THESE DE DOCTORAT

présentée à

L'UNIVERSITE DES SCIENCES ET TECHNOLOGIES DE LILLE

pour obtenir le titre de

DOCTEUR DE L'UNIVERSITE

spécialité électronique

par

Andrea COZZA

RAILWAYS EMC : ASSESSMENT OF INFRASTRUCTURE IMPACT

Soutenue le 22 juin 2005 devant la Commision d'Examen

Membres du jury :

M Paul-Alain ROLLAND	**Président**	Professeur à l'USTL-IEMN
M Sergio PIGNARI	**Rapporteur**	Professeur au Politecnico di MILANO
M Walid TABBARA	**Rapporteur**	Professeur à PARIS VI
M Flavio CANAVERO	**Co-Directeur de Thése**	Professeur au Politecnico di TORINO
M Bernard DEMOULIN	**Co-Directeur de Thése**	Professeur à l'USTL-IEMN
M Jean-Marie BODSON	**Invité**	ALSTOM Transport SA
M Victor SABATE	**Invité**	Consultant CEM
M Jean-Marie VANZEMBERG	**Invité**	Centre d'Essai Ferroviarie de Valenciennes

RAILWAYS EMC : ASSESSMENT OF INFRASTRUCTURE IMPACT

ABSTRACT

This work addresses EMC issues related to the railway domain, as brought up by industrial experience in applying the European standard EN 50121. The need to test rolling stocks on non-standardized facilities is here shown to be a major source of misinterpretation, eventually leading to overestimating the electromagnetic emissions radiated by a train. In particular, the test procedure described in the standard is shown to yield site-dependent results, due to the weakness of some basic assumptions on the propagation of electric signals along railway supply-lines. To this end, propagation and radiation phenomena along such lines are investigated, under a quasi-TEM assumption, proposing approximated descriptions validated through measurements on actual sites. Direct simulations can thus be used for assessing the impact of the infrastructure. Furthermore, an experimental characterization procedure is proposed in case of lack of a site description, based on magnetic field measurements.

CEM DES LIGNES FERROVIAIRES ELECTRIFIEES : EVALUATION DE L'INFLUENCE DE L'INFRASTRUCTURE

RESUME

L'étude porte sur la compatibilité électromagnétique des chemins de fer électrifiés définie par la norme Européenne EN 50121. La pratique de ce protocole nécessite de réaliser des mesures d'émission de véhicules sur des sites réels; il s'avère que l'armement des caténaires, leurs dimensions et les sous stations d'alimentation influent notablement sur le

rayonnement mesuré au voisinage d'un train. De plus, une surestimation du champ est probable, principalement à cause des hypothèses trop restrictives sur la propagation des signaux le long des caténaires, négligeant l'importance du régime d'onde stationnaire. L'étude de ces phénomènes a abouti au développement d'un modèle simplifié, validé par des expériences sur des sites réels. Ces simulations peuvent donc être utilisées pour estimer l'impact de l'infrastructure. Pour conclure, une procédure de caractérisation du système est proposée à partir de données tirées de mesures de champ magnétique.

POLITECNICO DI TORINO

SCUOLA DI DOTTORATO
Dottorato in Ingegneria Elettronica e delle Comunicazioni – XVII ciclo

Tesi di Dottorato

Railways EMC : Assessment of Infrastructure Impact

Andrea Cozza

Co-Tutori
Prof. Flavio Canavero
Prof. Bernard Démoulin

Coordinatore del corso di dottorato

Prof. Ivo Montrosset

22 Giugno 2005

Summary

During the last three decades, electronic devices have conquered the railway domain, taking the place previously held by electromechanical devices, thanks to higher performances and lower costs. The price of this "revolution" is the fact that, in order to work properly and reliably, electronic systems must be fairly immune to the effect of external interferers, while, at the same time, they are not to electromagnetically pollute the environment they work in. These issues are dealt with by Electromagnetic Compatibility (EMC) whereas several international EMC standardization committees work on the definition of tests and rules the manufacturers must comply with.

In the European Union, the reference for EMC issues in the railway domain is set by the CENELEC standard EN 50121, which deals with several aspects of a generic railway system, from the power-supply infrastructure to rolling stocks and signalling circuits. The introduction of this standard in 1996 has had a strong impact on rolling stock manufacturers, who are now required to test their products for EMC compliancy. As opposed to the automotive domain, the testing of trains cannot be performed in standard facilities, such as anechoic chambers, so that they have to be tested on actual railway lines, typically on the customer's. Industrial experience has shown that results obtained in this way are usually site-dependent, something that is against the very idea of a standard.

The aim of this work is to prove the importance of the infrastructure in radiated emission tests, showing that the test results are site-dependent, thus subject to misunderstandings and misinterpretations. To this end, the features of a generic railway system are briefly described, pointing out the great variability in actual configurations, together with the absence of standard solutions.

Subsequently, the electromagnetic modelling of a railway system is introduced, dealing with both propagation and radiation phenomena; in particular, the main topic here addressed is the modelling of supply-lines, through a quasi-TEM approach. The finite conductivity of the soil is taken into account by means of a closed-form formulation, thus avoiding numerical methods, and overcoming the limitations of Carson's model. Moreover, special attention is paid to discontinuities that would increase the model complexity, proposing approximated descriptions supported by numerical results. Results obtained with this model are then validated through several measurement campaigns carried out on actual railway lines, proving the effectiveness of the approach here pursued.

The model is then employed in order to prove that some criteria in the standard EN 50121, specifically introduced in order to avoid site-dependency, are not realistic, thus leaving this issue unresolved. To this end, numerical examples are considered, assessing the

impact of the infrastructure by comparing results obtained with realistic site configurations and with the ideal one envisaged by the standard. These comparisons are at the base of a tentative procedure that would allow to avoid the misinterpretations that triggered this work.

Unfortunately, this approach requires an accurate description of the test-site. Since this is hardly the case, an alternative experimental characterization of the site is proposed, based on magnetic field measurements. This approach, involving the solution of an inverse problem, is shown to be feasible through a numerical validation, though its practical utilization requires efficient optimization techniques.

Acknowledgments

The investigations here described have been carried out under a cooperation agreement between two French societies, Alstom Transport and the CEF[1], and two universities, the Politecnico di Torino (Italy) and the USTL[2] (France). Therefore, a number of persons have given a contribution to this work.

First of all, I want to thank Prof. Flavio Canavero, my thesis co-Director, who gave me the opportunity to work on this subject, supporting my candidature at Alstom Transport and at the CEF. His energy, curiosity, love for discussions and dedication to scientific research have greatly influenced me and this work.

I am much indebted to Prof. Bernard Démoulin, my thesis co-Director, for his constant support. I greatly appreciated the many discussions we had, proving his great experience in many fields and his deep love for science.

The thesis co-direction was ensured on the industrial side by several persons. In particular, two persons have given the most important contributions in setting the right direction, Jean-Marie Vanzemberg, Head of the CEF, and Victor Sabaté, EMC consultant for Alstom Transport. I also want to thank Dr. Christian Boneill and Jean-Marie Bodson (Alstom Transport), who co-directed my thesis for the industrial side.

An important role has also been played by Gérald Nottet and Eric François, Alstom Transport engineers, who greatly helped me during experimental campaigns.

I want to thank Prof. Walid Tabbara (Supélec[3], France) and Prof. Sergio Pignari (Politecnico di Milano, Italy) for having accepted to revise this manuscript as referees. In the same way, I want to thank Prof. Pierre Degauque, Head of the IEMN[4]/TELICE[5] laboratory where most of this work has been carried out, and Prof. Paul-Alain Rolland, Professor at the USTL, for having accepted to be the President of the Examining Commission.

I am much indebted to Dr. Lamine Koné, researcher at the IEMN/TELICE laboratory, for his kindness and availability, always giving precious suggestions, sharing with me part of his great experience in measurement techniques. Without him, experimental validations would have been far more difficult.

I wish to address special thanks to Prof. Stefano Grivet-Talocia and Prof. Renato Orta from Politecnico di Torino, for the time they dedicated to me.

---

[1]Centre d'Essai Ferroviaire (Centre for Railway Tests)
[2]Université des Sciences et Technologies de Lille
[3]Ecole Supérieure d'Electricité
[4]Institut d'Electronique Microélectronique et Nanotechnologie
[5]Télécommunications, Interférences et Compatibilité Electromagnétique

I also want to thank Dr. Marc Heddebaut, Research Director at INRETS[6], for having ensured access to INRETS during measurement campaigns.

Special thanks go to Rédha Kassi, engineer at the IEMN, for his availability and help in preparing and performing all the measurement campaigns. I like to regard his infinite patience as a proof of friendship.

The most part of this work has been carried out at the TELICE laboratory, where I really enjoyed the kindness of people living in the French region Nord. In particular, I want to thank Richard, Marc, Sébatien and Manue for their friendship.

The opportunity of working for three years as a Ph.D. student has been made real by the support of my parents: to them go special thanks.

As usual, the most important things come in the end. I want to thank Eleonora for having supported me during all this time with the most precious and nourishing of foods: love.

---

[6]Institut National de Recherche sur les Transports et leur Séurité (National Research Institution on Transportation and its Safety)

Table of contents

Chapter 1

Railways and EMC issues

In this chapter we recall some issues concerning Electromagnetic Compatibility (EMC) problems within the railway domain, mainly due to the ever-increasing use of electronic equipment on board of electric trains. The importance of EMC standards and their consequences on the manufacturing world are discussed, with special attention to the context of the European Union (EU). Critical issues are here discussed, pointing out the limitations of the present European standard EN 50121, calling for a deeper understanding of railway infrastructure impact on EMC tests. In particular, basic flaws in this standard are shown to lead to test-site dependent results, putting all the blame onto rolling stock manufacturers.

1.1 Introduction

During the last three decades, every manufacturer and user of electronic equipments has been affected by EMC. This discipline, which aims at ensuring the ability of an electronic device, equipment or system to work properly in an electromagnetically polluted environment with other devices, has known a formidable soar; its practitioner's role has passed from a sort of a "magician" trying empirically to put at work a system made up of several electronic devices, to a more formal one, where the target is to comply with a set of design constraints. This latter approach is becoming more and more compelling, forcing the manufacturer to intimately modify the research and development chain. This is actually justified by the dramatic increase in the number of electronic devices now being used in every aspects of modern life; more precisely, it is not the mere number of devices a cause for troubles, but rather their spacial density (or integration), stimulated over the past 30 years by a steady improvement in the semiconductor technology. This increase in the devices integration, allowing the development of systems performing more and more complex functions, together with ever-decreasing technological costs, had been appealing industrial manufacturers from every domain.

The railway industry has not been immune from this lure: whereas thirty years ago any function was still performed by electromechanical devices, nowadays nearly all of them are carried out through electronic devices. Besides being used for logical functions, controlling,

safety and other software operations, or more hardware ones such as transducing, these technologies have also conquered the high-power sector in the railway domain, i.e. the energy conversion [12], where switched-mode converters have successfully outstripped the electromechanical conversion. The reasons for this success are essentially the improved reliability of electronic converters: no mechanical parts moving during the process implies no damages due to their wearing away. Furthermore, it is by far simpler to substitute a thyristor on a printed board than an alternator. Another reason [1] is the requirement for a train to be able to switch between two or more kind of power-supply lines; this feature is extremely important in realities such as the European Union, where networks using several kind of power supplies are actually coexisting. This ability to switch from one voltage level (and in case even frequency) to another without causing any major inconvenience can be suitably achieved only by a switched-mode converter, whereas an electromechanical conversion would require a far greater amount of space on engine wagons.

One obvious drawback to switched-mode converters is related to the very idea of modulating the energy flow. This is achieved by switching on and off (or rather deviating) important current flows and voltages: as a matter of fact, a train can absorb up to some MW of power which, depending on the power-supply, may imply some thousands Ampères. Since the switching must be performed in a few score nanoseconds (in order to limit the amount of energy lost during voltage and current transitions), this leads to very important levels of electromagnetic interferences (EMI) [2]. These are in part directly radiated by the converter wiring, thus inducing voltages and currents all over the neighbouring wiring, but much worse effects are due to interferences conducted towards the overhead supply-line (cf. Figure 1.1). Since the level of these EMI would be catastrophic, all converters are provided with a series of filters at each port.

The filters design is not a simple matter, due to the very nature of the conducted EMI: in fact, they are due to transitions whose amplitude may vary of several thousands Ampères in a few score nanoseconds, thus producing EMI with a very rich spectrum, attaining the GHz range. So these filters, that have to be purely reactive being inserted on the power-supply circuit, have to work properly on many decades; this requires a number of filters working on smaller frequency-ranges, cascaded at each port.

Looking at Figure 1.1, another aspect is brought into play: since the train needs to be supplied, the converter is inevitably connected to an external line, so that part of the EMI produced by the train converters are injected into the supply line. Hence, several phenomena take place:

- since a railway line is practically a horizontal wire antenna, conducted EMI propagating along it inevitably excite generating an electromagnetic field. This may pose a serious threat to nearby telecommunication lines, also polluting the frequency spectrum used by radio broadcasters [3];

- the railway line can also be regarded as a multiconductor transmission line (cf. Chapter 3). Therefore it allows the propagation of such EMI signals; since other devices and equipments are connected to the same supply-line (according to the system architecture, see Chapter 2), the disturbances generated by in one point may
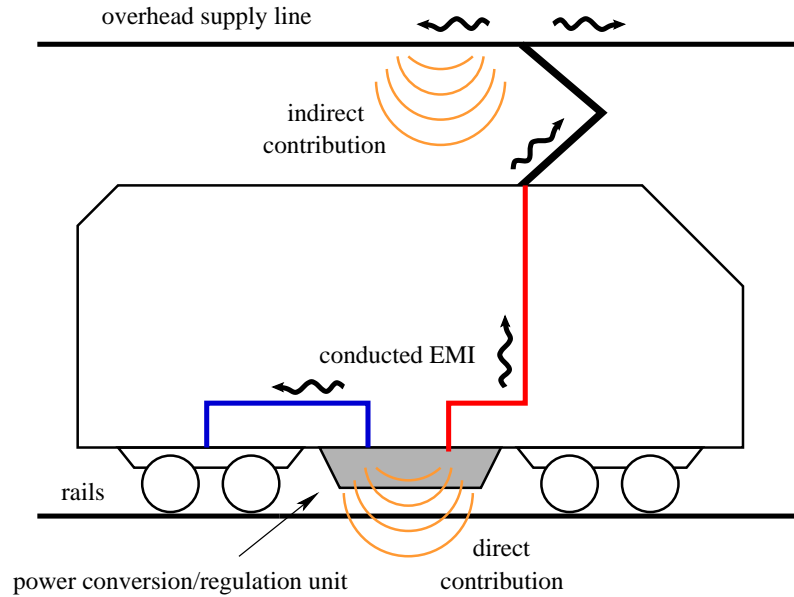
Figure 1.1. A schematic representation showing the two main contributions to the electromagnetic field measured near a train.

perturb the proper working of other devices, even many kilometers away from the EMI source;

- a railway line is usually not single-track, but it rather presents several parallel tracks (two, four or even more), as near as possible one to each other. This leads to electromagnetic couplings between the lines (or crosstalk), thus presenting another possible "gateway" for EMI to perturb other parts in the railway system, e.g. control signals propagating along the rails.

These three points certainly call for some sort of controls and restrictions for the EMI generated by a train, in order to assure the railway system and nearby ones to operate properly. Indeed, conducted EMI not only may disturb the electronic circuits dedicated to controlling and safety inside the train, but even the signalling circuitry connected to the rails [2, 4]. Faults in the detection of the train position and status may incur into catastrophic results. These considerations become even more pressing if one considers the spreading and the development of high-speed linking. For these reasons, it is paramount and even vital to provide a set of rules to be enforced on the manufacturers. This target is the raison d'être of EMC standardisation bodies, i.e. imposing sets of reasonable obligations and tests the industrial world have to comply with, according to the basic ideas and scopes of EMC.

In the railway domain, the most important standard in the EU context, but increasingly abroad too, is the so-called CENELEC EN 50121 [5]; this document, divided into five parts, describes the tests to be performed in order to point out EMC problems within a railway

system. Together with these tests, limits are imposed, both to conducted and radiated EMI.

1.2 Radiated emission tests under the CENELEC standard EN 50121

This standard, prepared by the CENELEC committee, deals with EMC issues in the railway domain. It is divided into five parts, addressing different aspects, here briefly recalled:

- Part 1 : General. A general description of the electromagnetic behaviour of a railway system is given, summarizing the most important phenomena that can lead to EMC problems.

- Part 2 : Emission of the whole railway system to the outside world. A setup is described for electromagnetic field measurements and limits are set. Basic statistical tools are introduced in order to get a representative estimation of the measured quantities.

- Part 3 : Rolling stock. This part is divided into two subparts, taking a closer look to emissions generated by electric trains, both as a whole and by its elementary parts.

- Part 4 : Emission and immunity of the signalling and telecommunications apparatus. Further tests are described in order to assess the EMC-compliancy of signalling devices.

- Part 5 : Fixed power supply installations. Emission and immunity tests are described for devices performing power-supply tasks.

In the context of the research project described in Section 1.4, the most important parts are the second and the third one, dealing with radiated emissions tests for rolling stocks as a whole. The basic setup for these tests is sketched in Figure 1.2. Here, the electromagnetic field is measured 10 m away from the mechanical axis of a railway track, on which the train to be tested is running. The mechanical centre of the antenna is set at a certain height with respect to the top of the rails. The actual height depends on the test to be performed. Radiated emissions are characterized by measuring the lateral component of the magnetic field over the frequency range 9 kHz-30 MHz, with the antenna height set in the range 1-2 m. On the other hand, the horizontal and vertical components of the electric field are measured over the frequency range 30 MHz-1 GHz, with the antenna height set to 3 m. Signals from the antennas are measured in the frequency domain, usually by means of spectrum analyzers.

This setup is shared by tests with and without trains. In the latter case, the train is tested under stationary and slow moving conditions (about 60 km/h for main-line trains). The need to test moving objects requires special attention in the setting of the resolution

4

Mechanical center
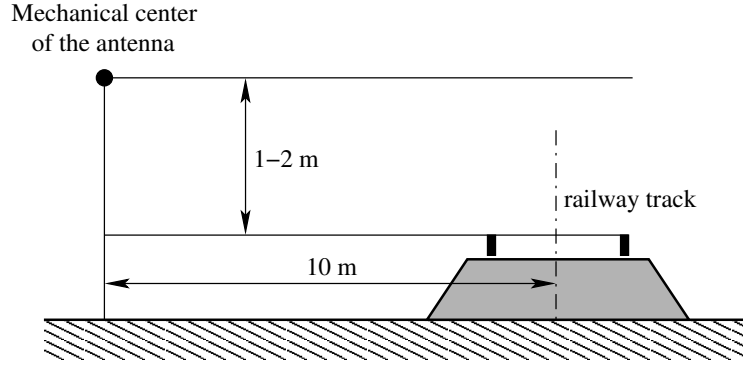of the antenna

1–2 m

railway track

10 m

Figure 1.2.   The setup required by the standard EN 50121 for measuring radiated emissions from rolling stocks running on an electric railway track. The antenna height of 1-2 m refers to the magnetic field tests, while for electric field ones it is set to 3 m.

bandwidth of the spectrum analyzer, in order to ensure the measurement of the peak-value in a short time, with respect to the time taken by the train for crossing the antenna position. In all these tests, the maximum peak-value is always considered.

In the last few years, updates of the standard have been discussed, proposing new setups based on quasi-peak measurements rather than peak one, in order to avoid worst-case characterizations. Moreover, new limits are under discussion, based on the feedback given by industrial experts.

1.3   Consequences of the standard for train manufacturers

The introduction of the standard in 1996 has obviously had very important consequences from the manufacturer's point of view. Besides the inevitable increase in the research and development costs, justified by further constraints in the design and testing of each equipment, a notable result has been the need to prove to the customer the ability of the product to comply with the standard limits. Indeed, in order to sell his products, the manufacturer not only has to provide a train that respects all the required electro-mechanical features, which are the basic reason for the customer to order a train; nowadays, the customer requires the manufacturer to prove the EMC compliancy of the train, not only by certificates or documents resulting from tests performed in the manufacturer's own facilities, but he even calls for the tests to be performed again on his own site or facility.

Of all the aspects considered in the previous section, the one that is always performed again on the customer's site is the near-field test. As already mentioned in the previous section, the magnetic and electric fields are measured at a fixed distance away from the railway line (usually set at 10 m).

As we have seen at the beginning of this chapter, the conducted EMI generated by switched-mode converters on the engine wagon are injected on the catenary. Hence, the

field measured is partly due to this indirect contribution, together with a direct contribution radiated by the train itself.

Although the direct contribution is due to the design of the train circuitry, the indirect one strongly depends on the site infrastructure (cf. Chapter 4). Far worse is the fact that since the architecture of the railway system varies from country to country, the relationship between the conducted EMI spectrum and the radiated field calls into question the infrastructure of the customer's site. Hence, the importance of a deeper knowledge in the intrinsic contribution of the site itself on the measured field.

As stated at the chapter beginning, we just want here to introduce a broad description of some of the main EMC issues in the railway domain which prompted this research project; hence, further details are to be found in the next chapters. Anyway, some important considerations can be already drawn:

- any actual configuration presents two fundamental features, i.e. the line length is always finite and it is usually connected to terminations not matched to the characteristic impedance of this multiconductor line (cf. Section 3.3). These two facts inevitably lead to the generation of reflections at the line ends: therefore, the current distribution along each wire presents standing-wave patterns. This means that for certain ranges of frequency the current distribution modulus has maxima that can be several times more important than for a matched (or infinitely long) line. Since the electromagnetic (e.m.) field, generated by the EMI propagating along the line, is directly related to the current modulus, the more important the current, the stronger the field. Hence, the e.m. field indirectly generated by a train is strongly affected by the line own architecture, which can strongly amplify the expected e.m. field;

- the same line supplying the train under test is usually connected to other devices. They may be divided into two groups: either sub-stations or other trains. Depending on the architecture, the substation may be a power transformer or a switched-mode converter (cf. next chapter). In this latter case substations and trains can be regarded as devices of the same nature, both generating and injecting disturbances on the catenary. A direct consequence is that not only the EMI generated by the train will produce an e.m. field, but also these extra-sources are bound to give contribution to the overall field.

These two considerations imply that the mere measuring the field at a certain distance away from the train is an ambiguous result. In particular, from the manufacturer's point of view, it would be disastrous to find out that a train is not being accepted by the commissioning customer for its non-compliancy with a standard, especially in the case of an EMC-compliant one! Indeed, the two points just highlighted leave this possibility unclosed. For these reason the standard EN 50121 provides two important requirements to be met:

- the site contribution to e.m. field must be known. To this end, before measuring the overall field with the train, this latter is kept disconnected from the catenary,

turned off. Then, the procedure envisaged by the standard is applied, in order to assess the site contribution. The resulting spectrum is usually referred to as ambient noise. At this point the actual measurements with the train can be performed: by comparing these results to the ambient noise spectrum, one can check the presence of any important contribution from the site. In this case, two possibilities can be envisaged for each frequency sample:

– the amplitude of the measured field is the same with and without the train. This implies that the train contribution is negligible with respect to the site. Thus, there is no possibility to extract the train contribution from these measurements, and the frequency sample is to be dropped. This does not mean that the train contribution is standard-compliant: maybe the site contribution is just several times stronger than the limits imposed by the standard, thus eclipsing the train non-compliancy;

– the overall field is stronger than the site contribution. In this case, the threshold chosen for considering the train contribution as dominant, is 6 dB. Thus, the train contribution has to be at least as strong as the site for considering the overall spectrum as significant.

- The line should be infinitely long. This assumption, which is physically never met, involves the absence of any standing-wave pattern. Another way of expressing this constraint is to ask for a matched line. Again this is never the case: a practical means for obtaining the same result is to consider the railway line as a lossy one. As we will see in the next chapter, this is actually the case, so that it is just a matter of imposing minimum lengths for obtaining a sufficiently strong attenuation. The standard assumes a length of 3 km to suffice for main commercial lines in order to be regarded as infinitely long. This value is unfortunately unrealistic. Indeed, the next chapters will provide the means for assessing the attenuation of electrical signals propagating along a railway line, pointing out an extremely low attenuation at low frequencies (up to some hundreds kHz).

The standardization commission had some point introducing such requirements. The underlying idea is again trying to provide an actual standard, i.e. a mean for testing a device in an unambiguous manner. Although the first point, assessing the site contribution, is self-consistent, allowing the manufacturer to argue for a margin of error, the second point has not yet been sufficiently investigated. The direct result of this lack of knowledge is the importance of resonance-related effects in the measured field. This is not just a matter of standardization: for a manufacturer it is paramount to prove the EMC-compliancy of his trains.

1.4 The research project

As one of the most important design and manufacturing group of rolling stock, Alstom Transport is deeply concerned with these problems. Having gone through several experiences with customers unsatisfied by the results obtained during near-field tests, related to

supply-line resonances, this company has proposed a research project about the electromagnetic modelling of a railway line. This project has involved two universities, i.e. the Politecnico di Torino, (Turin, Italy) and the laboratory IEMN[1]/TELICE[2], at the USTL[3] (Lille, France). Furthermore, the CEF[4], a railway test facility in Valenciennes, France, has provided the means for performing experimental tests on an actual railway track. This collaboration was sealed through a CIFRE[5] contract.

The aim of this project was the development of a theoretical model for studying the propagation and radiation properties of a railway line. In particular, the model was required to be implementable as a software tool: the railway system, described from a geometrical and topological point of view, provided of a certain number of electrical devices, would be simulated in order to verify the importance of the infrastructure contribution to the measured field. A straightforward consequence of owning such a tool, is the possibility to show by simulation the differences between the field measured nearby an actual line and the ideal infinite line considered by the standard (cf. Chapter 5). This is to be performed on site in front of the customer, who is comprehensibly suspicious of any document or justification indirectly delivered by the manufacturer. Therefore, this simulation tool ought to have a reasonable computation-time, e.g. not more than a few minutes. Furthermore, it has to follow the industrial principle of been reasonably accurate, i.e. it should yield results in a fairly good agreement with the reality, but using a reasonably simple model, with a limited computation-time; that is the more with the less.

The model need not provide both the electric and magnetic field radiated by the line: industrial experience has shown that the resonances affect the measurements up to a few hundred kHz, at the most one MHz; the same conclusion will be drawn in Chapter 4 through theoretical modelling. This frequency limitation allows to drop the study of the electric field: in fact, the standard prescribes to measure just the magnetic field up to 30 MHz.

The modelling of railway systems requires the study of both the supply-line (overhead line and rails or third-rail) and the power devices connected to it. Although the work here presented allows the inclusion of power devices, equivalent models for real-life devices are hard to be defined. In fact, theoretical equivalent models have been proposed, but in order to be applied, experimental tests have to be performed on actual devices. The problem is that such devices are hardly available for experimental investigations, being bulk devices that can weigh several hundred kilograms, and what is worse, connected to high-voltage lines whose supply is seldom interrupted.

Therefore, the main topic here addressed deals with propagation and radiation phenomena along the supply-line; this implies that the model here proposed cannot yet be fully applied to actual sites, due to this lack of device models. Nevertheless, it is an important step in the development of a more general simulation tool, since it already includes the potentiality for including power devices.

---

[1] Institut d'Electronique Microélectronique et Nanotechnologie

[2] Télécommunications, Interférences et Compatibilité Electromagnétique

[3] Université des Sciences et Technologies de Lille

[4] Centre d'Essai Ferroviaire (Centre for Railway Tests)

[5] Convention Industrielle de Formation par la Recherche (Industrial Agreement of Training by Research)

1.5   Conclusions

In this chapter we have introduced some important issues related to EMC standards in the railway domain. In particular, we have focused our attention on the European standard EN 50121, showing that it has some basic flaws in the definition of radiated emission tests. Indeed, it does not point out the fact that the magnetic field measured near a train is not only due to its intrinsic design, but also to the electrical configuration of the site where it is being tested.

These problems have a strong impact on rolling stock manufacturers, since they are on their own in proving that non-compliancies may be related to the test site rather than to the train itself. This has led to set up a research project, in order to assess the importance of the infrastructure in the overall results of radiated emission tests, by means of simple theoretical models.

Chapter 2

Railway system features

The aim of this chapter is to provide a brief, yet general, description of the main features of electric railway systems. To this end, the most widely spread configurations will be introduced, starting from a geometrical description of supply lines, up to a topological one, describing how these structures are actually used for supplying a train with the electrical power made available by substations.

2.1 Geometry of a typical electric railway track

In this section we recall the main features of electric railway tracks. From a mechanical point of view, railway tracks can be regarded as a mechanical support for rolling stock; in this respect, they can be described as made up of two parallel rails laying on a rock substrate known as ballast, specifically designed for supporting the mechanical stresses typically generated by rolling stock. Nowadays, railway traction is achieved by electric motors, which can be internally or externally supplied. In the former case, electric energy is generated onboard of the train itself, whereas in the latter case it is generated elsewhere and provided to the train by means of specifically designed distribution networks. The first solution has been increasingly turned down for the second one; as a matter of fact, electrical energy can be more efficiently generated in energy plants and subsequently adapted to railway needs by means of energy substations (cf. next section). An inevitable drawback of this solution is the need to transmit electrical energy from the substations to the trains: to this end, supply lines were firstly introduced.

The most widely spread configuration is the overhead one, sketched in Figure 2.1, showing the different components of a typical electrical railway track [8, 9], which are here briefly described; the most part of this data has been collected during [6] and refers to high-speed tracks in France (known as TGV lines), while other sources are indicated. It should be noticed that actual configurations come often in two or even four parallel tracks. Anyway, they share the same features as for the single-track configuration.
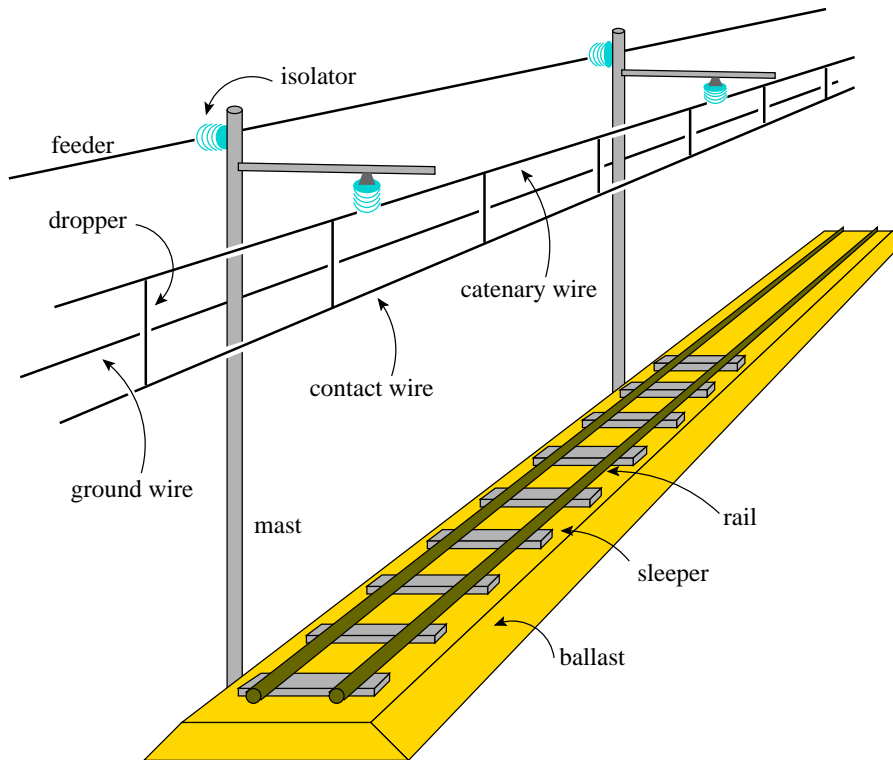
Figure 2.1. A simplified representation of a generic electric railway line, with an overhead supply line or catenary system.

Ballast

It is made of rocks and it provides the mechanical substrate for the actual track. A typical cross-section is shown in Figure 2.2a: a homogeneous layer of rocks (some centimeters wide) is usually considered, with an minimum thickness of 40 cm, while a lower layer of tar a few centimeters thick plays a draining role, in order to avoid water retention within the ballast. Actually, the ballast can be less thick in the surroundings of stations. The rocks employed in the ballast have a low conductive profile, in order to ensure a good insulation of the rails (cf. further on for more details).

This configuration is usually employed for main lines, whereas in underground links not ballasted tracks are sometimes used [10]. In this case a flat reinforced concrete bed substitutes the ballast.

Rails

They are kept in place on the ballast by means of transversal sleepers, traditionally wooden ones, whereas nowadays they are usually made of reinforced concrete. At least 4 cm must be allowed between the ballast and the bottom of the rails in TGV lines. The distance between the rails may vary according to the country: typical values are 1 m
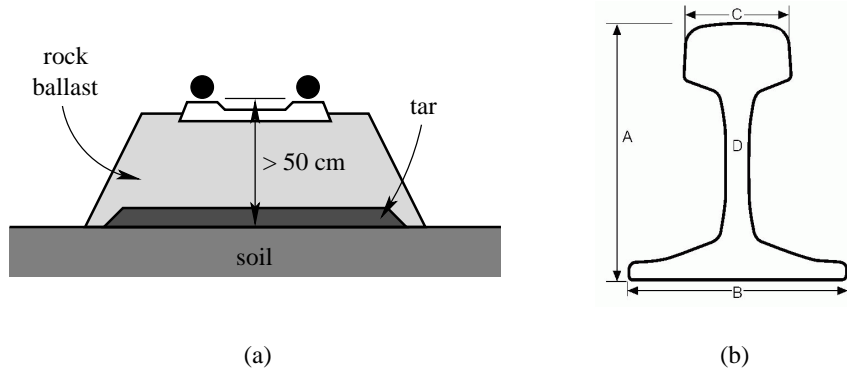
(a) (b)

Figure 2.2. The typical ballast cross-section for a TGV track (a) and the standard rail UIC60 [7] (b). Dimensions are A = 172 mm, B = 150 mm, C = 74 mm and D = 17 mm.

(mainly Germany), 1.435 m (the most widely spread in Western European countries) and 1.6 m. Their role is not only mechanical, but they also ideally act as return conductors for the supply line. The most widely spread cross-section is shown in Figure 2.2b [7]; the material they are made of is steel, but the only properties that are standardized are the cross-dimensions, the average density and the moments of inertia [7]. Its conductivity too is not imposed by any standard, although experimental results are of the order of 5 MS/m [11]. The materials employed also have ferromagnetic properties, with a relative magnetic permeability around 60 at 50 Hz.

Adjacent rails are soldered together over a length that can reach 800 m. Small gaps between these 800 m lengths are necessary to allow thermic expansion; in order to ensure electric continuity braided connectors are soldered between two rails. Anyway, a railway track must be divided up into subsections about $1 \div 5$ km long for the sake of signalling and automatic control. To this end, gaps filled with isolating materials are used.

Since the rails act as the return conductors for the supply line, they should be ideally insulated from the ground, in order to limit the fraction of current passing through the soil, both for safety reasons and for avoiding electrolytic corrosion of nearby metallic objects. Unfortunately, floating rails would be a hazard due to step and touch voltages, so that a sort of compromise is necessary. To the best of our knowledge, no standard values are imposed, but for a minimum impedance value of 2 Ω/km between the rails and the soil, for high-speed lines in France. In fact, rails are electrically insulated from sleepers by means of dielectric sheets. The most likely way of ensuring a fixed impedance is to ground the rails periodically, thus obtaining an average impedance over a certain length. As a matter of fact, rails are usually grounded at substations (cf. next section). On the other hand, step and touch potentials are limited by means of non-linear devices that can ground the rails in case of faults [16].

Overhead line

It is a multiconductor structure whose conductors are ideally at the same potential at any position, thus providing a stable electrical energy source to the train. Together with the rails it constitutes the actual power transmission structure, whereas other devices here described just have a secondary role, in this respect. It is often referred to as catenary (here too), though this label should just be applied to the wire hanging from masts: the very definition of a catenary implies a finite camber, i.e. the difference between the height at which the wire is connected to masts and the lower position it reaches in-between two masts. Actual layouts strongly depend on the overhead configuration (cf. Figure 2.3).
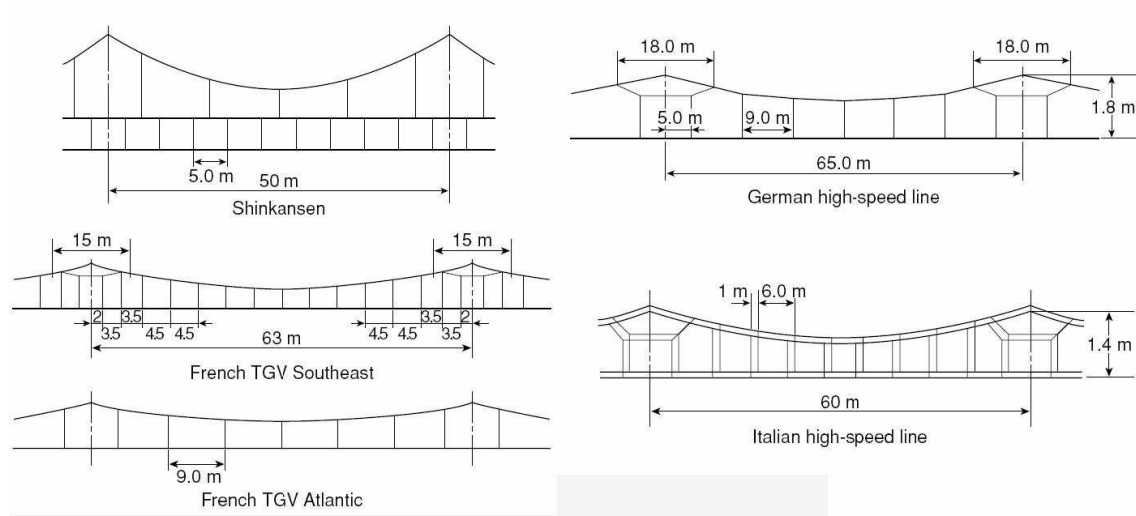
Figure 2.3. Some examples of overhead lines currently used [13].
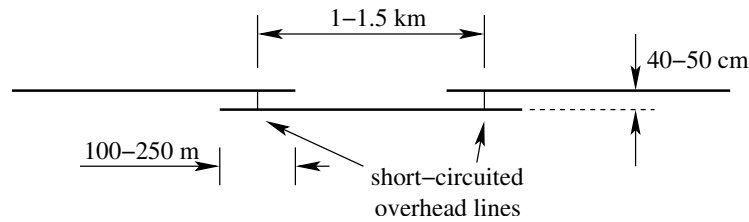
Figure 2.4. A typical configuration for railway lines longer than 1 km.

The length of actual overhead wires is clearly finite and it is in the range $1 \div 1.5$ km. Greater lengths are obtained by connecting together adjacent sections as in Figure 2.4. To this end, there are coupled portions, where two catenaries coexist facing one each other over about $100 \div 250$ m.

A very important parameter is the height of the contact wire, which is set to 5 m, with

respect to the rails, in TGV lines. Other wires are connected to the catenary wire through vertical metallic connections known as droppers (cf. Figure 2.1). The lower wires, which actually come into electrical contact with the pantograph, are known as contact wires; other intermediate wires can be employed both for having better mechanical properties (i.e. elasticity) and/or for increasing the overall conducting section of the overhead line (cf. Section 2.2). The droppers spacing is set by mechanical needs, in order to ensure a certain elasticity to the contact wire: typical values are $3 \div 9$ m. They do not have only a mechanical function, since they also provide equipotential connections along the overhead line; actually, droppers are not soldered to the overhead line wires, since this would not provided the best mechanical performances. In fact, actual droppers have configurations similar to the one in Figure 2.5a: therefore, the surfaces involved in these connections are subject to oxidation, so that the contact resistance can be non-negligible, although configurations as in Figure 2.5b are increasingly being adopted.

In order to ensure equipotentiality at the power-supply frequency and limit ohmic losses due to poor contacts, soldered connections are employed along the catenary. Their spacing is usually far greater than for droppers, although it strongly depends on the amount of current flowing through the catenary: in AC systems they are employed at the end of each catenary portion (i.e. $1 \div 1.5$ km), whereas in DC systems at each mast. Materials usually employed are copper (especially for contact wires) and bronze (especially for the catenary wire, due to better mechanical properties). The radii depend on the current to be supplied, though typical values are about 6 mm. In order to gain more conductive section, a further wire can be mounted on masts, referred to as feeder, with a radius usually greater than other overhead-line wires; a common value is about 9 mm. This wire is not connected through droppers, but only through soldered connections with a greater spacing.

(a)   (b)
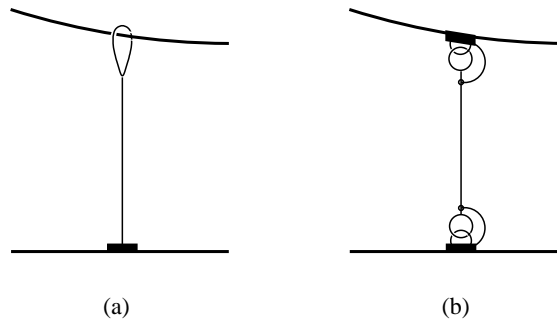
Figure 2.5.   A schematic representation of actual droppers: a classical connection that does not ensure electrical continuity (a) and a more complex one ensuring it (b).

Masts

They keep the overhead line hanging through the catenary wire. Their shape is mainly cylindrical, but their profile can quite differ from country to country: H-shaped bars in France, trellises in Italy, and in general tapered circular-section cylinders. They may not

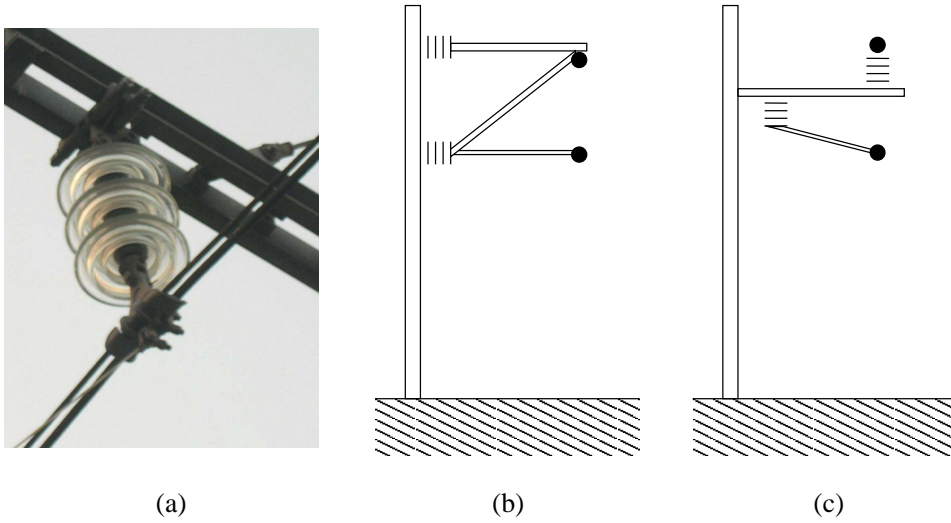(a)   (b)   (c)

Figure 2.6.   A power-isolator for 25 kV tracks (from CEF, France) (a) and two actual arrangements for power isolators on masts (b)-(c).

even be rectilinear, as in the Netherlands, where curvilinear shapes are used. They are almost periodically spaced in rectilinear tracks, whereas in curves the spacing is reduced, in order to approximate them through polygonal lines. The spacing in rectilinear tracks depends on the overhead line mechanical properties and ultimately on the power supply configuration (cf. Section 2.2): average distances are in the range $55 \div 70$ m.

The average distance from the track axis is about 3 m in single and double tracks. Due to safety reasons, the catenary wire (supplied by high-voltage sources) is connected by means of power-isolators, as for feeders. Their shape is usually as in Figure 2.6a with a length varying from 20 cm (DC supplies) up to 50 cm (AC supplies). They are usually made out of glass or ceramic materials and they can be mounted in several ways: two examples are shown in Figure 2.6b-c. Another safety measure is the grounding of masts: although this would seem as obvious, we have found no evidence or reference to actual grounding to the soil through dedicated low-impedance connections. On the other hand, masts are usually put into place as in Figure 2.7, within a concrete bedding, which does not provide a low-impedance path towards the ground.

Another safety measure is the connection of all the masts together by means of a dedicated wire, here referred to as ground-wire. It is periodically connected to the rails through connections that are enabled only during safety faults, usually by means of non-linear devices whose response is similar to a Zener diode, thus acting as a protection against over-voltages and over-currents (mainly induced by lightnings) [16]. Ground-wires are mainly employed in the neighbourhoods of railway stations, but they may also run along the entire length of a track, as in TGV lines. Another type of connection is shown in [14], where masts are directly connected just to one rail. On the other hand, along TGV tracks the ground-wire is connected to rails as in Figure 2.8; this connection acts as

a low-impedance path for currents flowing from the ground-wire towards the rails, whereas it has a much higher impedance between the two rails, thus limiting its impact on control signals propagating along the rails.
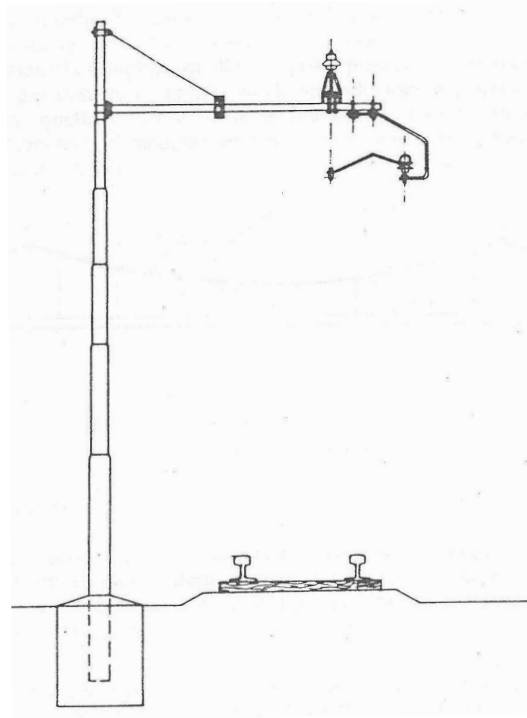

Figure 2.7.   A typical example of mast [15]; remark the fact that its bottom is surrounded by concrete, without direct grounding connections with the soil.
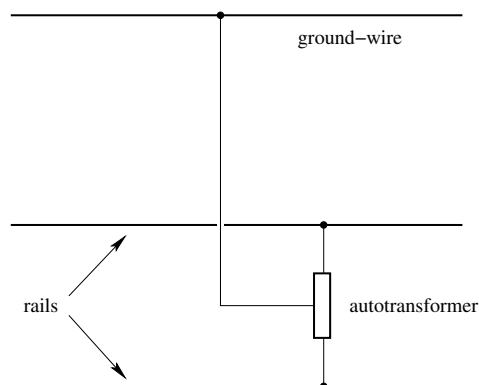

Figure 2.8.   The connection of the ground wire to the rails for over-voltage and fault protection.

17

Third rail

The catenary system is not the only way for transmitting electric power. An alternative solution is provided by the so-called third rail system, which employs a further rail, aside the two main ones, for transmitting electric power, as in Figure 2.9. The actual implementation of this system may vary over a wide range of configurations, according to how the third rail is oriented and how the energy is collected (laterally, at the bottom of the rail or on top of it). In this case the pantograph cannot be used any more, and other laterally mounted devices are used instead of it.

The third rail system is mainly employed in underground lines; an exception to that is the railway network in southern England. An even more peculiar idea is the four-rail system employed in some underground lines, with the fourth rail, insulated as the third one, is used as the return conductor, whereas the two main rails are not involved in power transmission; this arrangement was conceived for limiting corrosion problems due to part of the current returning through the ground. Another reason for resorting to the third rail is to avoid the visual impact of overhead lines, such as in Singapore.
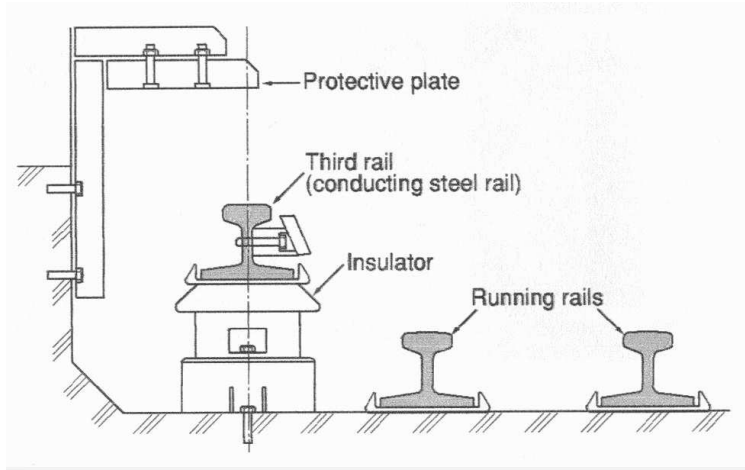
Figure 2.9.   An actual implementation of the third rail system [13].

2.2   Basic configurations of electric railway systems

So far the supply line has been introduced as a power transmission line, without any detail about the actual way it is employed. For instance, one may wonder how power substations are connected to the railway track and at which distance one from another. These features are more of a topological nature and they strongly depend on the type of energy supply [15, 16, 17].

In this respect, two broad families can be identified: DC supplies and AC ones. Each of these families is divided into several subgroups, depending on the nominal voltage

level applied to the railway track. Moreover, for AC voltages the frequency for power transmission can be chosen among several values. This wealth of configurations is due to the historical development of electric railways: each country, and even regions within the same country, defined different solutions to the engineering problems they faced, according to what they regarded as the most important issues, some of which are recalled in the next two sections. This freedom of choice was granted by the fact that at the beginning of the XX century, power distribution grids were not yet fully developed, or unable to ensure the power required by railway systems in the most trafficked lines. Therefore, railway companies had to develop their own power distribution grids, for their own use: this implied that the only constraints were set by railway needs.

This development did not bring any problem until interoperability became a top issue, namely within the European Union [1], where a great deal of supplies are still in use. Interoperability aims at developing railway links between countries where different electric supplies are used, a target that can be met by using switched-mode converters; Table 2.1 can give an idea of this scenario.

System Type			Japan[1]		World (including Japan)		
			km	%	km	%	Main Countries
DC	Less than 1,500 V		915	5	5,106	2	Germany, UK, Switzerland, USA
	1,500 V to 3,000 V (Mostly 1,500 V)		10,484	61	22,138	9	France, Spain, Netherlands, Australia
	3,000 V or more (Mostly 3,000 V)				78,276	33	Russia, Poland, Italy, Spain, South Africa
Single-phase AC	50 Hz • 60 Hz	Less than 20 kV			245	0	France, USA
		20 kV	3,741	22	3,741	2	
		25 kV	2,037	12	84,376	36	Russia, France, Romania, India, China
		50 kV			1,173	0	USA, Canada, South Africa
	25 Hz • 11 kV to 13 kV				1,469	1	USA, Austria, Norway
	16.66 Hz	11 kV			120	0	Switzerland
		15 kV			35,461	15	Germany, Sweden, Switzerland
Three-phase AC			30	0	43	0	Switzerland, France
Unknown					3,668	2	Kazakhstan[2], France
Total			17,207	100	235,816	100	

Notes: [1] Statistics include Japanese subways and AGTs.
[2] Kazakhstan is 3,528 km (3,000 V dc and 50 Hz 25 kV ac) but details are not known.

Sources: [1] *Railway Electrical Engineering Association of Japan, vol.8, no.10, pp.3–5, Oct. 1997*
[2] *Ibid., vol.8, no.11, pp. 77–78 and pp. 81–83, Nov. 1997*

Table 2.1. A summary of the electric supplies currently employed in electric railways, updated to 1996 [13].

In the context of this work, we are mainly concerned with the difficulties of defining simple descriptions for the simulation of railway infrastructures. As a matter of fact, it is not possible to have a priori knowledge of the actual geometry and topology of a test site, since they would not only depend on the power supply it employs, but also on engineering choices peculiar to the very test site, such as the type of substations, the number of conductors in the overhead line, and so on. In other words, we are dealing with systems whose features are more tailor-made rather than set by standards.

DC supply structures

Electric traction based on DC supplies has historically been the first to develop. This choice was due to electromechanical performances of DC motors better suited to traction applications (at the beginning of XX century); furthermore, the impedance of the supply line is limited to a resistive contribution, whereas in AC systems the reactive contribution plays a major role, decreasing power-transmission efficiency (relatively to the same effective voltage).

These advantages come with a number of practical drawbacks: since DC voltages could not be simply regulated inside locomotives (switched-mode voltage regulators were not still available), the voltage had to be regulated at the substation level, thus limiting the actual range of values. Furthermore, power insulation was a major issue. These two reasons limited the maximum voltage levels to a few thousand Volts. Actual values that are still in use are 1.5 kV and 3 kV for railway tracks, and 600 V and 750 V for underground and tramway lines.

Having a limited voltage, these systems are characterized by strong currents in the supply line, thus requiring larger conducting sections in order to limit power-transmission losses. Therefore, DC overhead lines are usually heavier than AC ones, with a greater number of conductors. The need for higher currents also means that losses are relatively higher in DC systems so that, in order to ensure a certain minimum voltage to locomotives, the distance between substations must be in the range $12 \div 20$ km under a 1.5 kV supply, and $35 \div 40$ km under a 3 kV. In the latter case distances are more typically limited to $15 \div 25$ km in highly trafficked lines [15]. In DC systems several substations can be directly connected to the same track: actually, a track is always divided into isolated portions known as sections, for several reasons such as signalling, safety and maintenance.

A typical layout for a DC supply is shown in Figure 2.10 [17] for a two-track system, where two substations are connected to each section. Each substation supplies two sections and the two tracks, in what is known as bilateral supply scheme. The two tracks can be put in parallel by means of power switches in the middle of the tracks; in the same way they can be broken into two parts for safety or maintenance reasons.

Another drawback of DC supplies is electrolytic corrosion in metallic objects and pipes buried in the ground near the tracks. As a matter of fact, the finite overall resistivity of the ballast implies that a portion of the return current flow through the soil. This problem is greatly worsened by the fact that the current never changes phase.
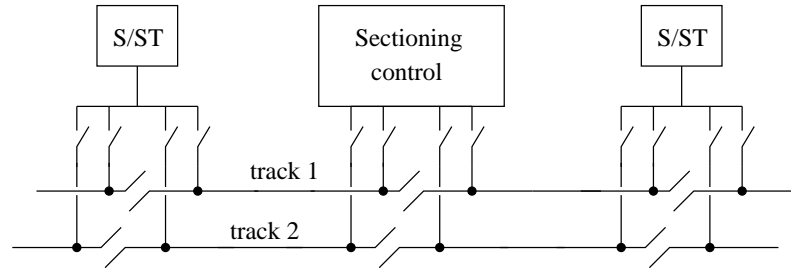
20

Figure 2.10. A general bilateral layout for a DC supply for a two-track line. The sectioning control unit allows the tracks to be connected in parallel or to cut off one half of them.

AC supply structures

On the other hand, AC systems have another balance of advantages and drawbacks. As a matter of fact, they allow simple voltage regulation on-board of locomotives through transformers, implying that the voltage supplied can be fixed to a certain level independently from the motor needs. By recalling that transmission losses are more important in AC systems (due to the higher track impedance), one can consider to supply higher voltages, thus having relatively minor losses; in the same way, by setting higher voltages the distance between substations can be increased. For instance, in 50 Hz tracks substations are $60 \div 100$ km apart [17].

In order to exploit DC motors, thanks to the freedom of choice for early engineers in electric traction, the frequencies chosen were $16\frac{2}{3}$ Hz or 25 Hz, often referred to as special frequencies. Nevertheless, as soon as electrical technology improved and 50-60 Hz power distribution grids spread, AC systems based on industrial frequency started to develop, driven by the possibility to directly connect substations to industrial distribution grids, avoiding the additional costs of special distribution grids. Indeed, in this case substations are basically based on transformers tapping energy from two phases of a three-phase high-voltage distribution line. Since this would mean an unbalanced load, consecutive substations use alternative phases, thus acting as an overall balanced load. But this also implies that the output of consecutive substations cannot supply the same line, due to the phase-shift in their phases, thus requiring the sectioning of a railway track. Due to the minor importance of losses, AC systems do not usually use bilateral configurations as in DC ones; therefore only one substation feeds the middle of each section.

In order to reduce transmission losses and radiated emissions, special configurations have been developed for AC systems. The two most successful are schematically shown in Figure 2.11. In the first one boosting transformers are periodically distributed along the supply line, where a further conductor is employed as a return conductor. Boosting transformers impose a differential current distribution between these two conductors, reducing the current returning through the rails and the soil, thus also reducing radiated emissions thanks to a less open current loop.

In the second special configuration the substation is a 50 kV source, connected between the actual catenary and a parallel feeder, while rails connected at the central point of the

transformer secondary. Autotransformers are connected along the line, in order to ensure a 25 kV supply as seen from the train. In this way, transmission losses are made relatively less important, so that the distance between substations can be increased. In this case too, radiated emissions are reduced.
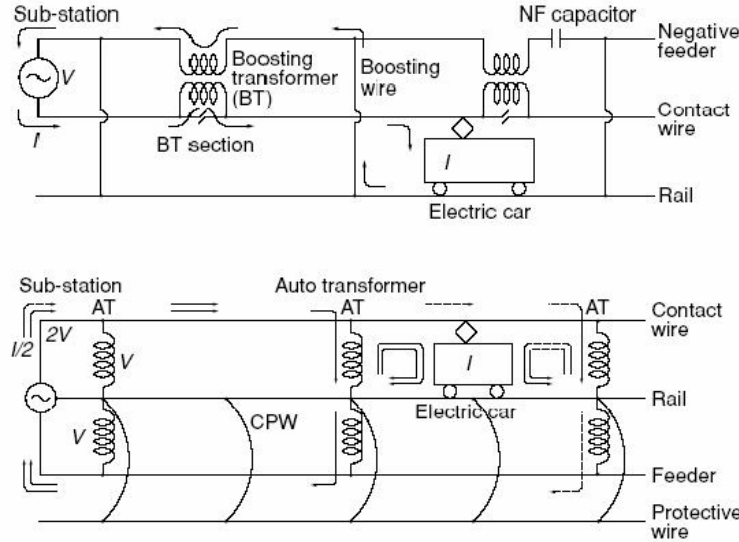
Figure 2.11.   The layout for a 25 kV supply line with booster transformers (a) and for a 2×25 kV configuration with autotransformers (b) [13].

On the other hand, for special frequencies users, there has been a strong drive to abandon their own distribution grids and to apply frequency-conversion substations. In the beginning that was achieved through electromechanical systems, whereas switched-mode inverters are now more increasingly used. The layout of substations along the track is in this case very similar to the DC case and a bilateral supply is adopted. In systems based on special and industrial frequencies the impact of the line reactance is more important in the latter case. For this reason, voltages are usually set to 15 kV and 25 kV respectively.

2.3   Conclusions

A general description of the most common features of railway lines has been presented in this chapter. In particular, special attention has been payed at discussing the differences between supply lines, mainly based on the form of electric energy supplied. This points out the difficulties involved in describing the configuration of actual railway lines, especially in what concerns power devices (e.g. transformers) and protection ones (e.g. isolators, over-voltage limiters). This is a major issue in the application of modelling tools to real-life systems: not only because of the lack of data about the actual configuration of a line

(mainly on a topological level), but also for the difficulty in the modelling of such devices above the industrial frequency range.

Chapter 3

Modelling of a uniform multiconductor line above a lossy soil

The aim of this chapter is to introduce the models that are at the base of the modelling of a railway system. The main features that this model should meet are summarized, pointing out the possibility to apply the transmission-line theory. To this end, this basic tool is introduced, together with other results for the analysis of propagation and radiation phenomena along transmission-line structures, such as the modal theory and antenna-theory models. Due to the presence of a non-ideal soil, its impact is addressed, summarizing the state of the art in the modelling of such a configuration and the limitations to the use of the transmission-line theory. Finally, the electrical properties of actual soils are discussed, together with a qualitative description of its impact on propagation and radiation phenomena.

3.1   Introduction

In Section 1.4 we have introduced the idea of modelling a railway system for EMC purposes. In order to meet these goals, we have chosen to use modelling tools based on the transmission-line theory (TLT). This choice is basically justified by the mathematical and computational simplicity of this model, together with the good accuracy it has proven over more than one hundred years of extensive validations in many different contexts. The TLT can be suitably applied to railway lines due to their structure, basically conceived for the transmission of electric energy: in the same way, this structure allows the propagation of electrical signals over a wider frequency-range.

As a matter of fact, this approach has been extensively investigated by Hill et al. and by Pozzobon et al. in several papers [18, 2, 14, 19], obtaining a good agreement between experimental and theoretical results. Nevertheless, we have not employed their methodologies, since the line models they have used were based on detailed experimental

characterizations, both of the soil and of the line itself. This means that it would be necessary to perform extensive measurements on a site not connected to any energy supply, which is a very strong limitation to the use of such characterizations: in fact, it is nearly impossible to fulfill such requirement on commercial lines. On the other hand, the experimental results they presented have been obtained for a specific configuration (number of conductors, connections, cross-section geometry, etc.), so that in general they cannot be applied to any configuration. Moreover, these results are limited to a few tens kHz, hence over a frequency range too limited with respect to the targets here set. Because of the need of accurate modelling on sites with different characteristics, a theoretical approach is better suited, allowing the industrial expert to pass from one configuration to another without requiring a characterization with the site not supplied.

A railway system cannot be simply described as a transmission-line: devices are connected to it, behaving as sources and loads, together with discontinuities impeding them to be regarded as uniform lines. Due to the frequency range here considered, it is possible to consider such devices (or discontinuities) as lumped, thus representing them through equivalent electric circuits. The TLT can easily accommodate this description, due to its electric-network approach, thus providing a good environment for a thorough analysis of a railway system. Unfortunately, discontinuities lead to a more complex description, thus increasing the computational load of an analysis: to this end, the next chapter addresses this problem, proposing several ways for simplifying it.

The targets set in Section 1.4 do not deal only with the propagation of electrical signals along railway lines, but also with the electromagnetic field they excite. To this end, antenna-theory models have been considered, in order to link propagation to radiation. In particular, these two aspects can be considered as a two-step analysis of railway systems, by computing the current distribution and then solving for the electromagnetic field.

The simplicity of the TLT comes with a price, that is a series of limitations, such as the need for a structure to be uniform and a high-frequency limitation due to its simplified approach. All these aspects are discussed in this chapter and in the next one. Moreover, in applying the TLT one usually considers the soil as a perfect electric conductor (PEC). This approximation is here shown to be unsuitable in the context of this work. Therefore, a thorough analysis of the further limits imposed by the presence of a non-ideal soil is presented. In the same way, antenna-theory models are regarded in the prospective of a non-ideal soil.

3.2 Electromagnetic waveguides

In order to understand the properties and limitations of the TLT, we need to recall some ideas from the theory of electromagnetic waveguides. But first, we should define what a waveguide is: in this work, a waveguide is a structure that can convey active electromagnetic power. In particular, we will refer to one-dimensional waveguides, i.e. structures that allow only one degree of freedom for the propagation, by defining a suitable reference system (in general a curvilinear one). Their main feature is indeed the ability to *guide* active electromagnetic power from one point to another. This does not require the

waveguide to be lossless (and in particular not to radiate e.m. energy); a waveguide should just be regarded as opposed to an antenna [20].

Hereafter we will consider a simpler version of waveguide, as shown in Figure 3.1. In this case, the structure presents a rectilinear axis, parallel to the z direction, and it is infinitely long. Furthermore, its cross-section is homogeneous, i.e. not dependent on the z coordinate. This particular choice is usually referred to as a uniform cylindrical waveguide. Therefore, the entire line can be univocally defined by its cross-section, applying a translation symmetry. In general, the full-wave electromagnetic modelling of waveguides is
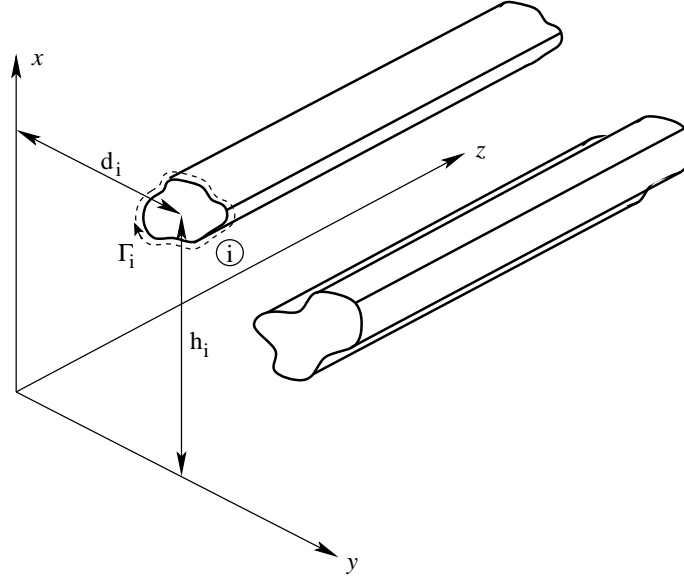
Figure 3.1.   The generic structure of a uniform open multiconductor transmission-line.

achieved by decomposing electromagnetic waves into several modes. In this dissertation, we will not enter this topic; a detailed description of the modal theory for such a structure can be found in [31] and a full-wave analysis of transmission-line structures has been presented in [21]. The only idea which is important in this context is just that the electromagnetic field propagating along a waveguide can be represented by means of a function basis. Each of these basis functions is usually referred to as a mode. In particular, from a more physical point of view, the modes present a different nature, which can be basically divided into two families:

- discrete modes: within this group, the modes are numerable, that is they form a discrete set. Propagation modes represent eigensolutions to the electromagnetic propagation along the waveguide. Each mode is characterized by a specific transversal electromagnetic field topography $\mathbf{\Phi}_0(x,y)$, which propagates along the waveguide. Whenever the propagation of a mode is considered, it presents the same transversal

topography at any longitudinal position, just scaled by a complex factor:

$$\mathbf{\Phi}(x,y,z) = \mathbf{\Phi}_0(x,y)\mathrm{e}^{-\gamma_p z} \tag{3.1}$$

The parameter γ_p is usually referred to as the propagation constant of the mode. Actually, this parameter is constant only in very specific cases, such as for a lossless line with no dispersion. In general, the propagation constant depends on the frequency and the electromagnetic properties of the media surrounding the waveguide.

- continuous modes: in this case the modes are not numerable, since they are not related to structure attached modes, but rather to the excitation of electromagnetic waves getting away from the waveguide. This category includes radiation and surface modes.

Propagation modes are usually classified by their transversal topography. For instance, a mode whose electric field has only transversal components is referred to as Transversal Electric, or TE. In the same way Transversal Magnetic modes, or TM, are defined. Structures presenting a dispersive behaviour allows the excitation of a further group of propagation modes. This group does not allows any simple classification as for TE and TM modes. In this case, the transversal topography presents mixed features: for this reason, they are usually referred to as hybrid modes. All these propagation modes present a cut-off frequency which is never equal to zero. This means that these modes can be excited, i.e. deliver active power, only at frequencies higher than their cut-off frequency. In particular, the cut-off frequency is related to the waveguide cross-section: a good rule of thumb is that these modes are excited whenever the guided wavelength is comparable to the cross-section.

For a waveguide or multiconductor transmission-line (MTL) as in Figure 3.1, defined with perfect conductors surrounded by a homogeneous isotropic lossless dielectric, in a not simply connected configuration, waveguide theory [20] shows that these structures allow a particular group of propagation modes whose electromagnetic field has only transversal components, i.e. Transversal Electric Magnetic or TEM. Its most important feature is to have a cut-off frequency equal to zero or, in other terms, to have no cut-off frequency at all. A direct consequence is that the only modes excited in an MTL are TEM modes as long as the maximum frequency concerned is lower than the lowest cut-off frequency for other propagation modes. This situation is sketched in Figure 3.2, highlighting the fact that there exists a frequency-range where a transmission-line can be effectively modelled by a TEM propagation model. Figure 3.2 also points out the reason why TE and TM modes are usually referred to as higher modes. On the other hand, radiation modes are always excited in open structures: indeed, the electromagnetic field is not confined to an impenetrable cavity, so that the flux of the lateral component of Poynting's vector is never equal to zero. Anyway, as long as transversal dimensions are smaller than the guided wavelength, the active power radiated by the line is negligible with respect to the power associated to the TEM modes, so that radiation losses can be neglected. In other terms, from an antenna-theory point of view, the open waveguide is considered as a poorly efficient antenna, since it cannot effectively *convert* electrical signals into radiated electromagnetic power.
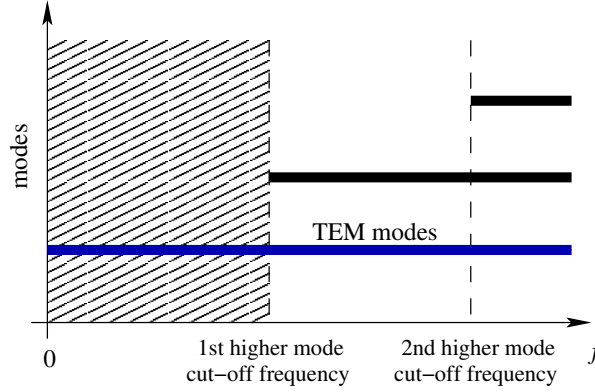
Figure 3.2. Mode-density vs. frequency for an MTL. For the shaded frequency range the propagation along the MTL is dominated by TEM modes.

3.3 Transmission-line theory

In this section we will refer to the structure in Figure 3.1, consisting of a uniform open MTL made of $N + 1$ parallel conductors, one of them acting as the reference conductor. All these conductors are considered as lossless, surrounded by a homogeneous and lossless medium. The results provided by the TLT are not related to a particular choice for the cross-section, which can assume, as in Figure 3.1, any shape.

The transmission-line theory (TLT) provides an analytical description of the propagation of electromagnetic waves along MTL. It is not a full-wave solution, i.e. it is not an exact solution to Maxwell's equations. In fact, TLT just describes the evolution of TEM modes, or better it assumes a TEM field topography. Therefore, TLT can be employed as long as the TEM mode is dominant in the MTL. As we have seen in Section 3.2, this assumption holds whenever higher-modes are not excited, i.e. as long as the transversal dimensions of the MTL are electrically small. In the present context we are interested in a circuit network approach to TLT. To this end, it is necessary to define voltages and currents.

Actually, a voltage could be defined, strictly speaking, only in static problems, where Maxwell's curl-equations are not coupled and the curl of the electric field is equal to zero. This is the reason why TEM approximations are also referred to as quasi-static approximations. The voltage is here defined as:

$$\mathscr{V}_i(z,t) = -\int_0^{h_i} \mathscr{E}_x(x,d_i,z,t)\mathrm{d}x \tag{3.2}$$

where $\underline{\mathscr{E}}(x,y,z,t)$ is the electric field, depending on the position (x,y,z) and the time t.

Other definitions can be considered, just choosing another contour point for the upper integration extreme. The resulting voltages are indeed equivalent, thanks to the quasi-static approach and having considered perfect conductors. In fact, this involves the electric field inside the conductors to be equal to zero, and thus the electrical potential to be constant over the conductor cross-section.

29

On the other hand, the current is supposed to be just of conductive nature, oriented along the z direction. Thus, the following definition holds:

$$\mathscr{I}_i(z,t) = \oint_{\Gamma_i} \underline{\mathscr{H}}(x,y,z,t) \cdot \mathrm{d}\underline{\Gamma} \tag{3.3}$$

where $\underline{\mathscr{H}}(x,y,z,t)$ is the magnetic field.

The TLT equations will be expressed in a matrix formulation, in order to obtain more compact expressions. To this end, we define the voltage and current vectors:

$$\mathscr{V} = \begin{bmatrix} \mathscr{V}_1 \\ \vdots \\ \mathscr{V}_N \end{bmatrix} \qquad \mathscr{I} = \begin{bmatrix} \mathscr{I}_1 \\ \vdots \\ \mathscr{I}_N \end{bmatrix} \tag{3.4}$$

Now, having defined voltages and currents, we can write TLT equations:

$$\frac{\partial}{\partial z}\mathscr{V}(z,t) = \mathbf{R}\mathscr{I}(z,t) - \mathbf{L}\frac{\partial}{\partial t}\mathscr{I}(z,t) \tag{3.5a}$$

$$\frac{\partial}{\partial z}\mathscr{I}(z,t) = \mathbf{G}\mathscr{V}(z,t) - \mathbf{C}\frac{\partial}{\partial t}\mathscr{V}(z,t) \tag{3.5b}$$

where $\mathbf{L}$, $\mathbf{C}$, $\mathbf{R}$ and $\mathbf{G}$ are the per-unit-length (p.u.l.) matrices for, respectively, the inductance, the capacitance, the resistance and the conductance. The elements of these matrices will be referred to as:

$$\mathbf{L} = \begin{bmatrix} l_{11} & l_{12} & \cdots & l_{1n} \\ l_{12} & l_{22} & \cdots & l_{2n} \\ \vdots & \vdots & \ddots & \vdots \\ l_{n1} & l_{n2} & \cdots & l_{nn} \end{bmatrix} \tag{3.6}$$

$$\mathbf{C} = \begin{bmatrix} \sum_{k=1}^{n} c_{1k} & -c_{12} & \cdots & -c_{1n} \\ -c_{21} & \sum_{k=1}^{n} c_{2k} & \cdots & -c_{2n} \\ \vdots & \vdots & \ddots & \vdots \\ -c_{n1} & -c_{n2} & \cdots & \sum_{k=1}^{n} c_{nk} \end{bmatrix} \tag{3.7}$$

$$\mathbf{R} = \begin{bmatrix} r_0 + r_1 & r_0 & \cdots & r_0 \\ r_0 & r_0 + r_2 & \cdots & r_0 \\ \vdots & \vdots & \ddots & \vdots \\ r_0 & r_0 & \cdots & r_0 + r_n \end{bmatrix} \tag{3.8}$$

$$\mathbf{G} = \begin{bmatrix} \sum_{k=1}^{n} g_{1k} & -g_{12} & \cdots & -g_{1n} \\ -g_{21} & \sum_{k=1}^{n} g_{2k} & \cdots & -g_{2n} \\ \vdots & \vdots & \ddots & \vdots \\ -g_{n1} & -g_{n2} & \cdots & \sum_{k=1}^{n} g_{nk} \end{bmatrix} \tag{3.9}$$

A physical interpretation of these p.u.l. matrices is provided by Figure 3.3, which presents the equivalent electrical network for an infinitely short portion of a three-wire MTL. These
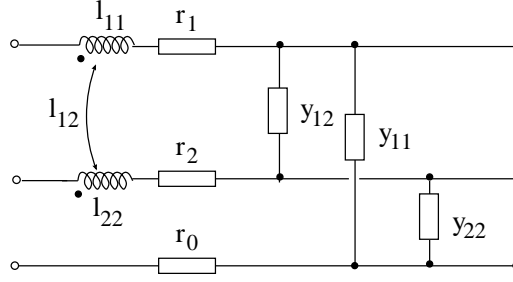
Figure 3.3. The electric-network interpretation of per-unit-length parameters of a three-wire line.

matrices entirely define the propagation along an MTL with no sources, under a TEM approximation. For this reason, the computation of such matrices is a central problem in the application of TLT to actual MTL, as it will be shown in Section 3.4.

Equations (3.5) can also be stated in the frequency-domain, assuming sinusoidal steady-state excitation. In this case voltages and currents are expressed as phasors, obtaining:

$$\frac{\partial}{\partial z}\mathbf{V}(z) \quad = \quad -\mathbf{Z}\mathbf{I}(z) \tag{3.10a}$$

$$\frac{\partial}{\partial z}\mathbf{I}(z) \quad = \quad -\mathbf{Y}\mathbf{V}(z) \tag{3.10b}$$

where $\mathbf{Z}$ and $\mathbf{Y}$ are respectively the impedance and the admittance p.u.l. matrices. These two matrices are defined as:

$$\mathbf{Z} \quad = \quad \mathbf{R} + j\omega\mathbf{L} \tag{3.11a}$$

$$\mathbf{Y} \quad = \quad \mathbf{G} + j\omega\mathbf{C} \tag{3.11b}$$

Equations (3.10) can be combined together, obtaining two second-order equations, in the form of Helmoltz's wave equation:

$$\frac{\mathrm{d}^2}{\mathrm{d}z^2}\mathbf{V}(z) \quad = \quad \mathbf{Z}\mathbf{Y}\mathbf{V}(z) \tag{3.12a}$$

$$\frac{\mathrm{d}^2}{\mathrm{d}z^2}\mathbf{I}(z) \quad = \quad \mathbf{Y}\mathbf{Z}\mathbf{I}(z) \tag{3.12b}$$

The results here recalled have been obtained under a TEM assumption, requiring the electromagnetic field to have no longitudinal component. Actually, this holds only for lossless lines; on the other hand, for conductors with a finite conductivity σ, Ohm's law states

$$\mathbf{E} = \frac{\mathbf{J}}{\sigma} \tag{3.13}$$

relating the electric field $\mathbf{E}$ inside the conductors to the current density $\mathbf{J}$. Considering a current flowing along the z direction, as required under a TEM assumption, equation (3.13)

31

clearly indicates that the longitudinal component of the electric field will be non-zero. Nevertheless, as long as it is negligible with respect to the transversal one, the TEM assumption can still be applied. Under this conditions, the propagation is referred to as quasi-TEM, meaning that the TEM assumption is not fully met. In other words, the losses can be treated as a perturbative effect, that is they do not strongly modify the propagation and the transversal field topography. Their major effect is to introduce an attenuation factor.

3.3.1 Per-unit-length parameters

It has been shown in Section 3.3 that TLT equations depend on p.u.l. matrices. The problem of computing them is here addressed.

In this section we will consider an MTL line with perfect conductors surrounded by a homogeneous and lossless medium. In this case matrices $\mathbf{R}$ and $\mathbf{G}$ are equal to zero. Due to the TEM assumption, p.u.l. matrices of inductance and capacitance are related to the static solution of Laplace's equation $\nabla^2\phi(x,y) = 0$ (where $\phi(x,y)$ is an electrostatic potential), as applied to the cross-section of the line. In particular, $\mathbf{L}$ and $\mathbf{C}$ are related by:

$$\mathbf{C} = \mu\epsilon\mathbf{L}^{-1} \tag{3.14}$$

where μ and ϵ are respectively the magnetic permeability and the dielectric permittivity of the surrounding medium. In case of circular conductors (hereafter referred to as wires), with currents uniformly distributed over their surface, closed-form expressions can be derived for the inductance and capacitance matrices. The uniformity assumption is fulfilled whenever the distance s_{ij} between two wires of radii $r_{w,i}$ and $r_{w,j}$ satisfies equation (3.15) (cf. Figure 3.4). Fulfilling this condition involves proximity effects to be negligible.

$$s_{ij} > 2(r_{w,i} + r_{w,j}) \tag{3.15}$$
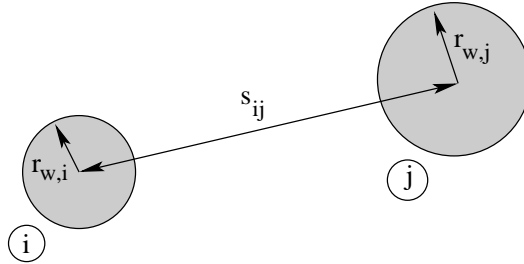
Under these assumptions, it can be shown that [22]:

Figure 3.4. The configuration for the definition of the wide separation condition.

$$l_{ii} = \frac{\mu}{2\pi}\ln\left(\frac{s_{i0}^2}{r_{w,0}r_{w,i}}\right) \tag{3.16a}$$

$$l_{ij} = \frac{\mu}{2\pi}\ln\left(\frac{s_{i0}s_j}{s_{ij}r_{w,0}}\right) \tag{3.16b}$$

where index 0 refers to the reference conductor. Matrix $\mathbf{C}$ can be directly computed thanks to equation (3.14). So far, the reference conductor has been considered as a further
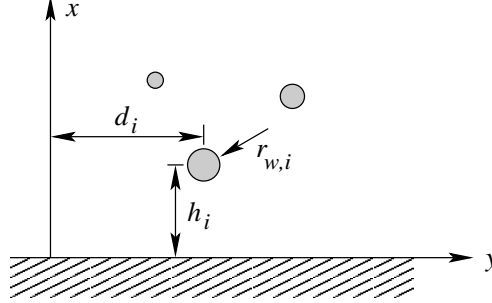

Figure 3.5. A uniform multiconductor transmission line above an ideal ground-plane. The conductors are assumed as infinitely long and the ground-plane is infinitely extended. The geometry parameters for the i-th wire are shown.

cylindrical conductor. In order to introduce the results presented in the next sections, we need to consider a slightly different setup, where the reference conductor is an infinite metallic plane, as in Figure 3.5. In this case the line has N wires. By assuming the reference plane, or ground-plane, to be a boundless perfect conductor, the image principle can be invoked, leading to [22]:

$$l_{ii} \;=\; \frac{\mu}{2\pi}\ln\left(\frac{2h_i}{r_{w,i}}\right) \tag{3.17a}$$

$$l_{ij} \;=\; \frac{\mu}{4\pi}\ln\left[\frac{(h_i+h_j)^2+(d_i-d_j)^2}{(h_i-h_j)^2+(d_i-d_j)^2}\right] \tag{3.17b}$$

These results hold only as long as we deal with circular conductors and condition (3.15) is fulfilled. Otherwise, numerical methods should be employed. There exists a great deal of possible numerical applications for computing p.u.l. parameters (e.g. LinPar). The choice should depend on the cross-section of the MTL: as an example, finite element methods are very useful whenever the surrounding medium is not homogeneous, or in case of complex-shaped conductors. These methods are very powerful thanks to their generality, but they are not computationally efficient . On the other hand, for very specific cases, more efficient routine can be developed. An example is the method of moments routine proposed in [23], which takes into account the non uniformity of the transversal current distribution along the wires surfaces. Hence, proximity effects can be included into the p.u.l. computation. This routine will be recalled in Section 3.4, regarding the modelling of rails.

The inductance and capacitance matrices for the overhead line represented in Figure 3.5 will be referred to as the external p.u.l. parameters of the line. So far, the wires have been regarded as lossless; although the conductivity of conductors used in the railway domain (mainly copper, bronze and steel) is quite high, they present a resistance that should be taken into account by the resistance matrix $\mathbf{R}$. Moreover, the finite conductivity also involves non-null magnetic fluxes *inside* the wires, thus adding a further contribution to

the inductance matrix. Since these effects take place inside the wires, the p.u.l. parameters related to them are referred to as internal. Furthermore, for the very same reason, mutual internal p.u.l. terms are negligible.

Assuming the current to be directed along the z direction, and with circular symmetry, the following expression holds for the internal p.u.l. impedance of the i-th wire of radius $r_{w,i}$ [22]:

$$z_{\text{int},i} = r_{\text{int},i} + \text{j}\omega l_{\text{int},i} = \frac{1}{\sqrt{2}\pi r_{w,i}\sigma_{w,i}\delta_{w,i}}\frac{\text{I}_0(q_i)}{\text{I}_1(q_i)} \tag{3.18}$$

where

$$q_i = \sqrt{2}\frac{r_{w,i}}{\delta_i} \tag{3.19a}$$

$$\delta_i = \frac{1}{\sqrt{\pi f \mu_0 \sigma_{w,i}}} \tag{3.19b}$$

and $\text{I}_0(x)$ and $\text{I}_1(x)$ are the modified Bessel's function of the first-kind, zeroth and first order respectively. Therefore the p.u.l. impedance matrix of a uniform MTL, surrounded by a homogeneous and lossless medium, can be written as:

$$\mathbf{Z} = \mathbf{Z}_e + \mathbf{Z}_{\text{int}} = \mathbf{R}_i + \text{j}\omega\left(\mathbf{L}_e + \mathbf{L}_i\right) \tag{3.20}$$

3.3.2 Modal theory applied to MTL

In order to model the propagation of electrical signals along an MTL, the linear system (3.10) need to be solved. This task is not straightforward, as the equations are coupled through full matrices (the p.u.l. matrices). If these matrices were in a diagonal form, the N equations would be uncoupled, that is they could be solved separately, without any interdependence.

The idea of decoupling linear equations can be exploited by recalling similarity transformations. The idea, from matrix analysis, is to seek an alternative representation equivalent to the original problem, where the coefficient matrices are in a diagonal form. In other words, we are looking for a suitable change of variables. A general result [24] states that two matrices $\mathbf{A} \in \mathbb{C}^{n \times n}$ and $\mathbf{B} \in \mathbb{C}^{n \times n}$ are similar if there exists a full-rank (thus invertible) matrix $\mathbf{X} \in \mathbb{C}^{n \times n}$ with the property that:

$$\mathbf{AX} = \mathbf{XB} \tag{3.21}$$

Under these assumptions, $\mathbf{X}$ is a similarity transformation. Now, let us consider a similarity transformation $\mathbf{T}$ relating matrix $\mathbf{A}$ to a diagonal matrix $\mathbf{\Lambda}$

$$\mathbf{AT} = \mathbf{T\Lambda} \tag{3.22}$$

being

$$\mathbf{\Lambda} = \begin{bmatrix} \lambda_1 & 0 & \cdots & 0 \\ 0 & \lambda_2 & \cdots & 0 \\ \vdots & \vdots & \ddots & \vdots \\ 0 & 0 & \cdots & \lambda_n \end{bmatrix} \tag{3.23}$$

where the $\{\lambda_i\}$ are the eigenvalues of matrix $\mathbf{A}$ and where

$$\mathbf{T} = [\mathbf{T}_1, \cdots, \mathbf{T}_n] \tag{3.24}$$

where $\{\mathbf{T}_i\}$ are the column unitary eigenvectors corresponding to the eigenvalues $\{\lambda_i\}$. Equation (3.22) can be rewritten as

$$\mathbf{A}\mathbf{T}_i = \lambda_i \mathbf{T}_i \tag{3.25}$$

which corresponds to the definition of the matrix eigenproblem applied to matrix $\mathbf{A}$. Thus, the sought similarity transformation exists and is defined by equation (3.22).

This procedure can now be applied to equations (3.12). Through the diagonalisation of matrix $\mathbf{YZ}$, the equations governing currents can be easily solved. Therefore, it suffices to define $\mathbf{T}$ as the juxtaposition of the eigenvectors of the matrix $\mathbf{YZ}$:

$$(\mathbf{YZ})\mathbf{T} = \mathbf{T}\mathbf{\Gamma}^2 \tag{3.26}$$

where $\mathbf{\Gamma} = \text{diag}\{\gamma_i\}$ is the diagonal matrix of the square-roots of matrix $\mathbf{YZ}$ eigenvalues. In this context the square root is taken in the algebraic definition, with a positive real part. The same procedure can be applied to voltages, considering the matrix $\mathbf{ZY}$. It can be shown that its eigenvalues are the same as for matrix $\mathbf{YZ}$ with a similarity transformation matrix $\mathbf{U}$ related to $\mathbf{T}$ as $\mathbf{U}^{\mathrm{T}} = \mathbf{T}^{-1}$. Therefore it suffices to solve the problem for the currents equation. Although it cannot be proven that a diagonal representation of $\mathbf{YZ}$ does always exist [22], for practical configurations a stable similarity transformation can be defined.

Having identified the matrix $\mathbf{T}$, it can be applied to the physical voltages $\mathbf{V}$ and currents $\mathbf{I}$, obtaining the new quantities $\mathbf{V}_m$ and $\mathbf{I}_m$:

$$\mathbf{V}(z) = (\mathbf{T}^{\mathrm{T}})^{-1}\mathbf{V}_m(z) \tag{3.27a}$$

$$\mathbf{I}(z) = \mathbf{T}\mathbf{I}_m(z) \tag{3.27b}$$

which, substituted into equations (3.10) yields the following solution:

$$\mathbf{V}(z) = \mathbf{Z}_c\mathbf{T}\left[\mathbf{P}^+(z)\mathbf{I}_{m0}^+ + \mathbf{P}^-(z)\mathbf{I}_{m0}^-\right] \tag{3.28a}$$

$$\mathbf{I}(z) = \mathbf{T}\left[\mathbf{P}^+(z)\mathbf{I}_{m0}^+ - \mathbf{P}^-(z)\mathbf{I}_{m0}^-\right] \tag{3.28b}$$

where matrices

$$\mathbf{P}^{\pm}(z) = \begin{bmatrix} e^{\mp\gamma_1 z} & 0 & \cdots & 0 \\ 0 & e^{\mp\gamma_2 z} & \cdots & 0 \\ \vdots & \vdots & \ddots & \vdots \\ 0 & 0 & \cdots & e^{\mp\gamma_n z} \end{bmatrix} \tag{3.29}$$

are the forward- and backward-travelling propagation matrices and $\mathbf{Z}_c = \mathbf{Z}\mathbf{T}\mathbf{\Gamma}^{-1}\mathbf{T}^{-1}$ is the characteristic impedance matrix of the MTL.

Equations (3.28) can be interpreted as the propagation along N independent two-wire transmission lines, as provided by the TLT, as sketched in Figure 3.6. The voltages and

35

currents are virtual quantities, related to the physical ones by equations (3.27). Actually, the propagation along each line corresponds to the N TEM modes allowed by a MTL, as introduced in Section 3.3. For this reason, this solution of the TLT equations is referred to as a modal approach. Hereafter, the quantities $\mathbf{V}_m$, $\mathbf{I}_m$ and $\mathbf{I}_{m0}$ will be referred to, respectively, as modal voltages, currents and excitation terms.
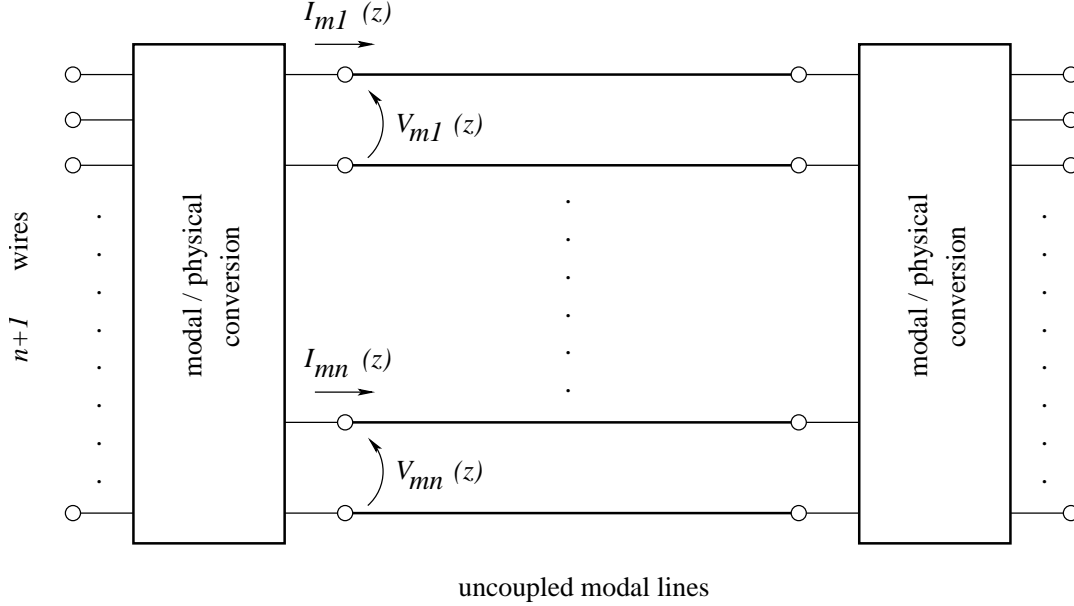

uncoupled modal lines

Figure 3.6. An electric-network interpretation of the modal theory, with uncoupled scalar modal lines, connected to two networks allowing the conversion from modal quantities back/to physical ones.

It should be born in mind that in this context the N modes are used to describe the TEM propagation, that is they can be regarded as a decomposition of the actual TEM propagation, by using a particular basis change. In particular, this decomposition is an extension of the common-mode/differential-mode decomposition often used in three-conductor lines. In the same way, for an $N+1$ conductor line, $N-1$ differential modes can be identified, together with a common-mode. Therefore, the modes can be regarded as a particular way of decomposing the current distribution along the MTL, as a combination of N basic configurations. An example is given in Figure 3.7, where a four-conductor line is considered. The weights defining the balance of the N modes are provided by the columns of matrix $\mathbf{T}$. For the example in Figure 3.7, the following matrix $\mathbf{T}$ has been considered:

$$\mathbf{T} = \frac{1}{\sqrt{3}} \begin{bmatrix} 1 & 1 & 1 \\ 1 & 1 & -1 \\ 1 & -1 & -1 \end{bmatrix} \tag{3.30}$$

Equations (3.28) point out one of the most important advantages of TLT: voltages and currents can be described as continuous quantities by using a discrete set of parameters.
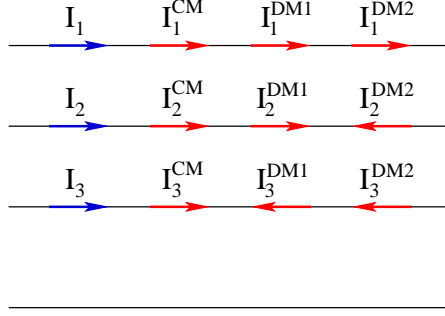
Figure 3.7. A modal expansion applied to a four-wire line, with the physical currents I_i decomposed into three sets of modal currents.

These parameters are the modal excitation terms $\mathbf{I}_{m0}^{\pm}$, which account for the excitation of the TEM modes by external sources. Thus, the TLT provides a complete, though simplified, description of the propagation phenomena, without solving Maxwell's equations as required by full-wave numerical methods. In fact, the computation of these parameters is just related to the termination circuits applied to the line ends, rather than to the boundary conditions all over the entire MTL structure. A detailed discussion about this topic is presented in Section 4.3.

Another important results from equations (3.28) is the chain matrix description of an MTL. The chain matrix directly relates voltages and currents at the two ends of an MTL of length $\mathscr{L}$

$$\begin{bmatrix} \mathbf{V}(0) \\ \mathbf{I}(0) \end{bmatrix} = \mathbf{\Phi} \begin{bmatrix} \mathbf{V}(\mathscr{L}) \\ \mathbf{I}(\mathscr{L}) \end{bmatrix} \tag{3.31}$$

where the argument 0 refers to the left-end and $\mathscr{L}$ to the right-end. The chain matrix, as derived from equations (3.28), is [22]

$$\mathbf{\Phi} = \begin{bmatrix} \mathbf{Y}^{-1}\hat{\mathbf{C}}\mathbf{Y} & -\mathbf{Z}_c\hat{\mathbf{S}} \\ -\hat{\mathbf{S}}\mathbf{Z}_c^{-1} & \hat{\mathbf{C}} \end{bmatrix} \tag{3.32}$$

being $\hat{\mathbf{C}} = \frac{1}{2}\mathbf{T}[\exp(+\mathbf{\Gamma}\mathscr{L}) + \exp(-\mathbf{\Gamma}\mathscr{L})]\mathbf{T}^{-1}$ and $\hat{\mathbf{S}} = \frac{1}{2}\mathbf{T}[\exp(+\mathbf{\Gamma}\mathscr{L}) - \exp(-\mathbf{\Gamma}\mathscr{L})]\mathbf{T}^{-1}$, where the exponentials are just applied to the main diagonal of $\mathbf{\Gamma}$.

3.4 TLT for a uniform multiconductor line above a lossy soil

As mentioned in Section 3.1, we want to model the uniform parts of a railway line as an MTL above an actual soil. So far, the results introduced in the previous section just deal with a perfectly conductive ground-plane. Although in the first place an actual soil can be regarded as a perfect conductor, its presence introduces several effects that cannot be taken into account by such a simplified approach. A qualitative description of these effects is presented in Section 3.7.

Although the importance of the soil has been recognized since the early days of telegraph lines, its effects were not investigated until the beginning of the twentieth century.
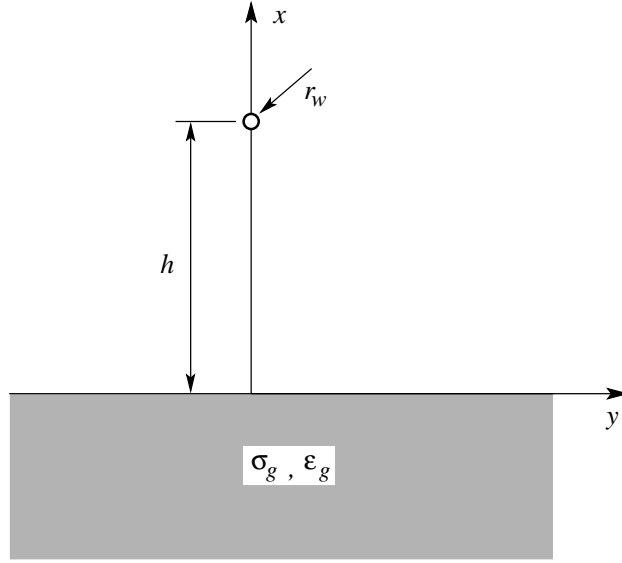
Figure 3.8.   A single-wire overhead line above a homogeneous soil.

In order to assess its importance on propagation, in 1926 Carson firstly proposed a modified expression for the p.u.l. impedance in [25], for the structure shown in Figure 3.8. The actual derivation of Carson's model will not be reported here, but it is very important to understand the assumptions under which he derived his model. Since he was interested in a model based on the TLT, he required the line to support a quasi-TEM propagation mode due to losses into the soil. Thus, as shown in Section 3.2, the line cross-section (delimited by the height h) must be electrically small. The soil was considered as a homogeneous isotropic medium, characterized by a conductivity σ_g and a relative dielectric constant ϵ_g. It was considered as not having any magnetic properties, namely with $\mu_g = \mu_0$. Typical values (cf. Section 3.4.1) are $\sigma_g = 10$ mS/m and $\epsilon_g = 10$. The behaviour of the soil depends on its complex permittivity $\tilde{\epsilon}$, defined as

$$\tilde{\epsilon} = \epsilon_g - \mathrm{j}\frac{\sigma_g}{\omega\epsilon_0} \tag{3.33}$$

For frequencies below the critical value $\omega_c = \sigma_g/\epsilon_0\epsilon_g$, it behaves as a finite conductivity conductor, whereas for frequencies well above this value it behaves as a lossy dielectric.

Carson worked under the assumption $\sigma_g \gg \omega\epsilon_g$; this condition corresponds to neglect the displacement currents into the soil. By regarding the wire under the thin-wire approximation, he showed that the presence of the soil can be taken into account by an additional series impedance Z_g, as in Figure 3.9. More details are given on the actual p.u.l. parameters computation in the next section.

In 1951, Kikuchi [26] proposed an extension to this model, taking into account the displacement currents into the soil. Although this model was valid over a wider frequency range, it only considered the quasi-TEM mode, neglecting the importance of other modes.
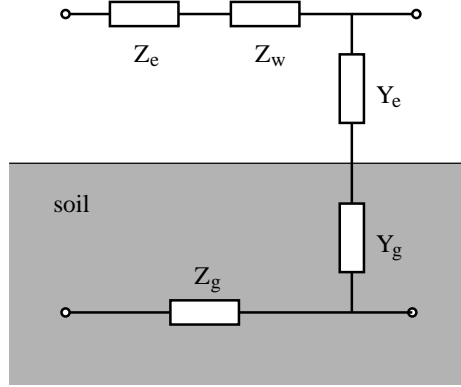
Figure 3.9. An electric-network interpretation of the per-unit-length parameters for a single-wire line above a finitely conducting soil, with the additional series and shunt terms accounting for the soil non-ideality.

Discussing about other modes than the quasi-TEM ones is not just a matter of speculative investigations. Even in the context of this project, it is very important to have a complete description of an MTL above an actual soil, since it is the only way to assess the validity of the quasi-TEM approach and to check its limits. Furthermore, both these models assumed a propagation constant equal to the free-space one.

For these reason, Wait proposed in 1972 [27] a modal equation obtained through a full-wave approach on a single-wire overhead line. The only assumptions were the thin-wire approximation and the description of the current-distribution through a complex exponential. Although he did not propose any solution to the modal equation, several researchers undertook this task. Among the most influential, King et al. investigated the validity of the quasi-TEM approach in [28] and [29], pointing out the following two conditions for the propagation to be dominated by a quasi-TEM mode:

$$|\tilde{\epsilon}| \quad \gg \quad 1 \tag{3.34a}$$

$$\frac{h}{\lambda_0} \quad < \quad 0.15 \tag{3.34b}$$

where λ_0 is the free-space wavelength. Furthermore, they proved that the attenuation of the quasi-TEM mode takes into account the radiation losses towards the soil and the dissipation at the soil interface. In other words, they proved that it is possible, under certain conditions, to consider a uniform line above the soil as a lossy transmission-line.

Chang et al. [30] reached the same results, but also showed that the first condition in (3.34) is needed for reducing the importance of another propagation mode, called the fast-wave mode. They also remarked that the attenuation associated with the quasi-TEM mode was greater than the fast-wave's.

The most complete modal description was carried out by Kuester et al [31]-[33], proving that a single-wire line above the soil supports a quasi-TEM or structure-attached mode, a fast-wave or surface-attached mode, a radiation mode in the air half-space, one in the

39

soil and a Zenneck type surface wave. In [33], examples are given about the topography of the transversal field for the two propagation modes, together with the trend of the propagation constants with respect to the wire height and the frequency.

The validity of this description was then experimentally investigated in 1983 by Degauque et al. [34], applying the modal description to an actual single-wire overhead line. Besides proving the accuracy of the results provided by the modal approach, Degauque et al. pointed out that satisfying conditions (3.34) does not allow to thoroughly neglect the other modes contribution. In fact, for a uniform matched line excited at his center by a sine-wave generator, the quasi-TEM description holds for distances from the source for which the attenuation does not exceed 60 dB. Further away, the other modes so far neglected begin to be dominant with respect to the quasi-TEM one. These results also prove that the attenuation of the quasi-TEM mode is greater than for the other modes, in particular as the frequency increases.

An example provided by Degauque et al. shows that at 1.5 MHz, this maximum distance is about a 12 km for a single-wire line at 9 m above the soil. Although this result could be considered as negative with respect to our need to model railway tracks several km long, this is actually good news, since for an attenuation of 60 dB the line can be regarded as matched, thus reducing its complexity to a "local level" (cf. Section 4.4).

A rather different approach has been pursued by Olyslager et al. in [35]; they have investigated how the p.u.l. parameters vary with respect to the soil conductivity. In order to check the validity of the quasi-TEM description, they have defined two different versions for the characteristic impedance, by means of a reciprocity theorem approach. These two versions consider, respectively, the quasi-TEM current or voltage as coincident with their respective physical quantity. Under this approach, only one of these two quantities has physical significance, whereas the other quantity has only a mathematical significance. Since these two formulations converge as the line becomes lossless, their disagreement is a meaningful check of the validity of the quasi-TEM approximation in lossy lines. Although the two formulations do not coincide for actual values of the soil conductivity, these differences are usually limited to a 10% error, but for local disagreements on very specific values with a resonance-like behaviour. Furthermore, the sensitivity of propagation phenomena with respect to the characteristic impedance is rather low, so that one can consider the quasi-TEM approximation as valid, even though the longitudinal components of the e.m. field are not negligible.

Knowing the conditions needed for a TLT approach, it would be possible to directly apply such a model to uniform railway tracks. Unfortunately, another condition must be fulfilled, that is the thin-wire assumption. It is common practice to consider it as valid for overhead lines fulfilling the condition $h/r_w \gg 1$. For an overhead supply line that would be alright, but a railway track is composed by rails too, together with further auxiliary conductors (cf. Chapter 2). Being in the proximity of the soil, the thin-wire hypothesis is to be carefully checked.

The first analysis verifying when the thin-wire approximation can be invoked was carried out by Pogorzelski et al. [36] in 1977. They extended the modal equation derived by Wait, describing the surface current density J_z along the wire surface through a cosine series expansion. In particular, they showed that the ratio between the constant term J_{z0}

and the fundamental cosine term J_{z1} is:

$$\left|\frac{J_{z0}}{J_{z1}}\right| \propto \frac{2h/r_w}{\ln(2h/r_w)} \tag{3.35}$$

Although this result was referred to as "proximity effect for a small height", it is based upon the assumption that the ratio $h/r_w \gg 1$. In fact, in that work "small height" just meant that h was small compared to both the skin-depth of the soil and the wavelength. Therefore this result cannot be applied to the rails.

A further analysis of the thin-wire approximation was undertaken by Bridges et al. [37] in 1989. In this case, no assumption was made on the ratio h/r_w. By using an approach based upon the method of moments, they proved that the actual condition for invoking the thin-wire approximation is just

$$\frac{h}{r_w} > 1 \tag{3.36}$$

which implies a wire almost at contact with the soil. In fact, although the longitudinal current present an azimuthal variation, it has no effect both on the propagation constant and on the electromagnetic field around the wire. Therefore, we are now in the condition to model a uniform railway line as an MTL above a lossy soil. A detailed description about the representation of rails as circular section conductors is presented in Section 3.4.5.

More recently, several authors have approached the analysis of a MTL above a lossy soil from a different perspective. Rather than studying the propagation properties of this system using a circuit network approach, they have considered the currents induced on it by an external electromagnetic wave [38, 39, 40]. This task has been motivated by a compelling need for a theoretical description of the currents induced by electromagnetic pulses such as lightning or nuclear and high-power pulses. Thus, these models having been developed for a time-domain analysis, they are not interesting in the context of this work. Further results more concerned with a frequency-domain modelling are recalled in the next section.

3.4.1 Summary of the p.u.l. formulations for a lossy soil

As asserted in Section 3.3, whenever the TLT can be applied, the propagation of electrical signals along an MTL is entirely described by its p.u.l. parameters, together with the line length. Having recalled in the previous section the possibility to describe the propagation along an MTL above the soil by means of the TLT, it is just a matter of computing its p.u.l. parameters. In this section, the main results available in the literature for this task are briefly recalled in a historical perspective.

The first expression proposed for the ground impedance is due to Carson [25]:

$$Z_g \simeq \frac{\mathrm{j}\omega\mu_0}{\pi k_g^2} \int_0^\infty \left(\sqrt{\lambda^2 - k_g^2} - \lambda\right) \mathrm{e}^{-2h\lambda} \mathrm{d}\lambda \tag{3.37}$$

where $k_g^2 = \mathrm{j}\omega\mu_0\sigma_g$. Eventually, he proposed a series expansion for the computation of the integral.

Another expression was derived by Vance [41]:

$$Z_g \simeq \frac{-\mathrm{j}\gamma_g}{4\pi h \sigma_g} \frac{H_0^{(1)}(\mathrm{j}\gamma_g 2h)}{H_1^{(1)}(\mathrm{j}\gamma_g 2h)} \tag{3.38}$$

where $\gamma_g = \sqrt{\mathrm{j}\omega\mu_g(\sigma_g + \mathrm{j}\omega\epsilon_g)}$ and $H_i^{(1)}(x)$ are cylindrical Hankel's functions of the first type. Vance also proposed a simplified expression for the ground shunt-admittance:

$$Y_g \simeq \frac{\gamma_g^2}{Z_g} \tag{3.39}$$

These two expressions have been compared in [42], showing their substantial agreement over the entire frequency-range of validity for the quasi-TEM approximation. Further approximated expressions have been proposed, such as in [43].

A special mention is deserved by the complex image method [44] which, although based on strong approximations, allows a simple physical interpretation of the soil effects, in particular for radiation phenomena. In this case the image principle (limited to a perfectly conductive soil) is extended to lossy soils by placing the image at a depth d_I

$$d_I \simeq h + (1 - \mathrm{j})\delta \tag{3.40}$$

where $\delta = 1/\sqrt{\pi f \mu_0 \sigma_g}$ is the soil skin-depth. Olsen et al. [45] have showed that this result is very close to the first term in the expansion proposed by Carson.

All these expressions share the common assumption that $\sigma_w \gg \omega\epsilon_0\epsilon_g$, i.e. the soil can be regarded as a finite conductivity conductor. Moreover, they also assume $\gamma_p \simeq \gamma_0$; in the literature, this hypothesis is often referred to as a quasi-static assumption. This label is quite strange, since the soil impact on the propagation constant is felt in the lower frequency-range too, as shown in the next section.

We are interested in a TLT model valid up to the MHz region, for actual soils; the lower limit for the critical frequency f_c is about 3 MHz for coastal lands (cf. Section 3.6), so that the assumption $\omega \ll \omega_c$ is not met up to the MHz region. For this reason, more general expressions are needed.

An answer to this need was given by D'Amore et al. in 1996. In [46] and [47] they derived the telegrapher's equations from Wait's model, with no approximation at all, but for a quasi-TEM assumption. A point deserving a clarification is the upper bound of the frequency range of validity of their results. In fact, D'Amore et al. have stated that the transmission-line mode is dominant even when the quasi-TEM approximation does not hold. This statement was based on the study of the attenuation of the propagation constant for the transmission-line mode. Indeed, this study showed a maximum in the attenuation, while going to zero at higher frequencies, thus leading D'amore et al. to consider it as dominant. Anyway, this analysis is not based on a complete modal description of the propagation, but it was rather based on an already simplified modal equation, assuming $\gamma_p \simeq \gamma_0$. Furthermore, previous works here recalled had already proven the limitation of the transmission-line mode.

Nevertheless, the results proposed by D'Amore et al. are indeed interesting because they do not regard the soil as a lossy conductor, but rather as a generic homogeneous medium. That is, as long as the quasi-TEM approximation is valid, no other approximation is considered, thus extending the p.u.l. expressions over a frequency range where $\omega \simeq \omega_c$.

Another important point is that the voltage definition may lose its physical significance. In fact, no quasi-static approximation has been considered by D'Amore et al.. This just means that the voltage acts as an auxiliary variable, or better as a state-variable. This may lead to problems in fixing the boundary conditions in the high-frequency limit, but in the context of this work the voltage definition is expected to be unambiguous, since conditions (3.34) are fully met.

3.4.2 Wide-frequency formulation of the p.u.l. parameters for a single-wire line

In this section the main results of the formulation proposed by D'Amore et al. in [46, 47] are briefly recalled. As previously mentioned, the telegrapher's equations they derived are based on Wait's model [27]. The main result obtained by Wait was a modal equation for a uniform infinitely long single-wire line above a lossy soil. In order to derive it, he expressed the longitudinal components of Hertz's vector potentials due to a complex exponential current distribution

$$I(z) = I_0 e^{-j\gamma_p z} \tag{3.41}$$

flowing along the z oriented wire, obtaining

$$
\begin{aligned}
\Pi_{e,z}(x,y,z) &= -\frac{j\omega\mu_0}{4\pi\gamma_0^2} I(z) \int_{-\infty}^{+\infty} \Big[e^{-u_0|x-h|} + \\
&\quad + R_e(\lambda)e^{-u_0(x+h)} \Big] \frac{e^{-jy\lambda}}{u_0} d\lambda \qquad x \geq 0 \tag{3.42a}
\end{aligned}
$$

$$\Pi_{m,z}(x,y,z) = -\frac{j\omega\mu_0}{4\pi\gamma_0^2} I(z) \int_{-\infty}^{+\infty} R_m(\lambda)e^{-u_0(x+h)} \frac{e^{-jy\lambda}}{u_0} d\lambda \qquad x \geq 0 \tag{3.42b}$$

with the scattering terms

$$R_e(\lambda) = -1 - u_0 \frac{2\gamma_0^2}{\Gamma_0^2} \left(\frac{1}{u_0 + u_g} - \frac{\gamma_p^2/\gamma_0^2}{\tilde{\epsilon}u_0 + u_g} \right) \tag{3.43a}$$

$$R_m(\lambda) = -\frac{\gamma_p\lambda}{j\omega\mu_0} \frac{2\gamma_0^2}{\Gamma_0^2} \left(\frac{1}{u_0 + u_g} - \frac{1}{\tilde{\epsilon}u_0 + u_g} \right) \tag{3.43b}$$

Hertz's vector potentials are related to the electromagnetic field as

$$\mathbf{E} = \nabla \times \nabla \times \mathbf{\Pi}_e - j\omega\mu_0 \nabla \times \mathbf{\Pi}_m \tag{3.44a}$$

$$\mathbf{H} = \nabla \times \nabla \times \mathbf{\Pi}_m + j\omega\epsilon_0 \nabla \times \mathbf{\Pi}_e \tag{3.44b}$$

43

By imposing the tangential electric field to be equal to zero at the wire surface (i.e. the wire is supposed to be a perfect conductor), the following modal equation is obtained:

$$\left(1 - \frac{\gamma_p^2}{\gamma_0^2}\right)\Lambda(\gamma_p,h,r_w) - \frac{2}{\gamma_0^2}\int_0^\infty \frac{\lambda^2 - u_0 u_g}{\tilde{\epsilon}u_0 + u_g}\mathrm{e}^{-2hu_0}\cos(r_w\lambda)\mathrm{d}\lambda = 0 \tag{3.45}$$

where
$$\Lambda(\gamma_p,x,y) = \mathrm{K}_0\left[\Gamma_0\sqrt{(x-h)^2 + y^2}\right] - \mathrm{K}_0\left[\Gamma_0\sqrt{(x+h)^2 + y^2}\right] \tag{3.46}$$

being $\mathrm{K}_0(\cdot)$ the modified Bessel's function of the second kind, zeroth order and

$$\Gamma_0^2 = \gamma_0^2 - \gamma_p^2 \tag{3.47}$$

The only unknown quantity in equation (3.45) is the modal propagation constant γ_p, which explains the term "modal". By including internal losses for the wire, the modal equation can be written as [46]:

$$\frac{2\pi}{\mathrm{j}\omega\mu_0}Z_\mathrm{int} \quad + \quad \left(1 - \frac{\gamma_p^2}{\gamma_0^2}\right)\left[\mathrm{K}_0(\Gamma_0\rho_1) - \mathrm{K}_0(\Gamma_0\rho_2)\right]$$

$$+ \quad 2S_1(\gamma_p,h,r_w) - 2\frac{\gamma_p^2}{\gamma_0^2}S_2(\gamma_p,h,r_w) = 0 \tag{3.48}$$

where Z_int is the internal impedance of the wire and

$$S_1(\gamma_p,x,y) \;=\; \int_0^\infty \phi_1(\gamma_p,x+h,\lambda)\cos(y\lambda)\mathrm{d}\lambda \tag{3.49a}$$

$$S_2(\gamma_p,x,y) \;=\; \int_0^\infty \phi_{\tilde{\epsilon}}(\gamma_p,x+h,\lambda)\cos(y\lambda)\mathrm{d}\lambda \tag{3.49b}$$

Two main approaches allow the derivation of the telegrapher's equations from an antenna theory model: these are shown described in [22] (power-based representation) and in [50] (reciprocity-based representation); the approach chosen by D'Amore et al. is the power-based representation. To this end, it is necessary to define a line voltage:

$$V(z) = -\int_0^h E_x(x,r_w,z)\mathrm{d}x \tag{3.50}$$

It should be noticed that the definition of a voltage does depend on the integration-path, having dropped the quasi-static hypothesis. By applying Maxwell's curl equations in their integral formulation, the two telegrapher's equations are derived, yielding:

$$Z_g \;=\; \frac{\mathrm{j}\omega\mu_0}{\pi(k_0^2 - \gamma_p^2)}\left\{k_0^2 S_1(\gamma_p,h,r_w) - \gamma_p^2\left[S_1'(\gamma_p,h,r_w) - S_1'(\gamma_p,0,r_w)\right.\right.$$

$$- \quad \frac{\gamma_p^2}{k_0^2}S_2(\gamma_p,0,r_w) + S_2'(\gamma_p,0,r_w) - S_2'(\gamma_p,h,r_w) + S_1(\gamma_p,0,r_w)\bigg]\bigg\} \tag{3.51a}$$

$$
\begin{aligned}
Y_g \;=\;& \mathrm{j}\omega\epsilon_0\pi(k_0^2 - \gamma_p^2)\Bigg\{ k_0^2\Bigg[S_1(\gamma_p,h,r_w) - S_1(\gamma_p,0,r_w) \\[2mm]
& -\; S_1'(\gamma_p,h,r_w) + S_1'(\gamma_p,0,r_w) + S_2'(\gamma_p,h,r_w) - S_2'(\gamma_p,0,r_w) \Bigg] \\[2mm]
& -\; \gamma_p^2\Bigg[S_2(\gamma_p,h,r_w) - S_2(\gamma_p,0,r_w) \Bigg] \Bigg\}^{-1}
\end{aligned}
\tag{3.51b}
$$

where

$$
S_1'(\gamma_p,x,y) \;=\; \int_0^\infty \frac{\lambda^2}{u_0^2}\phi_1(\gamma_p,x+h,\lambda)\cos(y\lambda)\mathrm{d}\lambda \tag{3.52a}
$$

$$
S_2'(\gamma_p,x,y) \;=\; \int_0^\infty \frac{\lambda^2}{u_0^2}\phi_{\tilde\epsilon}(\gamma_p,x+h,\lambda)\cos(y\lambda)\mathrm{d}\lambda \tag{3.52b}
$$

The kernel $\phi_\chi(x,\lambda)$ is defined as

$$
\phi_\chi(\gamma_p,x,\lambda) = \frac{\mathrm{e}^{-u_0 x}}{\chi u_0 + u_g} \tag{3.53}
$$

with

$$
u_0^2 \;=\; \lambda^2 - \gamma_p^2 + \gamma_0^2 \tag{3.54a}
$$

$$
u_g^2 \;=\; \lambda^2 - \gamma_p^2 + \tilde\epsilon\gamma_0^2 \tag{3.54b}
$$

As already mentioned, all the square roots are defined with a positive real part. The problem with equations (3.51) is the evaluation of the integrals $S_i(\gamma_p,x,y)$ and $S_i'(\gamma_p,x,y)$. In fact, this kind of integrals are known as Sommerfeld's integrals and no closed-form solution is available. These integrals, which arise in half-space scattering problems, are considered to present difficulties in their numerical evaluation. Actually, this is due to the oscillatory nature of the term $\cos(y\lambda)$; therefore the integration over an infinite support requires due care. Anyway, this approach would inevitably slow down the computation of the p.u.l. parameters. Furthermore, the propagation constant γ_p is needed. Actually, it should be computed by solving the modal equation (3.45) for the transmission-line mode.

This equation is hard to solve because of the presence of the unknown propagation constant γ_p into the integrals. Indeed, this is a non-linear integral equation. Usually, the integral dependence on γ_p is removed by assuming $\gamma_p \simeq \gamma_0$. This approximation, considered just for Sommerfeld's integrals, is the same used by Carson. By this means, the propagation constant can be computed as

$$
\gamma_p^2 = \gamma_0^2\frac{2\pi Z_{\mathrm{int}}/(\mathrm{j}\omega\mu_0) + \Lambda(0,h,r_w) + 2S_1(\gamma_0,h,r_w)r_w}{\Lambda(0,h,r_w) + 2S_2(\gamma_0,h,r_w)r_w} \tag{3.55}
$$

which coincides with the result recalled in [33] for a quasi-TEM approximation. In this case, the following small argument approximation should be used:

$$
\Lambda(\gamma_0,h,r_w) \simeq \ln\left(\frac{2h}{r_w}\right) \tag{3.56}
$$

45

due to numerical problems in the evaluation of Bessel's terms when $\Gamma_0 \simeq 0$. In [46] this approximation is expected to be a fair solution of the modal equation; anyway, no formal proof was given. A better estimation should be obtained by using this estimation of γ_p for the computation of Sommerfeld's integrals. Eventually, this idea leads to an iterative approach as

$$\gamma_{i+1}^2 = \gamma_0^2 \frac{2\pi Z_{\text{int}}/(j\omega\mu_0) + \Lambda(\gamma_i) + 2S_1(\gamma_i,h,r_w)r_w}{\Lambda(\gamma_i) + 2S_2(\gamma_i,h,r_w)r_w} \tag{3.57}$$

As previously recalled, a single-wire line supports two discrete modes (cf. Section 3.4). As shown in [33], the fast-wave and the transmission-line modes have propagation constants that can be quite similar at certain frequencies. Thus, equation (3.57) is affected by the same problems occurring in tracking dispersive eigenvalues in the frequency domain. Nevertheless, up to a few MHz, the two propagation constants are fairly distant [33], thus this approach is expected to work, sticking to the TLT mode.

An explanation to the validity of approximating γ_p in Sommerfeld's terms is their relative insensitivity with respect to it. This fact is shown in figures 3.10 and 3.11, where the modal equation is solved under three conditions: a) with $\gamma_p \simeq \gamma_0$, i.e. using equation (3.55), b) using four iterations of equation (3.57) and c) with the logarithmic approximation (3.65) presented in the next section. Solution (b) has been labelled "exact", since it converged to a stable result. Two line configurations are considered, with $h = 10$ m and $h = 10$ cm, with a wire radius $r_w = 1$ cm. The latter case is very important, since the rails are indeed very close to the soil. The soil is taken to be an average one (cf. Section 3.6), that is with $\sigma_g = 10$ mS/m and $\epsilon_g = 10$.

Four graphs are shown: the real and imaginary parts of the two Sommerfeld's integrals, the attenuation constant for the line and its effective dielectric constant ϵ_{ef}. The attenuation constant, i.e. the real part of γ_p, is here expressed in dB/m, whereas the effective dielectric constant is defined as:

$$\text{Im}\{\gamma_p\} = k_0\sqrt{\epsilon_{ef}} \tag{3.58}$$

that is as the dielectric permittivity required in a homogeneous medium to have the same phase velocity as in the half-space problem.

Indeed, the three solutions show a fairly good agreement. In particular, the logarithmic approximation provides a very good estimation of $S_1(\gamma_p,x,y)$, although $S_2(\gamma_p,x,y)$ is not as good. It also appears that the logarithmic solution is very close to the solution $\gamma_p \simeq \gamma_0$.

An interesting result is shown in Figure 3.11 for the 10 cm line. In this case, the effective dielectric constant is by far greater than unity. This means that the most part of the electromagnetic field is indeed in the soil. For the very same reason, the attenuation constant is far greater than for the 10 m case. On the other hand, a seemingly strange result is shown in Figure 3.10 for ϵ_{ef}: for $f > 2$ MHz, the phase velocity is greater than in free-space, being $\epsilon_{ef} < 1$. This result is confirmed in [33]. In the same way, the attenuation constant shows a maximum at the same frequency, decreasing for $f > 2$ Mhz. This behaviour can be explained as the result of two opposite trends: as the frequency grows higher, the soil gets more lossy, whereas the portion of field inside it gets smaller, thus less affected by its losses. Indeed, the skin-depth is just about 3 m at 2 MHz, whereas it is about 30 m at 20 kHz.
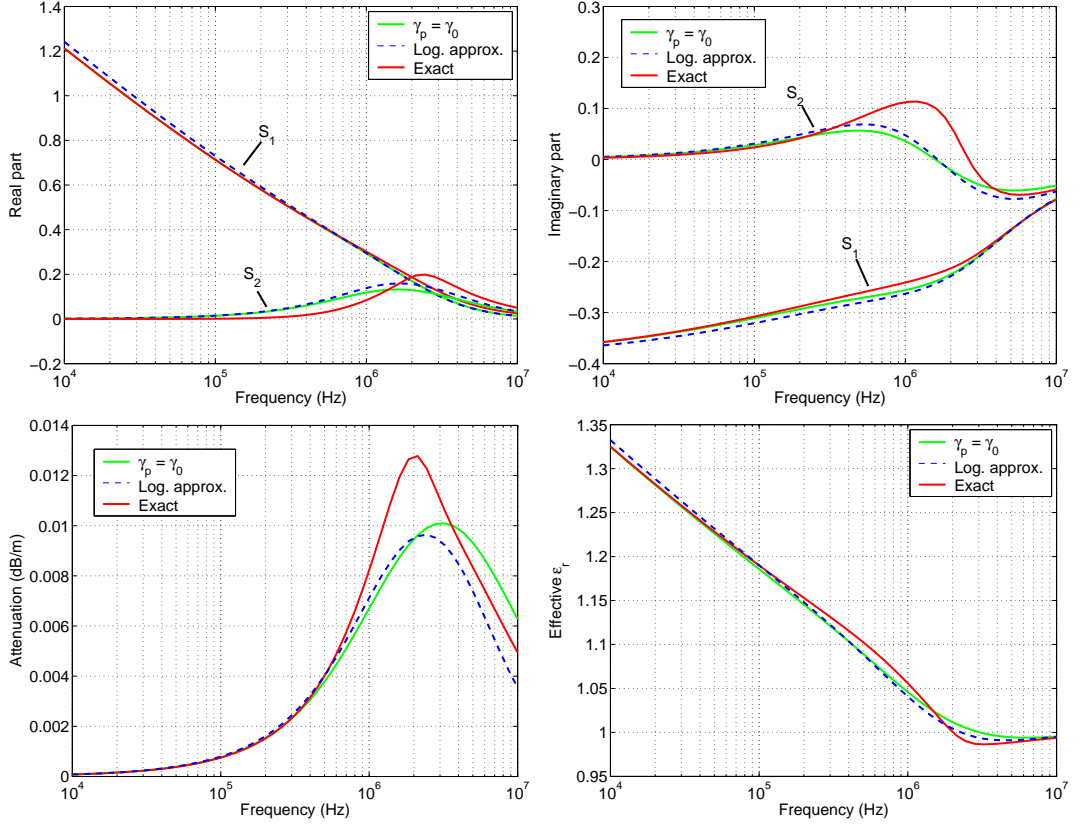
Figure 3.10.   Single-wire line (10 m high) over an average soil ($\sigma = 10$ mS/m, $\epsilon_g = 10$): Sommerfeld's integrals (a)-(b), line attenuation (c) and effective dielectric constant (d).

The results shown in figures 3.10-3.11 prove that Sommerfeld's integrals in (3.52) are indeed not very sensitive to the actual value of γ_p. As a matter of fact, for the case $h = 10$ cm the imaginary part of γ_p is about ten times γ_0; nevertheless, the results obtained with the approximation $\gamma_p \simeq \gamma_0$ are very close to the iterative solution. This proves that the integrals (3.52) can be effectively computed by means of this approximation.

Having solved the modal equation, the p.u.l. parameters expressed in equations (3.51) can be computed. The results obtained for the two previous examples, combined with the external parameters, are shown in Figure 3.12. As expected, the inductance is greater than for an ideal soil, due to the extra magnetic flux in the soil. Again, this is due to the penetration of the electromagnetic field into the soil, which also accounts for the extra resistance. Although the shunt conductance presents negative values, the passivity of the model solution is ensured by the fact that the attenuation constant is always positive.

One can also remark that the p.u.l. parameters are frequency-dependent. Although this is of little importance in a frequency domain approach, the time-domain solution of the TLT requires due attention. A general approach to the time-domain solution of transmission-lines with dispersive p.u.l. parameters is presented in [22], under the name of
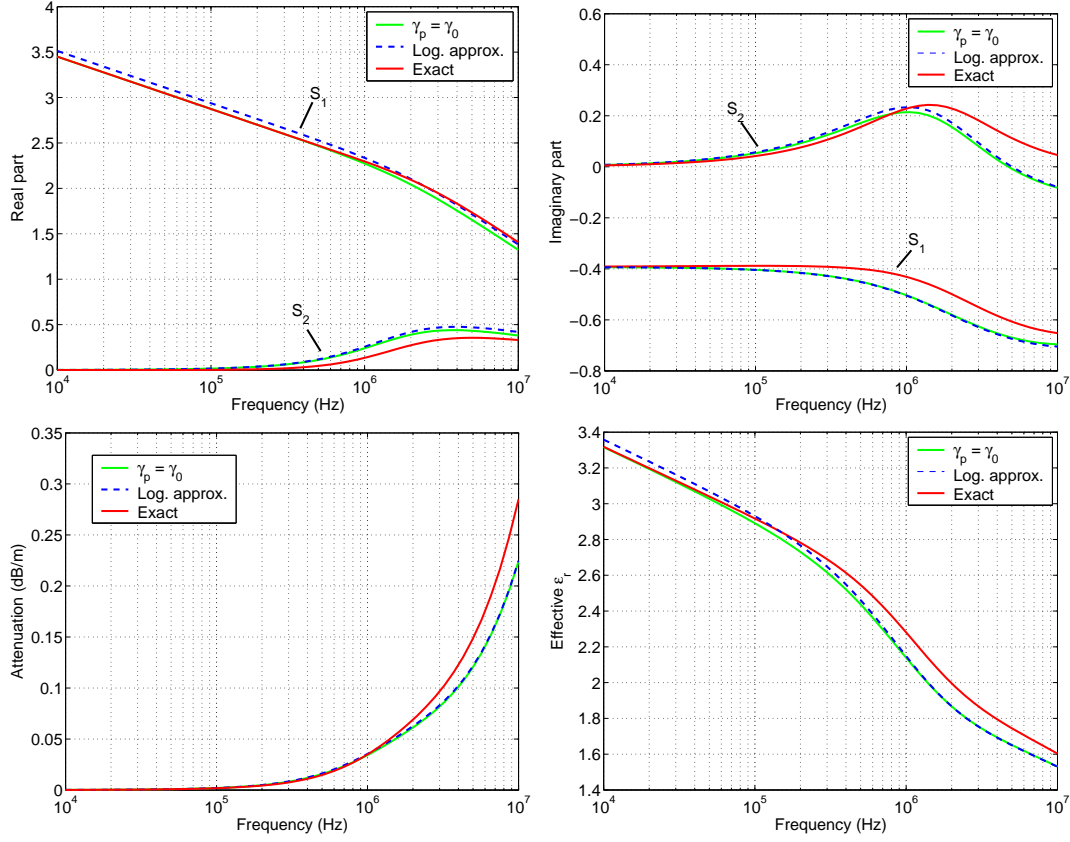
Figure 3.11. Single-wire line (10 cm high) over an average soil ($\sigma = 10$ mS/m, $\epsilon_g = 10$): Sommerfeld's integrals (a)-(b), line attenuation (c) and effective dielectric constant (d).

method of characteristics. Another possible solution is the discretization of equations (3.5), e.g. by means of an FDTD scheme. This approach has been pursued by van der Merwe in his Ph.D. thesis [51], obtaining a very good experimental validation of the results presented by D'Amore et al..

3.4.3   Logarithmic approximation of Sommerfeld's integrals

Although no closed-form solutions is known for the Sommerfeld's integrals (3.52), an approximated solution has been proposed by Pettersson in [52]. Here, he proposed the following approximation:

$$\frac{1}{\chi\lambda + \sqrt{\lambda^2 + \beta^2}} \simeq \frac{1}{\lambda(1 + \chi)} \left(1 - e^{-\lambda(1+\chi)/\beta}\right) \tag{3.59}$$

This approximation can effectively be used for simplifying the kernel (3.53). By assuming again $\gamma_p \simeq \gamma_0$, we obtain:
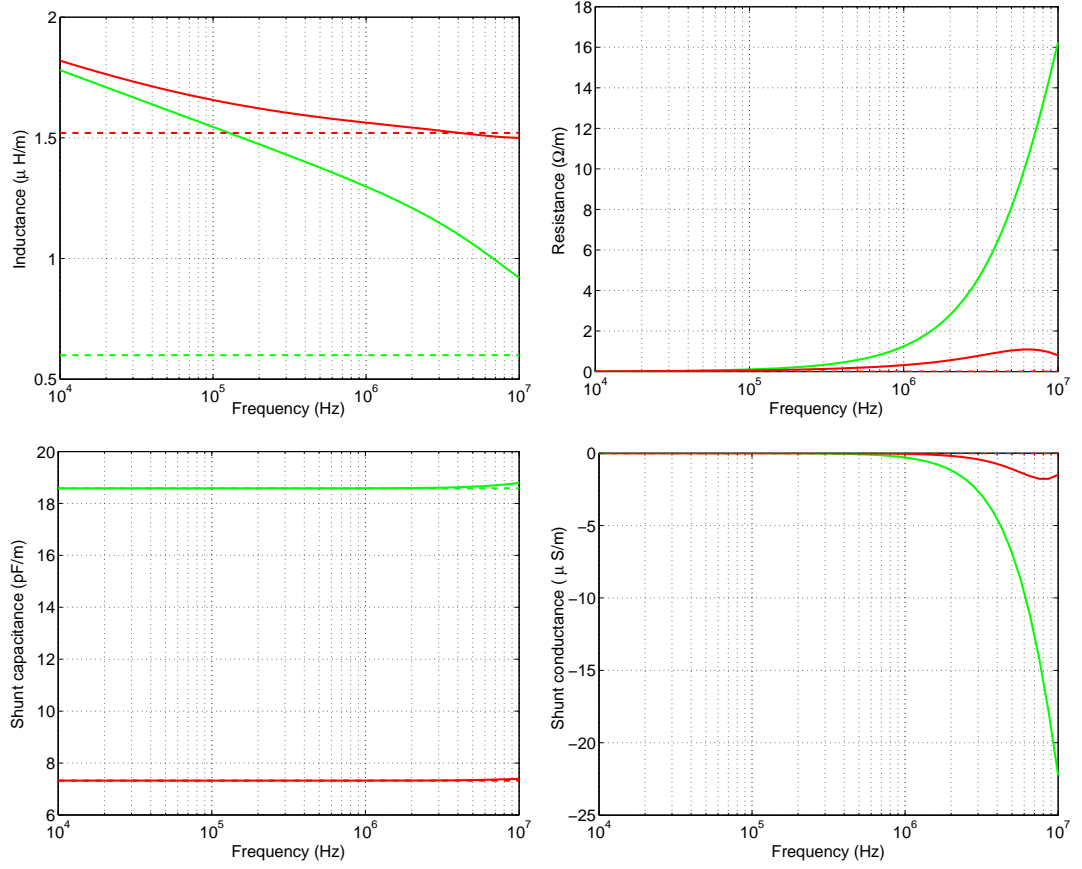
$$u_0 \quad \simeq \quad \lambda \tag{3.60a}$$

Figure 3.12. Per-unit-length parameters for a single wire line above a ground-plane, for $h = 10$ m (red line) and $h = 50$ cm (green line). Solid lines refer to an average soil ($\sigma_g = 10$ mS/m, $\epsilon_g = 10$), whereas dashed ones refer to a PEC soil.

$$u_g \quad \simeq \quad \sqrt{\lambda^2 + \gamma_0^2(\tilde{\epsilon} - 1)} \tag{3.60b}$$

which, substituted in equation (3.53) yields:

$$\phi_\chi(x,\lambda) \simeq \frac{\mathrm{e}^{-\lambda x}}{\chi\lambda + \sqrt{\lambda^2 + \beta^2}} \tag{3.61}$$

being

$$\beta = \gamma_0(\tilde{\epsilon} - 1) \tag{3.62}$$

Proceeding as in [52], one obtains:

$$\int_0^\infty \phi_\chi(x,\lambda)\mathrm{e}^{-\mathrm{j}\lambda y}\mathrm{d}\lambda \simeq \frac{1}{1 + \chi} \ln\left(\frac{x + \mathrm{j}y + c}{x + \mathrm{j}y}\right) \tag{3.63}$$

where

$$c = \frac{1 + \chi}{\beta} \tag{3.64}$$

49

Applying equation (3.63) to the definition of Sommerfeld's terms (3.52) yields:

$$S_1(\gamma_p,h,r_w) \quad \simeq \quad S_1'(\gamma_p,h,r_w) \simeq \frac{1}{4} \ln \left[\frac{(h+c_1)^2 + r_w^2}{h^2 + r_w^2} \right] \tag{3.65a}$$

$$S_2(\gamma_p,h,r_w) \quad \simeq \quad S_2'(\gamma_p,h,r_w) \simeq \frac{1}{2(1+\tilde{\epsilon})} \ln \left[\frac{(h+c_2)^2 + r_w^2}{h^2 + r_w^2} \right] \tag{3.65b}$$

with

$$c_1 \quad = \quad \frac{2}{\beta} \tag{3.66a}$$

$$c_2 \quad = \quad \frac{1+\tilde{\epsilon}}{\beta} \tag{3.66b}$$

3.4.4 Wide-frequency formulation of the p.u.l. parameters for an MTL

The results shown in the previous Section can be extended to a multiconductor configuration [47], thanks to the modal description presented in Section 3.3.2.

The configuration we are interested in is sketched in Figure 3.13. It consists of N metallic wires (i.e. with a circular cross-section) above a homogeneous soil. This line is supposed to be uniform, so that the cross-section is the same for any position z. As for
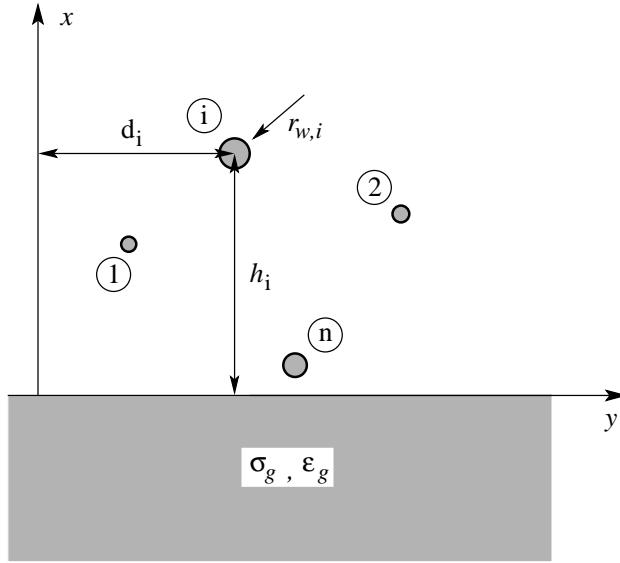

Figure 3.13. A multiconductor transmission-line above a homogeneous soil.

the single-wire configuration, a modal equation can be identified, this time in the form of a non-linear eigenvalue problem

$$\det \left[\gamma_k^2 \mathbf{1} - k_0^2 \mathbf{A}(\gamma_k) \right] = 0 \tag{3.67}$$

where $\mathbf{1}$ is the identity matrix and

$$\mathbf{A}(\gamma_k) = [\mathbf{\Lambda}(\gamma_k) + 2\mathbf{S}_2^h(\gamma_k)]^{-1} \left[\frac{2\pi}{\mathrm{j}\omega\mu_0} \mathbf{Z}_{\text{int}} + \mathbf{\Lambda}(\gamma_k) + 2\mathbf{S}_1^h(\gamma_k) \right] \tag{3.68}$$

The following expressions define the elements at the r-th row, i-th column for matrices $\mathbf{\Lambda}$ and $\mathbf{S}_{1,2}^h(\gamma_k)$

$$[\mathbf{\Lambda}(\gamma_k)]_{ri} = \mathrm{K}_0(\Gamma_k\rho_{t_1}) - \mathrm{K}_0(\Gamma_k\rho_{t_2}) \tag{3.69a}$$

$$\left[\mathbf{S}_1^h(\gamma_k)\right]_{ri} = \int_0^\infty \phi_1(\gamma_k, h_r + h_i, \lambda)\cos[(d_r + r_{w,r} - d_i)\lambda]\mathrm{d}\lambda \tag{3.69b}$$

$$\left[\mathbf{S}_2^h(\gamma_k)\right]_{ri} = \int_0^\infty \phi_{\tilde\epsilon}(\gamma_k, h_r + h_i, \lambda)\cos[(d_r + r_{w,r} - d_i)\lambda]\mathrm{d}\lambda \tag{3.69c}$$

$$\left[\mathbf{S}_1^0(\gamma_k)\right]_{ri} = \int_0^\infty \phi_1(\gamma_k, h_i, \lambda)\cos[(d_r + r_{w,r} - d_i)\lambda]\mathrm{d}\lambda \tag{3.69d}$$

$$\left[\mathbf{S}_2^0(\gamma_k)\right]_{ri} = \int_0^\infty \phi_{\tilde\epsilon}(\gamma_k, h_i, \lambda)\cos[(d_r + r_{w,r} - d_i)\lambda]\mathrm{d}\lambda \tag{3.69e}$$

where $\Gamma_k^2 = \gamma_0^2 - \gamma_k^2$, $\rho_{t_1} = \sqrt{(h_r - h_i)^2 + (d_r + r_{w,r} - d_i)^2}$ and $\rho_{t_2} = \sqrt{(h_r + h_i)^2 + (d_r + r_{w,r} - d_i)^2}$.

Solving equation (3.67) for all these parameters is equivalent to compute its eigenvalues. With this respect, the computation of the γ_k can be referred to as a non-linear integral eigenvalue problem. As for the single-wire configuration, the integral dependency on γ_k can be simplified by taking $\gamma_k = \gamma_0$ in the integral terms and in the matrix $\mathbf{\Lambda}$.

$$\left[\tilde{\mathbf{\Lambda}}\right]_{ri} = [\mathbf{\Lambda}(0)]_{ri} \simeq \frac{1}{2}\ln\left[\frac{(h_r + h_i)^2 + (d_r + r_{w,r} - d_i)^2}{(h_r - h_i)^2 + (d_r + r_{w,r} - d_i)^2}\right] \tag{3.70a}$$

$$\left[\tilde{\mathbf{S}}_1^h\right]_{ri} \simeq \frac{1}{4}\ln\left[\frac{(h_r + h_i + c_1)^2 + (d_r + r_{w,r} - d_i)^2}{(h_r + h_i)^2 + (d_r + r_{w,r} - d_i)^2}\right] \tag{3.70b}$$

$$\left[\tilde{\mathbf{S}}_2^h\right]_{ri} \simeq \frac{1}{2(1+\tilde\epsilon)}\ln\left[\frac{(h_r + h_i + c_2)^2 + (d_r + r_{w,r} - d_i)^2}{(h_r + h_i)^2 + (d_r + r_{w,r} - d_i)^2}\right] \tag{3.70c}$$

$$\left[\tilde{\mathbf{S}}_1^0\right]_{ri} \simeq \frac{1}{4}\ln\left[\frac{(h_i + c_1)^2 + (d_r + r_{w,r} - d_i)^2}{h_i^2 + (d_r + r_{w,r} - d_i)^2}\right] \tag{3.70d}$$

$$\left[\tilde{\mathbf{S}}_2^0\right]_{ri} \simeq \frac{1}{2(1+\tilde\epsilon)}\ln\left[\frac{(h_i + c_2)^2 + (d_r + r_{w,r} - d_i)^2}{h_i^2 + (d_r + r_{w,r} - d_i)^2}\right] \tag{3.70e}$$

Even though this solution to the matrix modal equation can be improved through the iterative approach previously discussed, in this case it is not as simple as for the single-wire line. In fact, the resulting propagation constants γ_k may be very similar (more on that later), so that the tracking of the eigenvalues and eigenvectors can be quite difficult, due to "crossings" in the approximated solutions. Furthermore, the analysis of the single-wire configuration has already proved that the approximation of the integral terms with $\gamma_p \simeq \gamma_0$ is acceptable.

For the multiconductor configuration, the utilization of the logarithmic approximation is even more important than for the single-wire case. In fact, in the latter case Sommerfeld terms could be easily (although slowly) integrated through numerical routines, thanks to the fact that the cosine argument depended on the wire radius. On the other hand, for an MTL, the cosine argument depends not just on the wire radius, but also on the distance between two wires. As the distance increases, the oscillations due to the cosine term can increase the complexity of the numerical integration. Happily, the logarithmic approximation does not depend on the cosine term, so that it is still valid, thus simplifying the task even more than for the single-wire configuration.

The exact expressions for the p.u.l. matrices are reported in [47]. Anyway, as showed in the previous Section, the logarithmic approximation provides fairly good results. For this reason, it is by far more practical to consider the p.u.l. matrices obtained under this approximation, marked as tilded quantities.

$$\tilde{\mathbf{A}} = (\tilde{\Lambda} + 2\tilde{\mathbf{S}}_2^h)^{-1}\left(\frac{2\pi}{j\omega\mu_0}\tilde{\mathbf{Z}}_{\text{int}} + \tilde{\Lambda} + 2\tilde{\mathbf{S}}_1^h\right) \tag{3.71a}$$

$$\tilde{\mathbf{Z}}_e = \frac{j\omega\mu_0}{2\pi}\tilde{\Lambda} \tag{3.71b}$$

$$\tilde{\mathbf{Y}}_e = j\omega\epsilon_0 2\pi\tilde{\Lambda}^{-1} \tag{3.71c}$$

$$\tilde{\mathbf{Z}}_g = \frac{j\omega\mu_0}{\pi}\left(\tilde{\mathbf{S}}_1^h - \tilde{\mathbf{S}}_2^0\tilde{\mathbf{A}}\right) \tag{3.71d}$$

$$\tilde{\mathbf{Y}}_g = j\omega\epsilon_0\pi\left(\tilde{\mathbf{S}}_2^h - \tilde{\mathbf{S}}_2^0\right)^{-1} \tag{3.71e}$$

As for the internal impedance matrix $\tilde{\mathbf{Z}}_{in}t$, it is defined as a diagonal matrix, where each element is represented by the internal impedance of each wire. Hereafter, we will always refer to these simplified expressions, though omitting the tildes for the sake of simplicity.

3.4.5 Approximation of rails as circular-section conductors

In order to apply the formulae so far introduced, the conductors are requires to have a circular section. Unfortunately the rails are far from fulfilling this assumption, their profile being quite irregular, and in particular presenting concavities. Under a thin-wire approximation it is usually assumed that as long as the conductor cross-section is electrically small and far from other conductors (with respect to its transversal dimensions), it can be regarded as dimensionless radiation-wise. But here we are interested in the per-unit-length parameters, which depend on the transversal dimensions of the conductor.

A common practice is to approximate the actual conductor with an equivalent one, by imposing the same area or the same perimeter, according to what principle the equivalent is based on [14]. For instance, same area equivalents ensure the same per-unit-length resistance, which is reasonable at low frequency where the current is uniformly distributed inside the conductor, whereas at higher frequencies the perimeter equivalent is better suited, since currents are mostly concentrated at the conductor surface. Anyway, the aim
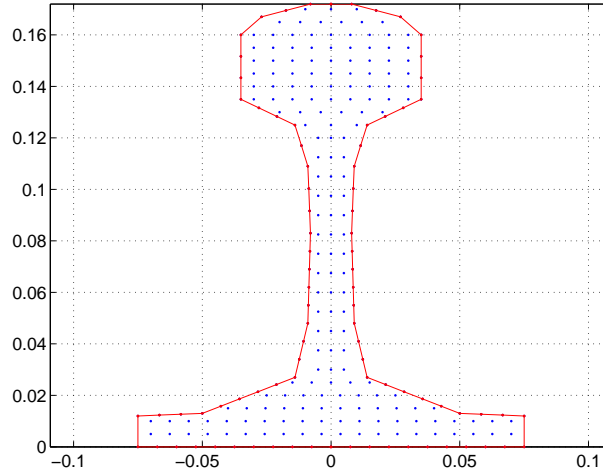
Figure 3.14.   The multi-wire approximation of a standard rail UIC60 employed for assessing the possibility to represent the rails as equivalent circular conductors. All the wires have a radius of 2 mm, with an average distance around 5 mm.

of these equivalent definitions is to ensure the same internal impedance, which is expected to be negligible over the frequency range here considered.

Rather than adopting one of these approximations, a different approach has been applied [22]. The actual rail (an UIC60) has been represented as a bundle of wires as in Figure 3.14, thus providing a rough discretization of the rail. These wires are regarded as connected one to each other by means of distributed short-circuits, so that they are kept at the same potential, thus simulating the equipotentiality of a single conductor. Considering wires far smaller than the skin-depth of the rail material, a uniform current distribution can be assumed flowing through each of them. Therefore the p.u.l. resistance of these wires is equal to their DC resistance. Due to the fact that the wires are very close one to each other, asymptotic formulae cannot be used for the computation of matrices **L** and **C**, requiring to take into account proximity effects. To this end, the numerical routine described in [23] has been employed, which was already available in our numerical libraries: nevertheless, proximity effects are negligible in practice. From this discretized description it is possible to derive an estimation of the overall per-unit-length parameters for the actual rail; to this end, the reduction technique described in Appendix C has been used. Subsequently, the equivalent radius required for obtaining the same results have been estimated by solving equations (3.71).

In order to check the accuracy of this equivalence, it has been applied to a simplified railway track, with two rails 1.435 mm apart, and an overhead wire with a 6 mm radius, 6 m high. The p.u.l. parameters have been computed for the rails at 10 cm and 50 cm above the soil interface, for two frequencies, 1 kHz and 2 MHz. The equivalent radius has been estimated as 76 mm maintaining the same barycentre than the actual rail. This result implies that the cross-surface of the equivalent conductor is 2.4 times greater than the actual rail, while the perimeter is 1.4 times smaller.

53

f	h (cm)	Z_{rr}	Z'_{rr}	$Z_{m,rr}$	$Z'_{m,rr}$
1 kHz	50	2.10e-3+j1.66e-2	1.98e-3+j1.67e-2	1.97e-3+j1.22e-2	1.96e-3+j1.22e-2
1 kHz	10	2.13e-3+j1.81e-2	1.99e-3+j1.81e-2	1.98e-3+j1.24e-2	1.98e-3+j1.24e-2
2 MHz	50	4.58+j13.4	4.59+j13.4	4.25+j4.65	4.26+j4.64
2 MHz	10	6.18+j13.7	6.21+j13.6	5.23+j2.59	5.24+j2.53
f	h (cm)	Z_{cc}	Z'_{cc}	$Z_{m,rc}$	$Z'_{m,rc}$
1 kHz	50	2.15e-3+j1.74e-2	2.15e-3+j1.74e-2	1.93e-3+j9.59e-3	1.93e-3+j9.59e-3
1 kHz	10	2.15e-3+j1.74e-2	2.15e-3+j1.74e-2	1.94e-003+j9.58e-3	1.94e-3+j9.57e-3
2 MHz	50	1.76+j19.5	1.76+j19.6	2.60+j2.22	2.61+j2.21
2 MHz	10	1.66+j19.2	1.65+j19.7	2.80+j0.990	2.79+j0.943

Table 3.1. Comparison of numerical results obtained for the per-unit-length matrix impedance with the multi-wire description of the rails and with the circular-section approximation (primed quantities), with radius 76 mm. Dimensions are in Ω/m.

f	h (cm)	Y_{rr}	Y'_{rr}	$Y_{m,rr}$	$Y'_{m,rr}$
1 kHz	50	+j4.18e-8	+j4.17e-8	-j3.22e-9	-j3.17e-9
1 kHz	10	+j7.95e-8	+j8.02e-8	-j9.87e-10	-j9.53e-10
2 MHz	50	+j8.35e-5	+j8.35e-5	-j6.44e-6	-j6.34e-6
2 MHz	10	+j1.59e-4	+j1.60e-4	-j1.97e-6	-j1.91e-6
f	h (cm)	Y_{cc}	Y'_{cc}	$Y_{m,rc}$	$Y'_{m,rc}$
1 kHz	50	+j1.51e-8	+j1.51e-8	-j1.14e-9	-j1.13e-9
1 kHz	10	+j1.50e-8	+j1.50e-8	-j6.06e-10	-j5.93e-10
2 MHz	50	+j3.01e-5	+j3.01e-5	-j2.29e-6	-j2.26e-6
2 MHz	10	+j3.00e-5	+j3.00e-5	-j1.21e-6	-j1.19e-6

Table 3.2. Comparison of numerical results obtained for the per-unit-length matrix admittance with the multi-wire description of the rails and with the circular-section approximation (primed quantities), with radius 76 mm. Dimensions are in S/m.

The results thus obtained are shown in Tables 3.1 and 3.2. The parameters shown are the self ones ({rr} for the rails, {cc} for the overhead wire) and the mutual ones ({m,rr} between the two rails and {m,rc} between a rail and the overhead wire). Indeed, the approximation is quite good, with a maximum error of about 3 % for the mutual admittance between the rails. One may wonder how it is possible that this equivalent conductor, far larger than the actual one, has the same internal impedance. In fact, the equivalent conductor only approximates the external parameters, whereas the internal ones are not correctly evaluated, although the order of magnitude is well identified. As a matter of fact, the internal impedance is negligible with respect to the additional series impedance of the ground. This result holds over the entire frequency-range here investigated, so that the rails can be effectively approximated by means of an equivalent circular conductor. The need for ensuring the same external parameters is particularly important for the capacitance, which is indeed dominated by the lower flat part of the rail, rather than the overall cross section.

Interesting results are also shown in Figure 3.15, where current density distributions
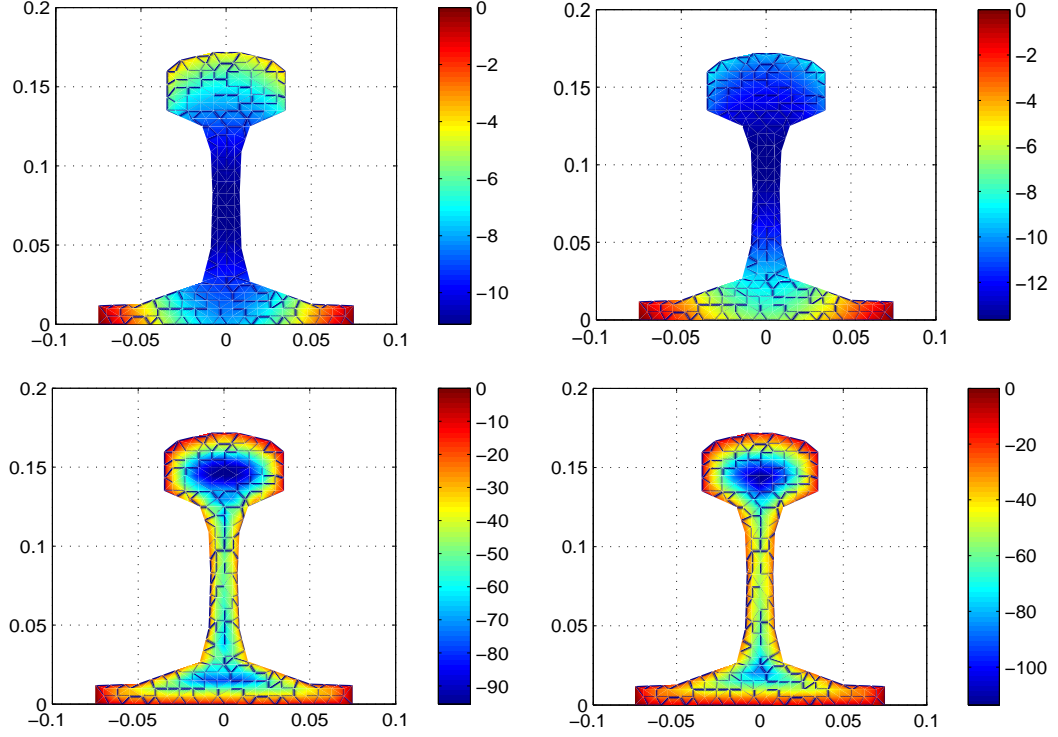
Figure 3.15.   The current density distribution inside a rail 10 cm above the soil interface, at 1 kHz (first row) and 2 MHz (second row), for an average soil (first column, $\sigma_g = 10$ mS/m, $\epsilon_g = 10$) and a perfectly conductive one (second column). The colors represent the normalized intensity of the current density, as expressed in dB.

are shown for a rail 10 cm above the soil, at 1 kHz and 2 MHz, for an average soil and a perfectly conductive one. As expected, for an average soil the proximity effects are less important than for the PEC case: this is due to the fact that for the perfectly conductive soil the current distribution across the soil is concentrated at its interface, whereas for the average soil the current is more deeply distributed into it, thus less affecting the one across the rail. This is particularly evident at 1 kHz, where the skin-depth is around 160 m, whereas at 2 MHz it reduces to just 3.6 m, so that the current distribution is quite similar to the PEC case.

These results have been obtained by assuming the rail conductivity equal to 5 MS/m [11] and a relative magnetic permeability $\mu_r = 1$. Actually, rails are made of ferromagnetic materials, with an average $\mu_r \simeq 60$ at very low frequencies (50-60 Hz), decreasing to one above a few kHz. Although ferromagnetic properties can be important for estimating the internal impedance, since they are limited in a very low frequency range, they have not been considered. Indeed, the lowest frequency considered in the standard EN 50121 is 10 kHz, where the rail internal impedance is already negligible with respect to the soil contribution.

55

3.5 The magnetic field generated by a uniform MTL

As stated in Section 1, this work deals with radiated emission tests. For this reason, the modelling of the electromagnetic field radiated by an MTL is a basic need. In particular, due to the requirements of the standard EN 50121 and to the frequency range here investigated (i.e. a few MHz), only the magnetic field will be considered. Its computation can be achieved through an antenna theory model, in order to relate the magnetic field to the current distribution computed by means of the TLT. Several solutions are available to this problem: only the most important for this work will be recalled in this section, as part of the model introduced in the next chapter.

3.5.1 Perfectly conductive soil

Before presenting the model for a lossy soil, the radiation from a current distribution above a PEC soil will be first considered. This will also allow a simpler introduction of some important results that will come in handy later on. Furthermore, for a zeroth order solution, these expressions can be useful. Although in this section the soil is regarded as

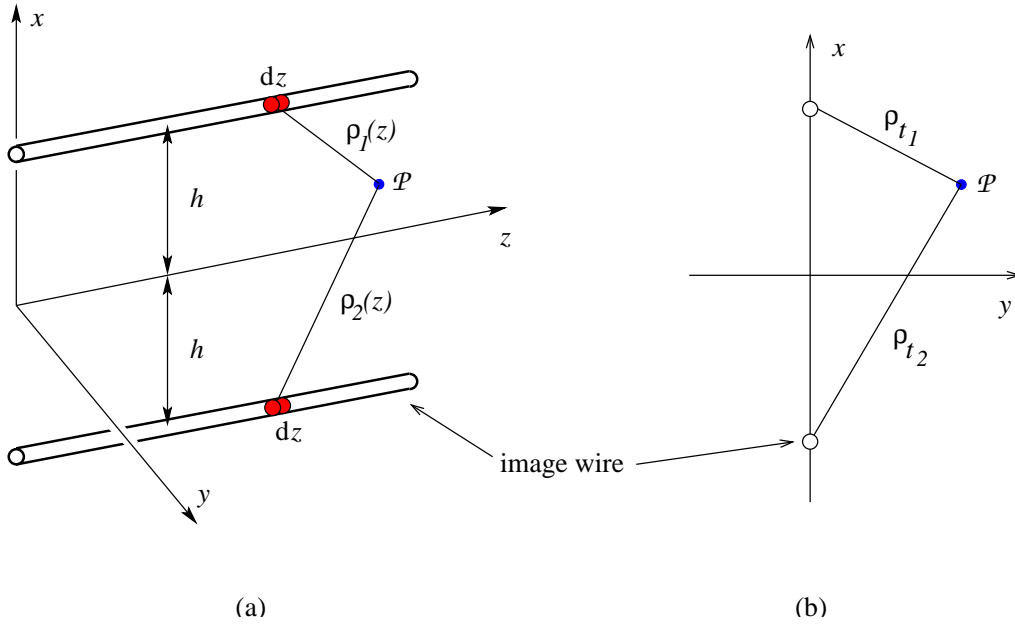(a)   (b)

Figure 3.16.   The definition of the quantities involved in the expressions for the magnetic field excited by a single-wire line.

a perfect conductor, the current distribution $I(z)$ is assumed to have been computed for a lossy soil. In other words, the propagation constants for the various modes will be, in general, different from γ_0. In fact, the soil is a perfect conductor only for the sake of the radiation computation.

Let us start with a single-wire line, as in Figure 3.16. Because of the ideality of the soil,

the image principle can be invoked. Thus, a single-wire line can be regarded as a two-wire line in free-space. The magnetic field as seen by an ideal observer in $\mathscr{P} = (x_0, y_0, z_0)$ is given by

$$
\begin{aligned}
H_x(\mathscr{P}) \;=\; & -\frac{y_0 - d}{\rho_{t_1}} \int_0^{\mathscr{L}} I(z)\rho_{t_1} \frac{1 + \gamma_0 \rho_1(z)}{\rho_1^2(z)} G(\rho_1(z))\mathrm{d}z \\
& + \frac{y_0 - d}{\rho_{t_2}} \int_0^{\mathscr{L}} I(z)\rho_{t_2} \frac{1 + \gamma_0 \rho_2(z)}{\rho_2^2(z)} G(\rho_2(z))\mathrm{d}z
\end{aligned}
\tag{3.72a}
$$

$$
\begin{aligned}
H_y(\mathscr{P}) \;=\; & \frac{x_0 - h}{\rho_{t_1}} \int_0^{\mathscr{L}} I(z)\rho_{t_1} \frac{1 + \gamma_0 \rho_1(z)}{\rho_1^2(z)} G(\rho_1(z))\mathrm{d}z \\
& - \frac{x_0 + h}{\rho_{t_2}} \int_0^{\mathscr{L}} I(z)\rho_{t_2} \frac{1 + \gamma_0 \rho_2(z)}{\rho_2^2(z)} G(\rho_2(z))\mathrm{d}z
\end{aligned}
\tag{3.72b}
$$

where ρ_{t_1} and ρ_{t_2} are the distances between the observer $\mathscr{P}$ and, respectively, the wire and its image

$$
\rho_{t_1} \;=\; \sqrt{(x_0 - h)^2 + y_0^2}
\tag{3.73a}
$$

$$
\rho_{t_2} \;=\; \sqrt{(x_0 + h)^2 + y_0^2}
\tag{3.73b}
$$

and $\rho_i(z)$ is the distance between $\mathscr{P}$ and the elementary current source $\mathrm{d}z$

$$
\rho_i(z) = \sqrt{\rho_{t_i}^2 + (z - z_0)^2}
\tag{3.74}
$$

and $G(\cdot)$ is the free-space Green's function

$$
G(\rho) = \frac{\mathrm{e}^{-\gamma_0 \rho}}{4\pi\rho}
\tag{3.75}
$$

accounting for the spherical propagation from a point-source.

Equations (3.72) represent the convolution of the electric current $I(z)$ with Green's function as the kernel. This solution holds as long as the current distribution can be represented as a line source. This means that its cross-section is regarded as equal to zero, with no lateral components; more generally it suffices that these two conditions are met:

- the wire radius $r_w \ll \lambda_0$, being λ_0 the free-space wavelength. This could be regarded as a looser version of the thin-wire approximation;

- the distance between the observer $\mathscr{P}$ and the current distribution is always greater than the wire radius. In other words, the cross-distribution is regarded as collapsed onto the wire axis.

The numerical solution of Equation (3.72) can lead to a significant computation-time, according to the actual geometry of the line. As remarked in equation (3.28), the current distribution along a transmission-line can be expressed as

$$
I(z) = I_0^+ \mathrm{e}^{-\gamma_p z} - I_0^- \mathrm{e}^{+\gamma_p z}
\tag{3.76}
$$

so that equations (3.72) can be rewritten as:

$$
\begin{aligned}
H_x(\mathscr{P}) \;=\; & -(y_0 - d)\left\{ I_0^+\left[\frac{\mathrm{F}(\mathscr{P},\gamma_p,h,0)}{\rho_{t_1}} - \frac{\mathrm{F}(\mathscr{P},\gamma_p,-h,0)}{\rho_{t_2}}\right] + \right. \\
& \left. -\; I_0^-\left[\frac{\mathrm{F}(\mathscr{P},-\gamma_p,h,0)}{\rho_{t_1}} - \frac{\mathrm{F}(\mathscr{P},-\gamma_p,-h,0)}{\rho_{t_2}}\right] + \right\}
\end{aligned}
\tag{3.77a}
$$

$$
\begin{aligned}
H_y(\mathscr{P}) \;=\; & I_0^+\left[\frac{x_0 - h}{\rho_{t_1}}\mathrm{F}(\mathscr{P},\gamma_p,h,0) - \frac{x_0 + h}{\rho_{t_2}}\mathrm{F}(\mathscr{P},\gamma_p,-h,0)\right] + \\
& -\; I_0^-\left[\frac{x_0 - h}{\rho_{t_1}}\mathrm{F}(\mathscr{P},-\gamma_p,h,0) - \frac{x_0 + h}{\rho_{t_2}}\mathrm{F}(\mathscr{P},-\gamma_p,-h,0)\right]
\end{aligned}
\tag{3.77b}
$$

having defined

$$
\mathrm{F}(\mathscr{P},\gamma,h',d') \;=\; \int_0^{\mathscr{L}} \mathrm{e}^{-\gamma z}\rho_t\frac{1 + \gamma_0\rho(z)}{\rho^2(z)}G(\rho(z))\mathrm{d}z
\tag{3.78a}
$$

$$
\rho_t \;=\; \sqrt{(x_0 - h')^2 + (y_0 - d')^2}
\tag{3.78b}
$$

$$
\rho(z) \;=\; \sqrt{\rho_t^2 + (z - z_0)^2}
\tag{3.78c}
$$

In the case of $\gamma_p = \gamma_0$, i.e. for a line in air, this expression could be effectively solved by means of McLaurin's series expansion, as proposed in [53]. Anyway, we are here interested in MTL with modal propagation constants $\gamma_k \neq \gamma_0$, so that this special case cannot be applied. For this reason, equation (3.77) has to be solved through numerical routines. Another interesting special case is the infinitely long line. In this case it can be shown that the magnetic field allows the following exact solution [53]

$$
H_x(\mathscr{P}) \;=\; \frac{I(z_0)}{\pi}\Lambda_x(\mathscr{P},\gamma_p,h,0)
\tag{3.79a}
$$

$$
H_y(\mathscr{P}) \;=\; -\frac{I(z_0)}{\pi}\Lambda_y(\mathscr{P},\gamma_p,h,0)
\tag{3.79b}
$$

assuming a current distribution $I(z)$ as in (3.76). The functions $\Lambda_{x,y}(\cdot)$ are defined as

$$
\Lambda_x(\mathscr{P},\gamma,h,d) \;=\; \frac{y_0 - d}{2}\Gamma_0\left[\frac{1}{\rho_{t_2}}\mathrm{K}_1(\Gamma_0\rho_{t_2}) - \frac{1}{\rho_{t_1}}\mathrm{K}_1(\Gamma_0\rho_{t_1})\right]
\tag{3.80a}
$$

$$
\Lambda_y(\mathscr{P},\gamma,h,d) \;=\; \frac{\Gamma_0}{2}\left[\frac{x_0 + h}{\rho_{t_2}}\mathrm{K}_1(\Gamma_0\rho_{t_2}) - \frac{x_0 - h}{\rho_{t_1}}\mathrm{K}_1(\Gamma_0\rho_{t_1})\right]
\tag{3.80b}
$$

Although it may look unlikely, this formulation can be effectively employed for practical configurations, as shown in the next section.

For the more general case of a multiconductor configuration as in Figure 3.17, the current distribution along each wire cannot be assumed anymore to be exponential. Nevertheless, the results for a single-wire line can be extended to an MTL by means of the modal theory presented in Section 3.3.2. In this respect, equations (3.77) can be extended
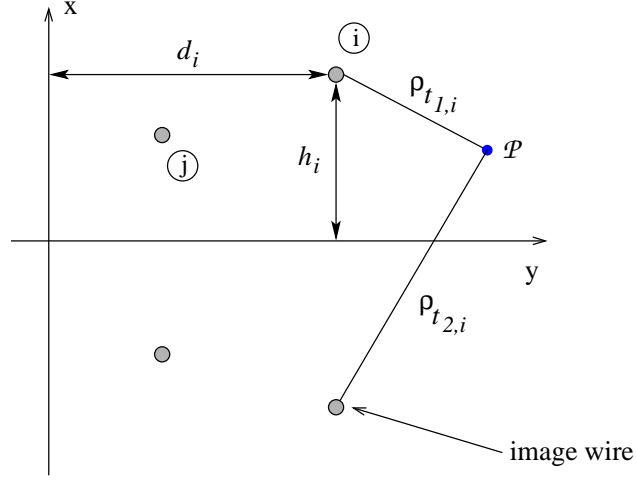
Figure 3.17.   The definition of the quantities involved in the expressions for the magnetic field excited by a multiconductor line.

to the MTL case by taking into account the contribution of each mode and each wire, obtaining

$$
\begin{aligned}
H_x(\mathscr{P}) \;=\; & -\sum_{i=1}^{N}\sum_{k=1}^{N}(y_0 - d_i)T_{ik}\left\{ I_{m0,k}^{+}\left[\frac{\mathrm{F}(\mathscr{P},\gamma_k,h_i,d_i)}{\rho_{t_1,i}} - \frac{\mathrm{F}(\mathscr{P},\gamma_k,-h_i,d_i)}{\rho_{t_2,i}}\right]\right. \\
& \left. - \; I_{m0,k}^{-}\left[\frac{\mathrm{F}(\mathscr{P},-\gamma_k,h_i,d_i)}{\rho_{t_1,i}} - \frac{\mathrm{F}(\mathscr{P},-\gamma_k,-h_i,d_i)}{\rho_{t_2,i}}\right]\right\}
\end{aligned}
$$
(3.81a)

$$
\begin{aligned}
H_y(\mathscr{P}) \;=\; & \sum_{i=1}^{N}\sum_{k=1}^{N}T_{ik}\left\{ I_{m0,k}^{+}\left[\frac{x_0 - h_i}{\rho_{t_1,i}}\mathrm{F}(\mathscr{P},\gamma_k,h_i,d_i) - \frac{x_0 + h_i}{\rho_{t_2,i}}\mathrm{F}(\mathscr{P},\gamma_k,-h_i,d_i)\right] + \right. \\
& \left. - \; I_{m0,k}^{-}\left[\frac{x_0 - h_i}{\rho_{t_1,i}}\mathrm{F}(\mathscr{P},-\gamma_k,h_i,d_i) - \frac{x_0 + h_i}{\rho_{t_2,i}}\mathrm{F}(\mathscr{P},-\gamma_k,-h_i,d_i)\right]\right\}
\end{aligned}
$$
(3.81b)

where $I_{m0,k}^{\pm}$ are the modal excitation terms introduced in equation (3.28) together with matrix $\mathbf{T}$. In the same way, the solution for the infinite line configuration, can be extended as

$$
H_x(\mathscr{P}) \;=\; \frac{1}{\pi}\sum_{i=1}^{N}\sum_{k=1}^{N}T_{ik}[\mathbf{\Lambda}_x]_{ik}I_{m,k}(z_0)
$$
(3.82a)

$$
H_y(\mathscr{P}) \;=\; -\frac{1}{\pi}\sum_{i=1}^{N}\sum_{k=1}^{N}T_{ik}[\mathbf{\Lambda}_y]_{ik}I_{m,k}(z_0)
$$
(3.82b)

where $I_{m,k}(z)$ stands for the current distribution along the k-th modal line

$$
I_{m,k}(z) = I_{m0,k}^{+}\mathrm{e}^{-\gamma_k z} - I_{m0,k}^{-}\mathrm{e}^{+\gamma_k z}
$$
(3.83)

59

The *ik*-th element of matrices $\mathbf{\Lambda}_x$ and $\mathbf{\Lambda}_y$ is defined as

$$[\mathbf{\Lambda}_x]_{ik} = \frac{y_0 - d_i}{2}\Gamma_k \left[\frac{1}{\rho_{t_{2,i}}}\mathrm{K}_1(\Gamma_k\rho_{t_{2,i}}) - \frac{1}{\rho_{t_{1,i}}}\mathrm{K}_1(\Gamma_k\rho_{t_{1,i}}) \right] \tag{3.84a}$$

$$[\mathbf{\Lambda}_y]_{ik} = \frac{\Gamma_k}{2} \left[\frac{x_0 + h_i}{\rho_{t_{2,i}}}\mathrm{K}_1(\Gamma_k\rho_{t_{2,i}}) - \frac{x_0 - h_i}{\rho_{t_{1,i}}}\mathrm{K}_1(\Gamma_k\rho_{t_{1,i}}) \right] \tag{3.84b}$$

3.5.2   Application of the infinite line solution to finite lines

As mentioned, the numerical computation of equations (3.81) can be time-consuming. Anyway, it need not be integrated all over the entire length $\mathscr{L}$: in fact, it is intuitive that the portion of line in proximity of the observer $\mathscr{P}$ gives the strongest contribution to the magnetic field. This intuition can be formally verified by studying the magnetic field near a line current distribution in free-space. This configuration can be effectively investigated as a 1-D problem, as in Figure 3.18.
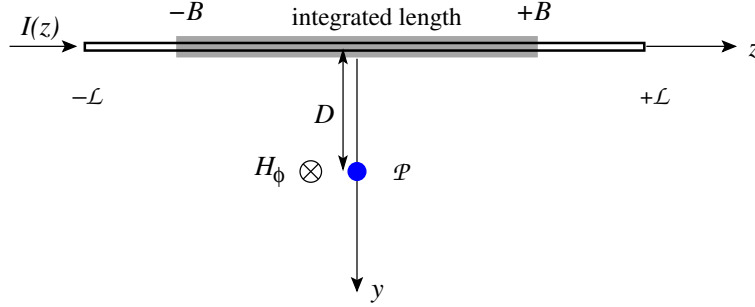

Figure 3.18.   The simplified configuration considered in order to check the accuracy of the magnetic field computed for reduced integration bounds.

Assuming a current distribution $I(z) = I_0\mathrm{e}^{-\gamma_0 z}$ along the length $[-\mathscr{L}, +\mathscr{L}]$, the magnetic field in $\mathscr{P}$ can be written as

$$H_\varphi = \lim_{B\to+\mathscr{L}} \frac{I_0}{4\pi} \int_{-B}^{+B} \mathrm{e}^{-\gamma_0(\rho+z)}\frac{D}{\rho^3}(1 + \gamma_0\rho)\mathrm{d}z \tag{3.85}$$

where $\rho = \sqrt{D^2 + z^2}$. In the same way, the magnetic field due to the current along the portion $[-B, +B]$ is defined as H_φ^B. The basic idea is to estimate for which value of B

$$|H_\varphi| \simeq |H_\varphi^B| \tag{3.86}$$

Whenever this condition is met, the contribution of the portions $[-\mathscr{L}, -B]$ and $[B,\mathscr{L}]$ is negligible. The same would hold for a longer wire, as long as the current distribution is the same. Hence, by extending this limit to infinite, it would be possible to apply the closed-form solution for an infinite line to a finite one, thus avoiding any numerical integration.

In order to estimate B, it is more convenient to have a look at the function being integrated. Its real and imaginary parts are shown in Figure 3.19, for $D = \{1,10,100\}$ m at 1 MHz. Here the longitudinal position z along the wire has been normalized to the observer's distance D and the values of the integrand have been normalized to the their maximum value, in order to compare all the results. In all the three cases the integrand contribution is more important in the region $z/D = [-5, +5]$, with very similar results for the distances 1 m and 10 m. Only for $D = 100$ m the integrand presents an oscillating behaviour; this is due to the term $\gamma_0\rho$, which does not affect the integrand shape unless the observer is electrically distant from the wire, as for $D = 100$ m. Therefore, in the present context, the integrand can be assumed to be proportional to a term $1/\rho^3$. Rather
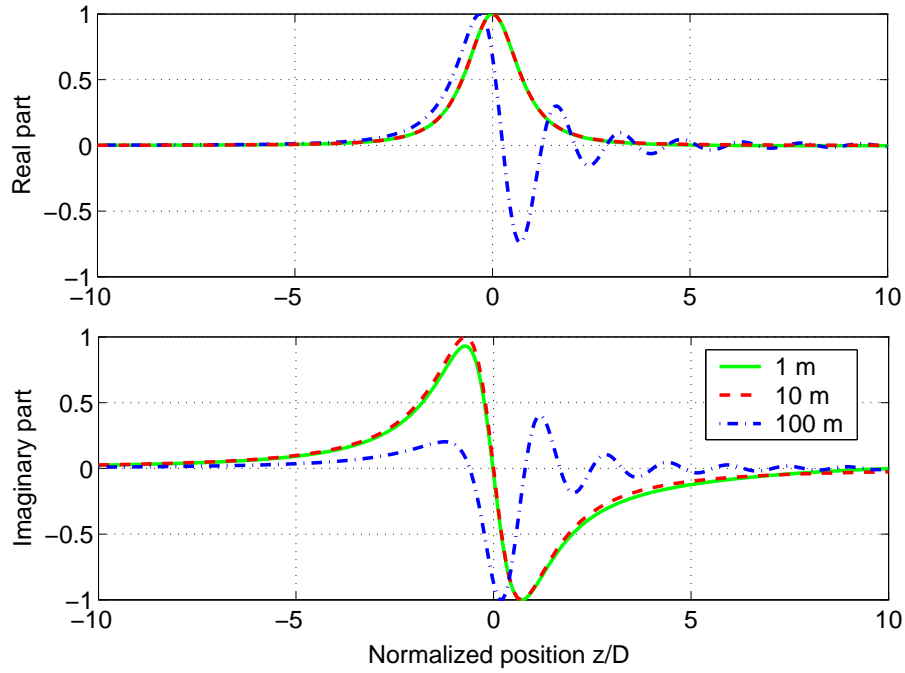

Figure 3.19. Normalized real and imaginary parts of the integrand in equation (3.85), for three observer's distances at 1 MHz.

than integrating the actual function, we can just consider its envelope, thus neglecting the exponential term, which actually acts as a phase term. The aim here is not to provide a quantitative solution to condition (3.86), but rather to have a thumb-rule.

Therefore we just consider the following function

$$\frac{D}{\rho^3}(1 + \gamma_0\rho) \tag{3.87}$$

61

defined by two terms proportional respectively to $1/\rho^2$ and $1/\rho^3$. By defining the integration accuracy η as

$$\eta\left[f(x)\right] = \frac{\displaystyle\int_{-B}^{+B} f(x)\mathrm{d}x}{\displaystyle\int_{-\infty}^{+\infty} f(x)\mathrm{d}x} \tag{3.88}$$

we obtain

$$\eta\left[\frac{1}{\rho^2}\right] = \frac{2}{\pi}\tan^{-1}\frac{B}{D} \tag{3.89a}$$

$$\eta\left[\frac{1}{\rho^3}\right] = \frac{B/D}{\sqrt{1+(B/D)^2}} \tag{3.89b}$$

These results, although derived under extremely simplified assumptions, provide an effective thumb-rule. By setting the required value for the accuracy η, an estimation of the bound B is readily available. In particular, it is interesting that the accuracy depends on the ratio B/D: thus, for a given accuracy level, this ratio is constant. Moreover, the second equation is the most important one, since the integrand in equations (3.85) is dominated by the term $1/\rho^3$. As an example, the practical case $\eta \geq 0.9$ (about 1 dB error) requires $B/D \geq 3$, which is compatible with the results in Figure 3.19. This is indeed a very important clue, since it means that whenever the line is uniform over a length $2B$, the infinite line solution can be employed, with no need to numerically evaluate the magnetic field. This thumb-rule has been checked in the next section by numerically evaluating the field contribution due to different portions of the current distribution for a more realistic configuration. Indeed, this rule appears to be valid.

3.5.3 Lossy soil

The problem of the magnetic field excited by an electric current above a lossy soil has already been introduced in Section 3.4, while dealing with propagation models. The simplest way for extending the results previously introduced for a PEC soil is the so-called complex image concept, already introduced in Section 3.4.1. This model holds only under the following assumptions [44, 54]

$$\rho_{t_2} \gtrsim 4\delta \tag{3.90a}$$

$$\omega \ll \omega_c \tag{3.90b}$$

Considering an average soil ($\sigma_g = 10$ mS/m, $\epsilon_g = 10$), an overhead wire 6 m above the soil, with the observer 10 m away from the line, 2 m high, the complex image model could be applied only over the frequency range $2 \div 4$ MHz.

These limitations can be overcome thanks to the model introduced by Wait [27]. He derived this model using a two-dimensional approach, so that his results can be applied only to infinitely long structures. Anyway, as shown in Section 3.5.2, under certain conditions the e.m. field near a line of finite length can be regarded as due to an infinitely

long one. Therefore, it suffices to extend Wait's model to a multiconductor configuration; once more, this can be achieved thanks to the modal approach introduced in Section 3.3.2, as proposed in [48]. For each cartesian component of the magnetic field, here generally indicated as H

$$H = \sum_{i=1}^{N} \sum_{j=1}^{N} \Theta_{ij} T_{ij} I_{m,j}(z) \tag{3.91}$$

where the modal current distribution $I_{m,j}(z)$ is defined as

$$I_{m,j}(z) = I_{m0,j}^{+} e^{-\gamma_j z} - I_{m0,j}^{-} e^{+\gamma_j z} \tag{3.92}$$

The radiation matrices $\mathbf{\Theta}_{x,y,z}$ are nothing but the same expressions defined in Wait's model, providing the magnetic field generated by an exponential current distribution. Their matrix form is here reported for the i-th row and j-th column element

$$\Theta_{x,ij} = \frac{1}{\pi}(\Lambda_{x,ij} - S_{4,ij}) \tag{3.93a}$$

$$\Theta_{y,ij} = \frac{1}{\pi}(-\Lambda_{y,ij} + k_0^2 S_{1,ij} + \gamma_j^2 S_{2,ij} + S_{3,ij}) \tag{3.93b}$$

$$\Theta_{z,ij} = \frac{\gamma_j}{\pi}(\Lambda_{5,ij} - S_{6,ij}) \tag{3.93c}$$

with

$$S_{1,ij} = \int_0^{\infty} \frac{1}{u_{0,j}} \phi_1(\gamma_j, x_0 + h_i, \lambda) \cos[\lambda(y_0 - d_i)] d\lambda \tag{3.94a}$$

$$S_{2,ij} = \int_0^{\infty} \frac{1}{u_{0,j}} \phi_{\bar{\epsilon}}(\gamma_j, x_0 + h_i, \lambda) \cos[\lambda(y_0 - d_i)] d\lambda \tag{3.94b}$$

$$S_{3,ij} = \int_0^{\infty} \frac{\lambda^2}{u_{0,j}} \phi_1(\gamma_j, x_0 + h_i, \lambda) \cos[\lambda(y_0 - d_i)] d\lambda \tag{3.94c}$$

$$S_{4,ij} = \int_0^{\infty} \lambda \phi_1(\gamma_j, x_0 + h_i, \lambda) \sin[\lambda(y_0 - d_i)] d\lambda \tag{3.94d}$$

$$S_{5,ij} = \int_0^{\infty} \frac{\lambda}{u_{0,j}} \phi_1(\gamma_j, x_0 + h_i, \lambda) \sin[\lambda(y_0 - d_i)] d\lambda \tag{3.94e}$$

$$S_{6,ij} = \int_0^{\infty} \frac{\lambda}{u_{0,j}} \phi_{\bar{\epsilon}}(\gamma_j, x_0 + h_i, \lambda) \sin[\lambda(y_0 - d_i)] d\lambda \tag{3.94f}$$

where the kernel $\phi_\chi(\cdot)$ had already been introduced in (3.53), functions $\Lambda_{x,y}$ in (3.84) and $u_{0,j}^2 = \lambda^2 - \gamma_j^2 + \gamma_0^2$. All of these integrals can be effectively evaluated by means of the logarithmic approximation (cf. Section 3.4.3), but for S_1 and S_2. In order to avoid numerical integrations, Prony's method has been employed [55]. This technique allows to approximate, through a non-linear fitting procedure, a complex-valued function $f(\lambda)$ as a finite sum of N complex exponential terms:

$$f(\lambda) \simeq \sum_{i=1}^{N} c_i e^{a_i \lambda} \tag{3.95}$$

By applying it to the kernel of Sommerfeld's integrals, an analytical solution is easily found

$$\int_0^\infty f(\lambda)\cos(\lambda y)\mathrm{d}\lambda \quad \simeq \quad -\sum_{i=1}^{N} \frac{a_i c_i}{a_i^2 + y^2} \tag{3.96a}$$

$$\int_0^\infty f(\lambda)\sin(\lambda y)\mathrm{d}\lambda \quad \simeq \quad \sum_{i=1}^{N} \frac{\mathrm{j}y c_i}{a_i^2 + y^2} \tag{3.96b}$$

Besides the simple solution, once the parameters a_i and c_i are known, Prony's method provides another important advantage: the oscillating term depending on the distance y is analytically integrated, so that even for great distances where the integrand function is highly oscillating, the computation time is the same. As a matter of fact, the kernel does not depend on the distance y, so that the parameters $\{a_i\}$ and $\{c_i\}$ can be evaluated just once. The accuracy of this approach is based on the correct evaluation of Prony's parameters; a heuristic approach has shown that setting $N = 5$ suffices for obtaining a very good approximation of the original data. Therefore, the fitting procedure is applied to a vector containing the actual value of the kernel to be approximated. Prony's method has already been shown to be very sensitive to noise in the data and to the data window. The first problem is avoided since the data are numerically generated from a mathematical function. On the other hand, attention should be paid at the definition of the data window. Since all the kernels have an exponential decay, the exponential tail has been discarded as it gets below 1 % of the kernel maximum absolute value. Numerical results are compared in Figure 3.20, for the Lobatto's quadrature employed by MatLab and Prony's method, as applied to a realistic configuration.

Considering numerical integration routines, a suitable quadrature method for unbounded regions is the Gauß-Laguerre algorithm [56]. It has been applied considering 50 and 100 nodes on each intervals in the quadrature routine. Usual typical values for this parameter are about 20 nodes. Results in Figure 3.20 show that in order to have accurate results both in the low and high frequency range, the number of nodes required is quite important.

Another advantage of Prony's method is that the numerical integration routines usually found in software tools like MatLab are not suitable for oscillating functions. In fact, very small tolerances need to be employed, thus leading to a very important computation time. Compromises inevitably incur in errors in the numerical integration. A comparison of the computation time for the integration methods so far described are shown in Figure 3.21. These results prove that Prony's method in this case provides the best compromise between good accuracy and low computation times. For instance, the Gauß-Laguerre method has a comparable computation-time with respect to Prony's, for 50 nodes per interval; but in this case, non negligible errors occur in the low-frequency range.

So far we have addressed the infinite line model; whenever it cannot be used, the magnetic field has to be computed by numerically integrating the current distribution as made up by a series of elementary horizontal electric dipoles above a lossy soil. This subject, extensively studied by Baños [57], has been firstly investigated by Sommerfeld [58]
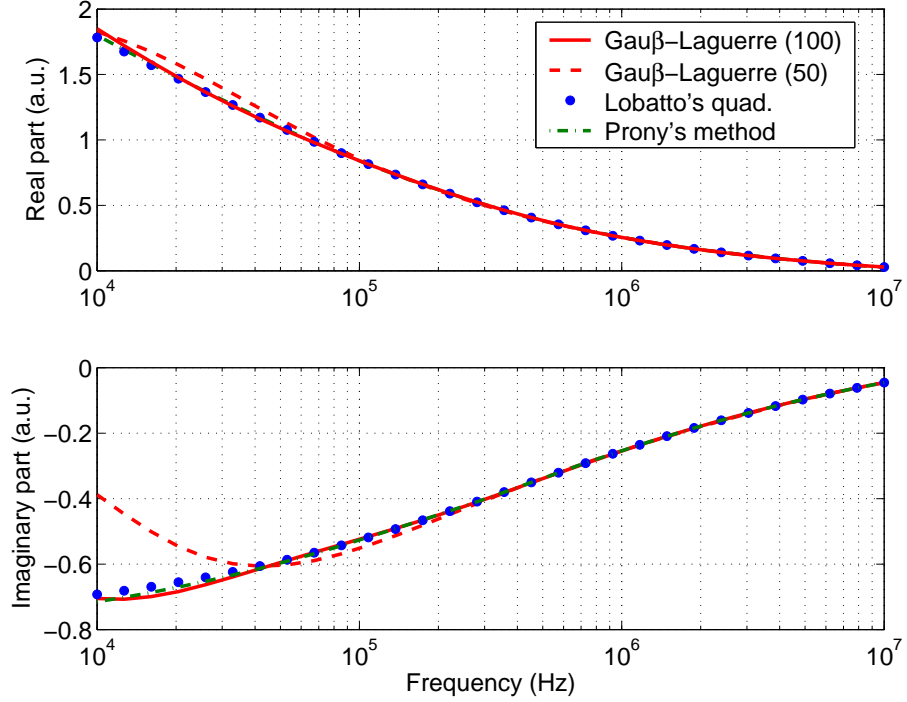
Figure 3.20.   A comparison between the results obtained with different numerical integration algorithms, as applied to $\mathscr{S}_3$, with $h = 5$ m, $x = 2$ m, $y = 10$ m, $\sigma_g = 10$ ms/m and $\epsilon_g = 10$.

for a vertical electric dipole. His results can be extended to horizontal electric dipoles, as performed in [59]: referring to Figure 3.22, Hertz's vector potentials are

$$\mathrm{d}\Pi_x \quad = \quad \frac{I\mathrm{d}z}{4\pi\mathrm{j}\omega\epsilon_0} \frac{\partial}{\partial z} \int_0^{+\infty} S(\lambda)\mathrm{e}^{-u_0(x+h)}\mathrm{J}_0(\lambda R)\mathrm{d}\lambda \tag{3.97a}$$

$$\mathrm{d}\Pi_z \quad = \quad \frac{I\mathrm{d}z}{4\pi\mathrm{j}\omega\epsilon_0} \int_0^{+\infty} \frac{\lambda}{u_0} \left[\mathrm{e}^{-u_0|x-h|} + R_m(\lambda)\mathrm{e}^{-u_0(x+h)} \right] \mathrm{J}_0(\lambda R)\mathrm{d}\lambda \tag{3.97b}$$

where $\mathrm{J}_0(\cdot)$ is Bessel's function of the first kind, zeroth order. Functions $S(\lambda)$ and $R_m(\lambda)$ accounting for the soil scattering are defined as

$$R_m(\lambda) \quad = \quad -1 + \frac{2u_0}{u_0 + u_g} \tag{3.98a}$$

$$S(\lambda) \quad = \quad \frac{2\lambda(u_g - u_0)}{\gamma_0^2(\tilde{\epsilon}u_0 + u_g)} \tag{3.98b}$$

Such a model can be used for assessing the thumb-rule previously derived for approximating a finite line above a PEC soil. To this end, a line 1 km long has been considered, for the typical configuration described in Appendix B, with the catenary reduced as described in Section 4.1.1. A 1 V excitation is applied at the line left end between the catenary and
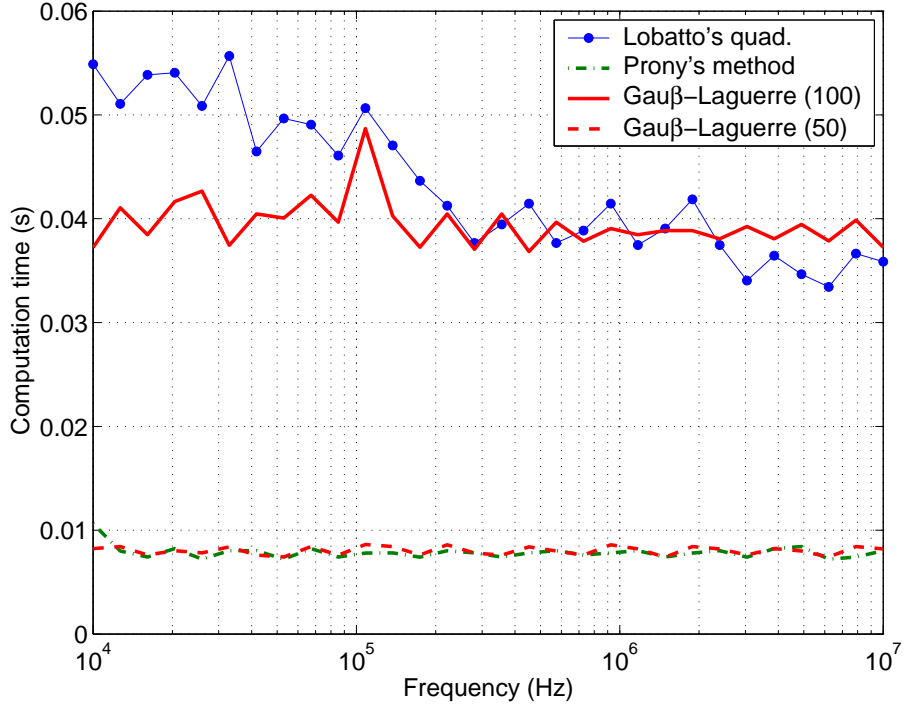
Figure 3.21. Computation-times required by the three numerical integration routines employed in Figure 3.20.

the two rails (short-circuited together), whereas the far end is open-circuited. The radiation model here employed regards the soil as lossy, so that these results can be realistically applied to actual lines. In Figure 3.23 the lateral magnetic field has been computed
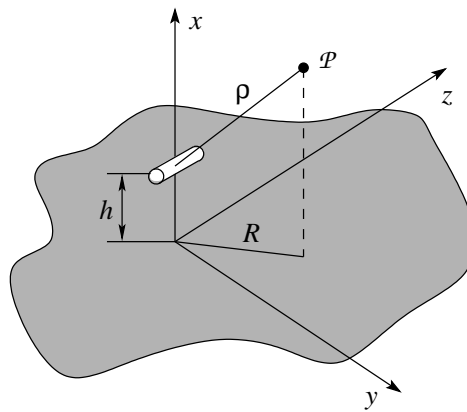

Figure 3.22. Definition of some geometrical quantities for expressions (3.97).

by means of Sommerfeld's model by integrating the current distribution on the region $[-B, +B]$ centered in $z_0 = 500$ m, for three values of B. This procedure has been carried out at two lateral positions y_0, namely 10 m away from the line axis and just under the overhead wire, in both cases at the height $x_0 = 2$. In particular for $y_0 = 10$ m the three lines refers to $B = \{10,20,100\}$ m whereas for $y_0 = 0$ m we chose $B = \{2,5,20\}$. These results show that the thumb-rule previously derived does hold also for this more complex configuration.

As a matter of fact, for $y = 10$ m, $B = 20$ m yields a spectrum almost indistinguishable from the case $B = 100$ m: the thumb-rule would have required $B \geq 30$ m. Similarly, for $y = 0$ m, the distance between the observer and the catenary (and also the rails) is about 2 m: the spectrum for $B = 5$ m and $B = 20$ m are indistinguishable, with the thumb-rule requiring $B \geq 6$ m.
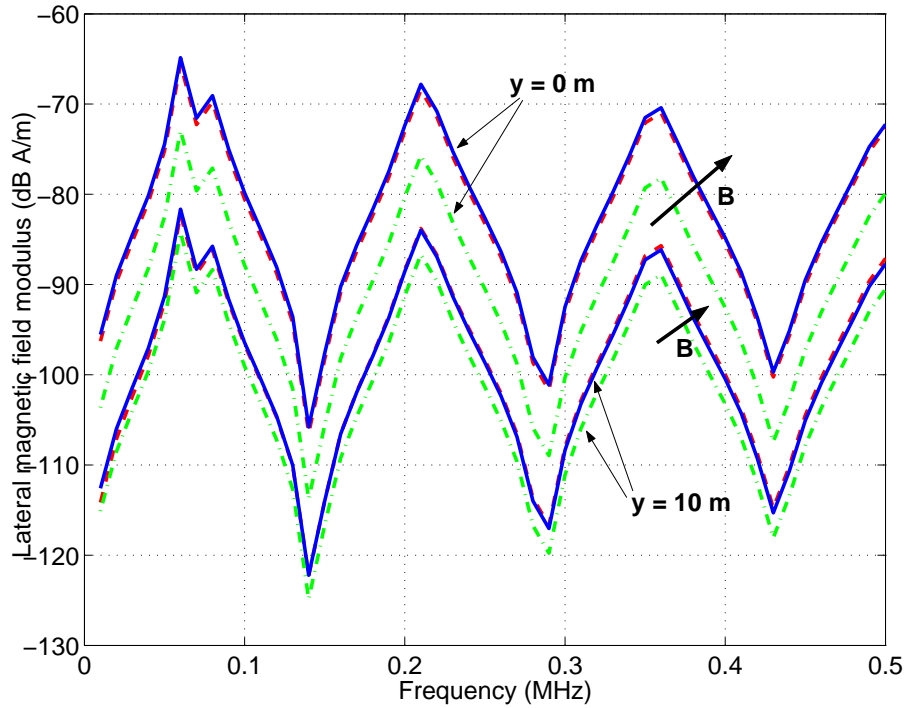

Figure 3.23.   The lateral component of the magnetic field as computed by Sommerfeld's model. The two groups of spectra refer respectively to $y = 10$ m and $y = 0$ m. In the first case three spectra have been computed for $B = \{10,20,100\}$ m and in the latter one for $B = \{2,5,20\}$ m. The arrows shows the evolution of the spectra as B gets bigger.

3.6   Electrical properties of actual soils

In order to model a lossy soil, its electrical properties need to be known. The two parameters needed are the soil conductivity σ_g and its dielectric constant ϵ_g. Having assumed the

soil as a homogeneous and isotropic medium, these quantities can be interpreted as equivalent values for a more complex configuration, e.g with stratifications of different media. Actually, even for a homogeneous medium, it would be necessary to know its magnetic permittivity μ_g too. Anyway, already during the model derivation in Section 3.4, this parameter has been assumed equal to one; this assumption is confirmed by Sunde in [60].

From a purely experimental point of view, the measuring of these two parameters has not yet led to a simple measurement setup. At low frequencies, the setup suggested by Sunde in [60] can be applied, based upon resistance measurements between two or four points. Since the frequency is very low, the soil basically behaves as a lossy conductor, so that only σ_g is estimated. The relationship between the resistance and σ_g is then based upon an integral model.

Soil conductivity (mS/m)	Occurrence	Typical soil
100	Unusually high	Clay
30	Very High	Chalk
10	High	Shale
3	Medium	Limestone
1	Low	Sandstone
0.3	Very Low	Slate, Sand, Gravel
0.1	Unusually Low	Granite, Quartz, Sand

Table 3.3. Frequency of occurrence for soil conductivity, as reported by Sunde in [60].

Another setup, usable over a wider frequency range, has been employed by Portela [61], using cylinder-shaped holders to get soil samples in a cylinder shape, while measuring the resistivity of the entire device. This method is ideally simpler and more accurate than Sunde's, but it needs special care in order to keep the soil samples in the same conditions as under the soil interface (humidity, pressure, etc.).

At radio frequencies, methods based on the analysis of reflection and transmission properties of the soil can be used, together with the modification in the input impedance of antennas electrically close to the soil. These are basically the same procedures used in soil prospection, using devices such as radars driving pulses into the soil.

The problem with all these methods is that the results obtained so far are not always comparable. One reason for this is that this kind of measurements are usually carried out by geophysicists, who are interested in the low frequency behaviour of the soil, mainly for deep layers prospections. On the other hand, electronic engineers are much more concerned with a higher frequency range, mainly for the analysis EMC topics, such as the effects of currents induced on overhead structures due to lightnings. Now, it is very common to find tables of values without any indication of the frequency at which they were measured, as pointed out in [62]. Moreover, these measurements are usually based on indirect techniques, which are more prone to systematic errors.

The results proposed by Sunde for the conductivity are listed in Table 3.3. They are interesting because he was more concerned in highlighting their frequency of occurrence,

rather than providing a list of values for very specific kind of materials. They refer to a DC excitation.

Further data, presented by Vance [41] for a broad classification of soils are shown in Table 3.4. These results are expected to be more representative to the present context, since Vance collected them for studying the effect of lightning pulses on overhead lines.
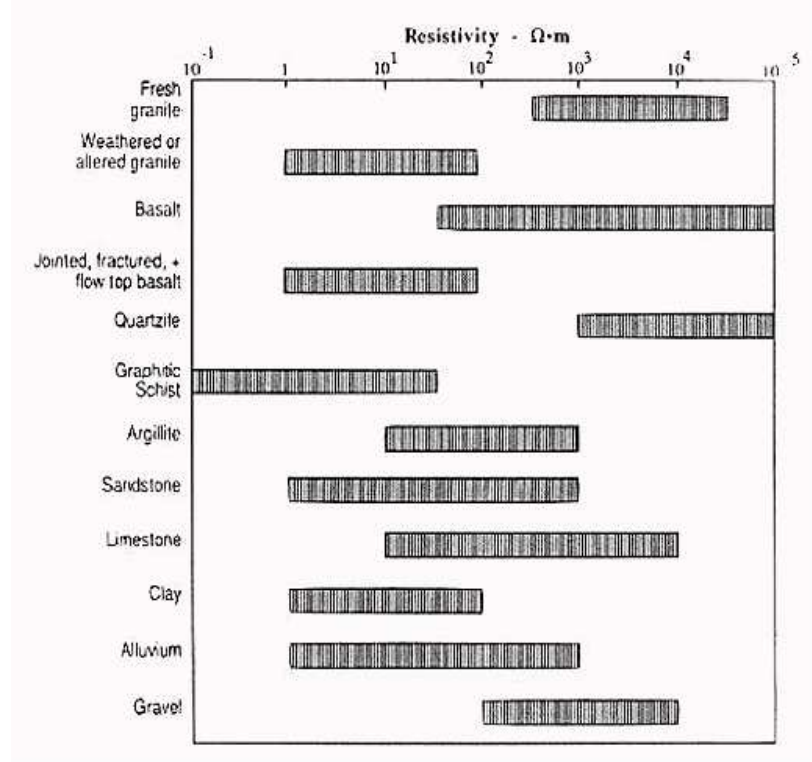

Figure 3.24. Resistivity values for various rocks and soils as reported by Maillol in [63].

The graph in Figure 3.24, after [63], shows the great variability of the conductivity for each family of materials. Maillol also pointed out the importance of water content for the permittivity value. The permittivity for pure, dry materials are bound to less then 10, whereas water has 80. Thus, due to the porosity of most rocks, water can indeed swing the permittivity value of more than one order of magnitude. The same effect is found in arid regions, due to hygroscopic salts dissolved into the soil.

The only recent study on the electrical engineering side was the one carried out by Portela. He showed that both σ_g and $\omega\epsilon_g$ have sub-linear trends, with $\sigma_g \in [1,25]$ mS/m over $0 \div 2$ MHz. The problem with these results is that ϵ_g reaches values up to 180, which is hard to explain on the basis of water content.

Obviously, the typical engineer have not a clue about the composition of the underneath soil, which is made worse by the fact that the soil morphology is very complex. For this

69

Soil	Relative dielectric constant ϵ_g	Conductivity (mS/m)
Dry, sandy coastal land	10	2
Marshy, forested flat land	12	8
Rich agricultural land	15	10
Pastoral land, medium hills	13	5
Rocky land, steep hills	10	2
Mountainous regions	5	1
Fresh water	80	5

Table 3.4. Average conductivity and relative permittivity for actual soils as reported by Vance in [41].

reason, rather than trying to give a precise description of the soil, average values would be by far more useful. Although these results are quite variable, the typical values for σ_g are in the range [1,100] mS/m, with $\sigma_g = 10$ mS/m for an average soil, and ϵ_g in [5,15], reaching up to 40 depending on the water content [41].

Since we are dealing with a model in the frequency domain, the frequency dependency of soil parameters can be readily taken into account. Anyway, that would require accurate information on the soil, which are not usually available. Furthermore, the results presented by Portela show a weak frequency dependency, so that soil parameters will be considered as constants. The need to simplify the soil description can easily lead to errors in the model results. The importance of these two parameters will be therefore checked by means of a sensitivity analysis in Section 4.5.

3.7 Effects due to the presence of an actual soil

In this section, a qualitative description of the main effects due to the presence of an actual soil will be given. To this end, the theoretical tools introduced in this chapter will be applied to actual line configurations. The following description is deliberately made in passing, since an accurate analysis of these phenomena is beyond the targets of this work. Anyway, they provide some insight into the physical phenomena underlying the propagation.

3.7.1 Effects on the current distribution

As early mentioned, the most evident effect due to the soil is an increased attenuation in the propagation along the line. That is straightforward for an infinitely long line; but for a finite line, a peculiar effect can be seen in the current distribution of MTL, such as the two-wire line in Figure 3.25, with its far-end closed on a 50 Ω resistance. The 3 km long line is excited by an ideal voltage generator and closed at its far-end on a 50 Ω load, simulating a power-draining load. For a perfectly conductive soil, the current distribution would be expected to be the same along the two conductors, but for a 180° phase-shift,

due to the ideal differential excitation. On the other hand, for a homogeneous soil with $\sigma_g = 10$ mS/m and $\epsilon_g = 10$ at 1 MHz, the current distribution is shown in Figure 3.26, as computed by using the p.u.l. expressions (3.71).
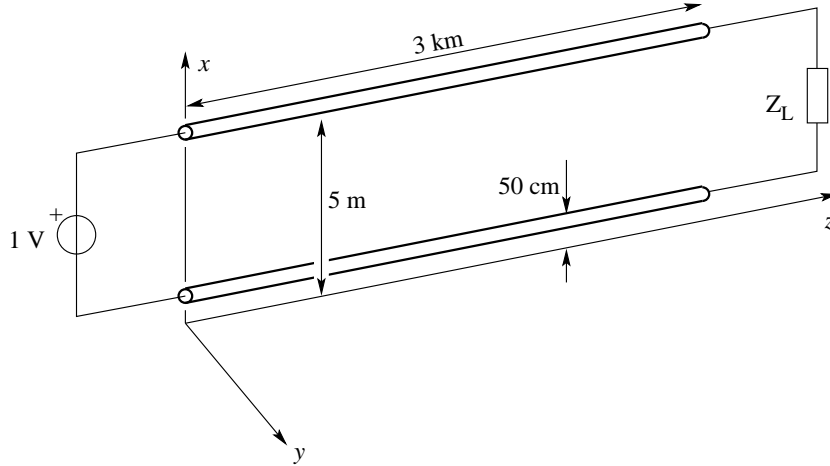

Figure 3.25.   The two-wire line used in the next examples.

Here it is shown that along the lower wire the current decreases for a certain length, than gets "steady" in its decay and finally increases, whereas along the upper conductor the current acts as subject to an exponential attenuation. The same phenomenon repeats at the other line end. This sort of spatial transient is due to the fact that near the line ends the current on the upper wire passes to the lower one, which is more strongly coupled to the soil. In particular, the current starts to pass more and more into the soil (far end), until it comes to an equilibrium between the two return-paths offered by the lower wire and the soil. On the other hand, the opposite phenomenon occurs at the near end, where the current has to go back to the lower wire, in order to fulfill Kirchoff's current law.

The existence of such space-transients in the current distribution is something that is not common in lines over a perfectly conductive soil. The same remarks can be drawn by looking at the current flowing through the soil. It has been computed as the missing term needed to satisfy Kirchoff's current law at a generic z position, by assuming negligible lateral currents. Again, this behaviour is far from straightforward: in fact, the soil presents a resistivity far greater than the wires one. The reason for an important portion of the current to return through the soil is its wide cross-section, which allows the soil to have an overall p.u.l. resistance comparable with the wires one.

This simple example can be useful in the analysis of discontinuities along a railway line. In fact, the electromagnetic field radiated by the line in the transient regions and in the steady-state one are expected to be different. This could lead to misunderstanding and misinterpretations in experimental results during test campaigns. This is the most likely reason why the standard EN 50121 requires the observer as far away as possible from substations and discontinuities, during the tests.
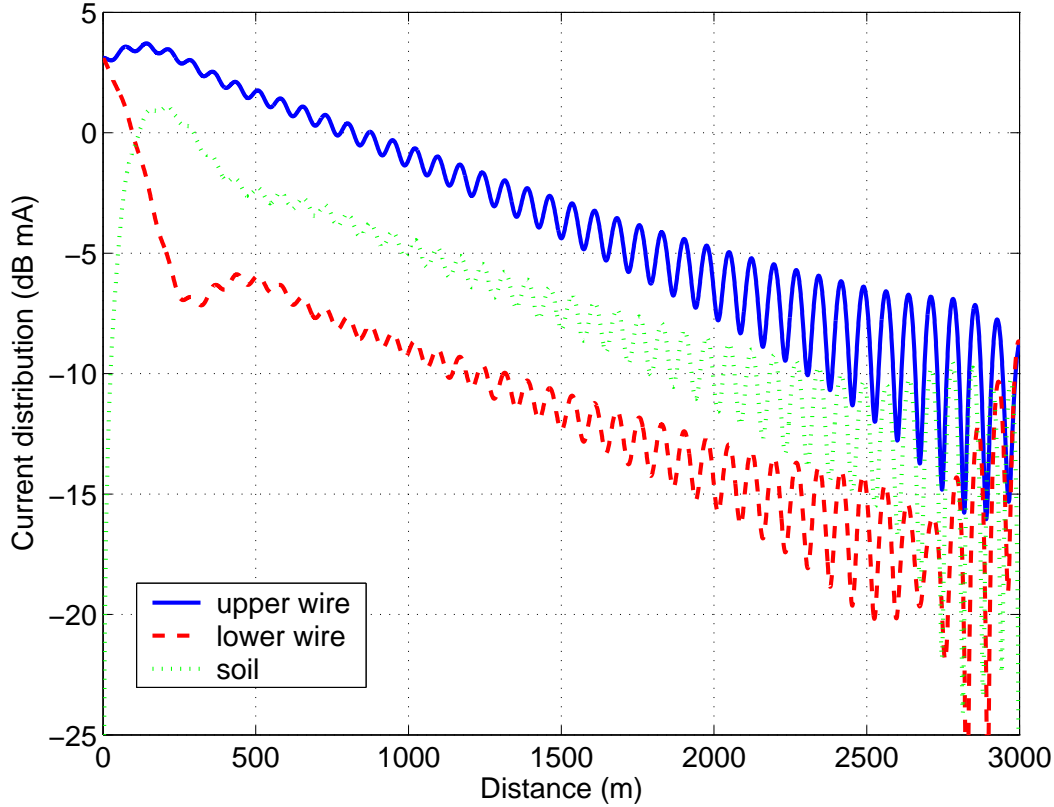
Figure 3.26.   The current distribution along the two conductors of the line in Figure 3.25, for a far-end load of 50 Ω, at 2 MHz.

Another interesting result from Figure 3.26 is that the propagation along the two conductors is different. Actually, this has already been shown in Section 3.4.4 with an example of computation of the propagation constants. Anyway, Figure 3.26 points out another problem: even with a purely differential excitation, the current distribution presents an important common-mode current.

As mentioned above, the soil as a current-return conductor cannot be treated as a wire, since the current is spread over a wide cross-section, depending on the frequency. This means that the coupling (or cross-talk) with nearby lines can be stronger, because of the current in the soil affecting the cross-section of these lines too. As a matter of fact, nearby lines share the soil as a reference conductor. The same conclusion holds for the coupling of a line with external incident electromagnetic waves, as shown in [42]. Here, Tesche et al. pointed out that considering a lossless line as the worst case, due to its lower attenuation, does not hold, due to the soil limited reflection, that leads to higher induced currents.

3.7.2 Effects on the field topography

The analysis of the effects of an actual soil on the e.m. field has been carried out on a line slightly more complex than the one shown in Figure 3.25. The catenary has been considered as made up by three wires plus a feeder, kept at the same potential by shunt connections. Finally, a ground-wire runs along the line at about 4 m above the soil interface; it is connected to the soil by means of short-circuits at the two ends of this 3 km line. The actual position of each wire is marked by black dots in figures 3.27 and 3.28.
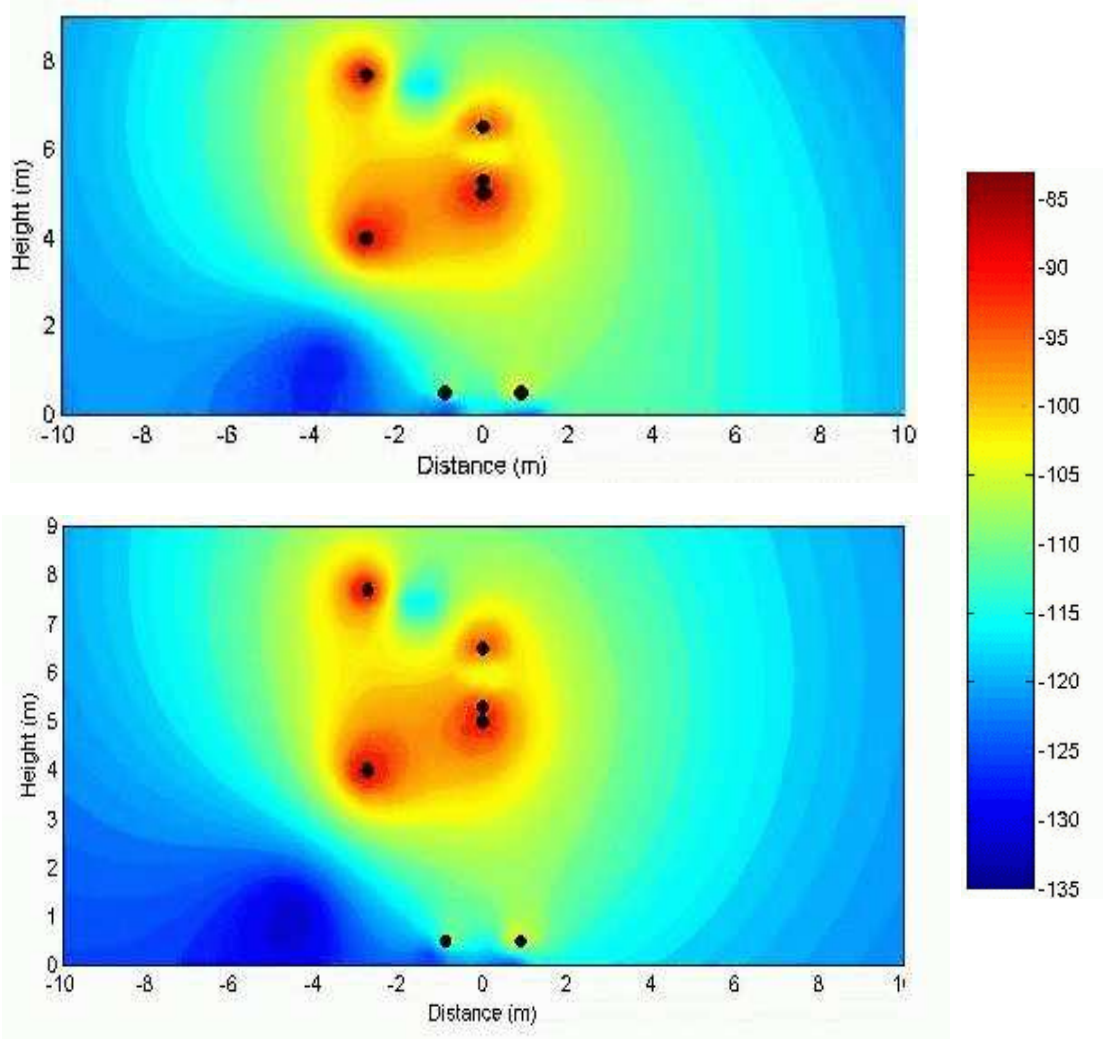

Figure 3.27. Transversal field topography at $z_0 = 1500$ m for 3 km long railway line: (a) PEC soil, (b) average soil ($\sigma_g = 10$ mS/m, $\epsilon_g = 10$). The frequency here investigated is 1 kHz, dimensions in dB A/m.

In order to highlight the differences due to the radiation model, the same current distribution has been considered, both for the PEC soil and for the lossy one. To this end,
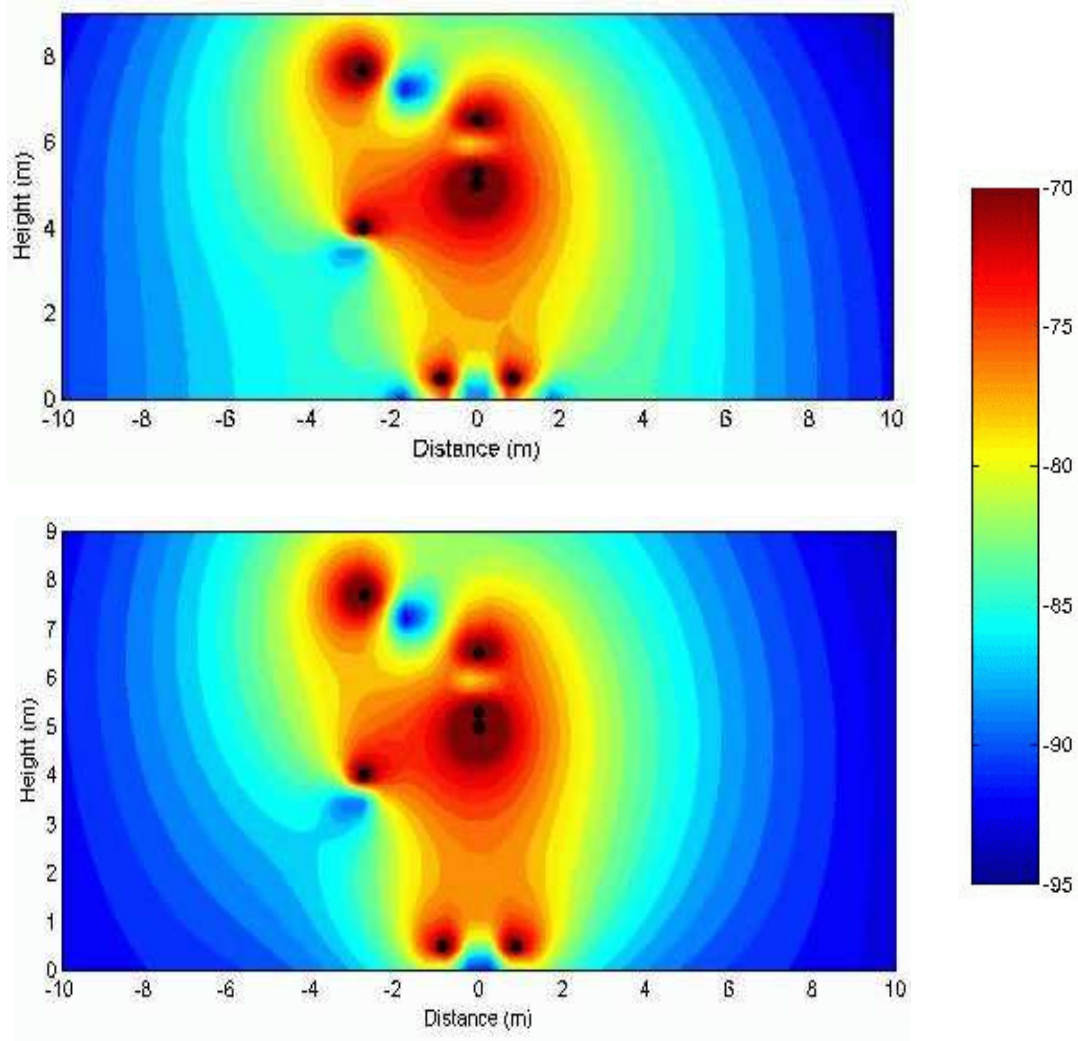
Figure 3.28.   Transversal field topography at $z_0 = 1500$ m for a 3 km long railway line: (a) PEC soil, (b) average soil ($\sigma_g = 10$ mS/m, $\epsilon_g = 10$). The frequency here investigated is 2 MHz, dimensions in dB A/m.

it has been computed for an actual soil, as in the previous example.

The magnetic field has been computed by means of the infinite line radiation model, applying equations (3.81) and (3.82), obtaining a transversal cut of the field topography. The results shown in figures 3.27 and 3.28 represent the intensity of the total transversal magnetic field at $z_0 = 1500$ m for two frequencies, respectively at 1 kHz and 2 MHz. Each Figure compares the results obtained with a PEC soil and with an average soil, in order to point out the most important differences.

Although the results are quite similar, there is an important difference: looking at the level lines, one can notice that they are almost perpendicular to the soil interface for the

PEC soil. This recalls the symmetry of a balanced line and it is due to the image of the actual line, thus implying that the lateral component of the magnetic is more strong near the interface, where the contributions of the line and its image have the same phase. On the other hand, for an actual soil, the field topography has no symmetry at all imposed by the soil, resembling the topography for a single-wire line. In other words, the line above a lossy soil acts as a more common-mode source rather than a differential one as for the PEC case. This is due to the weaker interaction between the line and the soil.

A straightforward effect of these differences is that the magnetic field near the soil interface is about 6 dB smaller with respect to a PEC soil. This is another way of stating the importance of applying a model that does take into account the soil non ideality.

Another result that is actually not related to the soil nature is the screening effect of the protection cable. As expected, it reduces the field intensity on the left side of the line by several decibels, though mainly in the low-frequency range. This is the reason why the standard EN 50121 requires to perform the radiated emission tests on the opposite side, since the cable presence would lead to underestimating the field intensity.

3.8 Conclusions

In this Chapter, the basic tools for the modelling of a uniform multiconductor line above a homogeneous half-space have been introduced. The methods here discussed are based upon transmission-line and antenna theories, seeking to provide closed-form solutions both for propagation and radiation phenomena.

For the sake of propagation, the p.u.l. parameters have been recalled to be the fundamental "blocks" for modelling a transmission-line, summarizing the most used formulations, together with a more recent one [46] not limited by the approximation of a metallic soil. On the other hand, the radiation from an MTL has been solved by means of numerical integrations for a finite line and analytical formulas for an infinitely long one. It has also been shown that the infinite line model can effectively be applied to finite lines under certain conditions.

The properties of actual soil materials have been summarized, highlighting the great variability and uncertainty in the choice of the values for the soil parameters. Finally, a qualitative description of the main effects of actual soils on propagation and radiation has been given, in order to have a more intuitive idea of the importance of not modelling the soil as a perfect conductor.

Chapter 4

Modelling of a railway system

In this chapter, actual railway systems will be considered. As mentioned in Chapter 2, such a system is here regarded as a collection of uniform multiconductor lines and lumped discontinuities. Hence, the tools introduced in the previous chapter will constitute the basic "blocks" for the modelling of actual systems. Due to industrial constraints, namely simplicity and effectiveness, some investigations are pursued in order to simplify this model without undermining its overall accuracy.

In particular, the most important non-idealities, with respect to a uniform line configuration, are investigated, together with the conditions under which the overall system description can be simplified. The basic tools for a sensitivity analysis are also introduced, in order to assess the impact of systematic errors in the system description. Finally, the validity of the model is verified by means of experimental investigations.

4.1   Non-idealities in a railway line

As already observed in Chapter 2, the discontinuities along a railway line will be regarded as lumped ones. This can be done thanks to their dimensions being far smaller than the minimum wavelength here considered, namely one hundred meters in free-space at 3 MHz. Among these discontinuities, introduced in Chapter 2, we can recall:

- Loads and sources, such as electric locomotives, power sub-stations, power transformers and all the sort of power devices connected along a railway line. These devices are indeed electrically small up to a few MHz, thus they can be effectively modelled by means of lumped equivalent circuits.

- Nearly-periodical short-circuits along the catenary. These short parallel stubs ensure the equipotentiality of the wires which make up the catenary, at least at the power-operating frequency.

- Masts. Again they behave as lumped discontinuities along the line; anyway, they deserve a special treatment thanks to their "periodicity" and their mainly capacitive behaviour (cf. Section 4.1.2).

A further aspect that should be considered is the ballast, which is dealt with in Section 4.1.3.

Throughout the entire chapter, and thus even in the overall model, the discontinuities will be assumed as non-radiating. In other words, only the railway track is regarded as able to radiate, considering the discontinuities as just acting on the current distribution. This simplification makes sense as long as the discontinuities are suitably far away from an observer measuring the magnetic field along the line. This assumption is also consistent with the requirements of the standard EN 50121, requiring the antenna to be placed as far away as possible from discontinuities. An important exception is provided by the train under test; this point is addressed in Chapter 5.

4.1.1 Catenary discontinuities and p.u.l. parameters reduction

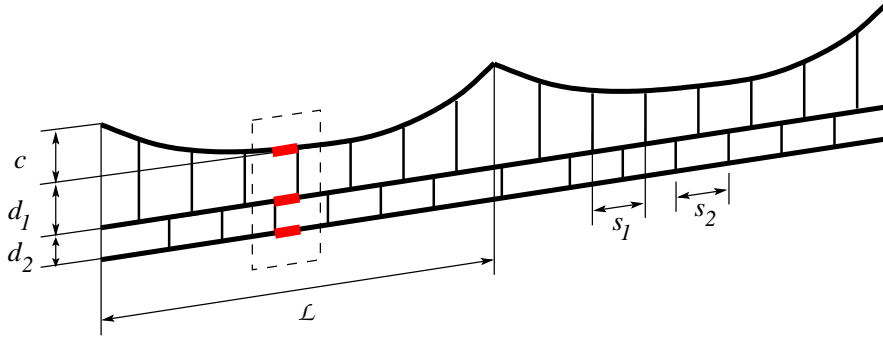The generic structure of a composite catenary is recalled in Figure 4.1, as introduced in Chapter 2.

Figure 4.1. The typical structure of a structured overhead catenary. The camber c is shown, together with the two series of droppers, with spacing s_1 and s_2.

The first impression of this line is of non-uniformity, depending on the importance of the camber c. Furthermore, even in the case of c equal to zero, the uniform line model could be applied only to tiny parts of the line, as highlighted in Figure 4.1. This approach would lead to catastrophic computation-times for the modelling of lines a few km long, requiring several thousands of such uniform portions. Furthermore, the infinitely long line model could not be used, thus requiring the numerical integration of the current distribution. In this section two approaches will be introduced in order to avoid these problems.

The first one is based on a reduction in the number of short-circuits. The basic idea is to show that the excitation of the catenary structure is such that the propagation along its conductors is nearly equipotential. In that regard, the short-circuits do not modify the propagation, because the current they carry is negligible with respect to the one in the horizontal wires.

Indeed, the catenary is always used in a common-mode configuration. In other words, it is always considered as a single-conductor structure, divided into several conductors just for the sake of mechanical properties. Moreover, all the connections to the catenary can

be regarded as the one in Figure 4.2a, where all the overhead wires are short-circuited together at the same longitudinal position. In fact, even for actual connections as in Figure 4.2b, the droppers ensure nearly the same behaviour as for Figure 4.2a. This is due to the fact that the spacing between the droppers is electrically small, so that propagation effects on the length Δs are negligible. Therefore, the droppers can be "virtually" moved as in Figure 4.2a.

Nevertheless, a pantograph is just connected to the lower conductor of a catenary, a configuration that would excite differential-modes in the catenary. Anyway, just a couple of series of droppers suffice for bringing the current distribution to a pure common-mode distribution. An example is shown in Figure 4.3. Hence, being the spacing about a few meters, the load can be regarded as in a common-mode configuration from a practical point of view.

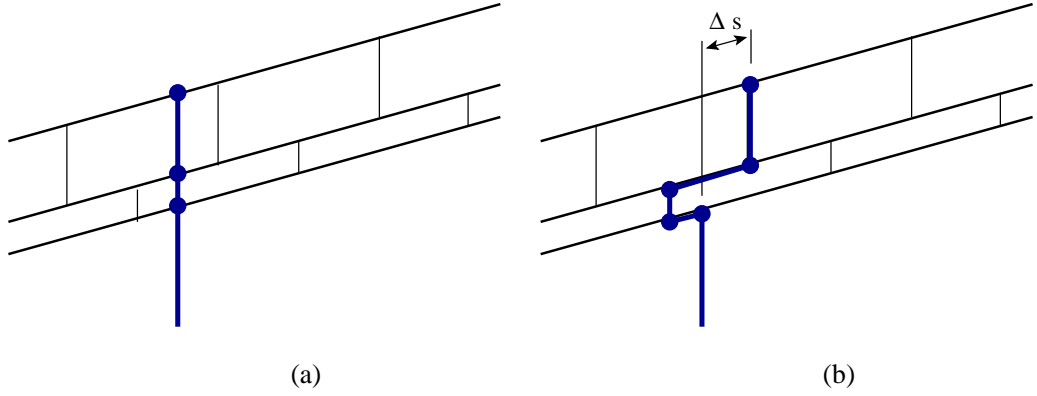(a)   (b)

Figure 4.2.   The ideal connection of a device to the catenary (a) and the actual one (b), with the device connected to the lower conductors. In this case the droppers ensure the equipotentiality of the catenary conductors.

Now, let us consider the propagation of electrical signals along a catenary without any dropper at all. Since the conductors are far away from the soil, signals propagate along them with nearly the same velocity and attenuation, as for an MTL in a homogeneous medium. In fact, the p.u.l. parameters related to the catenary wires are not very sensitive to their height above the soil. Thus, even though the catenary presents a camber, the p.u.l. matrices are nearly constant at each position z along the line. A reasonable remark can be that this observation holds only for the p.u.l. parameters relating the catenary wires to other conductors (e.g. the rails) and to the soil, whereas the p.u.l. parameters accounting for the coupling between catenary conductors are far from insensitive to the catenary camber. Indeed, this is true, but these values would affect only the propagation of differential-modes among the catenary conductors. Now, it has been shown that they are negligible, so that the simplification holds.

This means that having excited the catenary as a common-mode structure, it will behave as an equipotential structure at any position. Therefore, the short-circuits along the catenary will have nearly no impact on the propagation and on the radiation, since
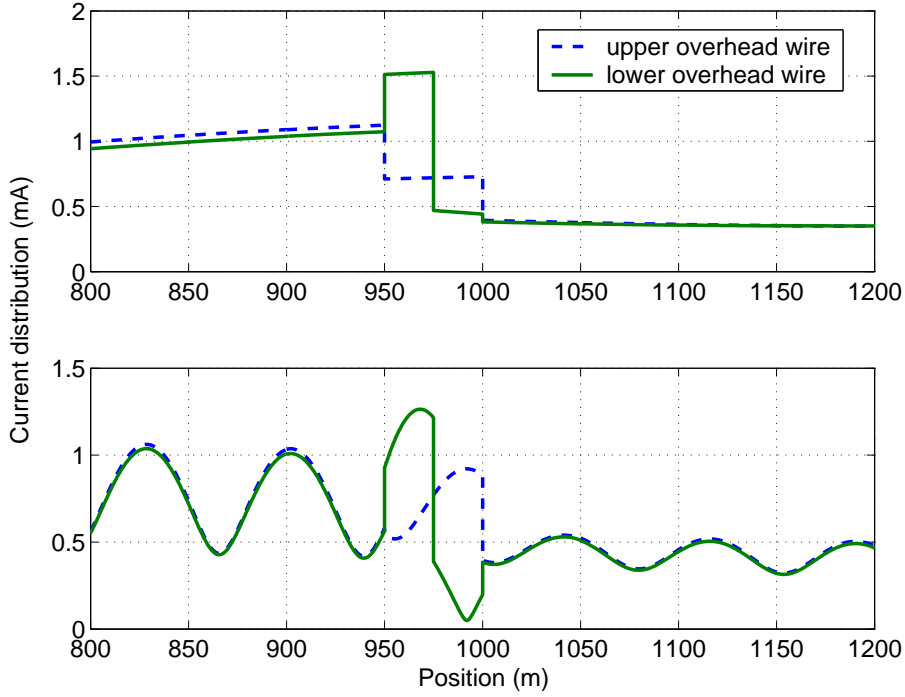
Figure 4.3. The current distribution along a two-wire catenary, 2 km long with droppers every 50 m, with a 200 Ω load at $z = 975$ m, connected as in Figure 4.2b. The two figures refer, respectively, to the current distribution at 100 kHz and 2 MHz. Although differential modes are excited in the proximity of the connection, a couple of droppers suffice for enforcing again a common-mode propagation.

they will carry negligible currents. Under these conditions, the catenary can be simplified by removing a large number of droppers.

This procedure is obviously an approximation: the propagation along the catenary wires is not exactly the same, since the surrounding medium is not homogeneous. These differences would be enhanced in long lines. Anyway, for line portions of suitable finite length this idea can be effectively applied. Furthermore, we are not interested in removing all the short-circuits, but rather in reducing the catenary complexity. Hence, it should be possible to consider a greater spacing in the model than in the actual line.

Numerical simulations of two configurations have been carried out, in order to ascertain the influence of several spacing between the catenary short-circuits. These results are shown in Figure 4.4, for the 2 km long three-wire line in the same Figure, considering a spacing of 20 m and 200 m between the droppers. Indeed, differences are very small (about 1 %) in the current distribution for the two configurations, as computed at 2 MHz, which can be regarded as a worst-case analysis, since at lower frequencies the droppers spacing is electrically shorter, thus less sensitive to the differences in the propagation along the two conductors.

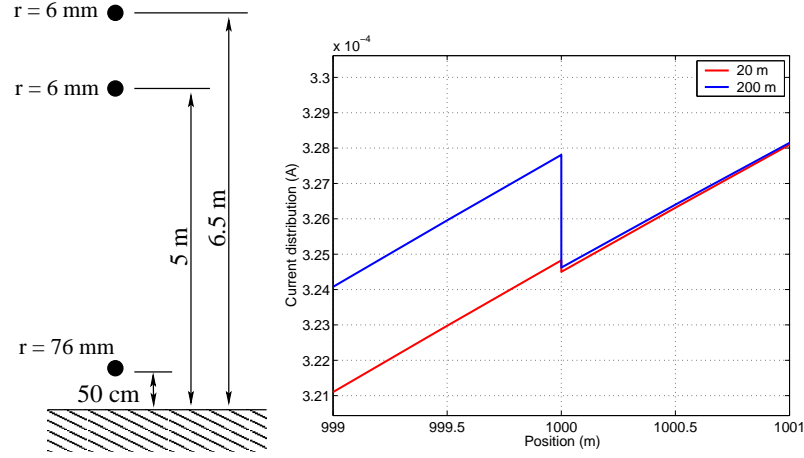Considering the magnetic field near the line, it is important to ensure a spacing that

Figure 4.4.   Reducing the number of droppers: (a) the configuration used in the numerical validation and (b) an excerpt of the current distribution at 2 MHz, with droppers spacing of 20 m and 200 m. The position 1000 m coincides with a dropper.

allows the use of the infinite line model. Since the results on the current distribution have shown that a spacing of 200 m suffices, this approximation can be applied. Since these results have been obtained at 2 MHz, the simplification of the catenary complexity is even more consistent at lower frequencies, were the short-circuits are electrically closer.

The second method here proposed is more powerful, allowing the substitution of the entire catenary with an equivalent single-wire line. Let us consider the configuration in Figure 4.5. Here, an infinitesimal portion (of length $\mathrm{d}z$) of an MTL, is described through its p.u.l. parameters. The upper conductors are continuously short-circuited at the ends

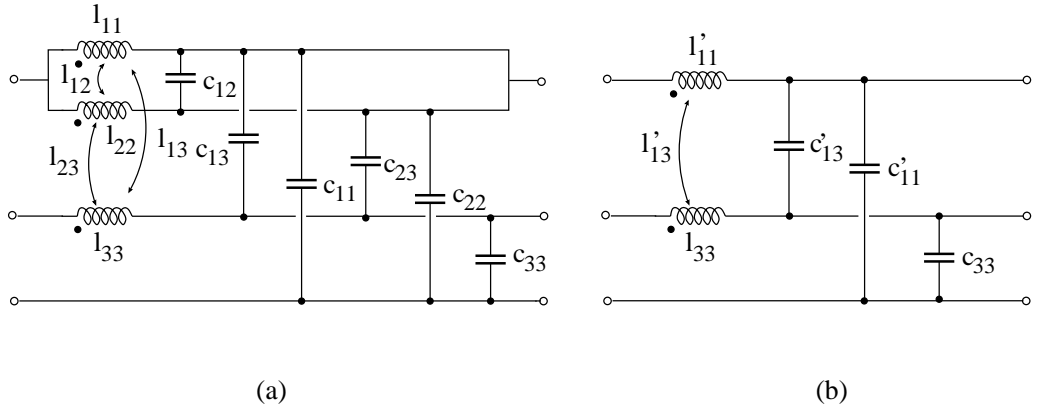(a)   (b)

Figure 4.5.   An example of reduction for an MTL with two conductors short-circuited together along their entire length. The new reduced line has just one conductor replacing the original two.

81

of the length dz. In other words, the short-circuits on the upper conductors (representing the overhead wires) are distributed all over the entire length of the line. Under these conditions, equivalent p.u.l. parameters can be defined, without loss of information, as shown in Appendix C. Such a procedure applied to a multi-wire catenary would reduce the number of conductors, and subsequently the computational complexity of the MTL. As a matter of fact, the computational cost of the analysis of an MTL through the TLT is at least proportional to N^2 (depending on how it is solved), being N the number of conductors in the line.
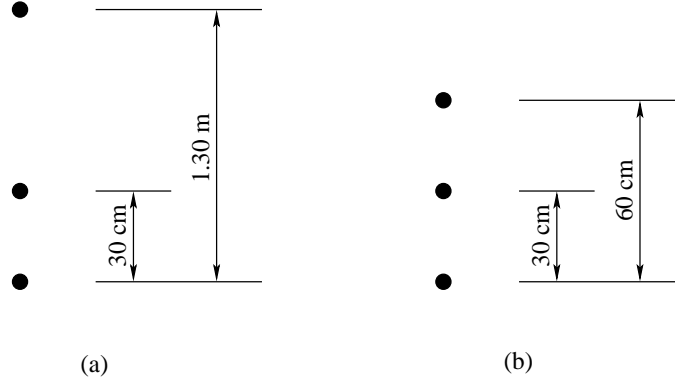

Figure 4.6. The configuration chosen for assessing the importance of the catenary camber on the per-unit-length parameters of the catenary. The two cases refer to the two extreme positions of the catenary camber, for a composite overhead line.

We now seek to apply this method to a railway line. In order to "spread" the lumped short-circuits along the entire line, their spacing has to be far smaller than the wavelength. Indeed, this is the case in the present context. In this case, the low sensitivity to the catenary camber is even more evident. To this end, let us consider the configuration described in Appendix B, representing an actual railway line. In order to assess the importance of the camber, two configurations are considered for the catenary wire, as shown in Figure 4.6. For these two configurations, the reduction procedure has been applied to the three overhead wires, at 100 kHz, obtaining the results of Table 4.1

These results prove that the camber in the catenary can indeed be neglected for the propagation analysis, since the maximum error is below 5 %. Besides, this analysis points

P.u.l. par.	(a)	(b)
Z_{cc}	3.87e-2+j6.00e-1	3.81e-2+j5.77e-1
Z_{cr}	5.22e-2+j1.04e-1	5.15e-2+j1.02e-1
Y_{cc}	j8.04e-6	j8.39e-6
Y_{cr}	-j4.83e-7	-j4.92e-7

Table 4.1. Comparison of some p.u.l. parameters for the two overhead configurations in Figure 4.6, applying the reduction technique described in Appendix C.

out that though the p.u.l. parameters of the catenary are not much affected by a camber, the number of conductors plays an important role. For instance, the series self-reactance of one contact wire is about $1\Omega/\text{m}$, whereas for the entire overhead line is about $0.6\Omega/\text{m}$. Therefore, attention should be paid in not neglecting the actual configuration of the catenary: rather than directly approximating it as a single conductor, its configuration should be used for the computation of an equivalent single-wire catenary.

On the other hand, from a theoretical point of view, these non-uniformities might have some effects on the magnetic field. As a matter of fact, the upper catenary wire gets more vertical as it gets nearer to the masts, the radiation pattern is expected to differ from the horizontal dipole one, increasing the longitudinal component. Anyway, this possibility has been neglected, in order to simplify the description of the line and in particular because the only component interesting for industrial applications is the lateral one, which is not much affected by this non-ideality. Indeed, the tilting acts on the xz plane, leaving unaffected the y direction; disagreements are rather expected on the vertical component, which is anyway not interesting in this context.

Therefore, this reduction procedure can be effectively applied to the propagation analysis. The problem is that their is a loss of information, since the results refer only to the common-mode propagation, without any information about the actual partition of the current among the catenary wires. Although this is not important for the propagation (as previously mentioned), it should be considered in radiation problems. In fact, the relative position of each current-carrying wire has to be taken into account. Now, this situation too can be simplified. Looking at equations (3.81), the magnetic field generated by each wire, as measured by the observer, depends on both their electrical and physical distance. For the catenary wires, the distances ρ_i get very similar as the observer gets far away from the line. In particular, for the practical case of an observer at 10 m away from the line, the catenary wires appear to be at nearly the same distance. Thus their position can be made to collapse into the mechanical center of the catenary. On the other hand, for an observer just under the catenary, the distances ρ_i differ, therefore this approach is expected to yield approximated results.

A numerical validation of the reduction procedure is shown in Figure 4.7: the current distribution at 2 MHz for the overall current flowing across the catenary and the lateral component of the magnetic field for a multi-wire overhead line are compared with the results obtained for the equivalent single-wire catenary. In particular, the magnetic field has been computed in two positions, one at 10 m away from the catenary, the other one just under the catenary axis, both 2 m above the soil, at the center of the line. The results are indistinguishable, even for the field measured under the catenary, which is somewhat unexpected.

The main drawback of this method is the need to invert the matrix $\mathbf{Z}$, as shown in Appendix C: anyway it reduces the dimension of the circuit matrix (cf. Section 4.3), which is the most important bottleneck in the computation of the current distribution. For the very same reason, also the radiation matrix is reduced: this is even more important, since its computation involves Sommerfeld's integrals. Therefore, the reduction eventually speeds up the overall analysis of the railway system. For instance, for the configuration in Appendix B, the computation of the magnetic field with the original configuration takes
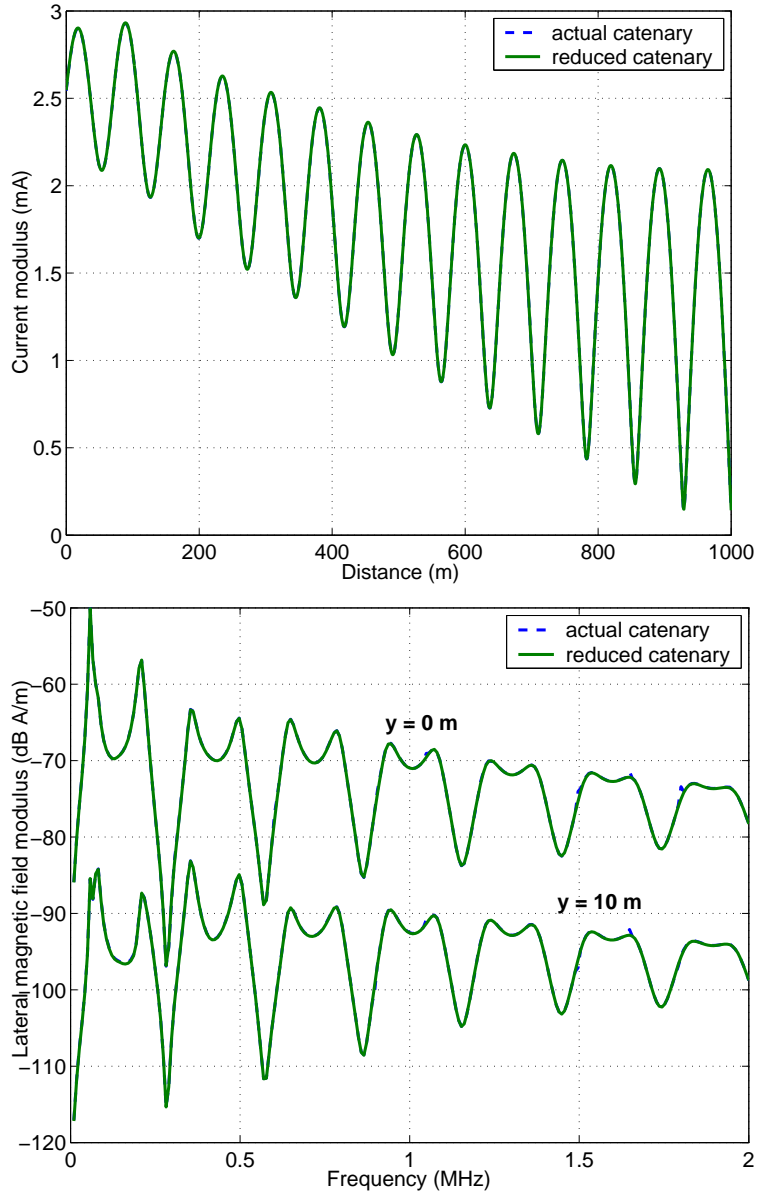
Figure 4.7.   A comparison of the results obtained with a multiconductor overhead line and the reduced one: (a) distribution of the overall current along the catenary at 2 MHz and (b) lateral magnetic field at 10 m and under the catenary, 2 m above the soil interface. The line here considered is described in Appendix B and 1 km long.

0.4 s per sample, whereas it takes just 0.14 s with the catenary reduction.

84

4.1.2 Masts

The poles acts as periodic connections between the catenary and another conductor, which can be either the soil or the rails, depending on the actual configuration. In order to be easily included into the overall model, an equivalent circuit is needed. To this end, the simplified pole in Figure 4.8a has been described under NEC, in order to estimate its input impedance. This has been accomplished over the frequency range $0.1 \div 3$ MHz, for a perfectly conductive soil. The impedance has been defined as between the connection to the catenary and the soil. The three configurations shown in Figure 4.8 have been studied, according to the actual configuration: the input impedance is well approximated by an inductance of about 13μH for a PEC soil (Figure 4.9).

For an actual soil the definition of the input impedance is ambiguous: in this case it changes according to the point of measurement in the soil terminal, because of the non equipotentiality of the soil. The results in Figure 4.9b, for the configuration 4.8b and an average soil ($\sigma_g = 10$ mS/m, $\epsilon_g = 10$), have been obtained by moving the lower terminal over a distance of $0.1 \div 4$ m away from the pole base. These simulations exploit the ability of NEC to model a soil as a homogeneous medium thanks to an approximated solution of Sommerfeld's model [64]. In this case, an additional series resistance $\leq 150\Omega$ has to be considered.

Although these results are interesting because of the possibility to study the frequency response of the masts, these structures are never directly connected to the catenary. Indeed, one or more power isolators are always placed between them and the catenary, for obvious safety reasons. These devices, basically acting as capacitors, are characterized by a very small capacitance, at least compared to railway standards: typical values are usually limited to a few pF. A tentative experimental characterization has been carried out on the model shown in Figure 4.10 by means of a network analyzer over the frequency range 30 kHz - 3 MHz. Unfortunately, the input impedance of this device was dominated by parasitic elements of the network analyzer. In fact, the same results were obtained with or without the terminals connected to the isolator. This peculiar result was not due to bad connections on the isolator metal terminals: both the connections were checked by means of a multimeter. This implies that its input impedance was by far greater than the common-mode impedance seen by the analyzer.

The experimental results can be very well approximated by a capacitance around 10 pF; for this reason, the isolator capacitance has to be smaller than the equivalent common-mode one. This limit is actually confirmed by practical knowledge of engineers working at Alstom Transport. Furthermore, the isolator in Figure 4.10 is for a 3 kV DC supply, so that isolators for 25 kV AC lines are expected to have an even smaller capacitance. Hence, the actual impedance to be considered for the masts is the series of the mast one and an equivalent capacitance smaller than 10 pF. Considering 2 MHz as the maximum frequency of analysis, the resulting shunt admittance Y_p is dominated by the isolator, so that masts can usually be neglected.

Recalling that the lumped shunt loads Y_p are nearly periodically distributed, with spacing s, one could think of considering them as an extra per-unit-length load $y_p = Y_p/s$. This approach, which would be rightfully valid only in a quasi-static analysis, is equivalent
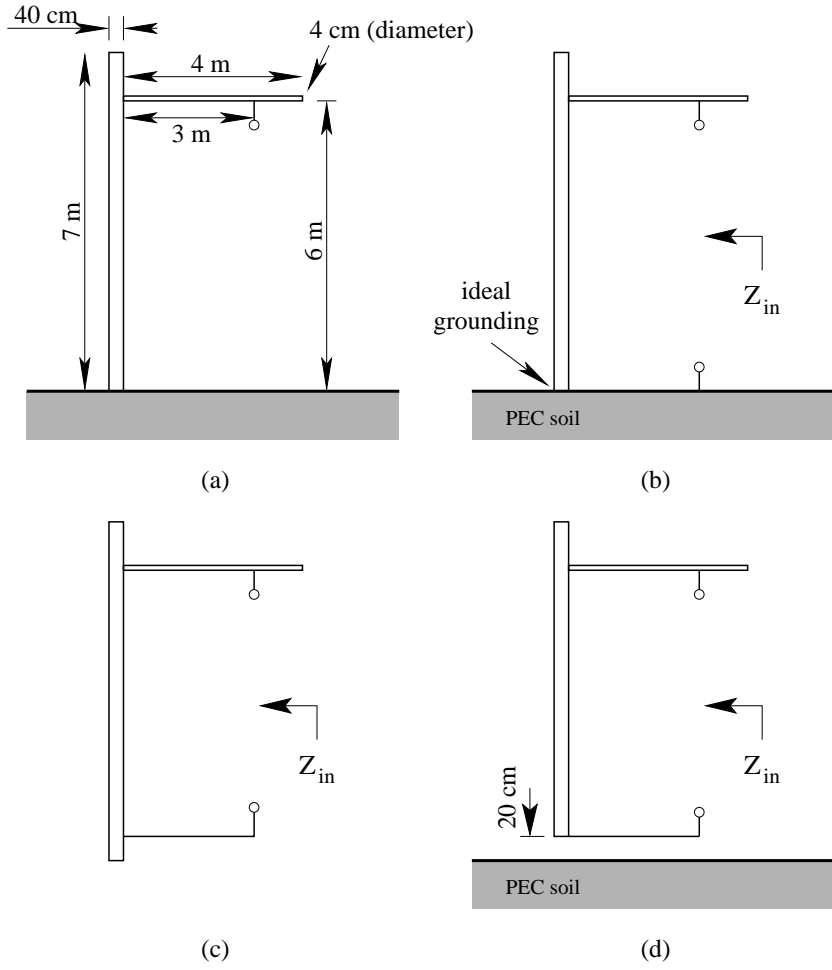
Figure 4.8. The simplified mast described under NEC, for the evaluation of a lumped equivalent circuit (a) and the three configurations investigated: with the mast ideally grounded to a PEC soil (b), in a free-space environment (c) and above a PEC soil but not grounded (d).

to "spread" these shunt loads all over the line. The p.u.l. admittance matrix can thus be modified by including the new per-unit-length admittance y_p as in Figure 4.11, for poles connected between the conductors indexed as i and j. The adding and subtracting of y_p is due to the peculiar structure of the matrix admittance, as recalled in Section 3.7 for the capacitance matrix.

This approach is certainly appealing due to the possibility to analyze a periodically loaded line, hence non-uniform, as a uniform line, thus greatly lightening the numerical burden of the simulation. Unfortunately, this approach obviously fails whenever the shunt admittance acts as a sharp discontinuity, introducing abrupt variations in the current distribution at its left and right. Indeed, in this case the distributed approach would
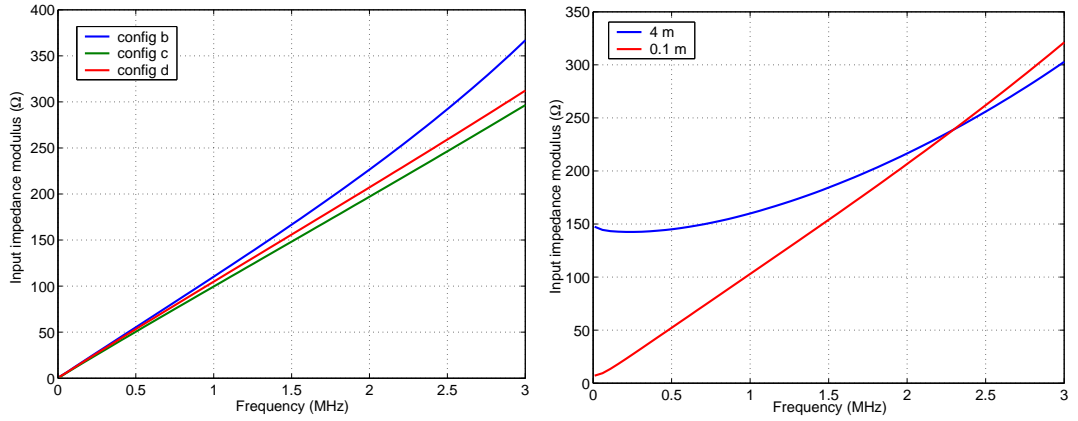
Figure 4.9. The input impedance of a mast, as computed with NEC, for the three configurations of Figure 4.8b-d (a) and for two reference positions with a finite conductivity ground-plane (Figure 4.8b) (b).

not be able to reproduce the abrupt variation in the current distribution. As already mentioned, Y_p is dominated by the isolator capacitance, so that this is not the case as long as the frequency does not exceed a few MHz, since the impedance of a 10 pF capacitance is about 8 kΩ at 2 MHz. But the isolator impedance is far greater than this value, so that it can be regarded as an open-circuit.

These considerations are based on measurements carried out with the isolator not connected to any high-voltage source. But in actual applications, they must support high-voltages; under such conditions, non-linear effects may occur, like ionization, that can

Figure 4.10. The 3 kV DC isolator used in the experimental characterization attempt (courtesy of RFI, Italy); attention was paid to ensure good ohmic contacts at the two extremities.
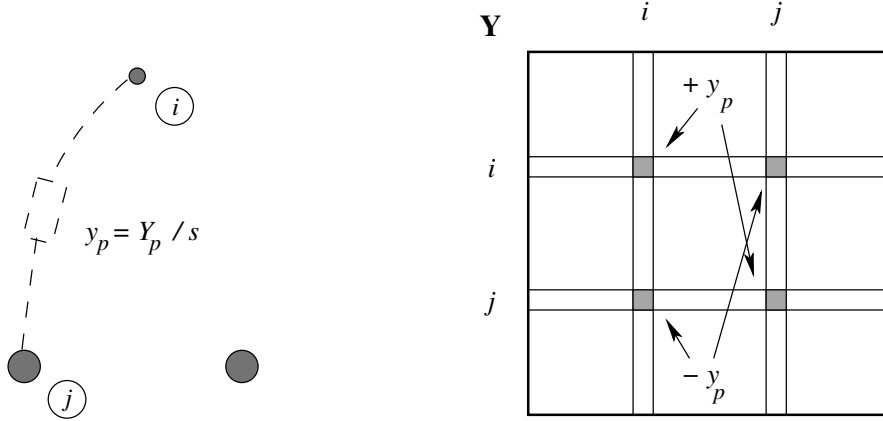
87

Figure 4.11.   An example of how identical lumped admittances Y_p periodically connected with spacing s can be included into the per-unit-length admittance matrix. The admittances are connected between the conductors i and j.

create conductive paths, equivalent to a shunt conductance, especially for a 25 kV supply. For such cases, the conclusions here claimed may prove wrong. Unfortunately, we have no information at all about the high-frequency effects of such non-linear phenomena.

In the end, we roughly consider the poles as periodic capacitances whose main effect is to "charge" the line, by increasing a part of the p.u.l. capacitance matrix, which could be interpreted as dealing with a non-homogeneous medium.

The current distribution obtained with different approaches is shown in Figure 4.12, for the reference line in Appendix B, with 10 pF capacitances spaced by 60 m, connected between the catenary and the rails. Here, the line has been considered with no poles, with periodic lumped poles and with "distributed" masts. This analysis has been carried out at 2 MHz, the worst-case because of the lower isolator impedance and because of the greater electrical distance between the masts. Figure 4.12 shows that the idea of spreading Y_p evenly along the line agrees with the actual periodically loaded line, even at 2 MHz, where the spacing is no longer electrically short. Nevertheless, the error in the current distribution computed with $Y_p = 0$ is smaller than 5 %; since these results have been obtained for a very conservative description, the masts can be definitely neglected for the propagation.

A more formal analysis of the impact of periodical discontinuities can be carried out thanks to Floquet's theorem, as proposed in [65]. It states that whenever a linear set of ordinary differential equations

$$\frac{\mathrm{d}^2\mathbf{x}(z)}{\mathrm{d}z^2} = \mathbf{M}(z)\mathbf{x}(z) \tag{4.1}$$

have non-constant but periodical coefficients $\mathbf{M}(z)$, with period d, its solution at position $z + d$ is directly proportional to that at z, as

$$\mathbf{x}(z + d) = \mathbf{x}(z)\mathrm{e}^{-\gamma_p d} \tag{4.2}$$
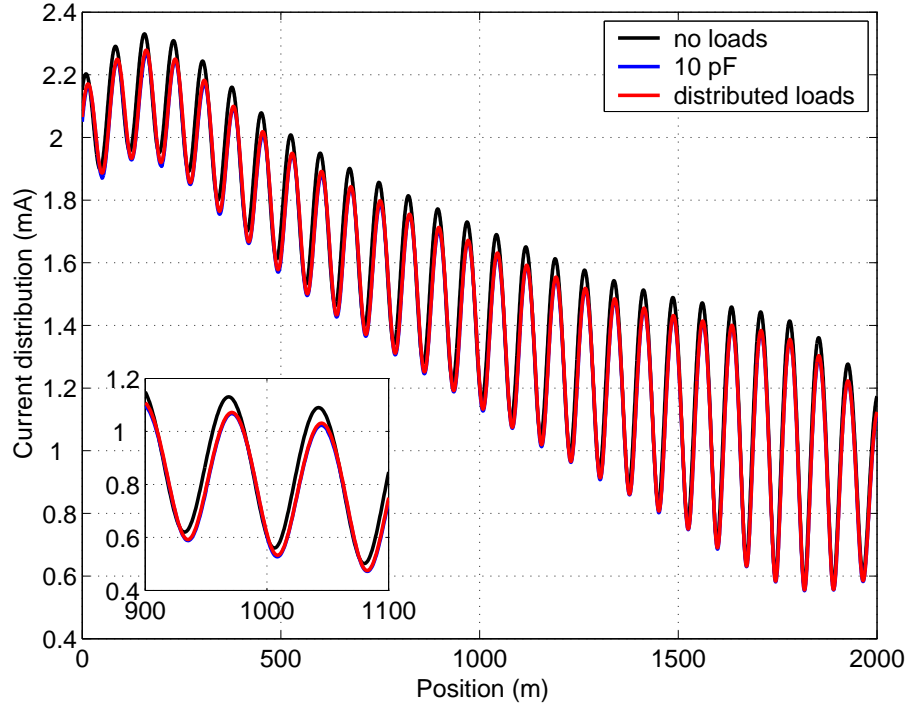
88

Figure 4.12. The current distribution of the overall current flowing in the overhead line of a line 2 km long (cross-section as in Appendix B), at 2 MHz. Three configurations have been studied: with no periodical loads, with 10 pF capacitances spaced by 60 m and with "distributed" extra capacitance in the p.u.l. admittance.

Floquet's theorem requires the function $\mathbf{x}(z)$ to be defined on the domain $(-\infty, +\infty)$, that is for an infinite line, thus implying an asymptotic analysis. Looking more closely to equation (4.1) one can notice that it is of the same kind as the second order telegrapher's equations 3.12, by considering $\mathbf{x}(z) = \mathbf{V}(z)$ and $\mathbf{M}(z) = \mathbf{Z}(z)\mathbf{Y}(z)$. Now, by applying a circuital approach to the definition of the per-unit-length parameters, one can see that they differ from the uniform case only around the lumped discontinuities. In particular, the only effect of shunt-admittances is to modify the per-unit-length matrix admittance, so that its values will change periodically in proximity of the discontinuities, i.e. with periodicity d. This is indeed the last hypothesis required by Floquet's theorem, which can therefore be invoked. Hence [65]

$$\mathbf{V}(z+d) = \mathbf{V}(z)\mathrm{e}^{-\gamma_p d} \tag{4.3a}$$

$$\mathbf{I}(z+d) = \mathbf{I}(z)\mathrm{e}^{-\gamma_p d} \tag{4.3b}$$

Now, since the coefficient γ_p is the same for the currents and the voltages, defining the chain matrix $\mathbf{\Phi}_c$ of a periodic cell

$$\begin{bmatrix} \mathbf{V}(z+d) \\ \mathbf{I}(z+d) \end{bmatrix} = \mathbf{\Phi}_c \begin{bmatrix} \mathbf{V}(z) \\ \mathbf{I}(z) \end{bmatrix} \tag{4.4}$$

89

one gets

$$\mathbf{\Phi}_c \begin{bmatrix} \mathbf{V}(z) \\ \mathbf{I}(z) \end{bmatrix} = \mathrm{e}^{-\gamma_p d} \begin{bmatrix} \mathbf{V}(z) \\ \mathbf{I}(z) \end{bmatrix} \tag{4.5}$$

This equation links the propagation constant of Floquet's solution to the eigenvalues of the chain matrix of the periodic cell. In particular, these eigenvalues yield the terms $\exp(\pm\gamma_p d)$ that satisfy Floquet's theorem. The γ_p coincide with the modal propagation constants as the periodic admittances goes to zero. Hence, in order to verify the impact of the admittances Y_p on the modal propagation constants, it suffices to solve the eigenvalue problem in (4.5) and compare the results with the case $Y_p = 0$. Results are shown in Figure 4.13 for the same configuration previously investigated, with both the rails and the catenary reduced to single conductors, thus obtaining a two-wire line above the soil. An ideal capacitance of 10 pF has been employed for modelling the poles, a value already
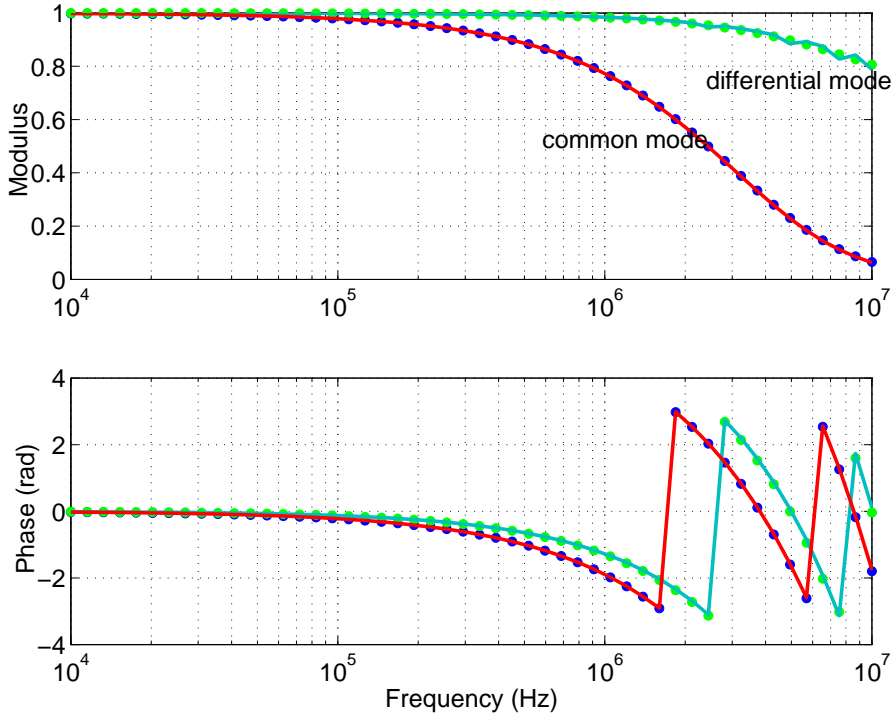

Figure 4.13. The attenuation and phase of the forward-travelling propagation exponential, as computed for a uniform two-wire line (dots) and for a periodically loaded one (solid lines), with spacing 60 m and periodical shunt-capacitances of 10 pF. The only visible effect of shunt-capacitances on the propagation is in the attenuation of the differential mode (the least attenuated one) in the higher frequency-range.

shown to be conservative. Nevertheless, the modal propagation constants appear not to be affected by the discontinuities, giving way just to very small variations in the higher frequency range. These results confirm the previous ones of Figure 4.12, so that it is possible to neglect the poles in the computation of the current distribution.

Scattering from masts

So far we have just considered the impact of periodic discontinuities on the propagation through a quasi-static approach. Anyway, the poles are basically vertical metallic cylinders, which behave as scatterers. In order to check the importance of the scattered field, the line in Figure 4.14 has been simulated with NEC, computing the transversal components of the magnetic field 5 m and 10 m away from the line, 2 m above the soil, both on the left and the right side. In this way, a shielding effect from the poles would be highlighted. As a matter of fact, the standard EN 50121 requires the antennas to be placed on the side with no poles, so to reduce any possible scattering from these objects.
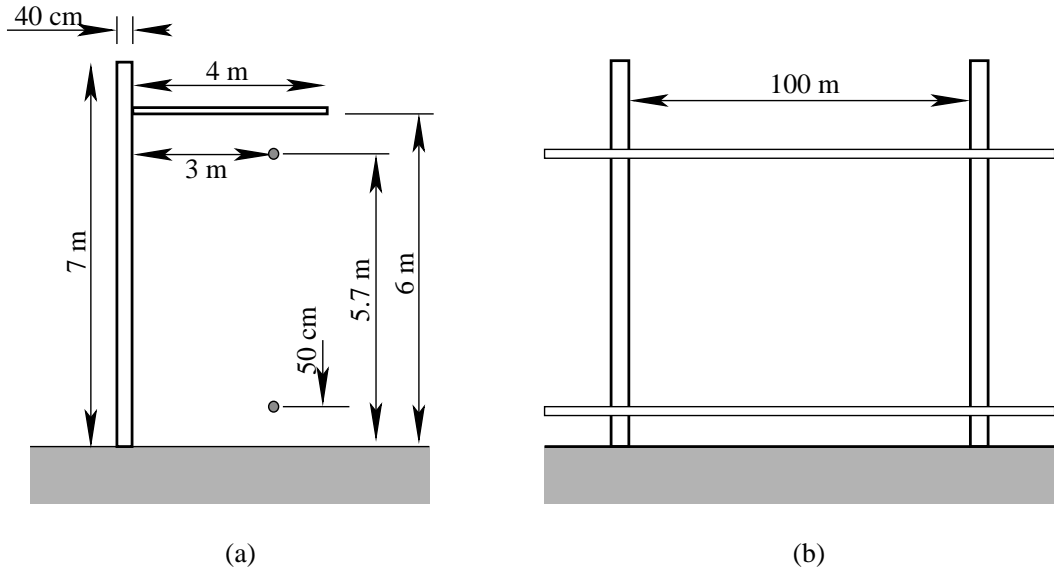

Figure 4.14.   The two-wire line studied in order to assess scattering from masts: transversal section (a) and longitudinal one (b).

Indeed, a shielding behaviour has been found, although tightly localized around the masts. A few meters suffice for neglecting them; in particular, the magnetic field measured on the opposite side is not perturbed at all by the poles, allowing them to be neglected for the radiation too.

4.1.3   The ballast

Actually, the ballast does not represent a discontinuity, since it can be assumed to run uniformly under the rails. It is rather a non-ideality with respect to the multiconductor line model presented in Section 3.4. The techniques introduced so far do not allow the description of a laterally bounded layer, unless approximating the ballast as laterally unbounded, thus considering a stratified soil description [66]. For such a configuration Wait's model, and therefore its quasi-TEM approximation, could still be applied.
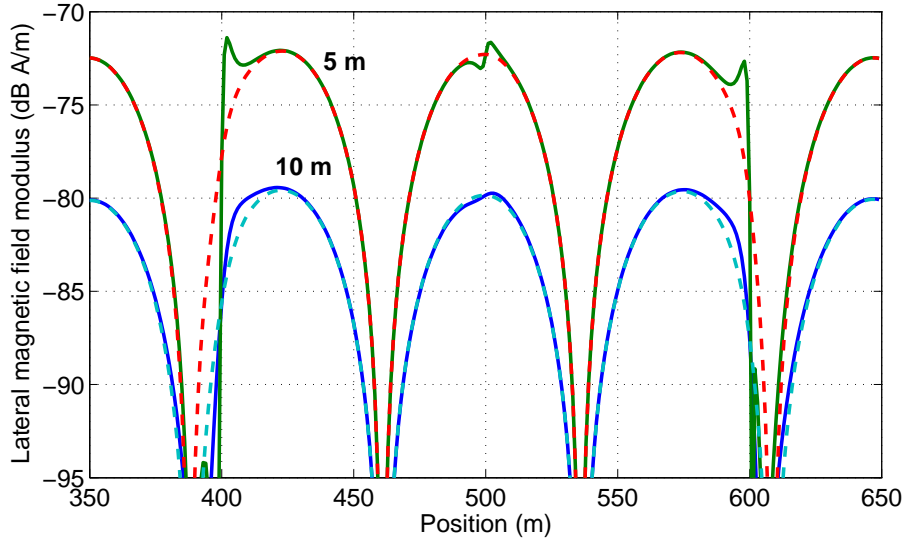
Figure 4.15.   Lateral component of the magnetic field 10 m and 5 m away from the line of Figure 4.14. The solid lines refer to the side with the poles, whereas the dashed lines refer to the opposite side.

Unfortunately, such approach is fine in theory but hard to implement. As a matter of fact, the electrical properties of the ballast should be specified, thus increasing the number of parameters needed by the model, parameters which are quite difficult to estimate. Furthermore, an equivalent description for the contact between the rails and the sleepers, and between the sleepers and the ballast would be needed. This would require a three-dimensional approach, exactly what we are trying to avoid in this work.

Nevertheless, the ballast can be neglected, thanks to the following reasons:

- a rock ballast is an aggregation of low-conductivity rocks (mostly quartzite) immersed in air, a configuration that does not assure the electrical continuity, even with an important humidity content. Furthermore, quartzite rocks have a typical conductivity of 0.1 mS/m, far lower than the typical value of 10 mS/m for a farmland soil. These two features identify the ballast as a very poor conductor: its overall bulk conductivity (including the air gaps) is expected to be smaller than 0.1 mS/m.

- As already mentioned, currents in the soil are justified by its enormous cross-section as a return conductor, thus providing an alternative return-path for the current. Furthermore, this current is not directly excited by the sources along the railway lines, but is rather induced by the current flowing along the railway track conductors. On the other hand, the ballast cross-section is negligible with respect to the soil, therefore it is expected to be less prone to provide a convenient return-path, as compared to the soil underneath.

While weighing these remarks, one should bear in mind that the rails are electrically insulated from the sleepers by means of a dielectric layer about some millimeters thick [6],

and the sleepers themselves are made of concrete several centimeters thick. On the other hand, the ballast is expected to slightly increase the capacitance of rails with respect to the soil, since quartzite has a relative permittivity of about $3 \div 5$. Nevertheless, this increase is expected to be negligible, since the rails lie on the border of the ballast, so that the electric field in mostly in air.

These remarks refer to a rock-ballast line. Anyway, as mentioned in Section 2 no-ballast lines are common configurations in underground lines. In this case there is no ballast at all, but nevertheless their structure is not homogeneous. However in this case there is a metallic grid running beneath the rails, which could be approximated as a perfectly conductive ground-plane. For such a configuration the model would get by far simpler than for an actual soil. Unfortunately, no experimental validation was performed for this configuration, so that the validity of this approximation has not been checked.

4.2 Approximated modal description

Another approach for reducing the model complexity can be defined by taking a closer look to the modal quantities Θ and γ. As a matter of fact, some propagation constants are quite similar to the free-space one γ_0: by approximating this subset with γ_0, the modal matrices can be simplified. To this end, we study the configuration in Appendix B, but without the central overhead wire, for the sake of simplicity: at 1 MHz, for an observer 10 m away from the line center, 2 m above an average soil, one has the results shown in table 4.2.

$\Theta =$

+1.05e-2 -j8.01e-4	+1.00e-2 -j8.54e-4	+9.75e-3 -j3.04e-3	+1.09e-2 -j3.44e-3
-1.04e-2 -j1.15e-3	-1.09e-2 -j1.60e-3	-9.86e-3 -j3.81e-3	-1.15e-2 -j3.19e-3
-1.17e-2 -j2.61e-3	-1.18e-2 -j2.59e-3	-1.10e-2 -j4.79e-3	-1.28e-2 -j6.19e-3
-1.15e-2 -j2.47e-3	-1.15e-2 -j2.50e-3	-1.07e-2 -j4.71e-3	-1.24e-2 -j6.10e-3

$\gamma/\gamma_0 =$

1.00 -j5.5915e-4
1.01 -j8.6308e-3
1.12 -j5.6188e-3
1.51 -j2.2233e-1

Table 4.2. Numerical results illustrating the possibility to simplify the modal description.

Looking closer to their actual values, one can remark a sub-structure as in Figure 4.16, identifying some sub-matrices with marked similarities. These are due to two reasons:

the propagation constants and the geometry. In the first case, the vector γ can be approximated by grouping together all the modes with propagation constants close to the free-space one, which can be dubbed as aerial modes, leaving just a few modes outside this set. These latter modes are related to field topographies more deeply immersed into the soil, accounting for the more important attenuations. Now, the propagation constants of the aerial modes can be effectively approximated by γ_0, thus allowing a reduction in the actual number of modes. This approximation had already been shown to be very effective in [67], as applied to uniform MTL in a non-homogeneous medium. In the present work the approximation of the aerial modes is used for justifying the similarities in the columns of $\boldsymbol{\Theta}$. On the other hand, we have already drawn attention on the possibility to regard the catenary as a single-wire; among other reasons, for measurements 10 m away from the line the actual position of these wires can be approximated with the catenary mechanical axis. This possibility is not limited to overhead wires, but it can be invoked as the relative distance between the observer and the wires gets comparable. In particular, the more distant the observer is from the line, the weaker the differences in the rows of $\boldsymbol{\Theta}$.

Now, pulling together these two remarks, one can easily explain the structure of the radiation matrix. For each sub-matrix, the geometry and the modal propagation are not very different, so that the radiation terms are very similar. Thus, rather than computing all the radiation terms in these sub-matrices, it suffices to computed just one term. Since Sommerfeld's integrals are involved, this simplification is indeed important for the overall computation time.

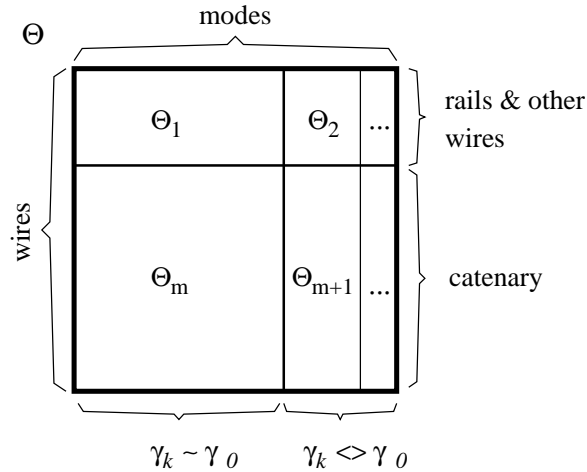Referring to the approximated value of the M sub-matrices as Θ_k, corresponding to

Figure 4.16.   Approximation of the radiation matrix by means of sub-matrices with similar elements.

the propagation constant γ_k, equation (3.91) can be simplified

$$H(\mathscr{P}) = \sum_{k=1}^{M} \Theta_k(x,y) \left[I_{eq,k}^{+} e^{-\gamma_k z} - I_{eq,k}^{-} e^{+\gamma_k z} \right] \tag{4.6}$$

having defined the equivalent currents $I_{eq,k}^{\pm}$ as

$$I_{eq,k}^{\pm} = \sum_{i,j} T_{ij} I_{m0,j}^{\pm} \tag{4.7}$$

considering all the couples (i,j) within each sub-matrix. This reduction approach may seem useless, having already proven the possibility to reduce the catenary to a single-wire line. Nevertheless, for configurations with extra conductors such as the ground-wire, the feeder or even nearby lines, the overhead conductors cannot be grouped together; in these cases, the line can be effectively simulated by applying the approach here proposed.

4.3 Computation of the current distribution

In the previous chapter, equivalent circuits have been sought for railway lines. Taking for granted the availability of equivalent lumped circuits for power devices and putting all these circuits together, thanks to a topological description, an equivalent electrical circuit can be defined, representing the entire railway system. By solving this electrical network, one can compute the currents and voltages across it, and therefore know the current distribution along all the conductors. As previously shown, this information suffices for computing the magnetic field radiated by a line: for this reason, the computation of the current distribution is paramount; thanks to the approach here pursued, this task can be accomplished by means of electrical network solvers.

A general and simple way of doing that is by means of the tableau method [68]. Here, the fundamental laws of electrical networks are imposed, mixing together topology constraints and equivalent models of electrical devices. For a generic electrical network characterized by N_n nodes and N_b branches, the topology can be taken into account by means of the incidence matrix $\mathbf{A} \in \mathbb{R}^{n_n \times n_b}$. This is defined as the matrix providing the matrix form for Kirchoff's current law (KCL):

$$\mathbf{A I}_b = 0 \tag{4.8}$$

where $\mathbf{I}_b$ is the column vector for the branch currents. The incidence matrix is therefore defined as

$$A_{ij} = \begin{cases} 0 & \text{branch } j \text{ is not connected to node } i \\ +1 & \text{current } I_j \text{ is oriented away from node } i \\ -1 & \text{current } I_j \text{ is oriented towards node } i \end{cases} \tag{4.9}$$

Kirchoff's voltage law (KVL) is defined in matrix form in a similar way:

$$\mathbf{V}_b = \mathbf{A}^{\mathrm{T}} \mathbf{V}_n \tag{4.10}$$

where $\mathbf{V}_b$ is the vector of the branch voltages and $\mathbf{V}_n$ is the nodal voltages vector. Attention should be payed at the orientation of branch voltages, which depends on the electrical conventions of users and generators. The last set of equations to be considered are the electrical models of the devices: these equations are usually referred to as constitutive equations and can be expressed in a very general mixed form as

$$\mathbf{Z}\mathbf{I}_b + \mathbf{Y}\mathbf{V}_b = \mathbf{W} \tag{4.11}$$

where $\mathbf{W}$ is the source vector. Matrices $\mathbf{Z}$ and $\mathbf{Y} \in \mathbb{C}^{n_n \times n_b}$ allows the representation of any linear electrical device. These three sets of equations can be written in matrix form as

$$\begin{bmatrix} \mathbf{A} & 0 & 0 \\ 0 & \mathbf{1} & -\mathbf{A}^{\mathrm{T}} \\ \mathbf{Z} & \mathbf{Y} & 0 \end{bmatrix} \begin{bmatrix} \mathbf{I_b} \\ \mathbf{V_b} \\ \mathbf{V_n} \end{bmatrix} = \begin{bmatrix} 0 \\ 0 \\ \mathbf{W} \end{bmatrix} \tag{4.12}$$

This representation is known as the tableau method. Once solved, all the $N_n + 2N_b$ currents and voltages in the circuit are available. Anyway, this representation can be effectively simplified by plugging the KVL equation into the constitutive one, getting the modified tableau representation

$$\begin{bmatrix} \mathbf{A} & 0 \\ \mathbf{Z} & \mathbf{Y}\mathbf{A}^{\mathrm{T}} \end{bmatrix} \begin{bmatrix} \mathbf{I}_b \\ \mathbf{V}_n \end{bmatrix} = \begin{bmatrix} 0 \\ \mathbf{W} \end{bmatrix} \tag{4.13}$$

In this case the number of unknowns is reduced to $N_n + N_b$.

As seen in Section 3.5, a modal description allows a simpler solution for computing the magnetic field. To this end, when dealing with transmission-lines, the modal excitation terms can be readily computed from the physical voltages and currents of the line, by means of the following relationship

$$\begin{bmatrix} \mathbf{V}(0) \\ \mathbf{I}(0) \end{bmatrix} = \begin{bmatrix} \mathbf{Z}_c\mathbf{T} & \mathbf{Z}_c\mathbf{T} \\ \mathbf{T} & -\mathbf{T} \end{bmatrix} \begin{bmatrix} \mathbf{I}_{m0}^{+} \\ \mathbf{I}_{m0}^{-} \end{bmatrix} = \mathbf{M}\mathbf{I}_{m0} \tag{4.14}$$

where $\mathbf{V}(0)$ are the nodal voltages at the left end of a line and $\mathbf{I}(0)$ are the currents entering into the line conductors at its left end. As already mentioned in Section 3.5, whenever an infinite line radiation model can be applied, the only data needed are the modal description for the nearest line to the observer. Otherwise, the actual current distribution has to be integrated, perhaps involving more than one line, as near a discontinuity. In that case, it suffices to apply equation (4.14) to each line and to compute the current distribution by means of equation (3.27).

4.4 Considerations on line attenuation and resonances

So far, the equivalent circuit approach seems to comprise the entire railway system, regardless of the actual behaviour of each device. It is spontaneous to ask themselves whether it would be possible to limit the extension of the equivalent circuit up to a certain point. This possibility would indeed allow a local description of the railway system as opposed to a global description. In this context, local just means near the observer; as a matter

of fact, we are interested into the magnetic field as measured in one point. Of course, its value is directly related to the current distribution, which in general depends on the entire system configuration.

Nevertheless, this dependence grows weaker as the frequency increases, since the attenuation introduced by the lines gets stronger. At the limit, a uniform line with an infinite attenuation acts as a sort of wave isolator, decoupling the system into two parts (cf. Figure 4.17). In this case, one end of the line sees the other one as matched, although not through the connection to a termination network $\mathbf{Z}_c$, but rather because of the very weak magnitude of reflected waves. A line behaving in this way acts as if it were infinitely long; here, this label is applied to the propagation rather than to the radiation.
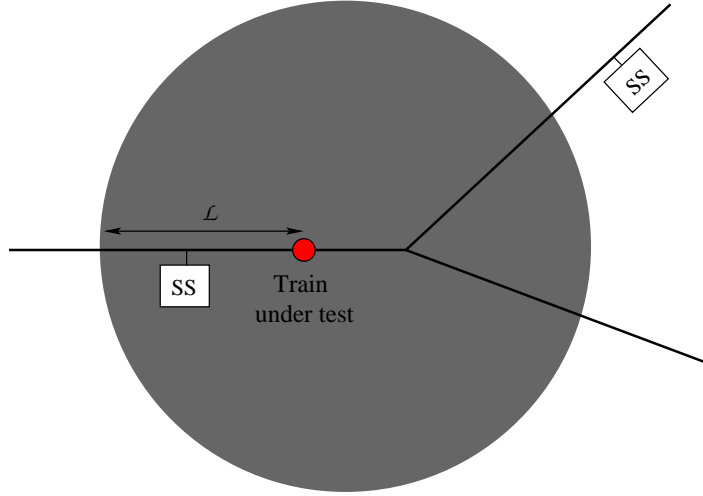

Figure 4.17.   A sketch representing the idea of local description. The observer's position is regarded as the center of a circle of radius $\mathscr{L}_\infty$: only the inner portion of the system is considered, regarding the outward lines as terminated by matched impedances.

To this end, it is important to know under which conditions this approximation can be invoked. Let us consider an MTL of length $\mathscr{L}$, whose far-end is connected to an electric network of matrix impedance $\mathbf{Z}_L$. We want to find a relationship between the forward- and the backward-travelling coefficient of the line modes. In matrix form

$$\mathbf{I}_{m0}^- = \mathbf{S}\mathbf{I}_{m0}^+ \tag{4.15}$$

where the matrix $\mathbf{S}$ is a sort of scattering matrix of the line, when connected to $\mathbf{Z}_L$. Imposing the boundary condition

$$\mathbf{V}(\mathscr{L}) = \mathbf{Z}_L\mathbf{I}(\mathscr{L}) \tag{4.16}$$

at the line far-end and plugging it into equations (3.28), one gets

$$\mathbf{S} = \mathbf{P}\mathbf{T}^{-1}(\mathbf{Z_L} + \mathbf{Z}_c)^{-1}(\mathbf{Z_L} - \mathbf{Z}_c)\mathbf{T}\mathbf{P} \tag{4.17}$$

97

where $\mathbf{P} = \mathbf{P}^+(\mathscr{L})$. Rather than comparing two vectors, it would be more useful to have just a scalar index assessing the importance of reflections. To this end we define the quantity Γ as

$$\Gamma = \frac{\|\mathbf{I}_{m0}^-\|}{\|\mathbf{I}_{m0}^+\|} = \frac{\|\mathbf{S}\mathbf{I}_{m0}^+\|}{\|\mathbf{I}_{m0}^+\|} \tag{4.18}$$

where $\|\cdot\| = \|\cdot\|_\infty$. Remark that Γ depends on the actual value of the modal excitation terms; in other words, it does not regard only the propagation along the line and the load termination, but it also takes into account the actual excitation of the line. Unfortunately, this equation is not very useful, since the excitation too depends on the actual configuration. In fact, we are looking for a general characterization of the propagation without any reference to the actual configuration. In other words, we need to assess the line mismatch on the basis of the modal propagation, regardless of the line excitation. To this end, the submultiplicative property of matrix norms [24] is applied twice to equation (4.18), yielding

$$\Gamma \leq \|\mathbf{S}\| \leq \|\mathbf{P}\|^2 \|\mathbf{T}^{-1}(\mathbf{Z_L} + \mathbf{Z}_c)^{-1}(\mathbf{Z_L} - \mathbf{Z}_c)\mathbf{T}\| = \|\mathbf{P}\|^2 \|\mathbf{S}_L\| \tag{4.19}$$

where $\mathbf{S}_L$ is the scattering representation for $\mathbf{Z}_L$. In general, a passive network fulfill the following condition

$$\|\mathbf{S}_L\| \leq 1 \tag{4.20}$$

yielding

$$\Gamma \leq \|\mathbf{P}^2\| \tag{4.21}$$

Recalling that $\mathbf{P}$ is diagonal, its infinite norm is the element with the greatest absolute value, that is

$$\Gamma \leq e^{-2\alpha_0 \mathscr{L}} \tag{4.22}$$

where α_0 is the smallest p.u.l. attenuation among the propagation modes. This result is very conservative and somewhat expected, simply stating that it suffices to have a strong attenuation on the least attenuated mode in order to ensure a good matching. Anyway, applying it to a three-conductor line (i.e. with a catenary reduced to a single-wire), the dominant mode is the one describing the differential propagation between the catenary and the rails, which coincides with the least attenuated. Since the propagation mainly follows this pattern, condition (4.22) is expected to be representative of the actual propagation. On the other hand, attention should be payed when applying condition (4.22) to an MTL catenary. In this case, the least attenuated modes are the differential modes circulating between two catenary conductors. This means that we are trying to infer the matching of the line by looking at the attenuation of modes that are not even excited.

This result can be employed in order to assess the validity of the infinite line condition required by the standard EN 50121 (cf. Section 2). In Figure 4.18 the minimum length is shown for the usual test case (Appendix B), with reduced catenary, requiring $\Gamma \leq 0.3$ (-10 dB); the validity of equation (4.22) is checked by applying a statistical approach to equation (4.18). In this latter case, for each frequency, 50 modal current vectors I_{m0}^+ have been randomly generated, assuming a normal probability distribution function, the scattering matrix $\mathbf{S}$ has been computed assuming an open-circuited line. The minimum
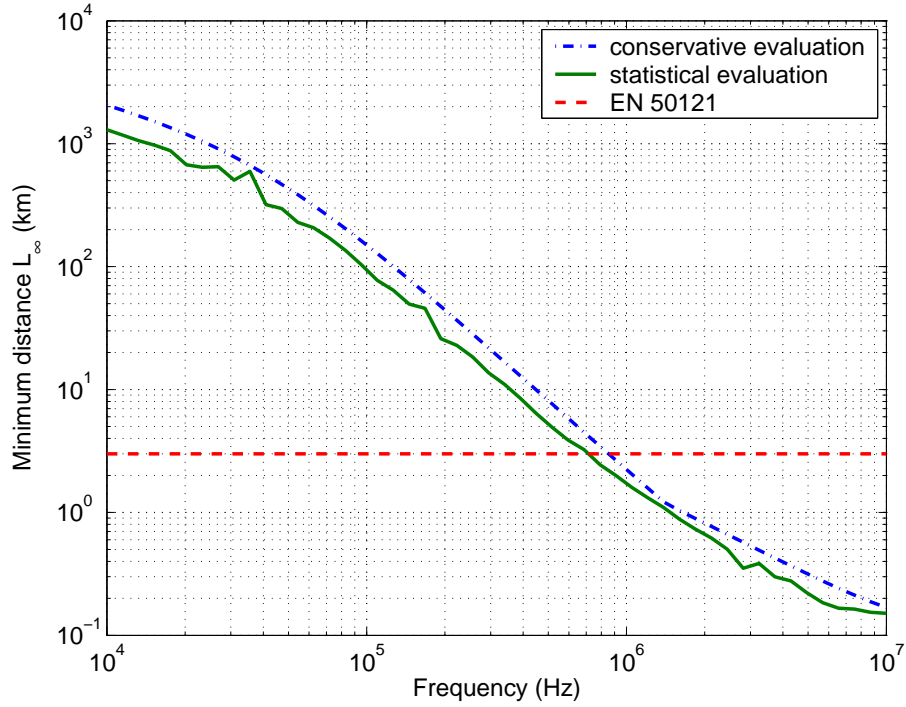
Figure 4.18.   An estimation of the minimum length $\mathscr{L}_\infty$ for regarding a railway track as an infinitely long MTL. Results refer to the typical configuration reported in Appendix B.

length has then been evaluated by a bisection zero-search routine for each random configuration. The agreement is quite good, thus proving that equation (4.22) can be effectively employed in actual configurations, having reduced the overhead line to a single conductor, thus avoiding differential modes along the catenary.

Over the frequency-range here considered, as the frequency increases the minimum length $\mathscr{L}_\infty$ gets shorter. Thus, the portion of system to be modelled can be greatly reduced, considering only a local description. This is not only a happy finding, but rather a need, since the configuration of actual railway systems is usually not available to the industrial engineer. Indeed, over certain frequency-ranges the model can be limited to the portion of system one can see from the measuring antenna. Unfortunately, as discussed in Section 4.6, it was impossible to perform any experimental validation of these results on long railway lines.

Anyway, the low-frequency range is expected to be the most critical for radiated emissions: the low attenuation of railway lines does not allow to consider a local description in this case, thus requiring a good knowledge of the entire system. Nevertheless, as mentioned in Section 2, railway lines undergo sectioning any few 10 km. Whenever the sectioning can be regarded as an abrupt interruption of a line, the system is indeed decoupled, thus limiting the extension to be modelled.

The most important result in Figure 4.18 is the fact that the standard EN 50121

overestimates the attenuation of a railway track, thus underestimating the importance of resonances in the lower frequency range. As a matter of fact, it just requires a uniform line to run for 3 km in order to regard it as infinitely long, whereas at 10 kHz, the minimum length is some 1000 km. This means that in this frequency range, resonances will be very strong, unless resistive loads are connected to the line, reducing the reflections. This point is very important, since the spectrum of the conducted EMI injected onto the catenary by switched-mode converters is more rich in the very same frequency range. Whenever harmonics in conducted EMI occur at the same frequency than a line resonance, conducted EMI generate important contributions to the magnetic field. The problem of resonances will be further investigated in Chapter 5.

4.5   Sensitivity analysis

So far, a perfect knowledge of the system description has been assumed, considering a somewhat ideal case. Unfortunately, this is never the case, but for very peculiar situations, such as a manufacturer testing rolling stock on his own test facility. More likely, the engineer willing to perform measurements along a railway track has a simplified knowledge of the actual configuration, depending on its complexity. Certainly, he would be able to effectively describe the line cross-section, but he would hardly know the exact length of a line and its termination loads.

This limited knowledge, to put it mildly, would strongly limit the use of the models introduced in the previous chapter to simulate actual railway systems and to estimate the magnetic field nearby a railway track. This problem is addressed in the next chapter, where an all-experimental characterization is proposed. Nevertheless, in the view of a fair knowledge of the configuration, it is interesting to assess the effects of systematic errors in the description of a railway system.

In this section we address this problem for small relative errors in the parameters employed for describing the system, such as the length of a line, the conductivity of the soil, the impedance of a load and so on. The small-error approach allows this problem to be analytically solved by means of the propagation of errors formula, by performing just one simulation run with nominal parameter values. On the other hand, larger errors must be treated in a different way, performing a complete simulation of the system for different values in the expected range of variability. For instance, for a parameter p with nominal value p_0, expected to vary over the interval $[p_1, p_2]$, simulation runs should be performed at least for $p = \{p_1, p_0, p_2\}$. In order to assess the overall effect of multiple errors, all the combinations should be considered for each parameter. Since the number of parameters can be important, this large-error approach is expected to be quite lengthy.

Although a small-error approach cannot substitute a large-error one, it can nevertheless provide important information on the sensitivity of the magnetic field with respect to a parameter, thus giving an idea of which parameters deserve a better accuracy or, in other words, which are the most critical parameters for avoiding gross errors in the modelling of an actual site. Furthermore, the small-error approach can be used for simplifying an eventual large-error analysis, just considering a smaller set of critical parameters identified

with the small-error analysis.

The propagation of error formula links the expected errors δp on the nominal arguments $\mathbf{p}_0 \in \mathbb{R}^{N_p \times 1}$ of function $f(\mathbf{p}) \in \mathbb{R}$ to the overall expected error. It is obtained by applying a first-order Taylor series expansion in $\mathbf{p}_0$

$$f(\mathbf{p}_0 \pm \delta\mathbf{p}) - f(\mathbf{p}_0) \simeq \sum_{k=1}^{Np} \left.\frac{\partial f}{\partial p_k}\right|_{\mathbf{p}=\mathbf{p}_0} \delta p_k \qquad (4.23)$$

In order to apply this result to the magnetic field model, we consider the real part of the magnetic field as $H_{\mathscr{R}}$, equation (4.23) yields

$$\delta H_{\mathscr{R}} = |H_{\mathscr{R}}(\mathbf{p}_0) - H_{\mathscr{R}}(\mathbf{p_0} \pm \delta\mathbf{p})| \leq \sum_{k=1}^{Np} \left|\frac{\partial H_{\mathscr{R}}}{\partial p_k}\right|_{\mathbf{p}=\mathbf{p}_0} |\delta p_k| \qquad (4.24)$$

which is valid since the parameters are real quantities. A similar result can be defined for the imaginary part of the magnetic field. Applying this result to equation (3.91) yields

$$\frac{\partial H}{\partial p_k} = \sum_{i=1}^{N}\sum_{j=1}^{N} \left\{ \frac{\partial\Theta_{ij}}{\partial p_k}T_{ij}I_{m,j}(z) + \Theta_{ij}\frac{\partial T_{ij}}{\partial p_k}I_{m,j}(z) + \Theta_{ij}T_{ij}\frac{\partial I_{m,j}(z)}{\partial p_k} \right\} \qquad (4.25)$$

where H is either the real or imaginary part of the magnetic field, for the sake of simplicity. The computation of all the partial derivatives is somewhat lengthy and is carried out in Appendix D. It is important to notice which parameters $\mathbf{p}$ are here investigated:

- the cross-section geometry, including the distances d, the heights h the wire radii r_w

- the line length

- the electric properties of the soil, σ_g and ϵ_g

- any parameters in the equivalent circuit of lumped discontinuities

- the position of the observer (i.e. the antenna)

In order to have scale-free sensitivities, thus comparable, we can define the normalized sensitivities $S_{p_k}^H$ as [68]

$$S_{p_k}^H = \frac{\partial H}{\partial p_k}\frac{p_k}{H} \qquad (4.26)$$

getting a new expression for equation (4.25)

$$\frac{\delta H}{H_0} = \sum_{k=1}^{N_p} S_{p_k}^H \frac{\delta p_k}{p_{0,k}} \qquad (4.27)$$

Attention should be paid to the fact that the expansion in equation (4.23) makes sense as long as the errors vector $\delta\mathbf{p}$ is small as compared to the nominal values $\mathbf{p}_0$.
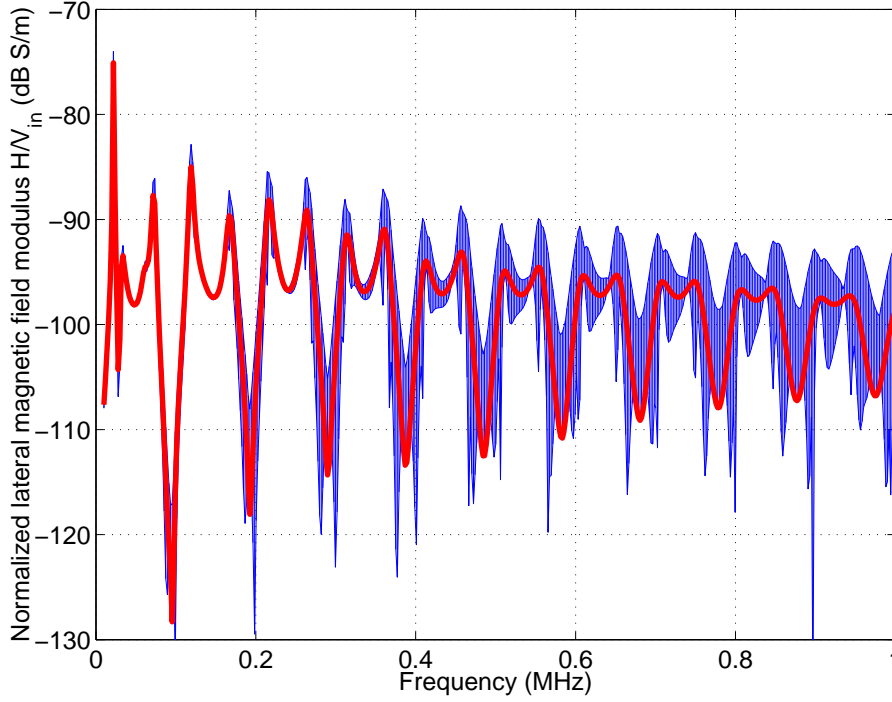
Figure 4.19. The magnetic field computed for the line in Figure 3.25, with its far-end open-circuited, for nominal values (solid line) and the σ_H margin (shaded area) estimated from the small-error sensitivity analysis, for relative errors set to 5 %, but for the line length, set to 1 %.

Usually, this analysis, based on a deterministic approach, is usually seen as too conservative: as a matter of fact, it considers the case where all the parameters have maximum errors at the same time and concurring to have the worst effect, by neglecting possible compensations. More representative results would be obtained by treating the errors vector $\delta\mathbf{p}$ as a random variable with its own probability density function. This would lead not to worst-case results, but rather to confidence margins, which are always less conservative. In general, such approach would greatly complicate the mathematical treating of the problem, since the covariance matrix of all the parameters should be derived. Nevertheless, in real-life cases it is reasonable to assume all the errors to be statistically independent and described by normal distributions, so that the covariance matrix reduces to a diagonal one, just considering the variances of each parameter.

Under such assumptions, the following relationship holds [68]

$$\sigma^2_{\delta H/H_0} = \sum_{k=1}^{N_p} (S^H_{p_k})^2 \sigma^2_{\delta p_k/p_{0,k}} \tag{4.28}$$

where the terms σ^2 are the variances of the expected relative error on each parameter.

This approach has been applied to the line in Figure 3.25, for an average soil, and the

observer 10 m away from the line axis, 2 m high. The expected relative errors have been set to 5 % for the soil parameters, the cross-section geometry and the antenna position, whereas the error on the line length has been set to 1 %. The results are shown in Figure 4.19, for a σ_H margin.

The results show that the magnetic field is relatively robust with respect to uncertainties in the low frequency range, while the expected error gets comparable to the nominal results as the frequency get higher. Therefore, at higher frequencies, the small-error approach is no more valid.

As already mentioned, it is very important to know to which parameters the magnetic field is more sensitive, especially around the maxima. To this end, the normalized sensitivities are shown in Figure 4.20 for the four maxima at 72, 215, 505 and 800 kHz. Here, it is made quite clear that the parameter mostly affecting the magnetic field computation is the line length, whereas the soil plays a less important role. On the other hand, the relative insensitivity for the cross-section geometry is good news, implying that a rough description can be applied. Anyway, the strong sensitivity to the length is an important limitation to the very idea of modelling a railway system, since it is actually very difficult to know such parameter with an accuracy as good as the one here considered, i.e. 1 %.
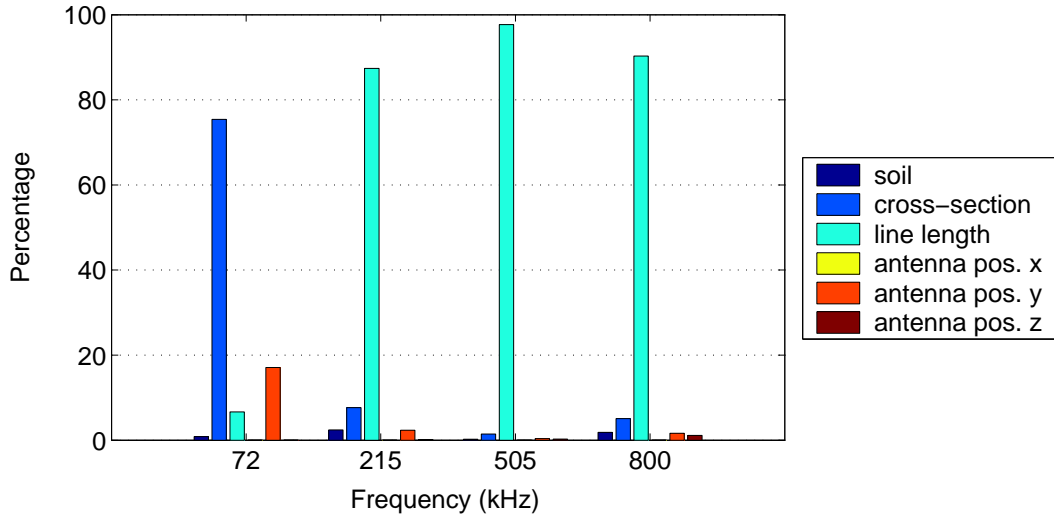

Figure 4.20. The tolerance of the magnetic field for the example in Figure 4.19, divided into six basic contributions. The four samples here shown refer to four peaks of the magnetic field in Figure 4.19.

Actually, this was quite expected: for a scalar line, its length can be regarded as a scale factor for all the electromagnetic quantities related to it, just leading to a stretch or a compression. On the the other hand, for multiconductor lines this holds, in general, only for modal lines: passing from modal quantities to physical ones, the effect of length errors are less predictable. Furthermore, in case of excitations in the middle of a line, these variations are even less easy to interpret. Therefore, even small relative errors on lengths are expected to have an important impact on the overall results.

To this end, the magnetic field has been computed for a configuration similar to the previous one, but with a slightly different longitudinal configuration: the excitation is placed between to lines, exciting the two of them at the same time, with nominal lengths $\mathcal{L}_1 = 500$ m and $\mathcal{L}_2 = 1000$ m for, respectively, the left one and the right one. The ends not connected to the excitation are open circuited. The magnetic field is measured at $z = 1$ km, 10 m away from the line, 2 m high above the soil. Assuming a 3 % error on both lengths, we have simulated the two configurations reported in figure 4.21a. Indeed, this error, that would normally be regarded as negligible, plays an important role, deeply altering the results even around 500 kHz: at that frequency, with $\Delta\mathcal{L}/\lambda < 0.075$ it is quite surprising to have an error of about 5 dB on the maximum field.

For the same configuration, a large-error analysis has also been applied to the soil parameters: here, four couples of values have been considered, obtaining the results shown in figure 4.21b. As expected, the resonances are not much affected, having already proven that the propagation constants are not very sensitive to these parameters. Nevertheless, variations of one order of magnitude in the conductivity can lead to errors reaching up to 10 dB on field maxima, due to the different scattering from soil. Although this means that the magnetic field is rather insensitive to soil parameters, since the conductivity has been varied on a very wide range, these results point out the importance of an acceptable estimation of the soil conductivity.

On the other hand, the permittivity is important only for very low conductivity values. Simulations for $\sigma_g = 10$ mS/m, results are indistinguishable for $\epsilon_g = 10$ or $\epsilon_g = 50$, whereas for $\sigma_g = 1$ mS/m differences appear to be much more important. Therefore, for extremely low conductive soils, such as sandy ones, a further source of uncertainty is to be expected.

4.6 Experimental validation

In this section the theoretical model so far described will be applied to actual systems. The aim is to verify its ability to provide accurate results both for the propagation and radiation phenomena. Since we are interested in MTL above an actual soil, these experiences have been carried out on outdoor sites.

It would indeed come natural to think of a commercial railway line as the best site for an experimental validation. Unfortunately, such sites are always associated with industrial exploitation, so that it is very hard (if not impossible) to schedule measurement campaigns. Another solution would be to gain access to test facilities, thus devoted to experimental activities rather than commercial ones. The problem is that such facilities are very expensive, since we are not talking about indoor laboratories, but rather of railway tracks stretching for several kilometers, requiring extensive maintenance and surveillance. Because of that, these sites are usually put up by societies in the railway business, who then use it for testing their own trains; therefore, they are difficult to be accessed too, due to thigh scheduling.

Nevertheless, this research project was sponsored by Alstom Transport and the CEF, so that some access to their facilities has been provided, although not as much as needed for purely experimental investigations. The results here shown have been obtained through
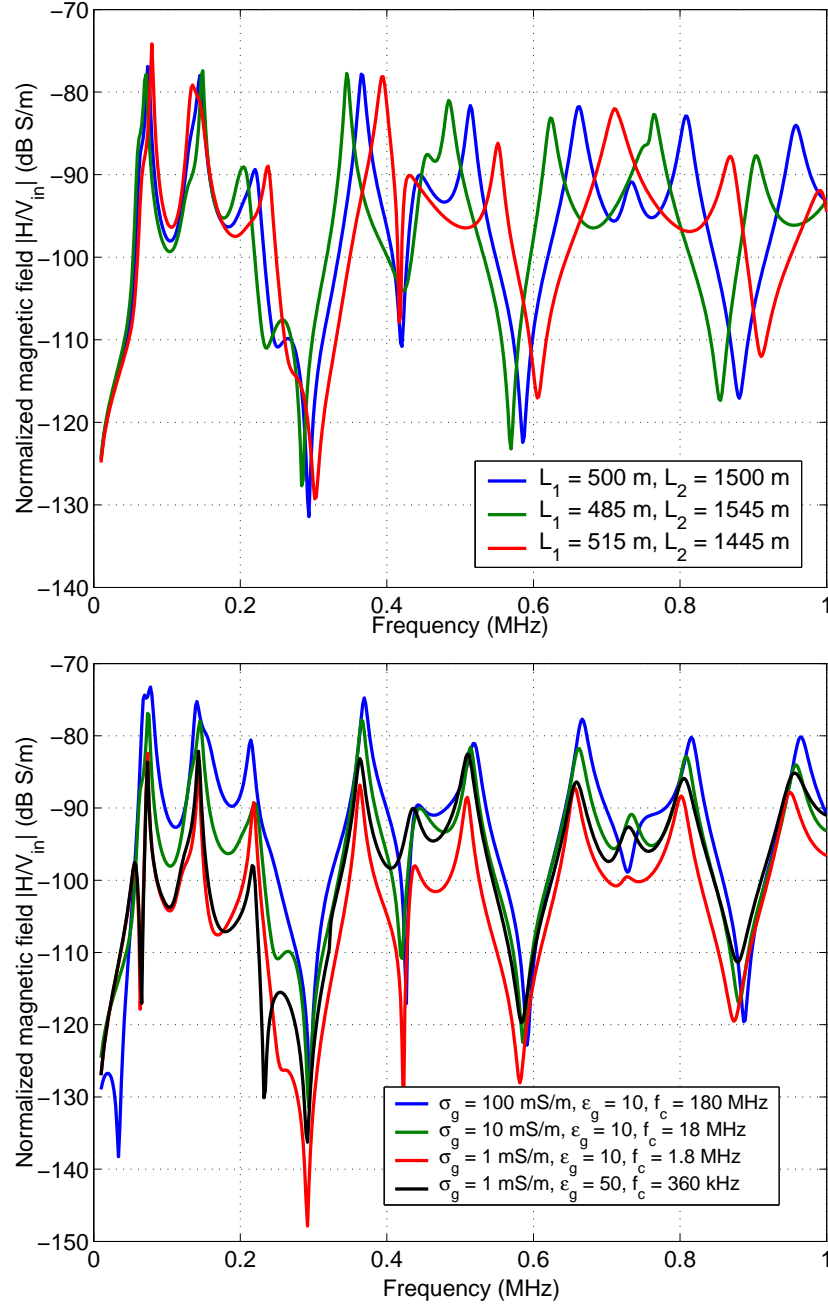
Figure 4.21. Large-error sensitivity analysis for a 3 % error on line lengths (a) and for different values of soil parameters (b).

measurements on different sites. Now this should be regarded as good news, providing a more robust validation; the problem is that these measurement campaigns have not been

105

carried out with the measurement setup described at the end of the next section, whose validity and robustness have been verified through a series of experimental campaigns, but rather with tentative setups, with basic flaws due to our inexperience. Valid measurements constitute a rather small subset of all the experimental tests carried out throughout this work. In order to avoid any confusion and to get comparable results, only the final ones are here shown. Nevertheless the results refer to slightly different setup configurations.

Three validations are here shown: the first one refers to preliminary tests performed on a scale uniform line; the other two deal with actual railway structures within the facility at the CEF and Alstom Transport's site in Valenciennes, France.

4.6.1   Measurement setup

The ultimate result to be validated is the magnetic field: anyway, the model here proposed is based on two steps, dealing with the propagation and subsequently with the magnetic field. In order to check both these aspects, two kind of measurements have been envisaged: the input impedance and the magnetic field. The input impedance has been considered as a good measure of the propagation along systems mainly constituted by transmission-lines, able to sum up all the contributions to propagation, including not only an indirect measure of the p.u.l. parameters, but also, for example, of the termination conditions at the ends of a line. Although it does not provide data on the entire current distribution, it is directly related to it through the input current.
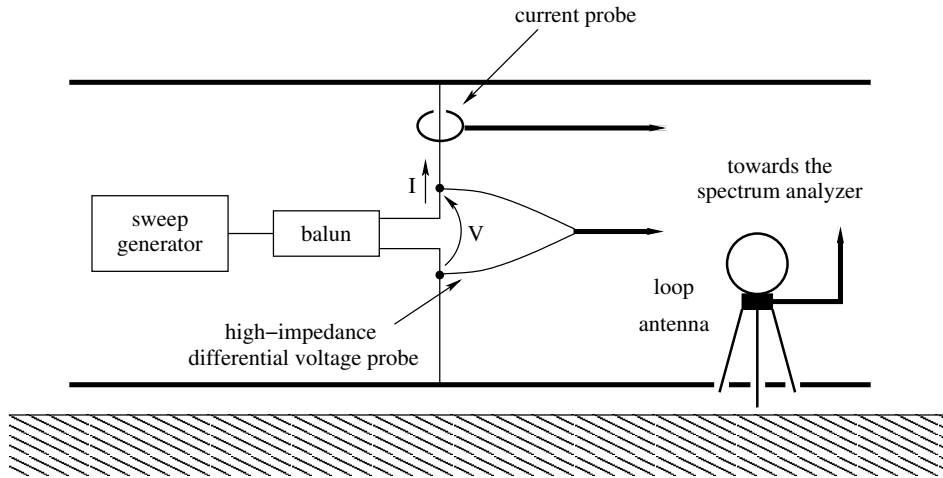

Figure 4.22.   The early setup employed for the experimental validation of the model. The input impedance was evaluated on the base of a V-I method.

The most simple setup for the impedance measurement is shown in Figure 4.22, as applied to a two-wire line above the soil. A sinusoidal sweep generator is applied, through a balun, to the two wires that excite the line; the actual voltage applied is measured by means of a high-impedance differential voltage probe, whereas the current injected into the line is retrieved through a current probe.

106

The line excitation is based on the use of a balun. This is a symmetric 1:1 broadband transformer (-3 db bandwidth over 1 kHz-30 MHz) mounted in the configuration shown in Figure 4.23. The idea is to provide an excitation not referenced to a particular voltage, namely the voltage generator ground. In fact, for the line in Figure 4.22, the lower conductor is not, generally speaking, at the same potential than the reference conductor of the sweep generator. Thus, without the balun, the sweep generator would indeed provide a short-circuit connection between these two conductors. Furthermore, the balun is important since it filters out the common-mode signal superimposed on the ideally differential output of the sweep generator. Since the experimental results are to be compared with theoretical ones, the actual configuration has to be described to the simulator. In case of a differential excitation this task is easily carried out; on the other hand, for common-mode excitations that is far from obvious and varies according to a wealth of parameters not easily known. Therefore common-mode signals can invalidate the experimental results, or even worse, lead to think that the model cannot provide accurate results. In order to avoid such problems and have comparable results, a balun was included. The balun also had two low frequency decoupling capacitors symmetrically mounted, in order to protect the measurement equipment from eventual high voltages on the line. This is due to static charge distributions (in particular in floating overhead conductors) and current and voltages induced by nearby electrified lines.
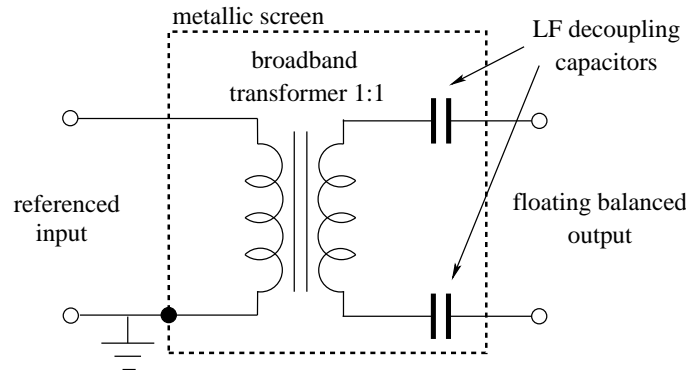

Figure 4.23.   The schematic of the balun.

The need for the voltage probe to have a high-impedance modulus is a basic requirement for all the voltage measurements. On the other hand, its being differential is required in order to avoid any influences of the measuring device on the system under test, for the very same reasons that led to the use of a balun for the line excitation, thus avoiding the excitation of common-mode currents between the reference conductors of the system uner test and the instrumentation.

The magnetic field is then measured by means of a screened loop antenna displaced along the line under test, for the three cartesian polarizations. Although this setup works reasonably well for the impedance, the magnetic field measurements are affected by sensitivity limitations. As a matter of fact, the passive screened loop antenna we used provided

107

output signals that were heavily affected by noise, showing just the resonance peaks above the noise background. This was due to the fact that the power generated by the sweep generator was limited to a few dBm, together with the limited sensitivity of the loop antenna.

Furthermore, this kind of measurements are intrinsically affected by problems due to external signals such as radio signals [69], picked up by the line under test acting as an antenna. The setup cannot discriminate between the signals coming from the excitation and those due to external interferences.

The simplest solution to this problem is to use a power amplifier as the output stage before the balun. This solution too has proven ineffective, due to mismatches at the power amplifier output port. As a matter of fact, a railway line is never matched, having usually open-circuited ends. Therefore, the input impedance seen by the power amplifier is mainly reactive, that is with a very high reflection coefficient. Under such conditions the output signal generated by the power amplifier undergo strong non-linear distortions that alter the frequency-spectrum of the excitation, due to protection circuits limiting the power reflected towards the amplifier. In order to avoid such distortions, the power actually injected into the line is nearly the same with or without the amplifier.
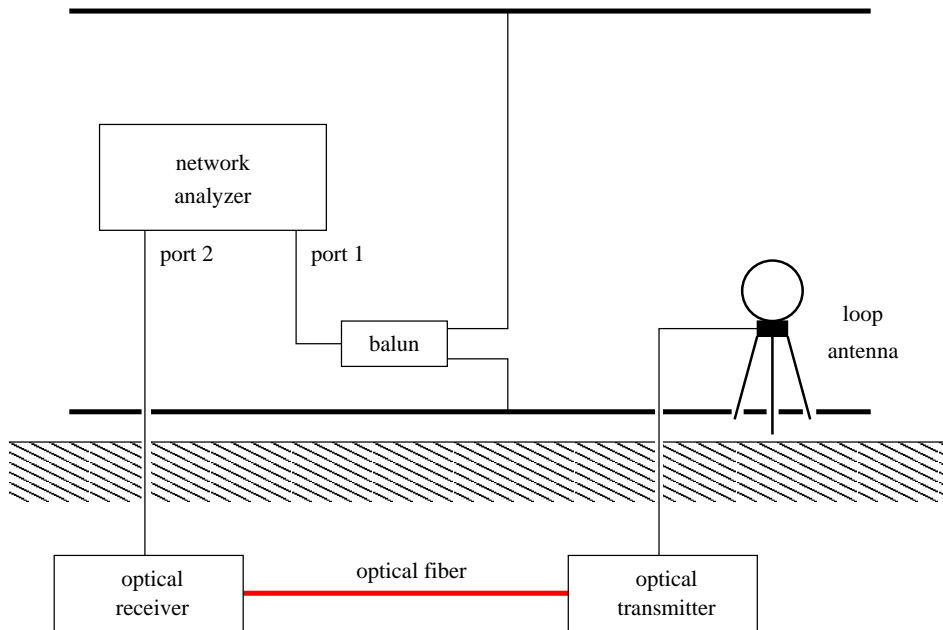

Figure 4.24.   The final setup employing a network analyzer, synchronizing the line excitation and the measurement.

An alternative setup, much more expensive, is shown in Figure 4.24. Here a two-port network analyzer is the core of the setup. In order to increase the overall sensitivity, the excitation and the magnetic field measurement are synchronized through the network analyzer phase-lock loop. This is easily achieved by mounting the balun on the first port, whereas the signals coming from the loop antenna enter the second port. Although the

loop antenna is the same as before, the overall sensitivity is greatly enhanced, because the phase-lock loop enables the network analyzer to "recognize" the signals due to the excitation rather than external sources. Moreover, the network analyzer ensures a noise rejection ratio reaching up 90 dB, thus strongly reducing the influence of thermal noise, thanks to averaging and filtering on very narrow frequency windows.

The balun is again employed and it should be included into the calibration chain, thus becoming invisible to the user. Its effects on the results are directly taken into account by the calibration setup: instead of standard calibration loads, low-end loads have been employed.

Another improvement in the setup is the use of an optical fiber link between the antenna and the network analyzer, rather than a coaxial cable link. Indeed, this synchronized configuration needs a long cable between the antenna and the excitation source. Actual lengths require about 100 m for the CEF site described in Section 4.6.3. Now, this would mean that the railway conductors run for 100 m side by side with the antenna coaxial cable, thus inducing currents on the coaxial screen conductor. These currents can modify the signals received by the network analyzer, thus distorting the magnetic field spectrum estimated from them. In other words, the coaxial cable would act no more just as a transmission-line, but it would also act as an antenna superimposing its signal to the one it should transmit. The optical link avoids all of these problems.

4.6.2 Outdoor mock-up line

The first experimental validation was aimed at verifying the accuracy of equations (3.71) for the computation of the p.u.l. parameters for a lossy soil. To this end, a simple line is the best configuration: results from more complex configurations may lead to flawed conclusions, since disagreements between the experimental results and the theoretical ones may be due not to errors in the p.u.l. parameters, but rather to an imprecise description of the actual system.

Unfortunately, as already mentioned, railway lines are accessed with difficulty and affected by tight scheduling. An easy solution to overcome this problem is the use of a simplified mock-up line, a procedure usually employed in laboratory tests before carrying them out on actual systems. The problem in this case is that the soil needs to be lossy, something that is not at all simple to be reproduced in a laboratory [51]. Thus, an open-area site has been considered, deciding to build an outdoor uniform line. It should be noticed that the aim is not to reproduce a scale railway line, but just to test the accuracy of the TLT. Furthermore, soil losses depend on the absolute values of the frequency and geometry, rather than on the electrical dimensions as for perfectly conductive structures. It suffices to remember that the electrical behaviour of the soil is set by the ratio ω/ω_c; now, a line scaled down by a factor two has to be studied on a frequency range multiplied by a factor two. This would alter the ratio ω/ω_c and the soil behaviour.

Therefore the tests should be performed in the same frequency range considered for actual railway systems, here limited to about 2 MHz. Nevertheless, due to practical reasons, the actual length of the mock-up line was limited to 30 m, whereas the wires height was limited to about 1 m. For such a configuration, the first resonance of the line

occurs around 2.5 MHz: therefore, in the original frequency range the line could not be considered as electrically long. As already shown in Section 3.7.1, the impact of the soil is more evident when the line is electrically long: in order to study such effects, it has been necessary to extend the frequency range up to 20 MHz, i.e. a line about two wavelengths long.
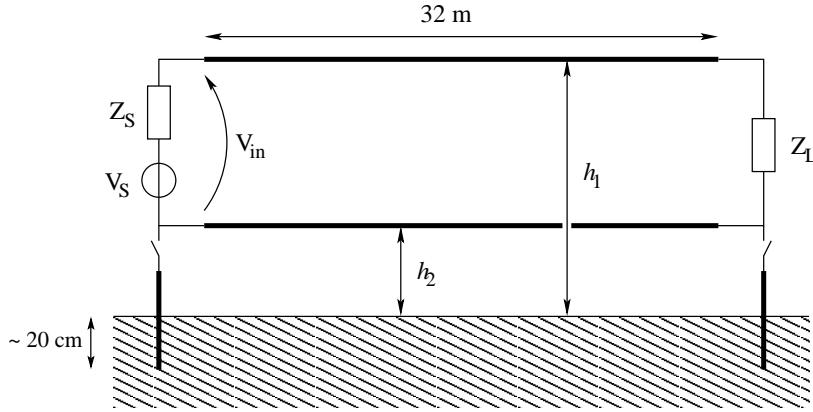

Figure 4.25.   The outdoor mock-up line in its more general definition.

The basic configuration of the mock-up line is shown in Figure 4.25. It has been built on a meadow in the backyard of the INRETS building in Lille, a French research institute on transport.

The 1 m height is compatible with the quasi-TEM approach even for the extended frequency range. Anyway, this configuration is basically different from an actual one, due to the extended frequency range; this implies that the dielectric nature of the soil will be more important.

The input impedance of the line has been measured for several configurations, changing the nature of the grounding connections at the line ends. For all of these investigations the model has shown a good agreement with the experimental results. The most important configuration is the floating line, with no grounding connections. As a matter of fact, in Section 2 it has been shown that actual railway systems mainly use this kind of configurations. Results are shown in figures 4.26 and 4.27, for $Z_L = 0\ \Omega$, $h_1 = 1$ m, $h_2 \simeq 15$ cm. The agreement is quite good, but on the impedance maxima. This is likely due to the fact that whenever the differential impedance (here investigated) gets higher, the input current comes to a minimum, so that it is more affected by common-mode currents, which therefore distort the impedance estimation.

These early validations were then followed up by investigations on the magnetic field. Since the most important model to be checked was the infinite line one, the antenna was placed in the middle of the line, which is the furthest position from the two ends. All of three polarizations have been measured, for a distance of 0 m, 2 m and 4 m, at an height of 70 cm and 1.70 m. Some results are shown in Figure 4.28 for the lateral component (along y), as measured at 2 m away from the line, 70 cm above the soil. The most important
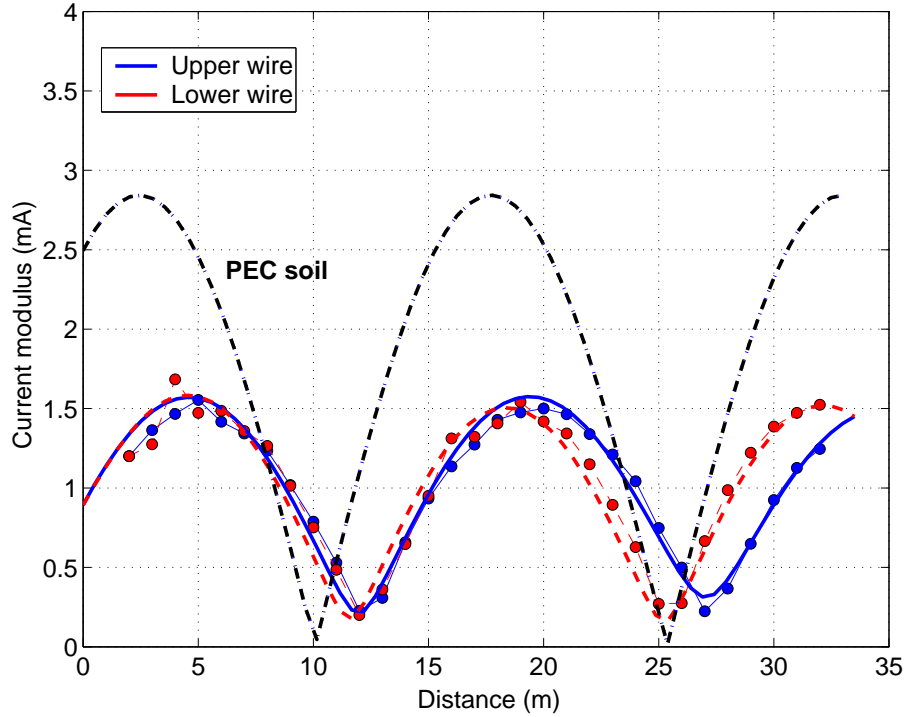
110

Figure 4.26.   The current distribution along the two conductors of the mock-up line for the floating configuration, at 9 MHz.

result is the good agreement on the magnetic field maxima. Indeed, as proposed in the next section, this is a basic requirement for applying this model in order to prove the impact of the infrastructure on radiated emission tests.

Another important result is also shown in Figure 4.29, representing the longitudinal component of the magnetic field. The agreement is quite good, and this result is important since it is directly related to the soil losses: a lossless soil would have been purely transversal (assuming lossless wires). Thus, this result allows a direct evaluation of the model ability to compute the field scattered by a lossy soil, at least in the frequency range here considered.

4.6.3   Actual railway lines

Several tests were carried out on actual railway tracks, since the first few months of this project. The aim had already been set as to experimentally characterize the site through input impedance and magnetic field measurements. Anyway, the most part of these experimental campaigns had just served as opportunities to test and fix the setup described in Section 4.6.1: indeed, this required a rather long trial and error approach which took the most part of the project duration. This, together with the rare opportunities to access to railway facilities, has strongly limited the number of reliable experimental results.
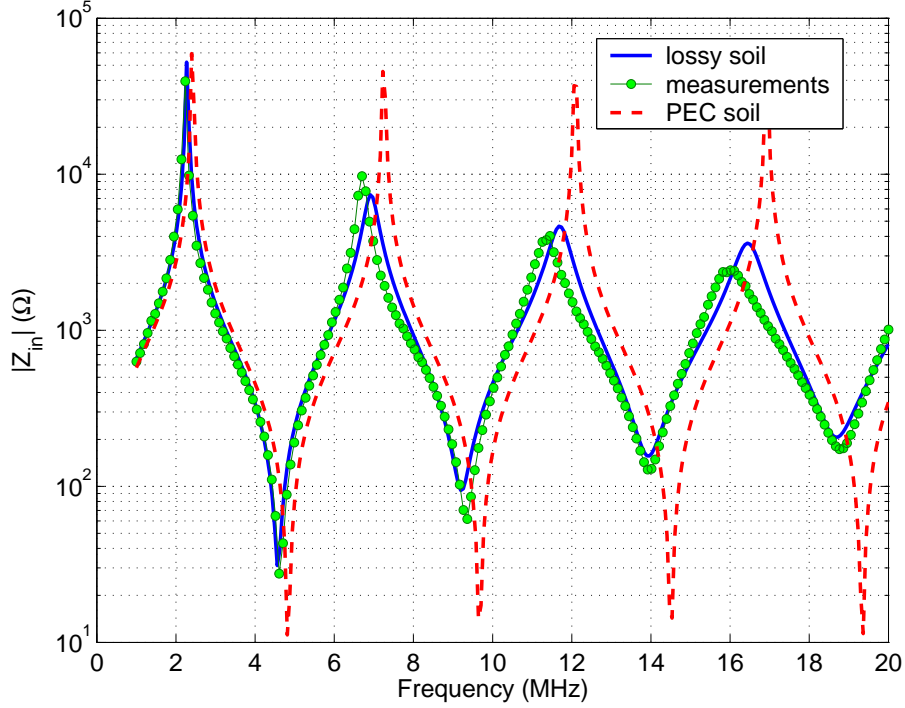
Figure 4.27.   The input impedance of the outdoor mock-up line for the floating configuration.

The results shown in this section refer to two sites. The first one is the already mentioned CEF, a railway test facility in Valenciennes, France; the second one is a test track within the industrial site of Alstom Transport, again in Valenciennes. The tests performed on these two sites are very similar, and they basically refer to the setup described in Section 4.6.1.

Centre d'Essai Ferroviaire (CEF)

The CEF is composed by several tracks mainly devoted to mechanical and acoustic tests of trains under construction; nevertheless, one portion of the so called VEV track is also employed in EMC tests. A functional sketch of this track is shown in Figure 4.30. The VEV is actually composed by three catenaries named S1, S2 and S3, with S2 and S3 short-circuited as in Figure 4.30, thus acting as a single track. A power substation feeds all the tracks in this site at the same time; but in this case its architecture is slightly different from the usual ones described in Chapter 1. This is due to the fact that the CEF is not limited to the testing of trains running under a specific supply, but rather it is able to accommodate all the main configurations currently employed all over the world. For this reason, the substation output is always generated by static semiconductors, even for the 50 Hz AC supply (cf. Figure 4.32). Two outputs of the substation are used for supplying the VEV track. In particular, the two main sections S1 and S2+S3 can be supplied under
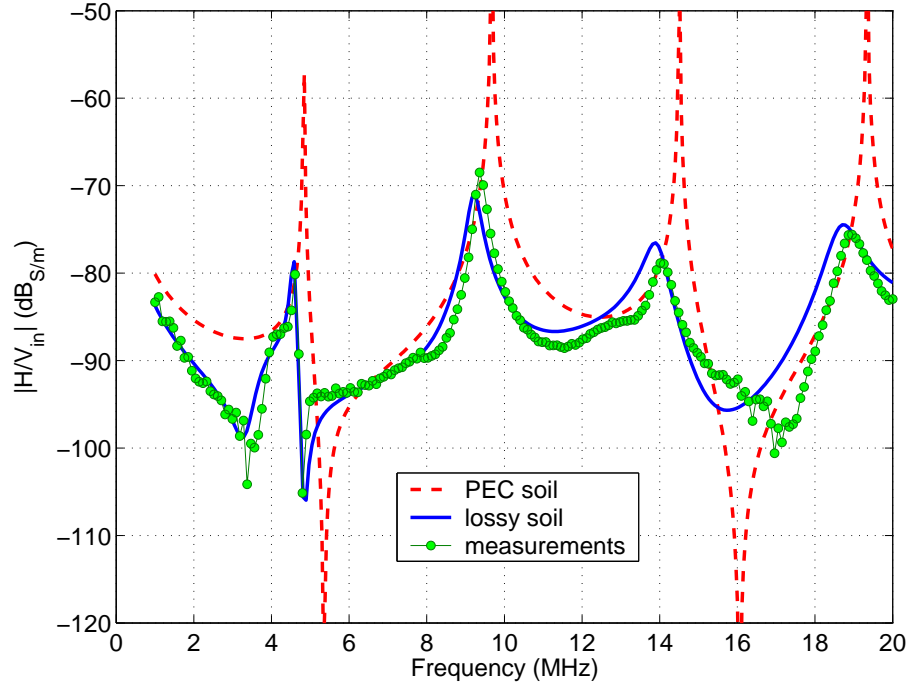
Figure 4.28.   The lateral component of the magnetic field as measured 2 m away from the mock-up line, 70 cm above the soil. Results refer to the floating configuration.

different voltages, an ability used for checking trains able to run under different voltage configurations.

The need to test trains running under different supplies has also led to a special type of catenary, shown in Figure 4.31. It allows strong currents to flow in it for DC supplies, maintaining a composite structure more typical of AC supplies.

In this case, applying the previously described setup requires due care. The two wires at the output of the balun should be connected to the catenary and the rails. Special attention has been paid at providing a good ohmic contact with the rails, by removing the layer of rust they were covered by. A sufficient pressure at these contacts has been provided by the vices shown in Figure 4.33a, the two rails have been short-circuited together through a further conductor. This configuration is actually realistic since the rails are usually short-circuited together at both the substation level and at the train wheels level, whilst usually maintaining a symmetrical structure. On the other hand, the connection to the catenary required the use of a special insulating hook pole shown in Figure 4.33b, with a wire screwed to the hook, in order to connect it to the excitation setup. The pole allowed a good connection only to the lower catenary conductors, but the droppers ensured the equipotentiality of the catenary wires, as already discussed in Section 4.1.1.

Before connecting the NA (or better the balun output) to the pole, special care has been required to temporary "ground" the catenary to the rails, by connecting a second pole between the catenary and the rails. This allowed a safer connection of the network
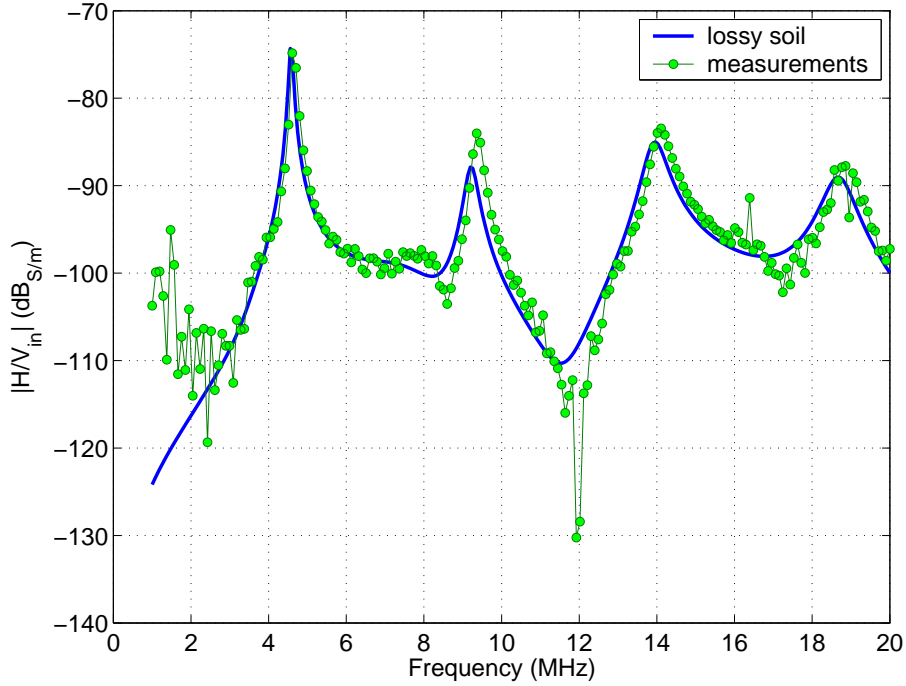
Figure 4.29.   The longitudinal component of the magnetic field as measured 2 m away from the mock-up line, 70 cm above the soil. Results refer to the floating configuration.

analyzer and the balun. As a matter of fact, the catenary is a very long floating wire, so that it acts as a quite big capacitance, whose potential can reach several tens Volts DC, with respect to the ground. Furthermore, the VEV track runs parallel to a TGV track for more than 1 km: since the distance between the two tracks is some 50 m, this 25 kV 50 Hz track induces about 100 V on the VEV track.

In this first experimental validation the network analyzer was placed just in front of the substation, whereas the loop antenna was about 120 m away. This choice was motivated by the presence of a wooden platform along the VEV, specifically built for antennas used in EMC tests. In particular this position is the only place along the VEV where it is possible to carry out field measurements 10 m away from the rails (1.6 m high with respect to the rails), as prescribed by the standards. On the other hand, a distance of 100 m between the excitation and the antenna has been chosen, in order to minimize the impact of the vertical wire connecting the pole to the network analyzer. As a matter of fact, it acts as a vertical antenna, much more efficient than the railway track, and near the rails its azimuthal component is orthogonal to the line, thus affecting the lateral component we are interested in. Furthermore, this arrangement allows to use energy sockets in the substation for supplying the instrumentation; and finally, only in front of the substation it is possible to park a small van for sheltering the instrumentation in case of adverse weather conditions, a major disrupting factor in outdoor tests in the French region Nord.

The VEV track was configured as follows: the substation was disconnected from the
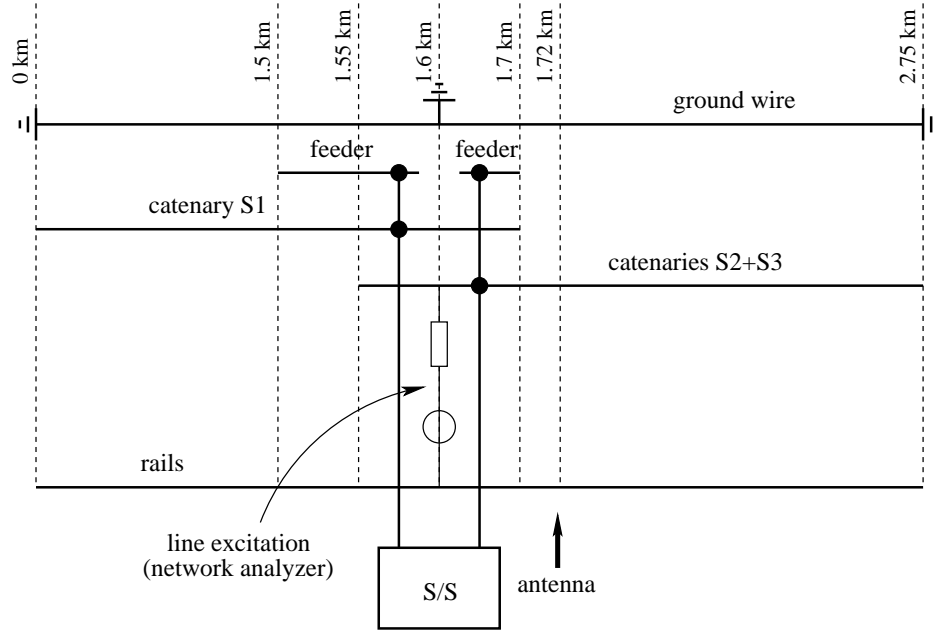
Figure 4.30.   A simplified description of the VEV track at the CEF.

two VEV catenaries by opening up sectioning switches at the output of the switched-mode converters, ideally leaving the catenaries as floating, but for a few meters of bar conductors inside the substation. The input impedance measured with this configuration is shown in Figure 4.34, together with the simulation results. The agreement stops at the first line resonance, whereas the second resonance takes place at different frequencies in the experimental (90 kHz) and the theoretical results (110 kHz).

Further investigations have shown that this disagreement was actually due to strong couplings in the "wiring" inside the substation. An experimental characterization of the substation was carried out with a network analyzer, by regarding the substation as a two-port device (cf. Figure 4.35) and measuring the impedance seen from these two ports under different conditions. The port not being measured was either short-circuited or left open. To this end, the substation was mechanically disconnected by the VEV catenaries. In the early description of the VEV track the substation was completely neglected due to its being assumed as disconnected from the catenaries. This example highlights the difficulty of applying a model to a real-life system, where it is not always possible to accurately describe all the relevant parameters. As a matter of fact, it is difficult to decide whether disagreements are due to flaws in the theoretical assumptions or just to a too much simplified (or inaccurate) description of the system.

Although a fitting procedure can be applied in order to derive an equivalent circuit representing the substation, the aim here pursued was to validated the railway track model, rather than to study the substation. For this reason, from that moment we always physically disconnected the substation from the catenaries. Anyway, up to 200 kHz the
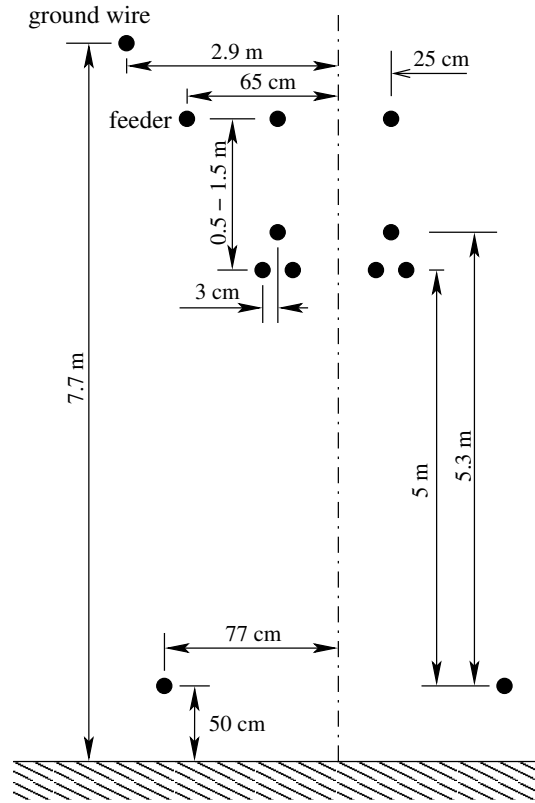
Figure 4.31. The cross-section of the VEV track (not in scale) near the substation, with the two catenaries running aside. Elsewhere, only one catenary is present. The radii of the wires are about 6 mm for the catenary conductors, 9 mm for the feeder and 5 mm for the ground wire.

substation can be modelled by the capacitive network in Figure 4.34a. This low frequency model has been included into the VEV model, obtaining the new results in Figure 4.34b, proving that the disagreements in Figure 4.34 were not due to the theoretical basis, but rather to an incomplete description.

Similar effects are expected for over-voltage protection devices: for instance, the equivalent capacitance of passive devices of this kind can exceed several μF, an enormous value that can easily modify the response of the entire site. Lack of information on the presence of such devices does jeopardize the very idea of modelling railway systems.

Another problem was due to the impossibility to use the optical link during the VEV campaigns; therefore we just used a BNC coaxial cable of about 120 m connecting the loop antenna output to the network analyzer. Anyway, in this case we are dealing with a further metallic conductor running parallel to the line under test for 120 m, at a distance of about 12 m from the line, which inevitably implies a non negligible coupling between them. For this reason the results of the characterization, shown in Figure 4.36, are limited to 500 kHz; here, the input impedance and the lateral component of the magnetic field are
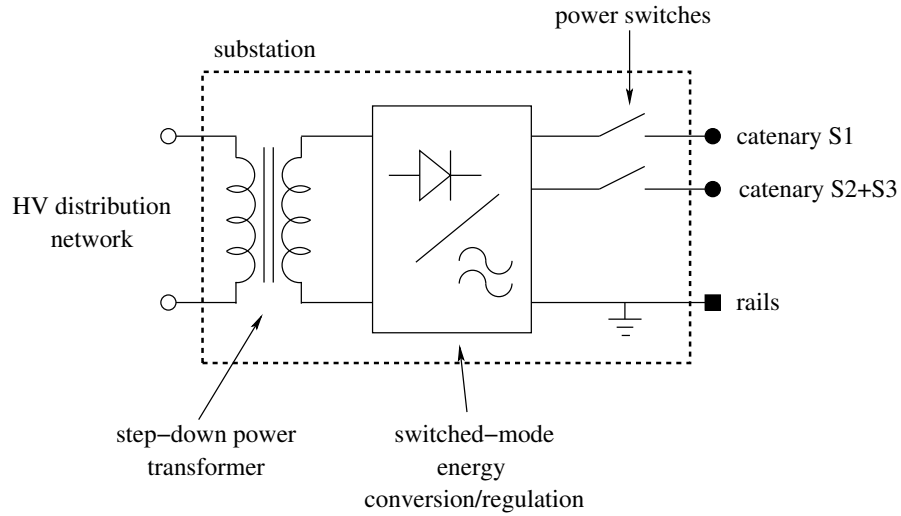
116

Figure 4.32.   A logical-block scheme of the sub-station at the CEF. The connections between the regulation block and the catenaries are implemented as metallic bars running for several tens meters.
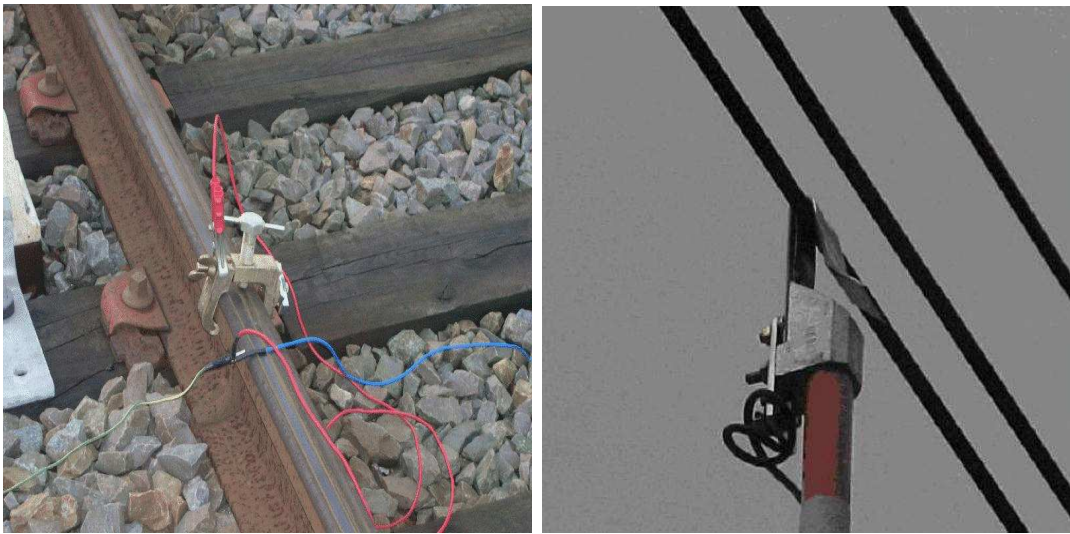
Figure 4.33.   The vices used for the connections to the rails (a) and the hook-pole for the catenary (b).

shown. The agreement with the theoretical results is fairly good; in particular, the model is able to assess the actual peaks in the magnetic field, whereas with an ideal soil there would have been a very important overestimation of these quantities. This point is fundamental, since the very idea of this project is to have a theoretical proof that the field maxima are due to the infrastructure rather than the train contribution. Therefore, it is vital that
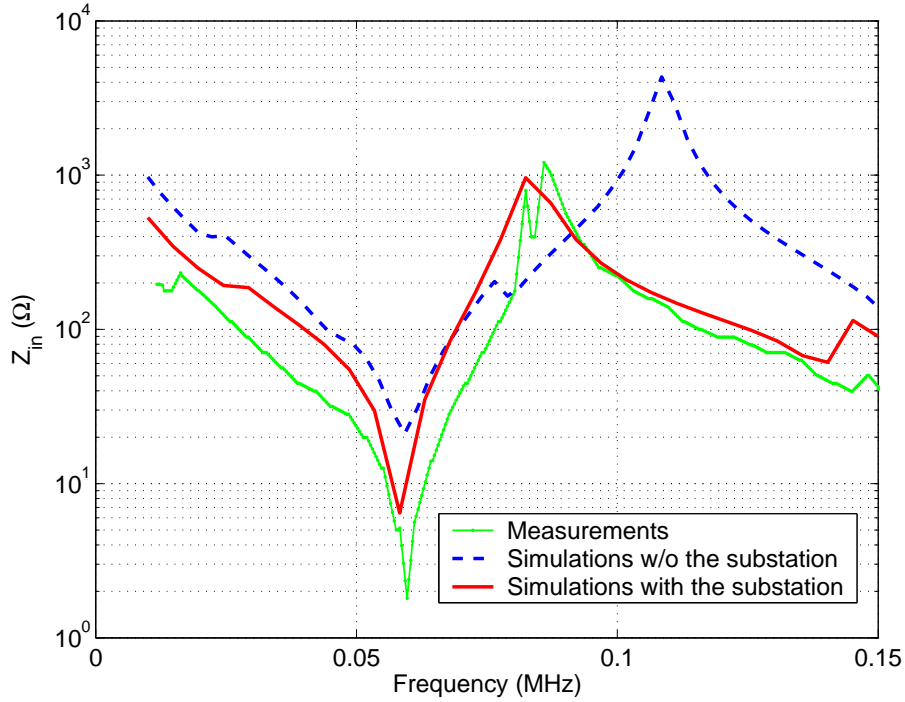
Figure 4.34. A comparison of the measured input impedance with the substation bars still connected, together with simulation results taking into account or neglecting the substation equivalent circuit.
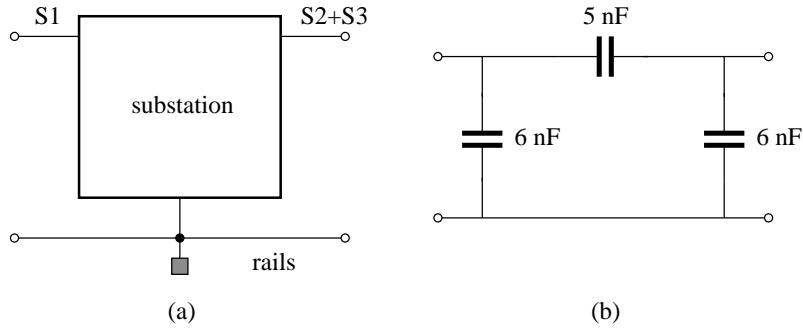
Figure 4.35. Experimental characterization of the substation internal bars (with energy-regulation circuits switched off): definition of the two-port equivalent (a) and low-frequency equivalent circuit (b).

the model be able to provide a good estimation of both the frequency of occurrence and the field magnitude around these maxima. It should also be noticed that these maxima are indeed quite strong with respect to the average magnetic field, due to the fact that we are dealing with a nearly reactive circuit, at least in the lower frequency range. As a

118

matter of fact, apart from power devices, a railway track is usually left unloaded, with very inefficient dissipative mechanisms, for reasons already mentioned in Chapter 2; under these conditions, the soil losses have a paramount importance. Therefore, considering the soil as an ideal conductor, the field maxima would be ideally unbounded, leading to a nearly useless model, unable to provide a realistic evaluation of these quantities.

Major disagreements occur above 400 kHz; this is likely due to an incomplete description of the VEV site, such as the lack of data about the overvoltage protection devices connected along the line and the grounding connections for the rails. As a matter of fact, the validation carried out on the Alstom test track Y12 (cf. next paragraph) yielded a better agreement, likely thanks to the simpler configuration. Moreover, the experimental results themselves are strange in this frequency range, where the trend of the magnetic field change quite abruptly. Maybe this was due to having used the coaxial cable.

Internal Alstom test track Y12

The procedure followed in this case was exactly the same as before. Nevertheless, this site had quite different features, a fact that is positive for an experimental validation, though some limitations are discussed later on.

The cross section is sketched in Figure 4.37: the catenary in this case is more similar to a DC configuration, while the most notable differences are due to the lower conductors. Here, four further conductors run parallel to the rails. The reason for their presence is the need to test trains rolling on pneumatic wheels, a solution usually employed in underground lines. These auxiliary conductors have different functions: the two nearest to the rails act as mechanical supports for the pneumatic wheels, whereas the other two are used by lateral wheels to keep the train in track. Obviously, testing underground trains requires a suitable supply, in this case a third rail running aside the lateral wheels guides.

In the experimental validation we were most interested in studying the line with the catenary, so that the third rail was kept floating. Furthermore, the auxiliary rails were periodically connected to the actual rails, with a spacing of about 20 m. The longitudinal configuration of the Y12 track is shown in Figure 4.38, again with the substation mechanically disconnected from the catenary.

Now, the problem with this line is the modelling of the auxiliary conductors. As a matter of fact, the actual rails are very close to the auxiliary ones, so that proximity effects cannot be neglected. To this end, the multiwire description applied to the rails (Section 3.4.5) has been used.

The tests were carried out with the setup shown in Figure 4.38: the distance between the excitation and the antenna loop was about 45 m, whereas the antenna was just 5 m away from the rails (1.4 m high with respect to the rails). This choice was due to the fact that in this case it had been possible to employ an optical link. Unfortunately, its length was limited to 50 m. The problem with this configuration is the increased importance of the magnetic field generated by the vertical wire exciting the catenary.

Some results are shown in Figure 4.39, for the open-circuited line. In this case, not only the catenary had been reduced to a single conductor, but also the auxiliary rails were divided in two groups and reduced to two single conductors, in order to avoid the
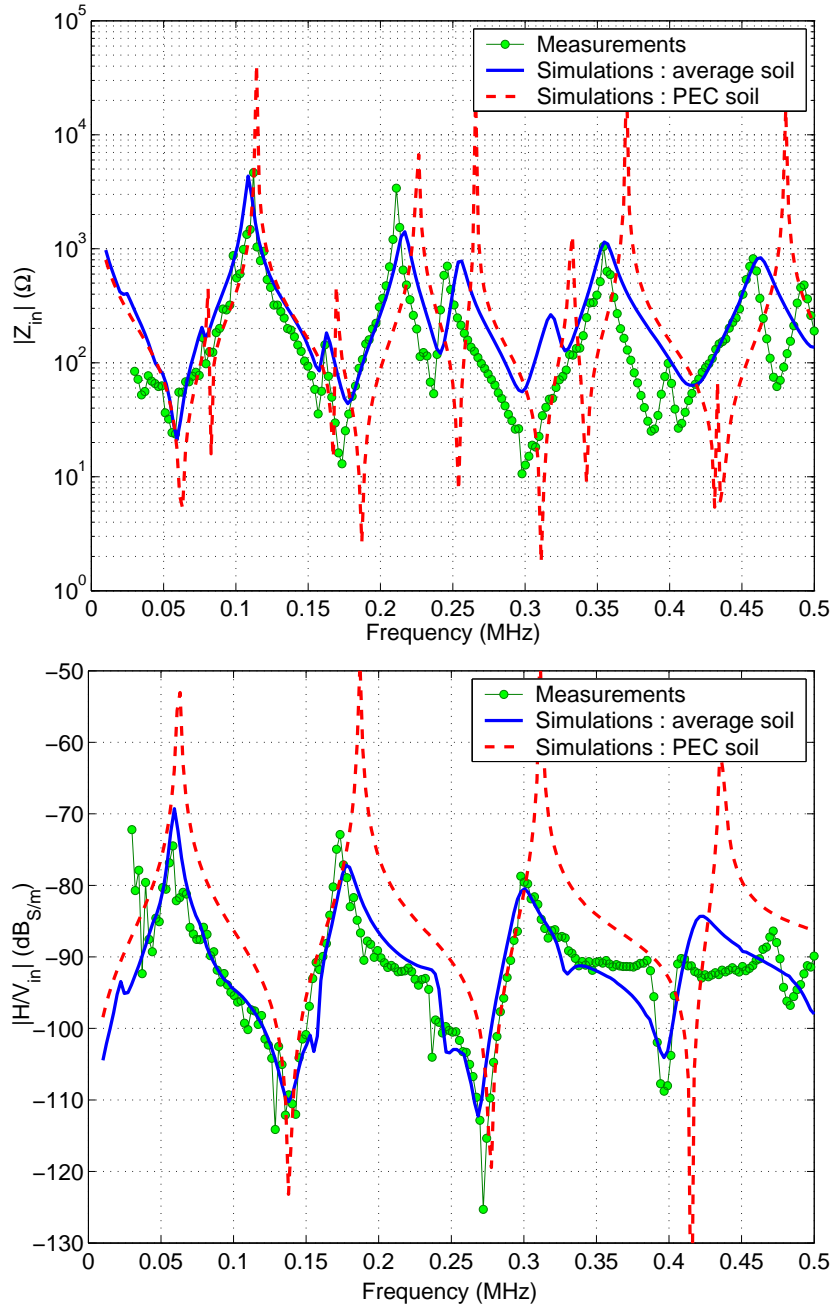
Figure 4.36. Validation on the VEV track at the CEF: input impedance (a) and lateral
component of the magnetic field (b) as measured 10 m away from the line.

description of the 20 m spacing connection with the actual rails. This solution has been
checked through simulations, showing no difference up to 2 MHz.
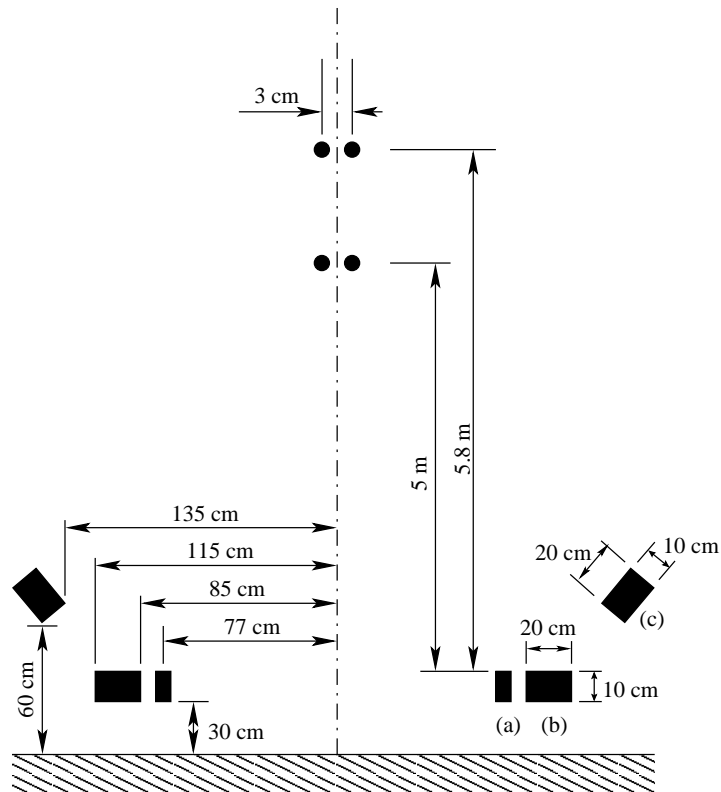
Figure 4.37.   The cross-section for the Y12 track inside the Alstom industrial site. The lower conductors are rails (a), auxiliary metallic bars for running train with tyres (b) and further metallic bars for lateral guiding wheels (c).
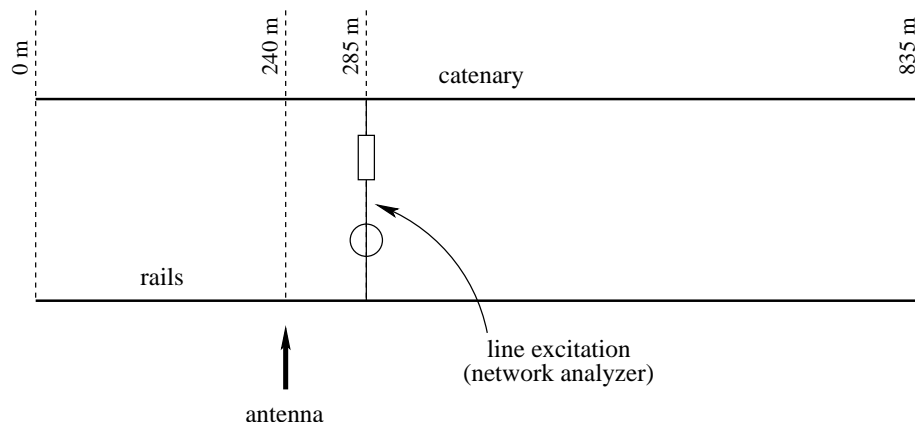
Figure 4.38.   A simplified description of the Y12 track.
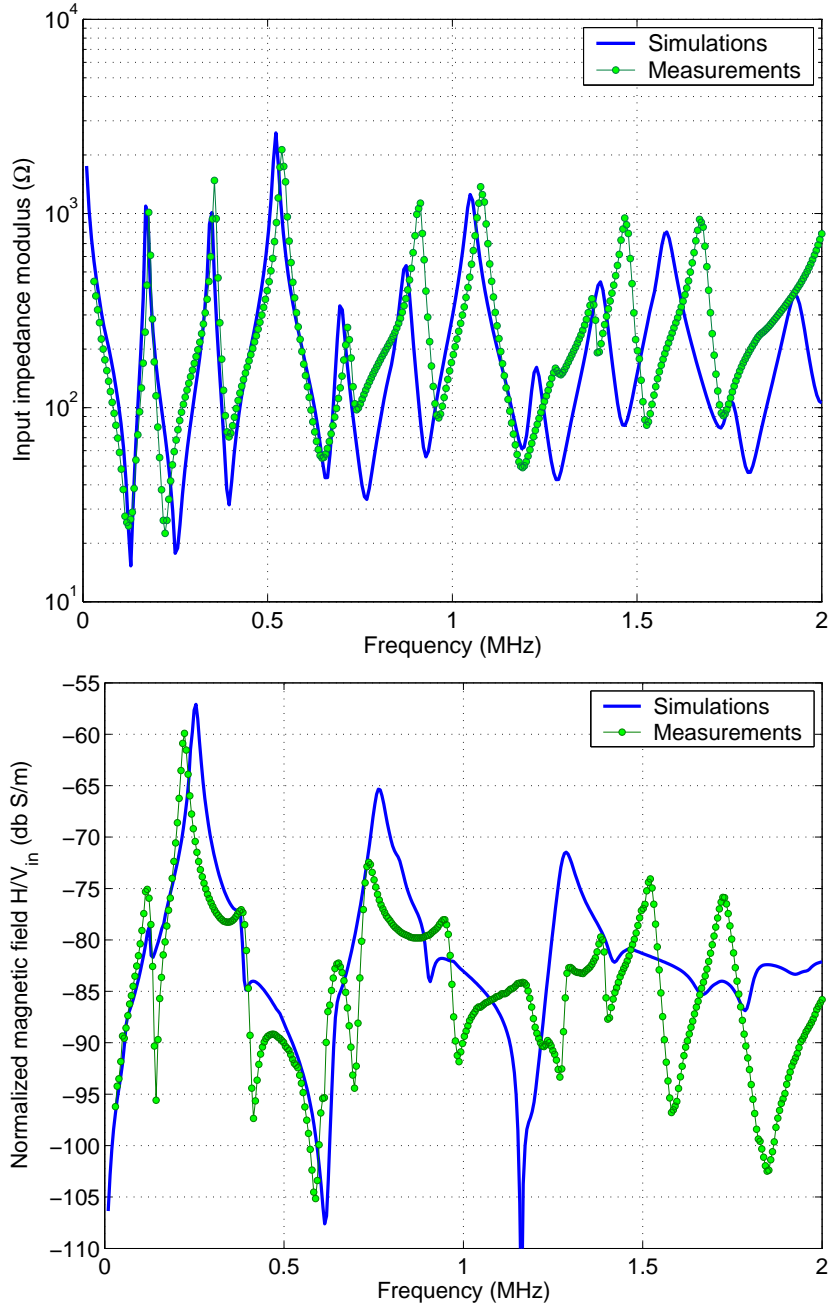
Figure 4.39. The validation for the input impedance (a) and the lateral magnetic field (b) for the Y12 track.

The agreement in this case is fairly good up to 1.2 MHz for the input impedance, except for a disagreement around 900 kHz. On the other hand, the magnetic field is validated only up to 700 kHz.

122

These results show once again the importance of the site description. In particular, detailed geometrical data were at hand for both sites, whilst nearly no information were available about power devices (substations), protection devices (overvoltage limitation circuits) and grounding connections for the rails at the substation level.

Assuming that the description fed to the model was accurate (which was not), the disagreements and limitations of the model are likely due to having neglected the effect of the ballast on the rails capacitance. This is the main discrepancy in the description of actual railway lines: thus, it would be necessary to include a description of the ballast, in order to extend the range of validity of the model.

4.7 Conclusions

In this chapter we have addressed the problem of applying the models introduced in the previous chapter to actual railway systems, according to the paradigm described in Chapter 2. Equivalent models for the discontinuities have not been investigated, since this topic would require a detailed study on its own; on the other hand, models introduced so far deal with uniform lines, with actual lines presenting non-idealities in this respect. To this end, droppers, masts and the ballast have been introduced, showing how their modelling can be simplified, while assessing the effects of such approximations. In particular, we have shown that a multi-wire overhead line can be effectively reduced to a single-wire line without losing in accuracy. Further simplifications have been introduced, based on an approximated modal description, especially effective in the computation of the magnetic field.

Since the magnetic field computation is based on the knowledge of the current distribution, this subject has been addressed, introducing the tableau method. Furthermore, we have shown that over a certain frequency range it is possible to limit the description of the site up to a certain degree, thanks to the attenuation introduced by the finitely conductive soil. This analysis has been used for assessing the validity of some basic assumptions in the standard EN 50121, proving their inaccuracy.

Besides, we have carried out a sensitivity analysis, in order to assess the criticality of the description accuracy, proving that inaccurate information on the length of a line have a strong impact on simulation results. On the other hand, the magnetic field has been shown to have a low sensitivity with respect to soil electrical properties; unfortunately, this is compensated by the great uncertainty in the soil conductivity, so that this parameter requires due attention.

Finally, results from experimental tests have been used for validating the models so far discussed. In particular, we have described the experimental setup employed for the characterization of a railway site, pointing out some major practical problems of this task. The results have shown the model to be fairly accurate up to about 700 kHz, thus partly satisfying the targets set at the beginning of this work.

Limitations in the frequency-range of validity are regarded as due to having neglected the impact of the ballast on the rails capacitance.

Chapter 5

Assessment of infrastructure impact

The model developed and validated in the previous chapters will be here applied to the problem introduced in the first chapter, namely the assessment of the overhead infrastructure impact in radiated emissions tests. It will be shown that this latter plays a major role, proving that a basic flaw is inherent in the standard EN 50121, pointing out the possibility to identify infrastructure-related field maxima. This possibility, being based on an ideal description of the site, its actual implementation is rather critical. To this hand, an alternative approach is proposed, based on an experimental characterization of a railway system through magnetic field measurements.

5.1 Contributions to the magnetic field in radiated emissions tests

Let us consider the system depicted in Figure 5.1: a train is supplied along a railway track, which is part of a railway system, as described in the first chapter.

As required by the standard EN 50121-3, the magnetic field is measured in front of the train, 10 m away from the track axis, thus giving a characterization of the train radiated emissions. This definition makes sense from the point of view of a potential victim, such as a telecommunication line, where we are interested in ensuring a limit to the maximum magnetic field, thus limiting its interference potential. As given in the standard, this definition seems to understate that this procedure assures a proper characterization of the train contribution. Actually, this idea neglects the contribution of the infrastructure, which can lead to an important overestimation of the train contribution.

In order to understand this statement, let us analyze, in a very simple way, the phenomena underlying the generation of radiated emissions. From the train point of view, the supply line ensures a certain voltage between the catenary and the rails. Although this voltage is not constant, its variability range is well defined along the entire railway system and set by the infrastructure, that is by the distribution of substations, the number of trains running along the same line, and so on. On the other hand, the input stage of the
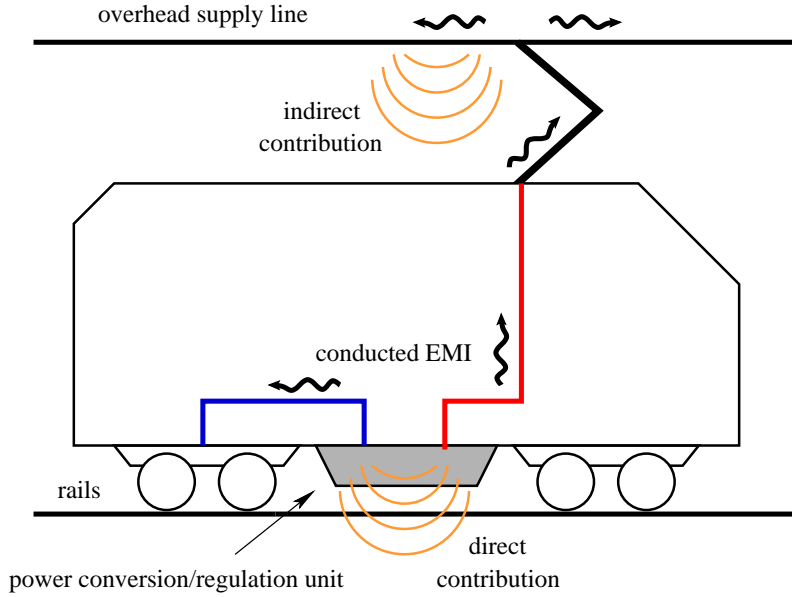
Figure 5.1.   A schematic representation of a train supplied along an electric railway line.

train, just after the energy-collecting pantograph, is basically constituted by a switched-mode converter, whose aim is to adapt the energy provided by the supply line into different forms, as required by the several users on-board of a train, such as traction motors and the signalling and control electronics. Obviously, nearly all the energy is used by the traction system which, accordingly to the actual architecture, can drain up to several MVA. The voltage is modulated, by means of fast-switching power transistors, with transition fronts of a few score nanoseconds. Therefore, very steep current and voltage derivatives are generated, which ultimately lead to important conducted emissions that propagate throughout the entire train. In this respect, a very important point is that these spurious signals are independent of the infrastructure, since they only depend on the voltage applied between the pantograph and the train wheels, and to the modulation employed by the switched-mode converter, together with the power drained by the train. This allows a different paradigm to be introduced, where the train input stage is regarded as a sort of conducted emissions generator in the frequency domain (cf. next section).

Two possible propagation-paths can be identified for conducted emissions, as shown in Figure 5.1: one is toward the supply infrastructure, whereas the other is within the train itself. Considering this latter case, spurious signals propagate through the train cabling, generating an electromagnetic field. This is a direct contribution of the train to the overall magnetic field measured during radiated emission tests; due to the nature of this contribution, i.e. due to conducted EMI almost independent from the test site, it is indeed an index of the train compliancy.

On the other hand, the other propagation path is towards the supply line which, acting as a horizontal antenna, radiates an indirect contribution to the magnetic field, depending

on the particular pattern of currents along the track conductors. The actual pattern is not entirely set by the train itself, which acts as a mere excitation source, but rather by the environment where the train lies. In fact, conducted emissions are subject to the reflections introduced by discontinuities connected to the railway tracks, thus modifying the actual current distribution along the supply infrastructure: therefore, the results of the radiated emission test are dependent on the actual infrastructure where the train is being tested. This alone is an indication of the fact that the standard definition is quite poor, since the results thus obtained are not directly comparable to results obtained on another site.

But the main flaw of the standard lies in the fact that the reflections along the infrastructure lead to resonances, which can amplify the radiation for some frequencies. Now, the standard regards the train under test as directly responsible for the field measured, which is in contrast with the fact that the field depends on the site infrastructure where the train is being tested.

Actually, this possibility is addressed in the standard, which requires the site to approximate an infinitely long line. In other words, the site infrastructure should not generate reflections for the signals propagating along its conductors. Since such a facility does not exist, the standard provides guide-lines for reducing spurious effects; in particular, it requires the line to have a minimum clear length of 3 km on both sides of the measurement point.

The main reason for providing such guide-lines is to ensure the comparability of test results performed on different sites. Actually, this is not the case, since the 3 km length does not suffice for ensuring low reflections. As shown in Section 4.4, the results in Figure 4.18 prove that the 3 km limit is valid only above 1 MHz, whereas for lower frequencies this length can attain several hundred kilometers. Anyway, as mentioned in the first chapter, the distance between two substations is usually limited to a few 10 km, so that in the low-frequency range the reflections they introduce are not attenuated enough. One could wonder about the existence of other mechanisms which could reduce reflections, such as resistive loads. Anyway, the very idea of a supply line is to transfer power from a source to the user, and resistive loads (other than trains), would increase the insertion losses of the supply line. Therefore, this structure is ideally purely reactive or, in other words, highly mismatched.

These considerations hold even in the case of the presence of other trains on the same line used for the tests. First, the input impedance of the train is not designed for this purpose, since it must ensure a good power transfer for the DC or AC supply. Second, even though the train ensured the line matching, this would reduce reflections only when it is at the end of a uniform line.

This scenario is worsened by the fact that the spectra of conducted EMI generated by switched-mode converters for traction has the most important harmonics below 1 MHz, so that there is a concrete risk of having harmonics amplified by the infrastructure resonances, whenever the two phenomena occur at the same frequency.

Moreover, a further source of confusion is the presence of harmonics not due to the train under test, namely conducted EMI generated by substations and other trains and power devices connected to the same supply line. As a matter of fact, it has been shown

that the attenuation of the line is very low below 1 MHz, so that signals injected several kilometers away from the train under test, have the same importance as they were injected just near the train. However, this problem is addressed by the standard, which advices to perform a magnetic field measurement with the train not connected to the supply-line. The result thus obtained is referred to as ambient noise, and it allows to assess the importance of EMI (both conducted and radiated) not related with the train.

Therefore, we can conclude that the guide-lines provided by the standard do not suffice for ensuring site-independent tests. In particular, the magnetic field measured during these tests is not only due to the train, but it is also affected by the actual configuration of the site, so that, paradoxically, a train standard-compliant on a site, may be non-compliant when tested on another one. Eventually, the limits imposed by the standard do not take into account these phenomena, having assumed that fulfilling the guide-lines ensures low reflections. Therefore, by comparing the test results to these limits, we are making a systematic error.
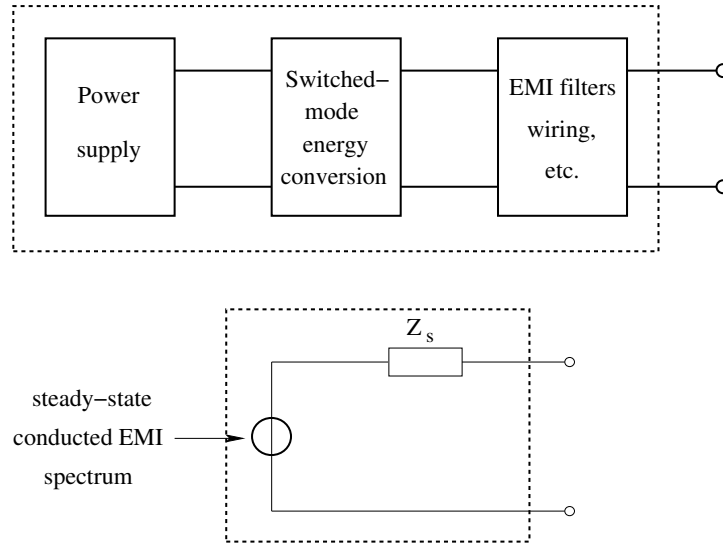
Figure 5.2.   Steady-state analysis of a switched-mode energy converter/regulator: a logical-block description (a) and a frequency-domain equivalent circuit, with the independent source accounting for the non-linear parts of the circuit.

5.2   Steady-state analysis of switched-mode converters

This description is mined by the fact that we are trying to describe a switched-mode converter, entirely based on non-linear devices, through a frequency-domain equivalent circuit, which is based on linearity assumptions. Nevertheless, such approach is valid in a steady-state analysis, as in this context. In particular, non-linear circuits performing modulation/regulation can be analyzed by means of Fourier series [70, 71], assessing the spectrum of the conducted emissions they generate, according to the modulation scheme

they implement. The resulting spectrum is almost independent from the load characteristics, but for the power factor seen by the switched-mode circuit [70].

Referring to Figure 5.2, switched-mode converters can be represented, for the sake of conducted EMI, as an independent generator in series with an impedance Z_s. While the generator accounts for the conducted EMI, the impedance Z_s represents all the remaining linear parts of the converter, such as wiring, EMI filters and so on [2, 72, 73, 74]. On the other hand, it is also possible to apply a time-domain analysis to the system, thus allowing the inclusion of non-linear circuits, as already mentioned in Section 3.4. Anyway, this goes beyond the scope of this work.

5.3   Assessing the infrastructure impact

Assuming to have a description of the equivalent circuit for the conducted EMI injected by the train into the catenary, it is straightforward to assess the impact of the infrastructure on the indirect contribution to the magnetic field. As a matter of fact, the model introduced in the previous chapters can be applied to a description of the actual site, as to the ideal site required by the standard. This latter case can be easily simulated by terminating a uniform line, with the same cross-section as the actual line, by its characteristic impedance matrix.

The infrastructure impact $W(f)$ is here defined as the ratio H_a/H_i, where H_a is the magnetic field measured for the actual site and H_i for the ideal one. The lateral component of the magnetic field is hereafter considered. We define the transfer function $\beta(f)$ of the site as

$$H(f) = \beta(f) \ I_{in}(f) \tag{5.1}$$

where I_{in} is the current injected by the train through the pantograph. Recalling that the equivalent generator for conducted EMI is almost independent from the site, it is possible to express the infrastructure impact as

$$W(f) = \frac{H_a(f)}{H_i(f)} = \frac{\beta_a(f)}{\beta_i(f)} \frac{Z_s(f) + Z_{in,i}(f)}{Z_s(f) + Z_{in,a}(f)} \tag{5.2}$$

where $Z_{in}(f)$ is the input impedance of the track, as seen from the train between the catenary and the rails. This kind of approach has the advantage of not requiring the knowledge of the excitation generator, but just of its internal impedance.

An example of results obtained with this procedure is shown in Figure 5.3, where the actual site is a uniform track 3 km long, with open-circuited ends, and the train placed in the middle of the track. As usual, the cross-section refers to the configuration described in Appendix B; the same cross-section has been considered for the ideal site. It is interesting to recall that in this latter case the computation of the current distribution does not require to consider a specific length for the track. In fact, having defined it as matched, the current-distribution is imposed by the source and the line cross-section, through the modal description of the propagation.

The internal impedance Z_s of the train has been assumed to be inductive, considering the two values j50Ω and j250Ω. These values are not meant to be representative of an

actual train, they are just considered as an example for discussing the infrastructure impact $W(f)$.
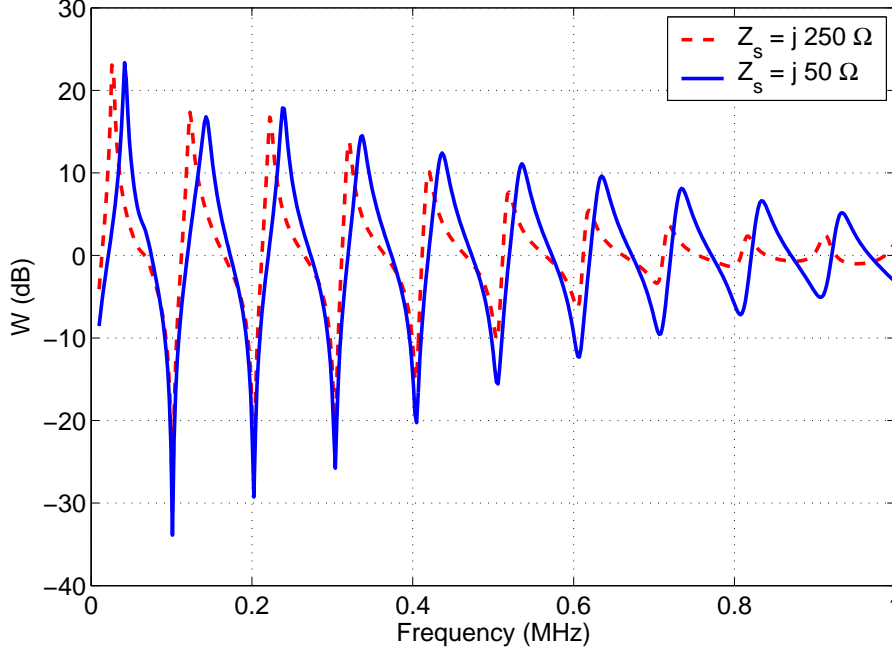

Figure 5.3.   Distortion factors showing the infrastructure impact for an open-circuited line 3 km long, with the train in the middle of the track. The magnetic field has been computed 10 m away from the line, 2 m high above the soil, 50 m at the right of the train. Two equivalent internal train impedances have been considered.

The results in Figure 5.3 are quite self-explaining; indeed, the resonances can distort the results of the radiated emissions test, in two respects: the most evident effect is the increase in the maxima, which can easily exceed 10 dB. But this is not the only effect, since whenever conducted emission harmonics occur at the same frequency of minima in the transfer function, their importance can be underestimated.

This kind of analysis can be easily applied to actual measurement campaign, in order to have a reference to ascertain the possible impact of the railway site where the train is being tested. Obviously, this procedure can be applied only to the indirect contribution due to the supply-line, and not to the direct contribution due to the train. To this end, it is possible to assess the relative importance of these two contributions by measuring the magnetic field in front of the train and at a certain distance from it. This is possible since the indirect contribution is not strongly affected by the distance from the train, whereas for the direct one the distance is very important, since it acts as a point source.

Besides, it is not possible to apply the model to compute the magnetic field in front of the train, since it cannot take into account the train chassis, which acts as a metallic scatterer. On the other hand, the indirect contribution can be evaluated a few meters away along the longitudinal direction, as long as this displacement Δz fulfill the condition

$\Delta z \ll \lambda$. An example is shown in Figure 5.4, for the line previously described, for $\Delta z = \{10,20,50\}$ m: indeed, the results are very similar up to about 400 kHz. Therefore, the spectra measured at 10 m and 50 m can be compared, highlighting the indirect contribution and the maxima due to the infrastructure. Once these alleged infrastructure resonances are identified, their nature can be checked by means of simulations, by applying the model developed in the previous chapters. Thanks to the fairly good validation, if the site is accurately described, the model should be able to reproduce the same resonances, thus proving the infrastructure contribution to the overall magnetic field.
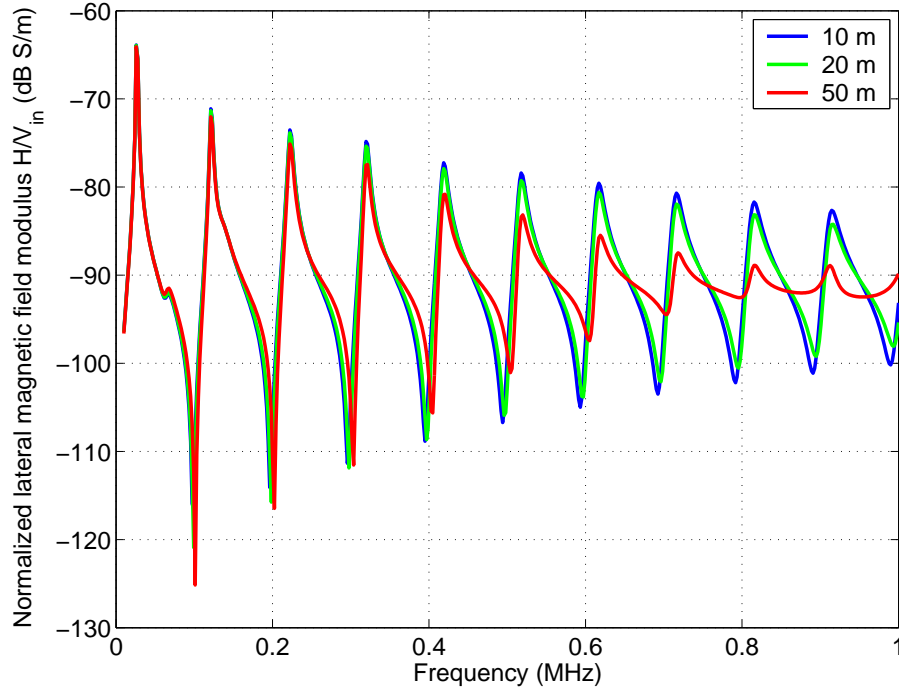
Figure 5.4. The magnetic field computed for Δz equal to 5 m, 10 m and 50 m away from an ideal voltage source in the middle of a 3 km long, open-circuited line (cf. Appendix B).

The procedure here described is based on the assumption of having a good knowledge of the topology and geometry of the actual site. Unfortunately this is hardly the case: as a matter of fact, in real-life situations, the customer requires the manufacturer to perform radiated emissions tests on its own site, for which the manufacturer has nearly no access to a complete and accurate description. Usually, the only information available is the nominal voltage of the power-supply, the distance of the train from the nearest substations and a rough description for the cross-section of the supply-line. Other important information, such as the capacitance and conductance of the power isolators, the connections of the masts to the ground or the soil, eventual grounding connections for the rails etc., are hardly available. It goes without saying that more advanced information such as equivalent circuits for substations and power devices are not known even to the site-owner.

131

Furthermore, as shown in Section 4.5, the current distribution and therefore the magnetic field are very sensitive with respect to the line length. In particular, errors of several hundred meters are usually regarded as negligible for lengths of several tens km, so that above a few kHz it is very likely to have errors of a quarter wavelength, clearly resulting in catastrophic errors on the resonances occurrence.

Nevertheless, predictive simulations can be usefully employed in order to have a practical assessment of the expected effect of the infrastructure, estimating the intensity of the resonances through tentative descriptions. Furthermore, predictive simulations can also be used for other applications, mainly on a more speculative level, for studying propagation and radiation phenomena in a railway system.

5.4 Feasibility study of an experimental characterization of a site

The difficulties in providing an accurate description of the actual site is obviously a major limitation to the use of the model as proposed in the previous section: there, the model had been employed for predictive simulations. Nevertheless, it is possible to conceive a different approach for assessing infrastructure impact; as opposed to the predictive characterization of the actual site, we try to define an experimental characterization, based upon measurements.

To this end, let us consider a portion of the actual site where the supply-line can be easily described, for instance along a uniform track, where no power devices are connected to it or, in the other case, an accurate equivalent circuit is available. In the following discussion we will consider the line as uniform, for the sake of simplicity; anyway, the same approach can be applied to more general cases, as long as equivalent circuits are available.

We consider a uniform track, long enough for applying the infinite-line radiation model, used as a reference. Electrical-circuit theory ensures that portions of a linear network, identified through a certain number of terminals, can be substituted by equivalent circuits. The equivalent representation we are going to use in this section is the multi-port formulation of Thevénin equivalent circuit, defined as:

$$\mathbf{V} = \mathbf{Z}\mathbf{I} + \mathbf{V}_s \tag{5.3}$$

where $\mathbf{V}$ and $\mathbf{I}$ are respectively the voltages and the currents at the terminals of the equivalent circuit, $\mathbf{Z}$ is the equivalent impedance matrix and $\mathbf{V}_S$ is a vector of source terms, accounting for independent sources inside the circuit portion to be replace by the equivalent representation. This idea can be applied to the actual line, where the train is being tested. In particular, the uniform portion of line previously introduced "sees" two equivalent circuits through its two ends, as in Figure 5.5. Applying this idea implies that the railway system can be regarded as linear.

The problem is how to estimate these equivalent representations. The idea here pursued is to use measurement results: the obvious advantage is that no previous knowledge is required about the railway system, while the equivalents would take into account the entire
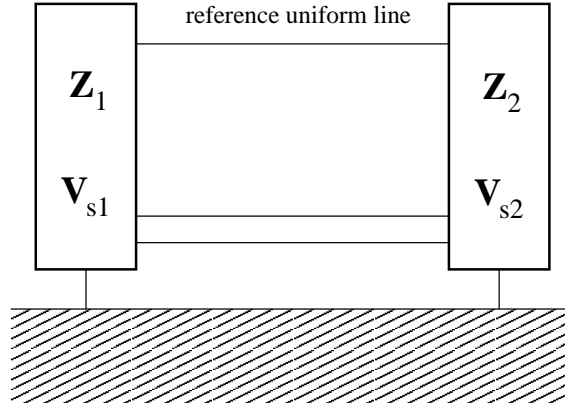
Figure 5.5.   The equivalent sought, based on a reference uniform line portion.

system, including source contributions due to substations and other trains connected to the supply infrastructure. Indeed, for predictive simulations the inclusion of such devices is not easy. On the other hand, measurements always hold the risk of making systematic errors, which can be hardly detected without a proper modelling, exactly what we are here trying to avoid.

The most direct way of estimating the two equivalent circuits would be to measure voltages and currents at the ends of the uniform line, or just currents for several configurations, in order to have enough data for estimating all the parameters of the equivalent representations. Although this is possible in investigations carried out in a railway facility, such an approach could not be proposed in an industrial testing, due to obvious security reasons, since the sensors would be very near to conductors subject to high voltages. Furthermore, special instrumentation would be necessary, not just low-end current-probes usually employed in industrial tests, but rather ad hoc solutions for measuring currents in rails and in catenary conductors. Solutions to this approach have been successfully proposed in [75], by developing special sensors; there, security problems where bypassed by mounting the current sensors for the overhead conductors on the masts, actually modifying the supply line. This approach is therefore more suited to facilities rather than to temporary testing on commercial sites, where usually it is not possible to disconnect the supply-line from substations.

The idea we propose here is to use magnetic field measurements for estimating the two equivalent circuits. Such an approach would be very attractive, since no security problems could arise, together with the fact that very simple instrumentation would be necessary.

The estimation of equivalent circuits from magnetic field measurements implies solving an inverse problem: indeed, this is exactly the opposite idea pursued in predictive simulations. This kind of approach is currently used in many practical problems, for instance in scattering problems [76], and it requires due care in the definition of suitable mathematical tools. Anyway, the aim of this work was not such study, but rather to check its feasibility: therefore, the approach we have considered is indeed very simple and in some measure

133
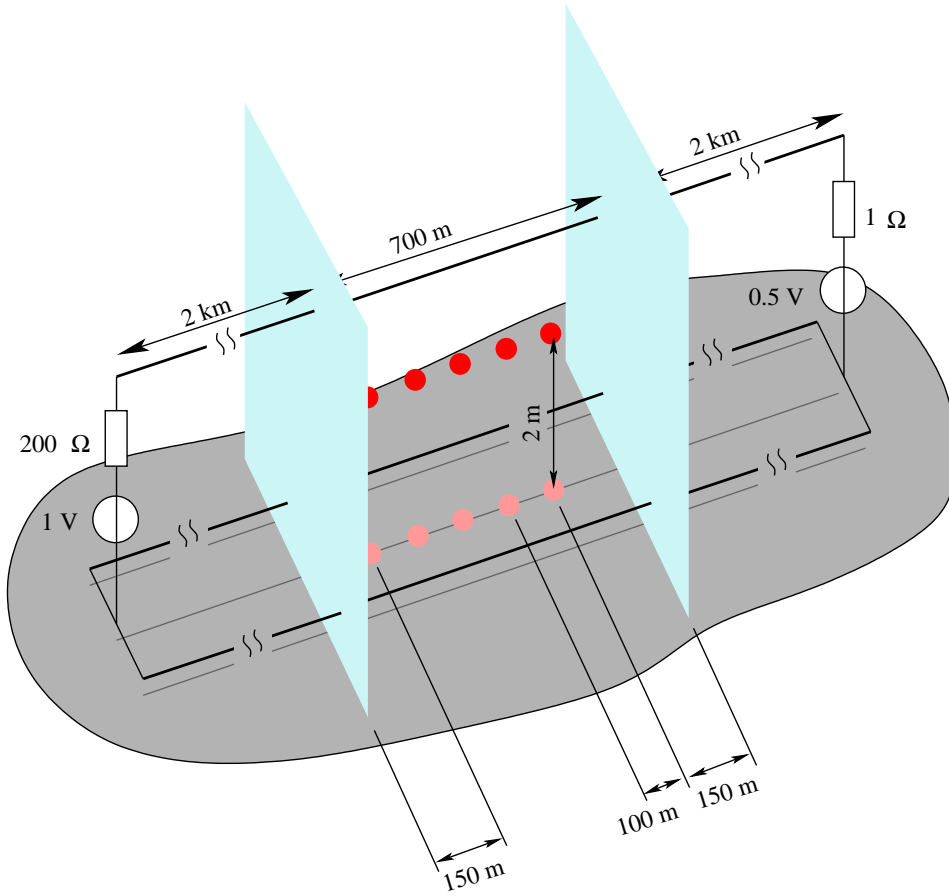
Figure 5.6.   The three-wire line considered for the numerical validation of the site characterization approach. The reference uniform line is defined by the two reference planes, together with the five positions where the magnetic field is sampled.

naive. Because of that, we regard this part as a feasibility study, rather than a complete work.

Since the aim is to characterize the site, the train under test should not be connected to the catenary. This means that the magnetic field measured for the equivalent circuits estimation is generated by the current distribution excited by conducted EMI injected by other power devices connected to the same supply-line. With this respect, this method exploits the sources of ambient noise; clearly, this implies to have a magnetic field spectrum far from flat, so that only some samples will be actually usable, corresponding to conducted EMI harmonics. Moreover, measurements will also record the contribution from faraway radio transmitters: here, the only possibility to distinguish them from the site contribution is either to apply previous knowledge (e.g. to know the frequencies they emit at), or to applying signal processing techniques trying to identify them. The most simple idea is to consider narrow peaks far above the average background noise as due to radio transmitters.

Anyway, external radiation source would just affect the experimental results at discrete frequencies, which are expected to be a negligible set with respect to the entire frequency range under investigation.

As already mentioned in Section 4.1.1, a railway line can be effectively described as a three-wire line, considering a reduced single-wire catenary. Therefore, the number of terminals in the two equivalent circuits is equal to three, plus the reference conductor. Hence, the number of parameters that can be assumed as independent is six for each matrix impedance (due to the reciprocity of a linear network) and three for each source vector, that is a grandtotal of eighteen parameters to be evaluated. Anyway, this number can be reduced by means of symmetries in the line configuration. In particular, the two terminals representing the two rails are assumed to be symmetrical, so that only four terms are required for each impedance matrix and two for each source vector, for a grandtotal of twelve parameters.

Constraints have been imposed on the impedances, requiring the two terminations to be passive (excluding independent sources already described in the vectors $\mathbf{V}_s$). To this end, it suffices to impose the matrix $\mathbf{Z} + \mathbf{Z}^{\mathrm{H}}$ to be positive defined, that is with positive eigenvalues [77]; the mark H indicates the conjugate transpose of a matrix. Since $\mathbf{Z}$ is symmetrical (due to the reciprocity of the system), the positive definite condition can be imposed just on $\mathrm{Re}\{\mathbf{Z}\}$.

The inverse problem can be formally defined as

$$\mathbf{H}_m = \mathbf{f}(\mathbf{p}) \tag{5.4}$$

where $\mathbf{p}$ is the vector of the equivalent circuit parameters, $\mathbf{H}_m$ is a vector of experimental data for the magnetic field and $\mathbf{f}(\cdot)$ is a function relating the equivalent description of the site (through the uniform line and the set of parameters $\mathbf{p}$) to the theoretical magnetic field. This last operation is performed by employing the model in a predictive way. The equal sign in (5.4) is to be taken in a weak sense, having chosen to look for a least square solution.

In particular, the magnetic field is measured at different positions along the uniform track and, since we are ultimately interested in the current-distribution, the most sensitive position is just under the catenary. As a matter of fact, in that position the measured field is more likely related to the current flowing just at the observer longitudinal position, rather than to the superimposition of a broader portion of line. Moreover, the lateral polarization is measured, being the strongest component, whereas the vertical component would give no more clues about the current-distribution in the catenary.

The idea of performing measurements at several positions can be practically carried out only by employing portable spectrum analyzers; otherwise, the displacement of non-portable models would be ultimately a major obstacle to this procedure.

The problem with this inversion is that there exist many parameter configurations that can provide nearly the same field as given by the experimental results. In particular, this is critical in the lower frequency-range, where propagation effects are not strong, due to the short electrical length of the uniform line. For this reason, it is a good idea not to consider the minimum length as fixed by the validity of the infinite-line radiation model,

but rather a far longer portion of the track, e.g. a few hundred meters, limited only by practical reasons of displacing the antenna and the spectrum analyzer.

These considerations are confirmed by studying the error function $e(\mathbf{p})$

$$e(\mathbf{p}) = \|\mathbf{H}_m - \mathbf{f}(\mathbf{p})\|_2 \tag{5.5}$$

Indeed, it is quite "bumpy", with a great number of local minima very close one another, whereas the global minimum is very narrow. Therefore, common tools based on gradient methods are not appropriate in this case. The simplest solution we considered is to generate randomly the parameters vector $\mathbf{p}$ for a certain number of runs, then applying a gradient method, keeping track of the one giving the lowest value of e. The random approach allows a rough inspection of the solution-space defined by $\mathbf{p}$. This approach is far from optimal, and its poor performances are worsened by the fact that there is no assurance to find the global minimum.

Even increasing the number of positions where the magnetic field is measured, this approach does not yield better estimations. In order to have a more selective solution, it is possible to perform the same measurements for several electrical configurations of the uniform line. This means just to connect load-pairs to the ends of the line, in order to modify the current distribution. These modifications would ideally not alter the sought equivalent representations, while yielding more data for a better insight of the equivalents.

The problem with this idea is the fact that loads should be connected between the catenary and the rails. These loads should not absorb power delivered in DC or 50/60 Hz, so that they should have a high-pass filter behaviour, cutting off the power-supply frequency. This can be easily achieved by inserting a series capacitance, whose actual value will depend on the load to connect. The actual problem is that the capacitances (of the order of a few tens nF) should be able to support high voltages, e.g. 25 kV in high-speed lines, which is a major limitation, since such devices could be quite expensive. Perhaps high-capacitance power isolators could be employed.

Connecting loads to the supply-line does not involve important safety problems, since they are not connected to the instrumentation for the magnetic field measurement. Due care must be payed to the use of isolated perches, which must include the isolator capacitance on its top, thus ensuring a safe low-voltage environment for the actual load. Moreover, it is paramount to achieve the connection to the rails and only afterwards to the supply-line, thus avoiding any potential risk of electrical shock.

In order to check the feasibility of this approach, a numerical validation has been carried out. An experimental one could not be performed, due to the constraints already recalled in Section 4.6. The virtaul site considered is sketched in Figure 5.6, where a 700 m uniform section has been used as the reference line. Therefore, the aim is to estimated the two equivalent representations at its ends. Two independent voltage generators have been used for simulating conducted EMI, and the magnetic field thus generated has been computed at the five locations marked by dots in Figure 5.6, under the catenary, two meters above the soil. This procedure has then been applied for nine configurations, obtained from the original one by applying load-pairs to the ends of the reference uniform line, thus obtaining a grand-total of 45 magnetic field spectra. The load configurations actually simulated are described in Table 5.1.

136

Config.	Left-end	Right-end
1	OC	OC
2	50 Ω	OC
3	OC	50 Ω
4	50 Ω	50 Ω
5	300 Ω	OC
6	OC	300 Ω
7	300 Ω	300 Ω
8	50 Ω	300 Ω
9	300 Ω	50 Ω

Table 5.1.   The nominal values of the resistive loads applied between the catenary and the rails at the two ends of the reference uniform line.

The frequency range has been limited up to 200 kHz, just for the first resonances of the site. This choice was not made just for the sake of simplicity, but because of the fact that the low-frequency range is the most critical for the estimation, since the reference line is not electrically long, so that the measurements along it give nearly the same results; in other words, less information about the site. In particular, in the low-frequency range it is not possible to exploit the information inherent to standing waves, which are directly related to the terminations condition.

The global minimum has been searched, for each frequency sample, by performing 50 runs. The choice of the guess-values for **p** is quite critical in this context, since all the parameters have a wide range of possible values. Indeed, the equivalent impedances can assume any values, being the line highly mismatched, whereas the equivalent generators depend on the importance of conducted EMI, which can vary of several orders of magnitude. Uniform probability density functions have been chosen for setting the guess-values. For impedances, the support was set over $[10\,\Omega, 10\,\mathrm{k}\Omega]$, both for the real and imaginary parts, whereas for source terms the support was $[0,1]$ V.

The accuracy of this characterization has been tested by computing the magnetic field due to a train under test on the same site, as in Figure 5.7. Since the entire procedure is based on a linearity assumption, superimposition can be invoked. Being interested just in the distortion effects due to resonances, the conducted EMI sources have been "turned off". As already stated, they had just been exploited for investigating the site configuration, not for the sake of knowing them.

The train has been regarded as a voltage generator with an internal impedance of j200 Ω. This choice was not based upon any knowledge of the internal impedance of an actual train, it has just been used as a reference for the validation. The magnetic field has been computed for two positions of the train, always far enough for applying the infinite line radiation model. The same simulations have been carried out for the actual site and the results are compared in Figure 5.8: indeed, the trend in the spectra is fairly well identified, even though there are important disagreements: in particular, as expected, in the low frequency range. Beside the validation of the characterization procedure, the
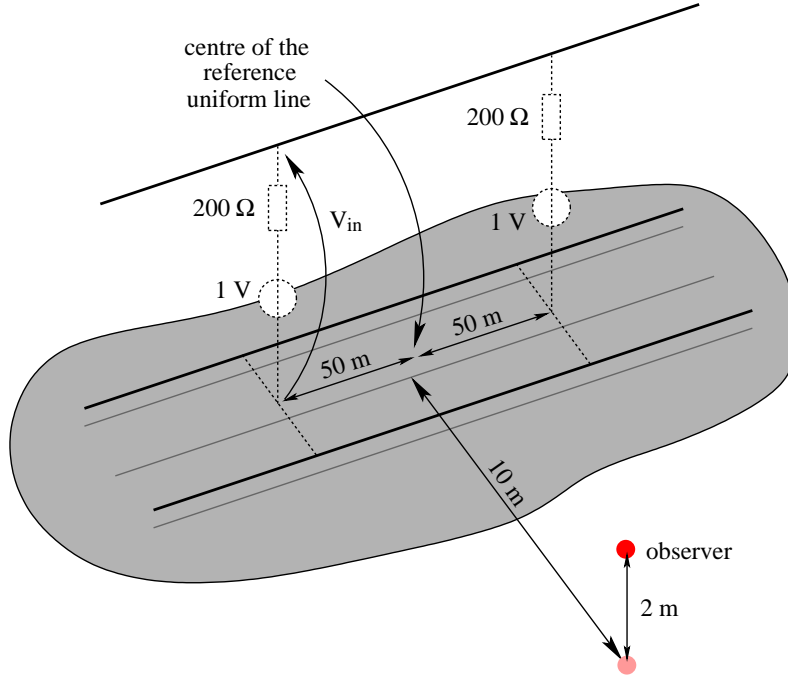
137

Figure 5.7. The two configurations tested for validating the site characterization.

infrastructure impact has been pointed out by substituting the two equivalent representations at the uniform line ends with the characteristic impedance matrix $\mathbf{Z}_c$; the magnetic field computed for this configuration is also shown in Figure 5.8.

Therefore, a procedure as the one here described would allow the manufacturer to characterize a site before actually testing the train, giving him a tool for assessing the impact of the infrastructure, by computing the magnetic field for the actual site and for the infinite line configuration, in the same way as described in the previous section.

5.4.1 Limitations to the proposed experimental characterization

The characterization procedure described in the previous section does need extensive investigations to get it ready for practical applications. In particular, the lack of reliability in the optimization routine should be solved; indeed there is a total lack of any convergence mechanism in the optimization routine we have used, based on random guess-values. A a matter of fact, during any run the probability to find the global minimum is the same as for previous runs. To this end, genetical algorithms may prove to be the right approach, in particular when associated with simulated annealing. As a matter of fact, this kind of approach is extensively employed in many optimization problems where the solution is based on a great number of unknowns, with a target (or error) function presenting many local minima. An example of successful application of such approach is the design of mechanical structures for airplanes, such as helices, or the design of reflector antennas

138

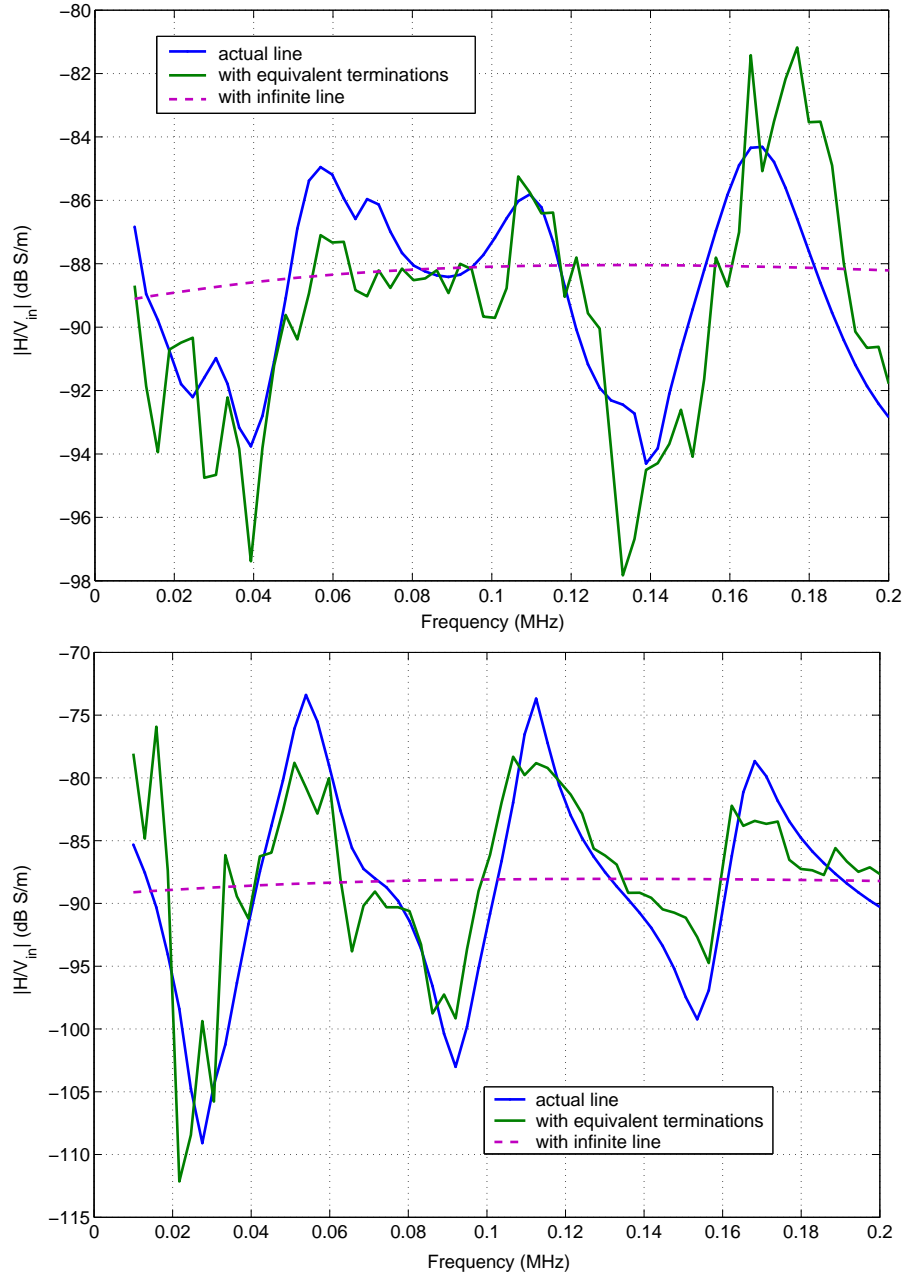Figure 5.8.   The results of the numerical validation for the experimental characterization of a site, showing the magnetic field for the actual site and the one computed by using the equivalent terminations for the train at the left side of the uniform line (a) and at the right side (b). The magnetic field for the infinite line required by the standard EN 50121 is also shown, thus giving an estimation of the infrastructure impact.

with a given radiation pattern. In both these examples the reliability of the solution is an important issue.

Furthermore, a better optimization routine could also relax the need for a great number of information, thus avoiding the utilization of load-pairs. Indeed, this need strongly affects the advantages of the proposed procedure, requiring special equipments (such as isolating perches, high-voltage loads, portable spectrum analyzers) and safety routines. Moreover, the range of nominal values for these loads is limited by the extra impedance of the decoupling capacitance, which sets a minimum bound for the actual impedance. Therefore, the use of loads may not be very effective in practice for getting more information on the site.

Another important point to be assessed is the influence of noise in the experimental results. Indeed, it is well known that inverse problems are strongly affected by noise, and in particular in this case we are not dealing only with white gaussian noise but also with narrow-band jammers (e.g. radio broadcasters).

5.5   Conclusions

In this chapter it has been shown that the actual configuration of the test site plays a major role in radiated emission tests. In particular, due to the mainly reactive behaviour of supply lines, resonances can strongly distort the test results: this implies that these results are site-dependent, since the resonances pattern is directly related to the site configuration. As already stated in Chapter 1, this is a major issue for rolling stock manufacturers, which must be able to prove that the train is EMC compliant.

To this end, it has been shown that the impact of the infrastructure can be effectively assessed by means of the model introduced in the previous chapters, following a predictive approach. Unfortunately, an accurate description of a site is hardly available, so that it has been necessary to propose an alternative approach based on an experimental characterization. In this case, a feasibility study has been carried out, showing that it is possible to derive an equivalent representation of the site, even with no a priori information. The limitations to this approach have been pointed out, highlighting the difficulties in solving the inverse problem and the practical problems in implementing an experimental approach.

Final considerations

In this section we recall the main issues addressed in this work, discussing about some important points which deserve deeper investigations. More detailed conclusions have already been discussed at the end of each chapter.

This work has been motivated by a fundamental industrial need, in response to the obligations imposed by the standard EN 50121. In particular, the third part of this standard does underestimate the impact of the infrastructure in radiated emissions tests, leaving all the responsibility on the manufacturer. This kind of problems have led Alstom Transport and the CEF to propose the present research project, seeking a rigorous proof of practical problems due to the infrastructure impact, by means of a theoretical model able to simulate a railway system.

To this end, a general description of what a railway system is has been given, showing how variable are actual realizations. In particular, the presence of several power devices connected along railway lines is a major source of uncertainty, due to the lack of knowledge about their high-frequency behaviour. Since their characterization would deserve an investigation on itself, the aim of this work has been set to the study of railway lines.

The problem of modelling this kind of systems has been tackled at several levels of complexity. By introducing some results from transmission-line theory, modal theory and antenna theory, the line has been firstly regarded as a uniform multiconductor line, addressing the effect of a finite conductivity soil in a second step. To this end, practical problems due to Sommerfeld's integrals have been solved, obtaining basic tools for the analysis of this kind of lines.

Subsequently, a more detailed description of a railway line has been considered, by taking into account non-idealities such as droppers, cambers, masts and the ballast. Approximated solutions have been proposed in order to keep the description of the actual system as simple as possible, with a special attention to the overall accuracy of the model.

These tools have then been used for checking the validity of a basic assumption in the standard EN 50121, that of a site approximating an infinitely long line, pointing out the inaccuracy of this assumption and giving a first estimation of the importance of the infrastructure.

Due to limited knowledge of the actual configuration of a railway system, a sensitivity analysis has also been carried out, highlighting the importance of accurate data about the line length, while showing that theoretical results are not much affected by inaccurate descriptions of the soil. In order to check the validity of the model, experimental investigations have been carried out on actual sites, showing a good agreement up to 700 kHz,

thus validating the approach here chosen. Limitations in the frequency-range of validity have been attributed to having neglected the dielectric nature of the ballast. On the other hand, the experimental investigations have pointed out the importance of providing accurate descriptions; in particular, in the present context, the presence of power devices is not always obvious, with hidden (buried) devices, that can alter the response of the entire system, leading to misunderstandings and misinterpretations.

Finally, the two main contributions to the magnetic field near a train have been discussed, showing that there exists an indirect contribution due to the infrastructure; the model can effectively be employed in order to estimate the impact of the infrastructure, showing how different an actual line would radiate with respect to the ideal one envisaged by the standard.

Due to the lack of knowledge about the site, the application of the model has been shown to be strongly affected by inaccurate descriptions. For this reason, rather than in a predictive way, the model has been applied in order to estimated an equivalent description of actual sites. To this end, we have proposed a characterization based on magnetic field measurements, employing the model in order to solve the inverse problem leading to an equivalent representation. A feasibility study has been presented with some simulation results, proving the feasibility of such an approach.

As a conclusion, we can state that the approach here presented has shown to be simple and fairly accurate over the most critical frequency range, up to 700 kHz, in accordance with the constraints set by the industrial domain. In particular, the analysis carried out in Chapter 4 has indeed yielded interesting results, leading to important simplifications and approximations.

Nevertheless, the present model cannot yet be applied in a predictive way to actual railway systems, due to two reasons. The first one is the almost total lack of data about the high-frequency behaviour of power devices. The problem of equivalent models must be thoroughly investigated in order to complete the description of a railway system. This task is far from simple, in particular from an experimental point of view: the definition itself of a suitable measurement setup is quite tricky, since the devices should be studied under their actual operating conditions, i.e. supplied by high-voltage sources. This requires the definition of a setup able to measure small amplitude signals superimposed on large-amplitude ones, avoiding saturation effects. To the best of our knowledge, the only way of achieving this goal is through electromagnetic field measurements, which are sensitive to the environment where the measures take place.

The second reason limiting the application of a model is the lack of knowledge of the configuration of actual sites. As a matter of fact, even having an ideally accurate model, one will always need to know what devices are present and how they are connected, together with an accurate estimation of the length of railway lines. This information can hardly be accessed, thus jeopardizing the entire effort of modelling a railway system.

On the other hand, as we have shown in Section 5.4, an experimental characterization of the site would overcome all these limitations. Because of all these considerations, further investigations should be undertaken in order to define a proper characterization procedure, acting on two fronts: first, suitable techniques should be studied for the characterization of the site; ideally, they should come with a low cost, using low-end devices

and equipments, while assuring a safe environment for the user, without any need to modify the site (e.g. inserting bypass wiring). These techniques should allow the user to collect as much data as possible about the electrical configuration of the test site, in order to estimate an equivalent representation. Second, suitable optimization techniques should be investigated. In particular, they should be able to deal with error functions with many local minima, providing some sort of statistical convergence criteria, so that the greater the number of iterations, the higher the probability of getting a good estimation of the global minima. These two points are deeply entwined, since stable and robust optimization techniques would likely require less experimental data, thus leading to a simpler characterization procedure.

Bibliography

[1] *Strategic Rail Research Agenda 2020*, First Report of the European Rail Research Advisory Council, September 2002

[2] R.J. Hill, "Electric Railway Tration: Part 6 Electromagnetic Compatibility - Disturbance sources and equipment susceptibility", *IEE Power Engineering Journal*, February 1997

[3] T. Konefal, D.A.J. Pearce, C.A. Marshman, L.M. McCormack, *Potential Electromagnetic Interference to Radio Services From Railways*, Final Report (AY4110) For Radiocommunications Agency, First issue, York EMC Services Ltd., University of York, UK

[4] R.J. Hill, "Electric Railway Tration: Part 7 Electromagnetic Interference in Traction Systems", *IEE Power Engineering Journal*, December 1997

[5] CENELEC Standard EN 50121, "Railway Applications - Electromagnetic Compatibility"

[6] Technical meeting, AMEC SPIE Rail, 11 June 2003, Cergy-Pontoise, France

[7] *The Track Handbook*, Corus Rail Businesses, http://www.corusrail.com

[8] "Railway Technical Pages - Electric Traction Power Supply", Last updated 1st February 2001, http://www.trainweb.org/railwaytechnical/etracp.html

[9] LTK Engineering Services, "Dictionary for Overhead Contact Systems with Pantograph and Trolley Pole Operations", *IEEE Overhead Contact Systems Committe for Rail Transit*, Draft July 2004

[10] G. de Pontbriand, *Non Ballasted Tracks*, Spie Enertrans, April 1999

[11] R.J. Hill, D.C. Carpenter, "Determination of Rail Internal Impedance for Electric Railway Traction System Simulation", *IEE Proceedings B*, Vol. 138, No. 6, November 1991

[12] Y. Oura, Y. Mochinaga, H. Nagasawa, "Railway Electric Power Feeding Systems", *Japan Railway & Transport Review*, No. 16, June 1998

[13] F. Lacôte, "50 Years of Progress in Railway Technology", *Japan Railway & Transport Review*, No. 27, June 2001

[14] A. Mariscotti, P. Pozzobon, "Determination of the Electrical Parameters of Railway Traction Lines: Calculation, Measurement, and Reference Data", *IEEE Transactions on Power Delivery*, Vol. 19, No. 4, October 2004

[15] F. Perticaroli, *Trazione Elettrica*, CLUP, Torino, 1988

[16] R.J. Hill, "Electric Railway Traction : Part 3 Traction Power Supplies", *IEE Power Engineering Journal*, December 1994

[17] P. Chapas, *Traction Ferroviaire*, Alstom Transport, September 1999

[18] R.J. Hill, D.C. Carpenter, "Rail Track Distributed Transmission Line Impedance and Admittance: Theoretical Modeling and Experimental Results", *IEEE Transactions on Vehicular Technology*, Vol. 42, No. 2, May 1993

[19] A. Mariscotti, P. Pozzobon, "Synthesis of Line Impedance Expressions for Railway Traction Systems", *IEEE Transactions on Vehicular Technology*, Vol. 52, No. 2, March 2003

[20] R.E. Collin, *Field Theory of Guided Waves*, McGraw-Hill Book Company, 1960

[21] V. Daniele, M. Gilli, S. Pignari, "Spectral Theory of a Semi-Infinite Transmission Line Over a Ground Plane", *IEEE Transactions on Electromagnetic COmpatibility*, Vol. 38, No. 3, August 1996

[22] C.R. Paul, *Analysis of Multiconductor Transmission Lines*, John Wiley & Sons, 1994

[23] J.C. Clements, C.R. Paul, A.T. Adams, "Two-Dimensional Systems of Dielectric-Coated, Cylindrical Conductors", *IEEE Transactions on Electromagnetic Compatibility*, Vol. 17, No. 4, November 1975.

[24] G.H. Golub, C.F. van Loan, *Matrix Computation*, Third Edition, The Johns Hopkins University Press, Baltimore, 1996

[25] J.R. Carson, "Wave Propagation in overhead Wires with Ground Return", *Bell System Technical Journal*, Vol. 5, 1926

[26] H. Kikuchi, "Wave Propagation Along an Infinite Wire Above the Ground at High Frequencies", Proc. Electrotech. J., Vol. 2, Dec. 1956

[27] J.R. Wait, "Theory of Wave Propagation Along a Thin Wire Parallel to an Interface", *Radio Science*, Vol. 7, No. 6, June 1972

[28] R.W.P. King, T.T. Wu, L.C. Shen, "The horizontal Wire Antenna over a Conducting or Dielectric Half Space: Current and Admittance", *Radio Science*, Vol. 9, No. 7, July 1974

[29] R.M. Sorbello, R.W.P. King, K.M. Lee, L.C. Shen, T.T. Wu, "The Horizontal-Wire Antenna Over a Dissipative Half-Space: Generalized Formula and Measurements", *IEEE Transactions on Antennas and Propagation*, Vol. 25, No. 6, November 1977

[30] D.C. Chang, R.G. Olsen, "Excitation of an Infinite Antenna Above a Dissipative Earth", *Radio Science*, Vol. 10, No. 8, August-September 1975

[31] E.F. Kuester, D.C. Chang, R.G. Olsen, "Modal Theory of Long Horizontal Wire Structures Above the Earth, 1, Excitation", *Radio Science*, Vol. 13, No. 4, July-August 1978

[32] R.G. Olsen, E.F. Kuester, D.C. Chang, "Modal Theory of Long Horizontal Wire Structures Above the Earth, 2, Properties of Discrete Modes", *Radio Science*, Vol. 13, No. 4, July-August 1978

[33] E.F. Kuester, D.C. Chang, S.W. Plate, "Electromagnetic Wave Propagation Along Horizontal Wire Systems in or Near a Layered Earth", *Electromagnetics*, Vol. 1, pp. 243-265, 1981

[34] P. Degauque, G. Courbet, M. Heddebaut, "Propagation Along a Line Parallel to the Ground Surface: Comparison Between the Exact Solution and the Quasi-TEM Approximation", *IEEE Transactions on Electromagnetic Compatibility*, Vol. 25, No. 4, November 1983

[35] F. Olyslager, D. de Zutter, "High-Frequency Transmission Line Models for a Thin Wire Above a Conducting Ground", *IEEE Transactions on Electromagnetic Compatibility*, Vol.37, No. 2, May 1995

[36] R.J. Pogorzelski, D.C. Chang, "On the Validity of the Thin Wire Approximation in Analysis of Wave Propagation Alog a Wire over a ground", *Radio Science*, Vol. 12, No. 5, September-October 1977

[37] G.E. Bridges, L. Shafai, "Validity of the Thin-Wire Approximation of Conductors near a Material Half-Space", *Antennas and Propagation Society International Symposium*, AP-S Digest, 26-30 June, 1989

[38] G.E.J. Bridges, L. Shafai, "Plane Wave Coupling to Multiple Conductor Transmission Lines Above a Lossy Earth", *IEEE Transactions on Electromagnetic Compatibility*, Vol.31, No. 1, February 1989

[39] F. Rachidi, C.A. Nucci, M. Ianoz, C. Mazzetti, "Influence of a lossy ground on lightning-induced voltages on overhead lines", *IEEE Transactions on Electromagnetic Compatibility*, Vol. 38, No. 3, August 1996

[40] F. Rachidi, C.A. Nucci, M. Ianoz, "Transient analysis of multiconductor lines above a lossy ground", *IEEE Transactions on Power Delivery*, Vol. 14, No. 1, January 1999

[41] E.F. Vance, *Coupling to Shielded Cables*, John Wiley & Sons, 1977

[42] F.M. Tesche, M.V. Ianoz, T. Karlsson, *EMC Analysis Methods and Computational Models*, John Wiley & Sons, 1997

[43] K.C. Chen, K.M. Damrau, "Accuracy of Approximated Transmission Line Formulas for Overhead Wires", *IEEE Transactions on Electromagnetic Compatibility*, Vol. 31, No. 4, November 1989

[44] J.R. Wait, K.P. Spies, "On the Image Representation of the Quasi-Static Fields of a Line Current Source Above the Ground", *Canadian Journal of Physics*, Vol. 47, 1969

[45] R.G. Olsen, J.L. Young, D.C. Chang, "Electromagnetic Wave Propagation on a Thin Wire Above Earth", *IEEE Transactions on Antennas and Propagation*, Vol. 48, No. 9, September 2000

[46] M. D'Amore, M.S. Sarto, "Simulation Models of a Dissipative Trasmission Line Above a Lossy Ground for a Wide Frequency Range - Part I: Single Conductor Configuration", *IEEE Transactions on Electromagnetic Compatibility*, Vol. 38, No.2, May 1996

[47] M. D'Amore, M.S. Sarto, "Simulation Models of a Dissipative Trasmission Line Above a Lossy Ground for a Wide Frequency Range - Part II: Multiconductor Configuration", *IEEE Transactions on Electromagnetic Compatibility*, Vol. 38, No.2, May 1996

[48] M.S. Sarto, "Electromagnetic Interference from Carrier Channels on Finite-Length Power Lines Above a Lossy Ground in a Wide Frequency Range", *IEEE Transactions on Power Delivery*, Vol. 13, No. 2, April 1998

[49] M. D'Amore, M.S. Sarto, A. Scarlatti, "Theoretical Analysis of Radiated Emission from Modal Currents in Multiconductor Transmission Lines Above a Lossy Ground", *IEEE International Symposium on Electromagnetic Compatibility*, Vol. 2, 21-25 August 2000

[50] F. Olyslager, *Electromagnetic Waveguides and Transmission Lines*, Clarendon Press, Oxford, 1999

147

[51] J. van der Merwe, *Uniform Multiconductor Transmission Lines Above a Dissipative Earth: Direct FDTD Analysis and Experimental Validation*, Ph.D. Thesis, University of Stellenbosch, October 1998

[52] P. Pettersson, "Image Representation of Propagation of Transients on Overhead Transmission Lines", *Proceedings of Cigré Symposium*, Lausanne, Switzerland, October 1993, paper 200-08

[53] J.R. Wait, "Electromagnetic Radiation from Cylindrical Structures", Peter Peregrinus, London, 1988

[54] P.R. Bannister, "Applications of Complex Image Theory", *Radio Science*, Vol. 21, No. 4, July-August 1986

[55] S.L. Marple, *Digital spectral analysis: with applications,*Prentice-Hall Inc., 1986

[56] H. Engels, *Numerical quadrature and cubature*, Academic Press, New York, 1980

[57] A. Baños, *Dipole Radiation in the Presence of a Conducting Half-Space*, Pergamon, New York, 1966

[58] A.N. Sommerfeld, "Über die Ausbreitung der Wellen in der Drahtlosen Telegraphie", *Annalen der Physics (4)*, Vol. 28, 1909, and Vol. 81, 1926

[59] J.R. Wait, *Electromagnetic Wave Theory*, Harper & Row Publishers, New York, 1985

[60] E.D. Sunde, *Earth Conduction Effects in Transmission Systems*, Van Nostrand, Dover, 1949

[61] C. Portela, "Measurement and Modeling of Soil Electromagnetic Behavior", *Proceedings IEEE 1999 International Symposium on Electromagnetic Compatibility*, EMC Society, pp. 1004-1009, August 1999, United States

[62] E.I. Parkhomenko, *Electrical Properties of Rocks*, Plenum Press, New York, 1967

[63] J.M. Maillol, "Overview of Physical Properties of Earth Materials", University of Calgary, Canada, http://www.geo.ucalgary.ca/ maillol/goph365/pp.pdf

[64] G.J. Burke, A.J. Poggio, *Numerical Electromagnetics Code (NEC) - Method of Moments. Part II: Program Description - Code*, Lawrence Livermore Laboratory, January 1981

[65] F.E. Gardiol, *Lossy Transmisison Lines*, Artech House, 1987

[66] J.R. Wait, "Electromagnetic Waves in Stratified Media", IEEE Press, 1994

[67] C. Poudroux, M. Rifi, B. Démoulin,"A Simplified Approach to Determine the Amplitude of the Transient Voltage Induced on a Cable Bundle", *IEEE Transactions on Electromagnetic Compatibility*, Vol. 37, No. 4, November 1995

[68] J. Vlach, K. Singhal, *Computer Methods for Circuit Analysis and Design*, Van Nostrand Reinhold, 1983, New York

[69] D. Morgan, *A Handbook for EMC Testing and Measurements*, Peter Peregrinus Ltd. on behalf of the IEE, 1994

[70] László Tihanyi, *Electromagnetic Compatibility in Power Electronics*, The IEEE Press, 1995

[71] J.A. Taufiq, J. Xiaoping, "Fast Accurate Computation of the DC-side harmonics in a Traction VSI Drive", *IEE Proceedings*, Vol. 136, Pt. B, No. 4, July 1989

[72] J. Shen, J.A. Taufiq, A.D. Mansell, "Analytical Solution to Harmonic Characteristics of Traction PWM Converters", *IEE Proceedings on Electric Power Applications*, Vol. 144, No. 2, March 1997

148

[73] X. Pei, K. Zhang, Y. Kang, J. Chen, "Analytical Estimation of Common Mode Conducted EMI in PWM Inverter", *26th Annual International Telecommunications Energy Conference INTELEC 2004*, 19-23 Sept. 2004

[74] L. Ran, S. Gokani, J. Clare, K.J. Bradley, C. Christopoulos, "Conducted Electromagnetic Emissions in Induction Motor Drive Systems Part II: Frequency Domain Models", *IEEE Transactions on Power Electronics*, Vol. 13, N0. 4, July 1998

[75] A.P.J. van Deursen, H.W.M. Smulders, R.A.A. de Graaff, J.B.M. van Waes,"Characterization of AT Railway Traction Power Supply, Measurement System and Results", *EMC'04 Sendai International Symposium on Electromagnetic Compatibility*, 1-4 June 2004, Sendai, Japan

[76] A.G. Tijhuis, *Electromagnetic Inverse Profiling: Theory and Numerical Implementation*, VNU Science Press, Utrecht, The Netherlands, 1987

[77] Eric W. Weisstein. "Positive Definite Matrix." From *MathWorld*–A Wolfram Web Resource. http://mathworld.wolfram.com/PositiveDefiniteMatrix.html

[78] Wilkinson, *The Algebraic Eigenvalue Problem*, Oxford University Press, London, 1965

Appendix A

List of acronyms

EMC	Electromagnetic Compatibility
EMI	Electromagnetic Interference(s)
e.m.	Electromagnetic
TLT	Transmission-line Theory
MTL	Multiconductor Transmission-line
p.u.l.	Per-unit length
PEC	Perfect Electric Conductor

Appendix B

Reference configuration

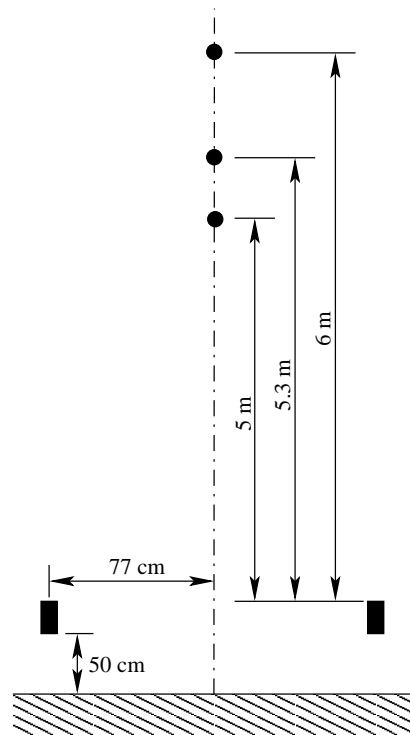Throughout this dissertation many examples refer to a reference test-case. This is here depicted in Figure B.1.

Figure B.1.   The cross-section configuration referred to throughout this dissertation. The radius of the three overhead wires is 6 mm.

Appendix C

Reduction of per-unit-length matrices

Let us consider an N-wire MTL, M of which are short-circuited together through "distributed" connections. For the sake of generality, the N wires constitute the set $\mathscr{C} = \{c_1, \ldots, c_N\}$, each wire identified by the index c_i; the subset $\mathscr{C}_M = \{c_1, \ldots c_M\}$ identifies the set of wires to be "reduced".

Two vector quantities can be defined :

$$\mathbf{I}_M = \begin{bmatrix} I_{c_1} \\ \vdots \\ I_{c_M} \end{bmatrix} \qquad \mathbf{I}_{NM} = \begin{bmatrix} I_{c_{M+1}} \\ \vdots \\ I_{c_N} \end{bmatrix} \tag{C.1}$$

the left one constituted by all the currents in the wires to be "reduced" and the right one by all the remaining currents. In the same way the vectors bV_M and bV_{NM} are defined.
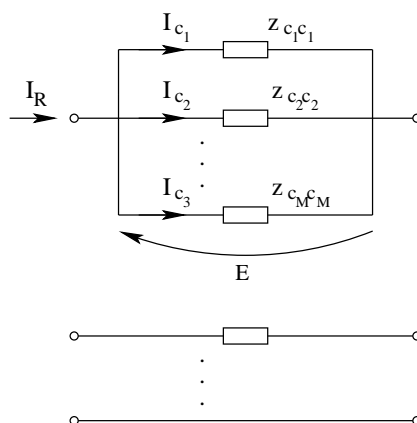

Figure C.1.   Reduction of p.u.l. parameters when a set of conductors are short-circuited in a distributed sens.

The problem of the reduction can be tackled separately for the series impedance and the shunt admittance. The series impedance relates currents and voltages as:

$$\begin{bmatrix} \mathbf{V}_M \\ \mathbf{V}_{NM} \end{bmatrix} = \mathbf{z} \begin{bmatrix} \mathbf{I}_M \\ \mathbf{I}_{NM} \end{bmatrix} \tag{C.2}$$

which can be inverted as

$$\begin{bmatrix} \mathbf{I}_M \\ \mathbf{I}_{NM} \end{bmatrix} = \begin{bmatrix} z'_M & \mathbf{z}'_{M,NM} \\ \mathbf{z}'^{\mathrm{T}}_{M,NM} & \mathbf{z}'_{NM} \end{bmatrix} \begin{bmatrix} \mathbf{V}_M \\ \mathbf{V}_{NM} \end{bmatrix} \tag{C.3}$$

With reference to Figure C.1, the conductors to be reduced are kept at the same voltage E, whereas the overall current flowing through the set $\mathscr{C}_M$ is I_R

$$I_R = \sum_{i \in \mathscr{C}_M} I_i \tag{C.4}$$

In order to obtain the new p.u.l. parameters for the reduced line, the currents and voltages for the set $\mathscr{C}_M$ should be substituted by the overall current I_R and the voltage E, obtaining

$$\begin{bmatrix} I_R \\ \mathbf{I}_{NM} \end{bmatrix} = \begin{bmatrix} z'_R & \mathbf{z}'_{R,NM} \\ \mathbf{z}'^{\mathrm{T}}_{R,NM} & \mathbf{z}'_{NM} \end{bmatrix} \begin{bmatrix} E \\ \mathbf{V}_{NM} \end{bmatrix} = \mathbf{z}' \begin{bmatrix} E \\ \mathbf{V}_{NM} \end{bmatrix} \tag{C.5}$$

where the reduced parameters z'_R and $\mathbf{z}'_{R,NM}$ are readily obtained from equation (C.3)

$$z'_R = \sum_{i,j \in \mathscr{C}_M} z'_{M,ij} \tag{C.6a}$$

$$\mathbf{z}'_{R,NM} = \sum_{i \in \mathscr{C}_M} [\mathbf{z}'_{M,NM}]_i \tag{C.6b}$$

where $\mathbf{z}'_{M,NM,i}$ is the i-th row of matrix $\mathbf{z}'_{M,NM}$. The reduced series impedance is then obtained by inverting matrix $\mathbf{z}'$.

$$* * *$$

On the other hand, for the shunt-admittance matrix the short-circuits just bypass the mutual admittances related to the sub-set $\mathscr{C}_M$, while the admittances between this sub-set and the remaining wires are just connected in a parallel configuration. Thus, the new parameters involving the equivalent wire are

$$y_R = \sum_{p=1}^{M} y_{c_p c_p} \tag{C.7}$$

$$y_{R,c_k} = \sum_{p=1}^{M} y_{c_p c_k} \qquad c_k \notin \mathscr{C}_M \tag{C.8}$$

where y_{ij} are the shunt-admittances between conductor i and j, and admittances towards the reference conductor for y_{ii}. Recalling the definition of the admittance matrix in Section 3.3, the parameters related to the equivalent wire for the reduced matrix will be $-y_{R,c_k}$ outside the main diagonal and

$$y_R + \sum_{k \notin \mathscr{C}_M} y_{R,c_k} \tag{C.9}$$

on the main diagonal.

Appendix D

Sensitivity analysis

The sensitivity analysis takes its start from equation (4.25), here reported for simplicity

$$\frac{\partial H}{\partial p} = \sum_{i=1}^{N} \sum_{j=1}^{N} \left\{ \frac{\partial \Theta_{ij}}{\partial p} T_{ij} I_{m,j}(z) + \Theta_{ij} \frac{\partial T_{ij}}{\partial p} I_{m,j}(z) + \Theta_{ij} T_{ij} \frac{\partial I_{m,j}(z)}{\partial p} \right\} \qquad \text{(D.1)}$$

where p is a generic parameter.

These derivatives should be computed for every parameter involved in the description of the railway system. But here we are evaluating the sensitivity with respect to the magnetic field due to one uniform line, since equation (D.1) assumes such configuration; in other words, the magnetic field is merely due to the current distribution along one uniform line. Hence, the sensitivities can be grouped into two classes:

- for local quantities: all the quantities related to the transversal analysis just depends on the cross-section parameters defining the line under analysis. Therefore, they are independent from the cross-section parameters of other other lines. As an example, consider the modal propagation constants γ_k: for each line they are just identified by the line cross-section, regardless of the other lines. For all these quantities, the sensitivities to other lines parameters can be set equal to zero;

- for global quantities: in this case, they depend on all the parameters. For instance, the current distribution along each line depends on the entire system

This distinction is important for a simpler approach. Of the three derivative terms in equation (D.1), the second one will be treated in the next section. The first one, dealing with the radiation matrices can be further expanded as

$$\frac{\partial \Theta_{x,ij}}{\partial p} = \frac{1}{\pi} \left(\frac{\partial \Lambda_{x,ij}}{\partial p} - \frac{\partial S_{4,ij}}{\partial p} \right) \qquad \text{(D.2)}$$

$$\frac{\partial \Theta_{y,ij}}{\partial p} = -\frac{1}{\pi} \left(\frac{\partial \Lambda_{y,ij}}{\partial p} - k_0^2 \frac{\partial S_{1,ij}}{\partial p} - \gamma_j^2 \frac{\partial S_{2,ij}}{\partial p} - S_{2,ij} \frac{\partial \gamma_j^2}{\partial p} - \frac{\partial S_{3,ij}}{\partial p} \right) \qquad \text{(D.3)}$$

$$\frac{\partial \Theta_{z,ij}}{\partial p} = \frac{\gamma_j}{\pi} \left(\frac{\partial S_{5,ij}}{\partial p} - \frac{\partial S_{6,ij}}{\partial p} \right) + \frac{1}{\pi} (S_{5,ij} - S_{6,ij}) \frac{\partial \gamma_j}{\partial p} \qquad \text{(D.4)}$$

The sensitivities of the modal propagation constants are treated in the next section. The radiation matrices are local quantities, so that only the line own parameters should be taken into account, namely h_i, d_i, the observer position $\mathscr{P}$, σ_g and ϵ_g. The contribution due to γ_j will be neglected, since it has been proven in Section 3.4.2 that Sommerfeld's integrals are not very sensitive to the actual propagation constant. Moreover, the same holds for the PEC soil terms, which have been reduced to the small argument approximation for the propagation terms (3.71). The PEC soil terms are:

$$\frac{\partial \Lambda_{x,ij}}{\partial x} = \frac{\Gamma_0}{2}(y - d_i) \left[\frac{x + h_i}{\rho_{t_2}} \frac{\Gamma_0 \rho_{t_2} \mathrm{K}_1'(\Gamma_0 \rho_{t_2}) - \mathrm{K}_1(\Gamma_0 \rho_{t_2})}{\rho_{t_2}^2} + \right.$$
$$\left. - \frac{x - h_i}{\rho_{t_1}} \frac{\Gamma_0 \rho_{t_1} \mathrm{K}_1'(\Gamma_0 \rho_{t_1}) - \mathrm{K}_1(\Gamma_0 \rho_{t_1})}{\rho_{t_1}^2} \right] \tag{D.5}$$

$$\frac{\partial \Lambda_{x,ij}}{\partial y} = \frac{\Gamma_0}{2} \left\{ \frac{\mathrm{K}_1(\Gamma_0 \rho_{t_2})}{\rho_{t_2}} \left[1 - \frac{(y - d_i)^2}{\rho_{t_2}^2} \right] - \frac{\mathrm{K}_1(\Gamma_0 \rho_{t_1})}{\rho_{t_1}} \left[1 - \frac{(y - d_i)^2}{\rho_{t_1}^2} \right] + \right.$$
$$\left. + \frac{(y - d_i)^2}{\rho_{t_2}^2} \Gamma_0 \mathrm{K}_1'(\Gamma_0 \rho_{t_2}) - \frac{(y - d_i)^2}{\rho_{t_1}^2} \Gamma_0 \mathrm{K}_1'(\Gamma_0 \rho_{t_1}) \right\} \tag{D.6}$$

$$\frac{\partial \Lambda_{y,ij}}{\partial x} = \frac{\Gamma_0}{2} \left\{ \frac{\mathrm{K}_1(\Gamma_0 \rho_{t_2})}{\rho_{t_2}} \left[1 - \frac{(x + h_i)^2}{\rho_{t_2}^2} \right] - \frac{\mathrm{K}_1(\Gamma_0 \rho_{t_1})}{\rho_{t_1}} \left[1 - \frac{(x - h_i)^2}{\rho_{t_1}^2} \right] + \right.$$
$$\left. + \frac{(x + h_i)^2}{\rho_{t_2}^2} \Gamma_0 \mathrm{K}_1'(\Gamma_0 \rho_{t_2}) - \frac{(x - h_i)^2}{\rho_{t_1}^2} \Gamma_0 \mathrm{K}_1'(\Gamma_0 \rho_{t_1}) \right\} \tag{D.7}$$

$$\frac{\partial \Lambda_{y,ij}}{\partial y} = \frac{\partial \Lambda_{2,ij}}{\partial x} \tag{D.8}$$

where

$$\mathrm{K}_1'(\Gamma_0 \rho) = -\mathrm{K}_0(\Gamma_0 \rho) - \frac{\mathrm{K}_1(\Gamma_0 \rho)}{\Gamma_0 \rho} \tag{D.9}$$

Furthermore

$$\frac{\partial \Lambda_{x,ij}}{\partial h_i} = \frac{\Gamma_0}{2}(y - d_i) \left[\frac{x + h_i}{\rho_{t_2}} \frac{\Gamma_0 \rho_{t_2} \mathrm{K}_1'(\Gamma_0 \rho_{t_2}) - \mathrm{K}_1(\Gamma_0 \rho_{t_2})}{\rho_{t_2}^2} + \right.$$
$$\left. + \frac{x - h_i}{\rho_{t_1}} \frac{\Gamma_0 \rho_{t_1} \mathrm{K}_1'(\Gamma_0 \rho_{t_1}) - \mathrm{K}_1(\Gamma_0 \rho_{t_1})}{\rho_{t_1}^2} \right] \tag{D.10}$$

$$\frac{\partial \Lambda_{x,ij}}{\partial d_i} = -\frac{\partial \Lambda_{x,ij}}{\partial y} \tag{D.11}$$

$$\frac{\partial \Lambda_{y,ij}}{\partial h_i} = \frac{\Gamma_0}{2} \left\{ \frac{\mathrm{K}_1(\Gamma_0 \rho_{t_2})}{\rho_{t_2}} \left[1 - \frac{(x + h_i)^2}{\rho_{t_2}^2} \right] + \frac{\mathrm{K}_1(\Gamma_0 \rho_{t_1})}{\rho_{t_1}} \left[1 - \frac{(x - h_i)^2}{\rho_{t_1}^2} \right] + \right.$$
$$\left. + \frac{(x + h_i)^2}{\rho_{t_2}^2} \Gamma_0 \mathrm{K}_1'(\Gamma_0 \rho_{t_2}) + \frac{(x - h_i)^2}{\rho_{t_1}^2} \Gamma_0 \mathrm{K}_1'(\Gamma_0 \rho_{t_1}) \right\} \tag{D.12}$$

$$\frac{\partial \Lambda_{y,ij}}{\partial d_i} \quad = \quad -\frac{\partial \Lambda_{y,ij}}{\partial y} \tag{D.13}$$

On the other hand, for Sommerfeld's integrals, the $\partial/\partial x$ are given by simply multiplying the kernel functions by a factor $-u_0$; the same results hold for $\partial/\partial h_i$. The derivatives with respect to y require the following substitutions

$$\cos(\lambda y) \quad \rightsquigarrow \quad -\lambda \sin(\lambda y) \tag{D.14}$$

$$\sin(\lambda y) \quad \rightsquigarrow \quad \lambda \cos(\lambda y) \tag{D.15}$$

For $\partial/\partial d_i$ just leads to the same results multiplied by -1. Since Sommerfeld's integrals are related to the soil characteristics they are quite sensitive to $\tilde{\epsilon}$. In order to simplify the analysis, the sensitivity $\partial \gamma_j / \partial \tilde{\epsilon}$ has been assumed negligible. Actually, this is a sound hypothesis, since the very foundation of the p.u.l. parameters expressions (3.71) are based upon the fact that Sommerfeld's integrals are weakly affected by the actual value of γ_p, but rather by $\tilde{\epsilon}$ in the kernel function ϕ_χ. Therefore, it suffices to operate the following substitution in all the terms $S_{k,ij}$

$$\phi_\chi \rightsquigarrow -\mathrm{e}^{-u_0(x+h_i)} \frac{(\partial \chi/\partial \tilde{\epsilon})u_{0,j} + (\gamma_0^2/2u_{g,j})}{(\chi u_{0,j} + u_{g,j})^2} \tag{D.16}$$

$$* \ * \ *$$

Concerning the sensitivities of the modal current distribution, they can be expanded as

$$\frac{\partial I_{m,j}}{\partial p} \quad = \quad \frac{\partial I_{m0,j}^+}{\partial p}\mathrm{e}^{-\gamma_j z} - \frac{\partial I_{m0,j}^-}{\partial p}\mathrm{e}^{+\gamma_j z} \tag{D.17}$$

$$- \quad \frac{\partial \gamma_j z}{\partial p}I_{m0,j}^+\mathrm{e}^{-\gamma_j z} - \frac{\partial \gamma_j z}{\partial p}I_{m0,j}^-\mathrm{e}^{+\gamma_j z} \tag{D.18}$$

In this case, the modal excitation terms are global quantities, since they may be strongly affected by all the boundary conditions. Therefore, all the parameters p_k should be taken into account. Anyway, it goes without saying that the most important ones are the length of the MTLs. As a matter of fact, railway track are never matched lines, so that resonances play an important role. Thus, a variation in the relative phase-shifting between forward- and backward-travelling modes strongly modifies the current maxima (and subsequently the magnetic field maxima). Furthermore, the lines lengths are the least accurately known parameters in actual systems. Anyway, the following derivation is kept in general terms, for the sake of simplicity.

The last two terms in equation (D.17) are related both to the sensitivities of the eigenvalues, treated in the next section, and the only terms dependent on the longitudinal

position z of the observer. On the other hand, the first two terms depend on the modal excitation terms. Their values are related to the voltages and currents at the left-end of a line by means of

$$\mathbf{g} = \begin{bmatrix} \mathbf{V}(0) \\ \mathbf{I}(0) \end{bmatrix} = \mathbf{M}\mathbf{I}_{m0} \tag{D.19}$$

where $\mathbf{M}$ and $\mathbf{I}_{m0}$ are defined in equation (4.14). Vector $\mathbf{g}$ is obviously a subset of the general solution $\mathbf{x}$ and they can be linked through the relationship

$$\mathbf{g} = \mathbf{Q}\mathbf{x} \tag{D.20}$$

where $\mathbf{Q}$ is a suitable matrix "selecting" the elements in $\mathbf{x}$ corresponding to the left-end voltages and currents. Vector $\mathbf{x}$ is obtained solving the tableau problem, here recalled as

$$\mathbf{C}\mathbf{x} = \mathbf{F} \tag{D.21}$$

corresponding to equation (4.13) defining the modified tableau method. Now, computing the derivative of the last equation with respect to p [68], and solving for $\partial \mathbf{I}_{m0}/\partial p$ yields

$$\frac{\partial \mathbf{I}_{m0}}{\partial p} = \mathbf{M}^{-1}\left\{ -\mathbf{Q}\mathbf{C}^{-1}\frac{\partial \mathbf{C}}{\partial p}\mathbf{x} - \frac{\partial \mathbf{M}}{\partial p}\mathbf{I}_{m0} \right\} \tag{D.22}$$

All these quantities are to be regarded as due to the nominal values of the parameters. The term $\partial \mathbf{M}/\partial p$ will be neglected, since it is a higher-order effect. It refers to the variations in the modal excitation terms due to the variations in the p.u.l. parameters with respect to the cross-section parameters. The other term $\partial \mathbf{C}/\partial p$ can be easily computed by recalling the definition of the circuit matrix $\mathbf{C}$ (cf. Section 4.3). For parameters related to MTLs, matrix $\partial \mathbf{C}/\partial p$ is an empty matrix but for the terms due to the derivatives of the chain matrix $\mathbf{\Phi}$. These derivatives will not be shown, since their computation can be straightforwardly carried out from equation (3.32) by applying the chain-rule, obtaining a result based upon the sensitivities for the p.u.l. matrices and the eigenvalues and eigenvectors.

$$* \ * \ *$$

On the other hand, the sensitivities for the p.u.l. matrices are here shown:

$$\frac{\partial \mathbf{Z}}{\partial p} = \frac{j\omega\mu_0}{2\pi}\left\{ \frac{\partial \mathbf{\Lambda}}{\partial p} + 2\frac{\partial \mathbf{S}_1^h}{\partial p} - 2\frac{\partial \mathbf{S}_2^0}{\partial p}\mathbf{A} - 2\mathbf{S}_2^0\frac{\partial \mathbf{A}}{\partial p} \right\} \tag{D.23}$$

$$\frac{\partial \mathbf{Y}}{\partial p} = j\omega\epsilon_0 2\pi\left[-\mathbf{\Lambda}^{-1}\frac{\partial \mathbf{\Lambda}}{\partial p}\mathbf{\Lambda}^{-1} \right] \tag{D.24}$$

having neglected the contribution from $\mathbf{Y}_g$. The last derivative terms share a similar structure

$$\frac{\partial \Lambda_{ij}}{\partial p} = \frac{\partial \rho_2^2/\partial p}{\rho_2^2} - \frac{\partial \rho_1^2/\partial p}{\rho_1^2} \tag{D.25}$$

$$\frac{\partial S_{1,ij}^h}{\partial p} = \frac{\partial \rho_2^2/\partial p}{\rho_2^2} - \frac{\partial \rho_1^2/\partial p}{\rho_1^2} \tag{D.26}$$

$$\frac{\partial S_{2,ij}^{h,0}}{\partial p} = \left(\ln \frac{\rho_2^2}{\rho_1^2}\right) \frac{\partial}{\partial p}\left(\frac{1}{1+\tilde{\epsilon}}\right) + \frac{1}{1+\tilde{\epsilon}}\left[\frac{\partial \rho_2^2/\partial p}{\rho_2^2} - \frac{\partial \rho_1^2/\partial p}{\rho_1^2}\right] \tag{D.27}$$

for

$$\rho_1^2 = (h_i + h_j)^2 + (d_i + r_i - d_j)^2 \tag{D.28}$$

where the definition of ρ_2 varies according to the function

$$\Lambda \rightsquigarrow \rho_2^2 = (h_i + h_j)^2 + (d_i + r_i - d_j)^2 \tag{D.29}$$

$$S_1^h \rightsquigarrow \rho_2^2 = (h_i + h_j + c_1)^2 + (d_i + r_i - d_j)^2 \tag{D.30}$$

$$S_2^h \rightsquigarrow \rho_2^2 = (h_i + h_j + c_2)^2 + (d_i + r_i - d_j)^2 \tag{D.31}$$

$$S_2^0 \rightsquigarrow \rho_2^2 = (h_j + c_2)^2 + (d_i + r_i - d_j)^2 \tag{D.32}$$

D.1 Eigenvalue and eigenvector sensitivities

As a first approximation, the p.u.l. parameters are weakly sensitive to small variations in the cross-section description, because of the logarithmic expressions employed in equations (3.71). Anyway, it may be interesting to assess their susceptibility. We consider the eigenvalue problem:

$$(\mathbf{A} - \gamma_k^2 \mathbf{1})\mathbf{X}_k = \mathbf{0} \tag{D.33}$$

Matrix $\mathbf{A}$ is here defined by a parameter p; in case of a small perturbation δp in p, around its nominal value p_0, we can write

$$\mathbf{A}(p_0 + \delta p) \simeq \mathbf{A}(p_0) + \frac{\partial \mathbf{A}}{\partial p}(p_0)\delta p \tag{D.34}$$

The evaluation of the eigenvalues and eigenvectors sensitivity for a matrix $\mathbf{A}$ perturbed by small variations $\delta p(\partial \mathbf{A}/\partial p)$ is still an open problem and a general solution is not yet available [24]. But in the present context, the matrix $\mathbf{YZ}$ always has simple eigenvalues, due to the inhomogeneity of the surrounding medium. For such a configuration the results proposed in [78] can be applied. To this end, the left eigenvectors have to be defined

$$\left[\mathbf{A}(p_0)^{\mathrm{T}} - \gamma_k^2 \mathbf{1}\right]\mathbf{Y}_k = \mathbf{0} \tag{D.35}$$

together with the auxiliary quantities β_{ij}

$$\beta_{ij} = \mathbf{y}_i^{\mathrm{T}}\frac{\partial \mathbf{A}}{\partial p}\mathbf{x}_i \tag{D.36}$$

where $\mathbf{x}_i$ and $\mathbf{y}_i$ are respectively the normalized right-hand and left-hand eigenvectors of $\mathbf{A}(p_0)$. The eigenvalue and eigenvectors sensitivities can be estimated as

$$\frac{\partial \gamma_k}{\partial p} = \frac{\mathbf{y}_k^{\mathrm{T}}(\partial \mathbf{A}/\partial p)\mathbf{y}_k}{2\gamma_k \mathbf{y}_k^{\mathrm{T}} \mathbf{x}_k} \tag{D.37a}$$

$$\frac{\partial \mathbf{x}_k}{\partial p} = \sum_{i \neq k} \frac{\beta_{ik}\mathbf{x}_i}{(\gamma_i^2 - \gamma_k^2)\mathbf{y}_i^{\mathrm{T}} \mathbf{x}_i} \tag{D.37b}$$

161

Appendix E

Instrumentation

Instrument	Model
Network analyzer	Agilent HP8753, 30 kHz - 6 GHz
Spectrum analyzer	Advantest R3271, 100 Hz - 26.5 GHz
Power amplifier	Amplifier Research, Model 25A 250A25 W, 10 kHz - 250 MHz
Functions generator	Philips PM 51360, 1 mHz - 5 MHz
Loop antenna	Rohde & Schwarz HFH2-Z2, 9 kHz - 30 MHz
Current probe	EATON Advanced Electronics, Model 91550-1L
Optical link	Electro Optic Development, SENTINEL 1000 FOL